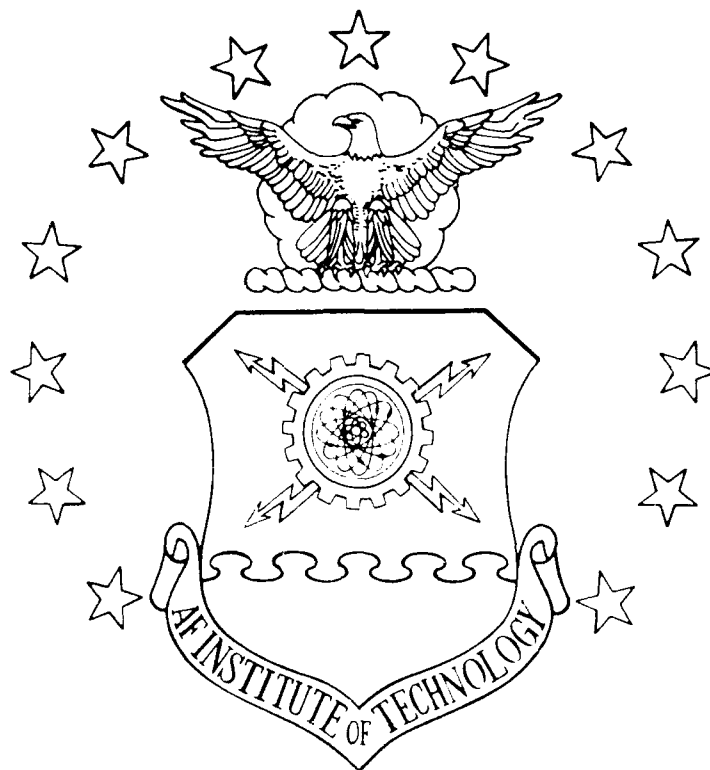


AD-A215 759



LUMINESCENCE OF LANTHANIDES
AND ACTINIDES IMPLANTED INTO BINARY
III-V SEMICONDUCTORS AND AlGaAs

Gernot S. Pomrenke
Major, USAF

AFIT/DS/ENF/89-4

DISTRIBUTION STATEMENT A

Approved for public release
Distribution Unlimited

DEPARTMENT OF THE AIR FORCE
AIR UNIVERSITY

AIR FORCE INSTITUTE OF TECHNOLOGY

Wright-Patterson Air Force Base, Ohio

89 12 26 16T

AFIT/DS/ENP/89-4

LUMINESCENCE OF LANTHANIDES
AND ACTINIDES IMPLANTED INTO BINARY
III-V SEMICONDUCTORS AND AlGaAs

DISSERTATION

Presented to the Faculty of the School of Engineering
of the Air Force Institute of Technology

Air University

In Partial Fulfillment of the
Requirements for the Degree of
Doctor of Philosophy

Gernot S. Pomrenke, B.S., M.S.

Major, USAF

December 1989

Approved for public release; distribution unlimited

LUMINESCENCE OF LANTHANIDES
AND ACTINIDES IMPLANTED INTO BINARY
III-V SEMICONDUCTORS AND AlGaAs

Gernot S. Pomrenke, B.S., M.S.
Major, USAF

Approved:

Robert L Hengehold 7 Dec '89
Chairman

Yung Kee Yeo 7 Dec '89

John Jones Jr. 7 Dec '89

Donald C. Reynolds 7 Dec '89

Accepted:

Robert A. Cahill
Interim Dean, School of Engineering

Preface

The study of lanthanides (rare earths) and actinides in semiconductors is a new area of investigation which allows for a multitude of directions for further investigations. Some of these directions I proposed in my 16 Feb 1988 Prospectus. Many opportunities exist for cooperative research among organizations outside and at Wright-Patterson AFB, such as the Avionics Lab (AADO-1), and specifically within AFIT between the Department of Engineering Physics (optical and gamma spectroscopy, theory, and radiation hardening) and Electrical Engineering (devices). The success of my experimental investigations has been reflected by the various presentations, invited talks, and publications which have been completed in the course of the program; a list of which appears at the end of the preface. Five MS thesis topics have been generated as a result of this research. Different directions were taken and many semiconductor-impurity systems were examined, the results for all not necessarily documented here (for example, for Ho, Th, some for Pr, and mul. implants). Many 'firsts' have been achieved and hope that the results will be of benefit to other investigators. The research essentially involved three types of experiments: selective excitation luminescence, photoluminescence, and lifetime measurements. For the latter two experiments the laboratory setup had to be essentially build or rebuild from the ground up.

The timely completion of the broad research program which I originally proposed was not realizable partially due to problems with contracted services and due to the various shortcomings of AFIT as it concerns funding, procurement (low priority), equipment, facilities, and support personnel. The final research direction also continued to be hampered by these conditions. Some major setbacks involved the high energy implantation service, availability of substrate material, laser excitation source in the green spectral range, infra-red detectors, reflectance gratings, and the limited access to the selective excitation experiment. As a result I am indebted to various outside agencies, government and civilian, which gave support that would allow for my eventual completion. I especially recognize Dr. Ian Brown of the Lawrence Berkeley Lab, University of California, Berkeley, CA, for his implantation work of the actinides and low energy ytterbium; and Jim Solomon of the University of Dayton Research Center and Materials Lab (WPAFB) for the secondary ion mass spectrometry (SIMS) analysis, aiding in both verifying the rare earth implant and determining the depth profile implant statistics. Mr. Solomon was responsible for several SIMS depth profile figures used in the dissertation. Also I sincerely thank Mr. Meisner of Wacker Siltronic Corporation (Burghausen, Federal Republic of Germany) for making available various semi-insulating and low-doped GaAs wafers.

I would like to thank the Air Force and my advisors, Dr. Robert L. Hengehold and Dr. Yung Kee Yeo, for giving me the opportunity to perform this research. Sincere appreciation goes to Prof. Dr. Juergen Schneider and Dr. Helmut^o Ennen of the Fraunhofer Institute (IAF), Freiburg, West Germany (FRG), for originally introducing me to the investigation of rare-earth doped semiconductors and their continued friendship and interest. I am indebted to Dr. Johannes Windscheif, also of the IAF, and Dr. Paul Klein of the Naval Research Lab (NRL), DC, for having had the opportunity to work with them in the past and gain from their broad experimental knowledge and straight-forward but professorial approach to a problem.

I would like to thank and recognize the assistance of the following people and organizations: Dr. William Mitchel and Robert Bertke of the Materials Lab (WPAFB) for polishing GaP samples and making Ge samples available; Dr. Cris Mudare and Eugene Soltis also of the Materials Lab for the use of their PbS detector; John Crist of the Avionics Lab (AADR, WPAFB) for making the annealing and sample cleaning facilities available and Dr. Phil Yu and Greg Smith for the temporary use of their annealing tube; also of the Avionics Lab, John Hoelscher for polishing crystals, Tim Cooper for electrical measurements, Lt. Paul Cook for the silicon nitride films, Jim Ehret and Ed Stutz for some GaAs wafers, Larry Callahan for his detector work, MSgt. Wilder for his technical support, and Dr. Rex Jones for the multilayer structure containing AlAs; of the Propulsion Lab (WPAFB),

Jim Ray for his superb glass work and the equipment support of Dr. Alan Garscadden, Dr. Sigmund Kizirnis, and Bob Knight; Donald (Sandy) Smith and Dr. Schepler of the electro-optics branch of the Avionics Lab (AADO) for the rare-earth doped glasses; Dr. Ernest Dorko of the Weapons Lab, Albuquerque, NM, for the Molelectron detector; Dr. Frank Pedrotti of Marquette University for some of the electrical measurements; Dr. Paul Klein of NRL for the PbS detector; Dr. Ziegler of IBM for the TRIM code; AFOSR of Bolling AFB for some of the initial funding; Implant Sciences Corp. for their quality 390 keV implantation work (funded privately) and computer code; and Prof. Karl Gschneidner of the Rare-Earth Information Center for his communications.

At AFIT I would like to recognize the technical staff which included Bill Evans and Rick Patton and toward the end of my program Greg Smith and Leroy Cannon; Dan Cook for his help as graduate assistant during the winter and spring of 1989; Mr. Don Smith of the AFIT electronic fabrication facility for some material support; Capts. Jeff Cavins and Jamie Varni for the spectra plotting software development; Dr. George John and Maj. Steve Berggren for their nuclear activity measurements; and the AFIT machine shop personnel which supported me for the past few years, Jack Tiffany, John Brohas, Ron Ruley, Dave Priscot, Tim Hancock, and Jan Lavallet. Special thanks go to Capt. Kevin Keefer for familiarizing me with the software and the excitement

spectroscopy experimental setup; Lt. Jose Colon for supporting a particular part of my research during his summer 1988 thesis work (photoluminescence of ytterbium); and Capt. Thad Bumgarner for his efforts on the time-resolved luminescence lab while working on his thesis during the summer of 1988.

Most importantly, I would like to thank my wife, Erna, and my son, Stefan, for tolerating this program and for their understanding; it is to them and my recently born daughter, Andrea, that I dedicate this dissertation.

Gernot S. Pomrenke

"Chess is much wider than calculation. It's wider than logic. You need fantasy and imagination."

- Kasparov -

Publications (PB) and oral presentations (OP) during the doctoral program (Jun 86 - Jul 89) reflecting directly or indirectly partial results from the dissertation research:

1. [OP] G. Pomrenke and P. Klein, "Excitation Spectroscopy on Rare-Earth Elements in III-V Semiconductors and Silicon", Ohio Section Meeting of the American Physical Society, 11 Oct 1986, Cleveland, Ohio. Abstract published in the Bulletin of the American Physical Society, Vol.32, No. 5, May 1987, p.1291.

2. [OP] P. B. Klein, H. B. Dietrich, and G. Pomrenke, "Time-Resolved Photoluminescence Measurements of Rare Earth Impurities in Si and III-V semiconductors", 1987 March Meeting of the American Physical Society, 16 March 1987, New York, NY. Abstract published in the Bulletin of the American Physical Society, Vol. 32, No. 3, March 1987, p. 439.

3. [OP] G. S. Pomrenke, T. F. Bumgarner, R. L. Hengehold, and Y. K. Yoo, "Time Resolved Luminescence of Ytterbium Implanted at High Energy into InP", Ohio Section Meeting of the American Physical Society, 8 Oct 1988, Toledo, Ohio. Abstract published in the Bulletin of the American Physical Society, Vol.34, No.4, April 1989, p.1261.

4. [OP] J. E. Colon, G. S. Pomrenke, R. L. Hengehold, and Y. K. Yoo, "Luminescence of Rapid Thermally Annealed III-V Semiconductors Implanted with 1 MeV Ytterbium Ions", Ohio Section Meeting of the American Physical Society, 8 Oct 1988, Toledo, Ohio. Abstract published in the Bulletin of the

American Physical Society", Vol.34, No.4, April 1989, p.1261.

5. [PB] P. B. Klein and G. S. Pomrenke, "Photoluminescence decay of the 1.54 μm Er^{3+} emission in Si and III-V semiconductors", Electronics Letters, Vol.24, No.24, 24 Nov 1988, p.1502.

6. [OP] G. Pomrenke, R. Hengehold, and Y. Yeo, "Thulium and Praseodymium Related Emissions in Rare Earth Implanted III-V Semiconductors", March Meeting of the American Physical Society, 23 March 1989, St. Louis, Missouri. Abstract published in the Bulletin of the American Physical Society, Vol.34, No. 3, March 1989, p.918.

7. [OP] J. E. Colon, T. F. Bumgarner, G. S. Pomrenke, R. L. Hengehold, and Y. K. Yeo, "Luminescence of III-V semiconductors and AlGaAs implanted with 1MeV Ytterbium Ions", March Meeting of the American Physical Society, 23 March 1989, St. Louis, Missouri. Abstract published in the Bulletin of the American Physical Society, Vol.34, No.3, March 1989, p.917.

8. [OP] P. B. Klein and G. S. Pomrenke, "Radiative and Nonradiative Recombination at Er Centers in III-V Semiconductors", March Meeting of the American Physical Society, 21 March 1989, St. Louis, Missouri. Abstract published in the Bulletin of the American Physical Society, Vol. 34, No. 3, March 1989, p. 551.

9. [OP] G. S. Pomrenke, R. L. Hengehold, and Y. K. Yeo, "Luminescence of GaAs, AlGaAs, and AlAs Implanted at 1 MeV with Erbium", Ohio Section of the American Physical Society, 29 April 1989, Oxford, Ohio.

10. [OP & PB] Gernot S. Pomrenke, Robert L. Hengehold, and Yung Kee Yeo, "Excitation Mechanism of Rare Earth (Yb, Tm, Er, Pr) Emissions in GaAs and InP", submitted and accepted for presentation at the 16th International Symposium on Gallium Arsenide and Related Compounds, 25-29 Sep 1989, Karuizawa, Nagano, Japan. Refereed paper to appear in proceedings of the meeting as an Inst. of Physics publication as in the past.

11. [OP] Gernot S. Pomrenke, "Luminescent Characteristics of Lanthanides Incorporated into III-V Semiconductors", invited talk for the Condensed Matter and Surface Sciences Seminar at Ohio University, Athens, Ohio, 20 April, 1989.

12. [OP & PB] J. S. Solomon, G. S. Pomrenke, R. L. Hengehold, and Y. K. Yeo, "SIMS and photoluminescence studies of rare earth implants in InP", submitted and accepted for presentation at the Seventh International Conference on Secondary Ion Mass Spectrometry, 3-8 Sep 1989, Monterey, California. Refereed article to appear in the proceedings of the conference.

13. [PB] Gernot S. Pomrenke, Robert L. Hengehold, Yung Kee Yeo, Ian G. Brown, and James S. Solomon, "Actinide activated luminescence in uranium implanted III-V semiconductors", to be published in the 15 February 1990 issue of the Journal of Applied Physics.

Table of Contents

	page
Preface	iv
List of Figures	xv
List of Tables	xix
List of Symbols	xx
Abstract	xxii
I. Introduction	1
II. Background and Theory	8
A. Overview	8
B. Semiconductors, Lanthanides, and Actinides	10
C. Solids Containing Rare Earth Ions	17
D. Investigations of 4f- and 5f- Doped Semi- conductors	21
Overview	21
Luminescence	22
Electrical Measurements	26
Excitation and Lifetime Measurements	29
E. Investigation Techniques and Physical Processes	32
Photoluminescence	32
Excitation Spectroscopy	34
Lifetime Measurements	36
F. Implantation and Annealing	40
G. Secondary Ion Mass Spectrometry (SIMS)	45
III. Experiment	49
A. Overview	49
B. Photoluminescence	50
C. Selective Excitation Luminescence	72
D. Lifetime Measurements	81
E. Sample Processing	91
Introduction	91
Sample Information	91

	page
Sample Preparation	94
Implantation	96
Post-implantation Sample Treatment	102
Sample Mounting	108
SIMS	109
IV. Results and Discussion	113
A. Photoluminescence	113
Photoluminescence of Yb^{3+}	114
Photoluminescence of Er^{3+}	139
Photoluminescence of Tm^{3+}	157
Photoluminescence of Pr^{3+}	180
Photoluminescence of Actinides	202
B. Selective Excitation Luminescence	217
Introduction	217
Experimental	219
Results and Discussion	222
Ytterbium	222
Thulium	225
Erbium	228
Praseodymium	232
Conclusion	237
C. Lifetime Measurements	239
Introduction	239
Results and Discussion	240
InP:Yb	240
AlGaAs:Yb	250
GaAs:Er and AlGaAs:Er	251
GaAs:Tm	253
Conclusion	253
V. Conclusion and Recommendations	255
Appendix A: Electronic Configuration of Lanthanide Ions	276
Appendix B: Electronic Configuration of Actinide Ions	277
Appendix C: Energy Level Diagram for Lanthanides (RE^{3+})	278
Appendix D: Energy Level Diagram for Actinides (An^{3+})	279
Appendix E: Photoluminescence of Ho^{3+} in GaAs	280
References	281
Vita	291

List of Figures

Figure	Page
1. Operation schemes of crystal lasers that emit on pure electron transitions.....	3
2. Photoluminescence spectra at 10 K for Er-implanted GaAs and annealed with the strip-heater, conventional, and quartz ampoule method.....	14
3. Recombination schemes in photoluminescence.....	33
4. Three-level system with one luminescent level and a rapid decay process between level 3 and level 2.....	38
5. Schematic of the photoluminescence setup.....	51
6. Schematic of the evacuation and cryogenic subsystem.	52
7. Atmospheric transmission at sea level over a 300 meter path.....	60
8. System response spectra.....	61
9. Schematic of the photon counting and acquisition subsystem.....	63
10. Experimental arrangement for germanium detector.....	66
11. Germanium detector mount.....	67
12. Experimental arrangement for the photoconductive detector (PbS).....	69
13. Infrared detector mount.....	70
14. Setup for the selected excitation experiment.....	73
15. Bandwidth of birefringent filter.....	77
16. Schematic of the experimental setup for lifetime measurements.....	82
17. Sample environment and evacuation and cryogenic subsystems for the lifetime measurement setup.....	83
18. High energy ion beam accelerator.....	98
19. Sample annealing methods.....	104

20. Conventional anneal furnace temperature profile for a 750°C anneal.....	105
21. Temperature/time profile of the rapid thermal anneal system.....	107
22. Cross-section of the DIDA ion microprobe.....	110
23. Luminescence spectra at 4.2 K and energy-level scheme for Yb ³⁺ with T _d symmetry in InP.....	119
24. Photoluminescence spectra at 6 K of 140 keV Yb-implanted InP.....	122
25. Photoluminescence spectra of Yb-implanted and 750°C annealed GaP and GaAs.....	123
26. Isochronal anneal study of Yb implanted InP at 6 K..	125
27. Isothermal anneal study at 6 K of InP implanted with Yb at an energy of 1 MeV.....	127
28. Photoluminescence at 6 K of Yb ³⁺ in n-type GaP.....	129
29. Photoluminescence at 6 K of Yb ³⁺ in Al _{0.15} Ga _{0.85} As....	132
30. Photoluminescence at 6 K of Yb ³⁺ in Al _{0.23} Ga _{0.77} As....	133
31. Photoluminescence at 6 K of Yb ³⁺ in Al _{0.30} Ga _{0.70} As....	134
32. SIMS depth profile of Yb implanted InP.....	137
33. Photoluminescence spectra of erbium implanted into GaAs, AlAs, and AlGaAs with different Al mole fractions.....	143
34. Photoluminescence spectra of erbium implanted into GaAs samples of different conductivity.....	144
35. Temperature dependence of the Er-specific emission in Al _{0.4} Ga _{0.6} As.....	146
36. Implant dosage dependence of the Er-specific emissions of semi-insulating GaAs at 7K.....	148
37. High resolution spectra at 7 K of the Er ³⁺ emission in two different but identically treated GaAs substrates.....	150
38. Photoluminescence at 7 K of Er implanted (CS) semi-insulating GaAs excited by two different sources....	151

39. Comparison spectra of Er implanted semi-insulating InP and GaAs.....	153
40. SIMS depth profile of Er implanted InP.....	155
41. Comparison spectra of the Tm^{3+} emission in InP and GaAs.....	163
42. Photoluminescence of encapsulated GaAs:Tm as a function of anneal temperature.....	167
43. Photoluminescence of nonencapsulated GaAs:Tm as a function of anneal temperature.....	168
44. Tm^{3+} emissions in GaAs as a function of sample temperature.....	171
45. Isochronal anneal study of Tm implanted InP.....	173
46. Photoluminescence of InP:Tm at two different laser excitations.....	175
47. SIMS depth profile of Tm implanted into InP.....	178
48. Comparison spectra of the Pr^{3+} emission at 6 K in GaAs and InP.....	185
49. Transitions between three sets of spin-orbit levels of Pr^{3+} in implanted GaAs.....	186
50. Isochronal anneal study of the GaAs:Pr emissions in the 0.73 - 0.96 eV spectral region.....	188
51. Isochronal anneal study of the GaAs:Pr emissions in the 0.90 - 1.55 eV spectral region.....	189
52. Intracenter emissions of Pr^{3+} in GaAs as a function of sample temperature.....	192
53. Spectra of Pr^{3+} emissions from two different implanted GaAs substrates.....	194
54. Isochronal anneal study of the Pr^{3+} emissions in InP for the 0.73 - 0.97 spectral region.....	196
55. Isochronal anneal study of the Pr^{3+} emissions in InP for the 0.95 - 1.50 eV spectral region.....	197
56. SIMS depth profile of Pr implanted InP.....	199
57. SIMS depth profiles of as-implanted and 750° annealed InP implanted with uranium.....	207

58. Photoluminescence spectra of GaAs and InP implanted with uranium at an average energy of 131 keV and subsequently annealed at 750°C for 15 min and 640°C for 10 min, respectively.....	209
59. Temperature dependence of the luminescence intensities of the various 5f uranium emissions observed in GaAs and InP.....	213
60. Yb ³⁺ luminescence spectra at 7K of InP:Yb excited with different laser lines; inset shows excitation spectra of the 1007 nm Yb ³⁺	223
61. Tm ³⁺ luminescence spectra of GaAs:Tm for two anneal temperatures; inset shows the excitation spectra of the dominant line for the 600°C/10min anneal.....	226
62. Er ³⁺ luminescence spectra as a function of excitation energies for (WA) GaAs:Er.....	229
63. Position of laser excitation lines for GaAs:Er with respect to the near-edge emissions.....	230
64. Excitation spectra of the dominant Er ³⁺ emission and background at 1541 nm of (CS) GaAs:Er at 7K.....	231
65. Excitation spectra of the dominant Er ³⁺ emission of InP:Er at 7K.....	233
66. Luminescence spectra of GaAs:Pr upon pumping with three different excitation energies.....	234
67. Excitation spectra of specific Pr ³⁺ emissions of GaAs:Pr at 7K.....	235
68. Decay curves for the Yb ³⁺ emissions in InP:Yb at 4.2, 80, and 90 K.....	244
69. Anneal temperature dependence of the Yb ³⁺ lifetimes in InP:Yb at 1002 nm.....	245
70. Example rise and decay waveform of the Yb ³⁺ luminescence in InP:Yb (2.9 μ s system time constant).....	246
71. Luminescence rise and decay waveform of the Yb ³⁺ 1006 nm emission in InP:Yb (fast Ge detector, 200 ns time constant).....	248
72. Decay curve for the Yb ³⁺ emission in Al _{0.3} Ga _{0.7} As:Yb..	251
73. Model for possible energy transfer mechanisms in rare earth doped III-V semiconductors.....	272

List of Tables

Table	Page
1. Properties of Important Group IV and III-V Semiconductors.....	12
2. Characteristics of Lanthanides and Selected Actinides.....	13
3. Calculated Projected Ranges and Stragglings for Lanthanides and Actinides Implanted into Selected Semiconductors.....	44
4. III-V Semiconductor Substrate Information.....	92
5. AlGaAs Sample Information.....	93
6. MEVVA Implant Parameters.....	102
7. Calculated and Measured Implant Parameters in as-implanted InP.....	112
8. Sample Information for the Ytterbium Implanted Semiconductors.....	118
9. Emission Line Assignment for Yb ³⁺ in InP.....	121
10. Sample Information for the 1 MeV Erbium Implanted Semiconductors.....	141
11. Sample Information for Tm Implanted GaAs.....	160
12. Sample Information for Tm Implanted InP.....	161
13. Sample Information for Tm Implanted GaP.....	162
14. Sample Information for the 380 keV Praseodymium Implanted Semiconductors.....	183
15. Sample Information for the Selective Excitation Study.....	220
16. Corrected Decay Lifetimes of Yb ³⁺ in InP for a System Response Time Constant of 2.9 μ s.....	247

List of Symbols

AD	= amplifier discriminator
amp	= ampere
arb. units	= arbitrary units
a. u.	= arbitrary units
cfm	= cubic feet per minute
cc	= carrier concentration
DA	= donor-acceptor
D ^o A ^o	= donor-acceptor
DIDA	= dynamic in-depth analyzer
ESR	= electron spin resonance
eV	= electron volt
f	= focal length
FB	= free-to-bound
fg	= forming gas
fwhm	= full width at half maximum
gr/mm	= grooves per millimeter
IR	= infrared
keV	= kilo electron volt
LED	= light emitting diode
LHe	= liquid helium
LN ₂	= liquid nitrogen
LO	= longitudinal optical
LPE	= liquid phase epitaxy
max	= maximum
MBE	= molecular beam epitaxy
MCA	= multichannel analyzer
MeV	= mega electron volt
MEVVA	= MEtal Vapor Vacuum Arc
min	= minute
MOCVD	= metal organic chemical vapor deposition
ND	= neutral density
NE	= near edge
nm	= nanometer
PC	= personal computer
PL	= photoluminescence
PMT	= photo multiplier tube
ppb	= parts per billion
ppm	= parts per million
psi	= pounds per square inch
RE	= rare earth
s	= second
sec	= second
SI	= semi-insulating
SIMS	= secondary ion mass spectrometry
TC	= thermocouple
TM	= turbo molecular
TRIM	= TRansport of Ions in Matter
und	= undoped
UV	= ultraviolet

VDC = volts direct current
VFC = voltage to frequency converter
 μ = micro (Greek letter 'mu')
 \emptyset = diameter

.

Abstract

Through luminescence experiments it was observed that lanthanides, or rare earths, and also actinides, may be successfully introduced into binary and ternary III-V Group semiconductors. The study supports the feasibility of producing infrared light emitting diodes (LEDs) for the 0.9 to 1.7 μm spectral range. Besides systematic spectral characterization through photoluminescence, excitation mechanisms and decay kinetics were also investigated.

Ytterbium (Yb), erbium (Er), thulium (Tm), praseodymium (Pr), and uranium (U) were successfully implanted into GaAs, InP, GaP, AlAs, or AlGaAs as observed through photoluminescence and also verified by secondary ion mass spectrometry (SIMS). The impurities were implanted through high (1 MeV), intermediate (380, 390 keV), and low (140 keV) energy standard and nonstandard implantation methods, followed by post-implantation annealing using both rapid thermal and conventional furnace annealing. Details on the implantation techniques are given and implantation statistics were determined.

The resulting characteristic sharp 4f- or 5f- emissions were seen around 1.0 μm for Yb^{3+} in InP, GaP, and AlGaAs; 1.5 μm for Er^{3+} in GaAs, InP, GaP, AlAs, and AlGaAs of four different Al mole fractions; 1.2 μm for Tm^{3+} in GaAs and InP; 1.1, 1.3, and 1.6 μm for Pr^{3+} in GaAs and InP; and from

1.6 to 1.7 μm for uranium in GaAs and InP. Preliminary evidence shows Ho-specific emissions in GaAs at 0.94 and 1.18 μm . Tm^{3+} emissions are assigned to transitions between the crystal-field-split spin-orbit levels $^3\text{H}_5 - ^3\text{H}_6$ while for Pr^{3+} , between the levels $^1\text{G}_4 - ^3\text{H}_4$, $^1\text{G}_4 - ^3\text{H}_5$, and $^3\text{F}_3 - ^3\text{H}_4$, respectively. The luminescence studies were performed by using semiconductor substrates of different conductivity, by varying laser excitation, sample temperature, and by varying anneal temperature, time, and technique.

Selected excitation experiments with a tunable dye laser were performed on the different systems in order to understand the excitation mechanism between the semiconductor host and the rare earth ion. It was established that free carriers were needed to excite the rare earth centers but below bandgap states such as donor-acceptor pairs and deep levels are also involved as seen for Er^{3+} and possibly Pr^{3+} . Lifetime measurements show the radiative (~ 1 millisecc for Er^{3+}) and more non-radiative (for Yb^{3+} 12.5 microseconds in InP and 15.5 microseconds in $\text{Al}_{0.3}\text{Ga}_{0.7}\text{As}$) nature of the different rare earth ions incorporated into the semiconductor.

I. Introduction

The study of rare-earth elements incorporated into Group III-V and Group IV semiconductors is of current interest due to their potential applications in optoelectronics and photonics in the visible and near infrared spectral region. Although the luminescence properties of rare-earth (4f) ions in solids have been studied in great detail for decades, the research was almost entirely concerned with the optical properties of 4f ions in dominantly ionic host crystals such as fluorides and oxides (for example Krupke, 1966 and Brown et al, 1974, and references therein). To a lesser extent, luminescence of 4f ions in more covalently bonded hosts, such as tetrahedral II-VI semiconductors has also been investigated (Brown et al, 1974). However, inspite of their potential as 4f-doped light-emitting diodes (LED) and lasers, it was not until the early 1980s that the luminescence properties of 4f-ions in III-V semiconductors and silicon were investigated to any significant extent.

It has been over the last seven years that various investigations have shown that it is possible to introduce a variety of rare-earth ions into semiconductors and to excite the internal 4f-4f luminescence transitions not only optically but also electrically. These 4f-intracenter emissions are identified with transitions between the weakly crystal-field split spin-orbit levels of the trivalent rare earth. Recent developments in the growth of rare-earth doped

III-V semiconductors by investigators in Japan, the development of a possibly new type of 4f-doped laser structures at AT&T Bell Laboratories, and the fabrication of Er doped GaAs LEDs in France, have broadened the international interest in these materials, which until 1987 was almost completely dominated by research efforts in the Federal Republic of Germany and the Soviet Union. The only other known U.S. efforts aside at the Air Force Institute of Technology has been at the Naval Research Lab in Washington, DC.

As motivation for the investigation of lanthanides and actinides in III-V and ternary semiconductors, Figure 1 is presented. Depicted are the laser transitions of trivalent and divalent 4f- and 5f-ions in ionic hosts, and as mentioned, these have been widely investigated in the past. Furthermore, many attempts were made to fabricate integrated systems in which these laser active ions could be incorporated into a semiconductor and which would then be excited through injection of minority carriers. Although 4f-ions show intense visible and infrared emissions in II_B-VI semiconductors, no acceptable pn-diode could be produced such that the 4f-ions could be electrically excited through electron impact in the n- or p-type II_B-VI layer. Since III-V semiconductors lend themselves easily to n- or p-type doping and the production of pn-diodes, it would appear that 4f-doped III-V semiconductor devices should be realizable.

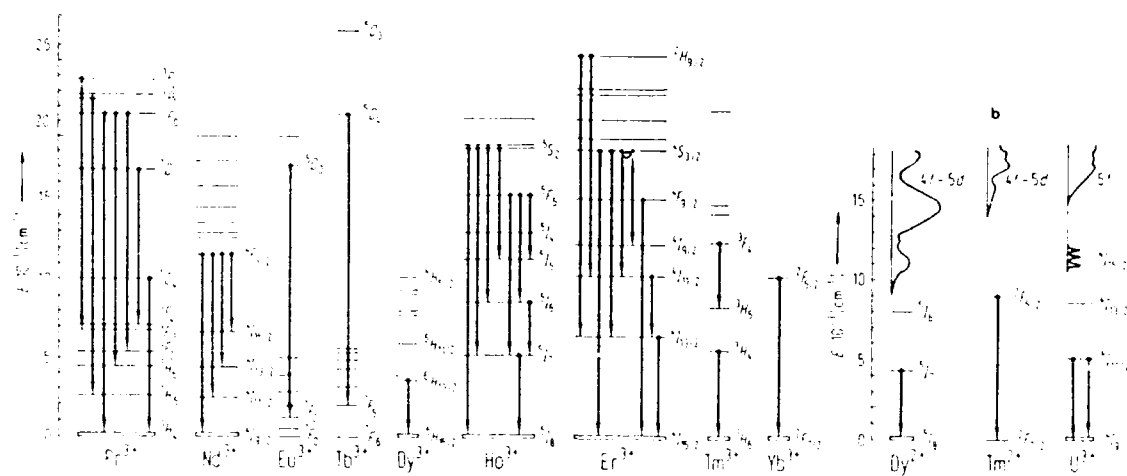


Figure 1. Operation schemes of crystal lasers that emit on pure electron transitions. (a) Trivalent rare earth ions. (b) Dy^{2+} , Tm^{2+} , and U^{3+} ions. (Kaminskii, 1981)

The doping of III-V compound semiconductors, such as gallium arsenide (GaAs), gallium phosphide (GaP), and indium phosphide (InP), and silicon (Si) with such rare-earth elements as ytterbium (Yb) and erbium (Er) allows for sharp optical transitions, with accompanying narrow line-widths, heretofore unachievable with other dopants (Ennen and Schneider, 1985). The emission wavelengths are not determined by the host semiconductor bandgap but by the transition energies within the $4f$ levels of the rare earth ion. Because the $4f$ shell is well-shielded from the external environment by filled $5s$ and $5p$ shells, these transition energies tend to be only weakly affected by the presence of external perturbations. Thus, a rare earth doped semiconductor source would be compatible with integrated

optics applications, as this laser medium may be incorporated into almost any host material, and the emission wavelength is relatively insensitive to the host material (Ennen et al, 1983) or temperature (Whitney et al, 1988).

Recent developments in this new research area could result in light-emitting diodes and perhaps a wide array of injection lasers which would operate with much narrower linewidths in those spectral regions important to present silica based fiber optics. Both Whitney et al (1988) and Rolland et al (1988) recently reported the fabrication of Er-doped GaAs light-emitting diodes emitting at 1.54 μm ; Haydl et al (1985) and Dimariev et al (1983) reported on Yb-doped InP LEDs emitting at 1.0 μm . Novel device structures using combinations of Si, III-V, and II-VI compounds doped with rare-earths are also being considered. Recently two multilayered heterojunction structures were proposed: the staircase impact electroluminescent devices (SIED) and the staircase photon amplifier converter (SPAC) (Lozykowski, 1988). The study of rare-earths in semiconductors represents a relatively broad area of investigation which supports the short and long term needs of the government for new materials and semiconductor devices.

The use for modern electronics of III-V and ternary semiconductors has been recognized by the technical community and the government for at least the last decade. As a result these semiconductors are natural candidates for rare earth doping. The high electrical carrier mobility and the

relatively large energy gap makes GaAs attractive for high speed devices. Also the fact that GaAs is a direct-gap material allows for the fabrication of a variety of light-emitting diodes and laser structures. The interest in superlattices and quantum well structures has further increased the importance of GaAs and its alloy, AlGaAs. The importance of InP results from the material's potential for applications in transferred-electron devices. The high mobility of InP is also thought to extend the frequency and power range in FETs; hence, making the material, like GaAs, attractive for various high-speed devices in both the microwave and opto-electronic area. Gallium phosphide is of continued importance as base material for light-emitting diodes. Initially the main impetus for using the III-V and ternary semiconductors lies in their potential for making lanthanide or actinide doped LEDs or laser diodes.

These rare-earth doped semiconductors are also of interest from a fundamental or basic physics point of view, as the interaction between the well screened 4f levels and those of the more covalent semiconductor host is not yet understood. Also the center may act as a shallow or deep level or as a resonant state. In order to extend the understanding of these materials, it is important in the immediate future, to perform studies to determine how the rare-earth ion is incorporated into the semiconductor crystal, determine what the emission characteristics are, as

well as to determine the quantum efficiencies, excitation mechanism, energy transfer, and lifetimes of these transitions which give rise to the 4f-luminescence. In furthering our understanding of these lanthanides it would also be meaningful to investigate the properties of semiconductors doped with actinide ions, specifically uranium (U) or thorium (Th), which are the only effectively non-radioactive elements in the unfilled 5f series. This would be the first time that an actinide doped III-V semiconductor would be investigated.

The proposed program was to investigate III-V Group semiconductors and AlGaAs which were implanted with selected lanthanides and actinides. The basic phenomenon investigated was the use of the semiconductor energy levels to activate the rare-earth element. The spectral region of interest spanned from the visible up to 2.5 μm with emphasis on the region around 1.54 μm as this wavelength is of technological importance since it coincides with the absorption minimum in silica based glass fiber. The investigation techniques were excitation spectroscopy, luminescence decay measurements, and photoluminescence; the latter technique was especially emphasized. The candidate lanthanide ions were ytterbium (Yb), erbium (Er), thulium (Tm), and praseodymium (Pr), and the candidate actinide was essentially uranium (U). The host semiconductors were aluminum gallium arsenide (AlGaAs), gallium arsenide (GaAs), gallium phosphide (GaP), indium phosphide (InP), and aluminum arsenide (AlAs). The rare-earth

ions were introduced into the semiconductor host through high, intermediate, and low energy implantation.

Aside from identifying the specific 4f- or 5f-intracenter transitions, the photoluminescence technique was used to analyze the emission structure as a function of semiconductor substrates of varying conductivity, laser excitation energy, emission or sample temperature, encapsulation, anneal temperature, anneal time, and anneal technique (rapid thermal and conventional furnace annealing). The selected excitation of the different systems with a dye laser was performed in order to understand the excitation mechanism between the semiconductor host and the rare earth ion which leads to the 4f-emissions. Lifetime measurements with a nitrogen-laser pumped dye laser were made to determine if the emissions are basically radiative or more nonradiative, in other words long lifetimes ($\geq 100 \mu s$) or short lifetimes ($< 100 \mu s$).

II. Background and Theory

A. Overview

The idea of rare-earth elements incorporated into the more covalent semiconductors such as GaAs and Si may be traced to a short communication in 1963 by R. L. Bell proposing a dc-pumped rare-earth laser. The idea was to use the recombination radiation of the semiconductor to raise impurity centers in the host to optically excited states which could then be lased. The energy levels of the usual donor and acceptor states are normally too broad but the narrow lines from the rare-earth 4f-shells might be applicable.

At about the same time, three unpublished reports appeared from Department of Defense sponsored research in rare-earth doped Si, GaAs, and InP. In their attempt to further understand and improve the injection laser, G. J. Lasher et al (1963) attempted to produce diodes by diffusing Zn into GaAs:Nd and InP:Tm, Ho, or Dy; however, no fluorescence other than the main band-to-band emissions was observed. In early 1964, C. R. Betz et al reported their findings on producing single silicon crystals doped with rare-earth elements (Gd, Sm, and La) and uranium. Spectroscopic analysis did not reveal appreciable rare-earth doping, and resistivity measurements indicated that only in one case was there appreciable doping; attempts to build diodes understandably also failed. Also in 1964, as part of a RCA-in-house and ARPA-supported electronic material

research effort, D. Richman (1964) investigated Nd doping of GaAs by vapor-transport technique. Faint luminescence emissions from Nd were observed from diodes produced from the rare-earth doped GaAs. As part of a program in doping semiconductors by ion bombardment, Gibbons et al (1965) reported electrical and optical data on Si:Tm, Si:Nd, GaAs:Nd, CdS:Nd, and ZnS:Nd; no 4f photoluminescence was observed for GaAs:Nd, Si:Tm, and Si:Nd.

Perhaps due to competing research efforts in glasses and II-VI semiconductors, or recognition of the difficulty in appreciably doping the materials with rare-earths, few efforts were reported for rare-earth doped III-V or Group IV semiconductors until increased Soviet efforts during 1979-1980. Prior to this time, H. C. Casey et al reported in 1964 on the diffusion and solubility of Tm in single crystal GaAs. In 1968, S. L. Pyshkin et al reported on the temperature dependent Hall measurements of GaP activated with Sm, Gd, or La. Then in 1975 Pyshkin published what appears to be the first report of rare-earth luminescence in a III-V compound by reporting on the luminescence of GaP:N:Sm.

Also during the period prior to 1979, M. I. Aliev et al (1978), reported on the electrical activity of Gd and Yb in GaSb and V. F. Masterov et al (1978) reported on the magnetic susceptibility of GaP crystals doped with rare-earth elements. The work involving lanthanides and actinides in silicon was tabulated in 1980 by J.-W. Chen and A. G.

Milnes, and essentially concentrated on electrical and magnetic measurements involving Gd, Sm, Ho, Nd, Ce, Eu, and the actinide, Th. Some of the limited investigations of rare-earths (Nd, Eu) in germanium (Ge) are referenced by Andrianov et al (1974).

The investigations of Kasatkin et al in 1979 and 1980 were quickly followed by other efforts into rare-earth doped/implanted III-V semiconductors and silicon by investigators both from the USSR and the Federal Republic of Germany (FRG). Of particular note was the achievement of electroluminescence of InP:Yb (Dmitriev et al, 1983) and the papers by H. Ennen et al (1983 and 1983a) reporting strong, sharply structured luminescence of ytterbium in InP, GaP, and GaAs, and erbium in InP, GaP, GaAs, and Si. Numerous papers have appeared since then, also by investigators in Japan (Uwai et al, 1987a; 1987b; 1987c), with efforts culminating recently with the reporting of highly single longitudinal emissions from possibly Er-doped InGaAsP lasers emitting near 1.5 μm (Tsang and Logan, 1986; van der Ziel et al, 1987), and the report of Er-doped GaAs LEDs by Whitney et al (1988) and Rolland et al (1988).

B. Semiconductors, Lanthanides, and Actinides

With the goal of developing novel type of optoelectronic devices, the last few years have seen the investigation of the luminescence of 4f-ions in solids concentrate on the technologically important III-V semiconductors and silicon. Besides the Group IV

semiconductors, Si and Ge, the Group III-V semiconductors are the most intensely studied and best understood of the semiconductors. Properties such as larger bandgap and greater electron mobility, have demonstrated the superiority of the III-V Group over the traditional Group IV semiconductors in such areas as higher device operating temperatures, higher radiative recombination efficiencies, lower power consumption, faster data rates, and benefits that result in tailoring the bandgap and mobility when alloying the III-V's. Specifically the superior characteristics of the III-V's are demonstrated in LEDs, laser-diodes, Gunn diodes, and FETS. The most important III-V semiconductors are GaAs, GaP, and InP, and more recently the alloy AlGaAs. Table 1 tabulates the important Group IV and Group III-V semiconductors and some of their characteristics. The optical and electrical characteristics of these materials are influenced strongly through impurity and defect related energy levels which occupy positions within the bandgap; one may differentiate these further as shallow or deep levels.

The rare-earth or lanthanide ions have all relatively similar chemical and physical properties and their atomic numbers range from 58 to 71 inclusive, commencing with cerium (58) and through lutetium (71). The chemical properties are similar because the outer electron shells are identical in the $5s^2 5p^6$ configuration; the differences in the elements resulting from the filling of the 4f shells. The neutral

Table 1 Properties of Important Group IV and III-V Semiconductors (Sze, 1981).

Semiconductor		Bandgap (eV)		Mobility at 300 K (cm ² /V-s) ^a		Band ^b	Effective Mass ^b <i>m</i> [*] / <i>m</i> ₀		ϵ_s/ϵ_0
		300 K	0 K	Elec.	Holes		Elec.	Holes	
Element	C	5.47	5.48	1800	1200	I	0.2	0.25	5.7
	Ge	0.66	0.74	3900	1900	I	1.64 ^c 0.082 ^d	0.04 ^c 0.28 ^f	16.0
	Si	1.12	1.17	1500	450	I	0.98 ^c 0.19 ^d	0.16 ^c 0.49 ^f	11.9
	Sn		0.082	1400	1200	D			
IV-IV	α -SiC	2.996	3.03	400	50	I	0.60	1.00	10.0
III-V	AlSb	1.58	1.68	200	420	I	0.12	0.98	14.4
	BN	~7.5				I			7.1
	BP	2.0							
	GaN	3.36	3.50	380			0.19	0.60	12.2
	GaSb	0.72	0.81	5000	850	D	0.042	0.40	15.7
	GaAs	1.42	1.52	8500	400	D	0.067	0.082	13.1
	GaP	2.26	2.34	110	75	I	0.82	0.60	11.1
	InSb	0.17	0.23	80000	1250	D	0.0145	0.40	17.7
	InAs	0.36	0.42	33000	460	D	0.023	0.40	14.6
	InP	1.35	1.42	4600	150	D	0.077	0.64	12.4

rare-earth atom electronic configuration is given by the following general expression: $[\text{Xe}]4f^n5d^{(1 \text{ or } 0)}6s^2$ ($n = 0-14, n \neq 2, 8$). The electronic configuration $[\text{Pd}]4f^n5s^25p^6$ may also be used as it is more illustrative in showing the 5s and 5p shielding. The lanthanides share a valence of primarily 3 and have a very strong affinity for oxygen. The 14 elements which constitute the lanthanide series and some pertinent characteristics are given in Table 2 (Sargent-Welch Scientific Company, 1980); two of the actinides are included. The electronic configuration for both the neutral and trivalent lanthanide state is given in Appendix A and for

Table 2 Characteristics of Lanthanides and Selected Actinides

Element	Symbl	Z	at.wt.	ox.states	cryst struc	neutral atom electron conf.
Cerium °	Ce	58	140.12	+3,+4	fcc	[Xe]4f ¹ 5d ¹ 6s ²
Praseodymium	Pr	59	140.91	+3,+4	hex	[Xe]4f ³ 6s ²
Neodymium	Nd	60	144.24	+3	hex	[Xe]4f ⁴ 6s ²
Promethium	Pm*	61	145	+3	hex	[Xe]4f ⁵ 6s ²
Samarium	Sm	62	150.4	+3,+2	rhomb	[Xe]4f ⁶ 6s ²
Europium	Eu	63	151.96	+3,+2	bcc	[Xe]4f ⁷ 6s ²
Gadolinium	Gd	64	157.25	+3	hex	[Xe]4f ⁷ 5d ¹ 6s ²
Terbium	Tb	65	158.93	+3,+4	hex	[Xe]4f ⁹ 6s ²
Dysprosium	Dy	66	162.50	+3	hex	[Xe]4f ¹⁰ 6s ²
Holmium	Ho	67	164.93	+3	hex	[Xe]4f ¹¹ 6s ²
Erbium	Er	68	167.26	+3	hex	[Xe]4f ¹² 6s ²
Thulium	Tm	69	168.93	+3,+2	hex	[Xe]4f ¹³ 6s ²
Ytterbium	Yb	70	173.04	+3,+2	fcc	[Xe]4f ¹⁴ 6s ²
Lutetium	Lu	71	174.97	+3	hex	[Xe]4f ¹⁴ 5d ¹ 6s ²
.....						
Thorium	Th	90	232.04	+4	fcc	[Rn]6d ² 7s ²
Uranium	U	92	238.03	+6,+5,+4,+3	orthr	[Rn]5f ³ 6d ¹ 7s ²

(* synthetically prepared; first oxidation state is most stable)

the actinides in Appendix B. The traditional spectroscopic code is used in assigning the ground state of the ions, i.e. $(2S+1)L_J$.

The shielding of the f-electrons from interaction with the environment is important in determining the spectral characteristics of the rare earths. Instead of the broad absorption or emission bands arising from d-electron transitions, the spectra consist generally of many sharp bands as illustrated in Fig. 2 (Pomrenke et al, 1986). This sharpness being the result of the lack of interaction between the f-levels and the crystal environment. The 5s² and 5p⁶ shells shield the 4f-orbitals from the crystalline or amorphous surroundings such that the spectra is very similar

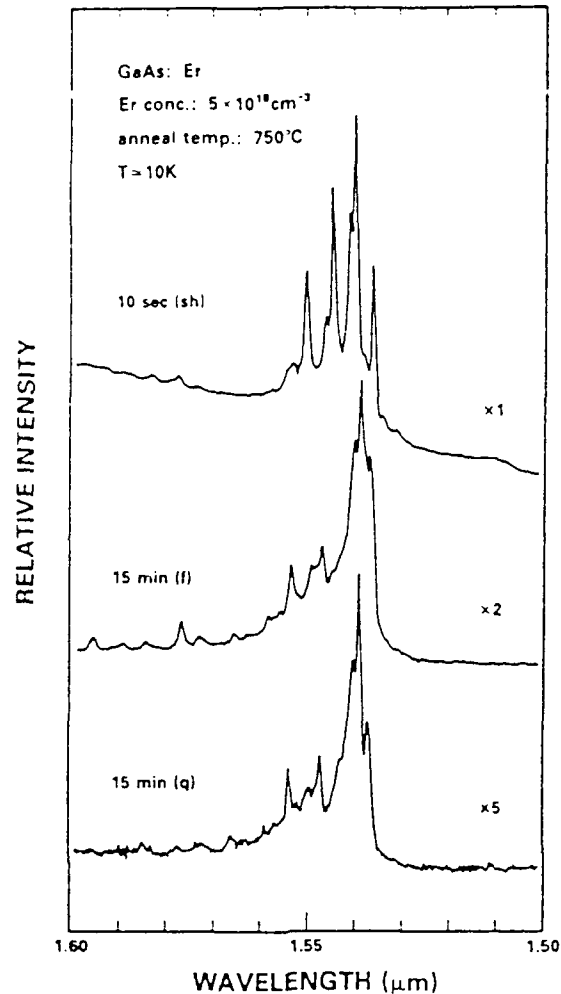


Figure 2. Photoluminescence spectra at 10 K for Er-implanted GaAs and annealed with the strip-heater, conventional, and quartz ampoule method. (Pomrenke et al, 1986)

to that of the free atom. However, the crystalline environment produces strong enough perturbations in the energy structure such that it may be spectrally analyzed. (The wavefunctions of the free ion may be used to describe the energy levels of the 4f-shell under the influence of the crystal field as shall be discussed later). The large number (tens of hundreds) of bands is attributable to the large number of configurations possible within the partially filled

f-subshell.(Sienko and Plane, 1966) Appendices C and D depict the observed energy levels of trivalent lanthanides and actinides, respectively, as tabulated by various researchers.

Even though the coupling of the 4f-electrons to the lattice is weak, the most important parameter is the crystalline electric field. Besides the sharp spectra, another aspect of the screening of the environment is that it weakens the coupling to the vibrational modes of the lattice such that many of the energy levels tend to have long lifetimes. Hence, the important optical properties of the rare-earth ions are due to the fact that they have long-lived fluorescent energy levels and strong narrow fluorescent spectra.(Brown and Shand, 1970) Furthermore, since the symmetry of the crystalline electric field is imposed on the electron spin resonance spectra of the 4f ground state as well as on the optical spectra, it is possible to deduce the environment around a particular rare-earth site in the lattice. Thus in general the rare-earth ion can fill two roles in an experimental study, as a strong fluorescing ion and as a probe for site symmetry. As previously indicated much of this knowledge has been gained through studies of optical properties in which the 4f-ions were incorporated in dominantly ionic host crystals such as oxides and fluorides.

The actinide series consists of the elements with atomic numbers 90 to 103, inclusively, beginning with thorium (90)

and through lawrencium (103). The electron configuration for both the neutral and trivalent state is given in Appendix D. A partial listing of the actinides was given in Table 2. In many respects the electronic structure and chemical properties of the actinide elements are similar to those of the lanthanide series, the 4f, 5d, and 6s subshells of the lanthanides corresponding to the 5f, 6d, and 7s shells of the actinides; however, significant differences exist. The energy levels lie closer together and the nuclei are unstable with respect to alpha emission. Thorium and uranium, although radioactive, have sufficiently long half-lives (1.40×10^{10} years for Th^{232} and 4.47×10^9 years for U^{238}) such that they occur in nature and are therefore the only actinide elements listed in Table 2. The actinides show a variety of oxidation states, for example, uranium forming compounds in the +3,+4,+5, and +6 states. The absorption and emission spectra generally consist of a large number of sharp peaks due to the shielding of the f-electrons; however, the peaks are not as sharp as those arising from 4f-transitions, primarily because the 5f-levels are not as well buried as the 4f-levels. (Sienko and Plane, 1966)

Limited experimental results exist for U^{3+} and U^{4+} incorporated in alkaline earth fluorides. The near-infrared absorption reported for these ions have been assigned to transitions within the $5f^n$ configuration (Brown and Shand, 1970). Most of the investigations of uranium in the solid state are somewhat dated with a great majority of past work

on the spectroscopic properties of uranium compounds tabulated by Dieke and Duncan, 1949.

C. Solids Containing 4f- and 5f- Earth Ions

In considering the incorporation of lanthanide and actinide impurities into semiconductors, one must consider the interaction that takes place between the host crystal and these impurity ions. The characteristic sharp emissions are from electrons in the partially filled inner 4f shell in the rare earths. Different arrangements of the 4f electrons in the available states of the partially filled 4f shell lead to different energy levels for the atom as a whole. This 4f shell is also well shielded against external influences by the electrons which occupy the 5s and 5p shells such that the energy levels caused by the 4f electrons of a specific ion remain relatively unaffected by the host crystal lattice into which the rare earth is placed. Due to the shielding effect the wave function of the free ion may be used to describe the energy levels of the 4f ions in the influence of a crystal field; the crystal field being regarded as a perturbation acting on the free-ion states.

Evaluation of the crystal splitting is carried forth by starting from certain unperturbed eigenfunctions. Three schemes are usually considered based on the strength of the crystal field in comparison to the electrostatic interaction between the electrons; these are the weak field, the medium field, and the strong field. For rare earths and actinides

the weak field scheme is generally used (DiBartolo, 1968; Boyn, 1988) where the crystal field potential is small in comparison with the spin orbit interaction. The Hamiltonian for the 4f ion in a lattice is in general terms given as

$$H = H_0 + H_{ee} + H_{cf} + H_{so}, \quad (1)$$

where H_0 is the Hartree-Fock part of the Hamiltonian, H_{ee} the Coulomb interaction between the electrons not contained in H_0 , H_{cf} the small crystal field potential, and H_{so} the spin-orbit coupling. More specifically, the Hamiltonian is given as

$$H = \sum_{i=1}^n \left\{ \frac{p_i^2}{2m} - \frac{e^2 Z}{r_i} + e^2 \sum_{j>i} \frac{1}{r_{ij}} + eV(r_i, \theta_i, \varphi_i) \right\} + \lambda \bar{L} \cdot \bar{S}, \quad (2)$$

where all the terms have the usual meaning (see Di Bartolo, 1968) with n equal to the number of electrons in the ion. By an expansion into spherical harmonics the perturbing potential is given as

$$V(r_i, \theta_i, \varphi_i) = \sum_{lm} A_{lm} r_i^{-l} Y_l^m(\theta_i, \varphi_i). \quad (3)$$

The free-ion levels, depicted in Appendix C and D, are a result from the splitting of the $4f^n$ configuration due to $H_{ee} + H_{so}$ and are designated by the widely used spectroscopic notation $2S+1L_J$. The free-ion levels are generally then

split into several components by the action of H_{cf} (the 'Stark components').

The Stark splitting is of the order of 100 cm^{-1} , while the energy separation between terms as a result of H_{ee} and H_{so} is at least 1000 cm^{-1} . The crystal-field splittings of the $5f$ levels are approximately twice the value as for rare earths. The number of levels into which a given term of a free ion is split by the crystal field may be determined through the group-theoretical method of Bethe (Bethe, 1929; Smith and Sorokin, 1966). Upon the application of group theory to the crystal field problem, the new levels created by the splitting can each be characterized by symbols, Γ_i , which are irreducible representations of the point group whose symmetry corresponds to that of the site occupied by the rare earth ion. It is essentially the free-ion J value which determines the specific irreducible representation of the point group. The complete quantitative description of the crystal field splitting requires a considerable sophisticated mathematical approach.

In a very general outline one approaches the problem of determining the energy levels by taking the formalism for the perturbing electric field to the sixth term with even terms dropping out. The result goes toward determining the matrix elements of the perturbation by using the free atom wavefunction usually through the Stevens operator equivalent method. As it is sometimes difficult to explicitly develop the crystal field parameters, one makes use of the results of

Lea et al (1962) for systems of cubic symmetry. The results can be diagonalized to determine the eigenvalues of the perturbed system. The ultimate goal is to establish crystal field models, the results of which can be compared to experimental data.

Finally, important considerations in studying the interaction between the lanthanide and the semiconductor are the excitation and de-excitation mechanisms, unfortunately many of these processes are not fully understood. A recent review article on the 4f-luminescence of lanthanides in II-VI semiconductors addresses some of the relevant processes (Boyn, 1988). The three types of schemes in which energy is transferred to the rare earth ion involves (1) the direct excitation of the 4f shell, (2) the excitation of impurity states external to the 4f shell with a nonradiative energy transfer to the 4f shell, and (3) the direct transfer of energy from electron-hole pairs and/or excitons to the 4f shell.

Although Boyn (1988) did not address the de-excitation mechanism in conjunction with the excitation mechanism, it is conjectured that the two processes are probably interrelated to give the characteristic 4f emissions from solids. The de-excitation processes are essentially divided into four groups: (a) intra-ion 4f-4f multiphonon transitions, (b) the energy transfer between the 4f states of two rare earth ions, also known as cross-relaxation, (c) energy transfer to

impurity states outside the 4f shell, and (d) Auger-type relaxation. A possible sequence for exciting the 4f ion might involve the nonradiative energy transfer from the DA states of the semiconductor to a first, second or third excited energy term of the 4f ion with a subsequent intra-ion 4f-4f multiphonon transition resulting in a transition from the first excited state to the ground state (for a proposed model see the conclusion to this document).

D. Investigations of 4f- and 5f- Doped Semiconductors

Overview

Even though research into rare-earth doped III-V and Group IV semiconductors has been relatively recent, a substantial number and a great variety of investigations have been undertaken. Interest in these systems has been in crystal growth along with the calculation of the diffusion and solubility coefficients (Casey et al, 1964). Some of the earliest works included the determination of magnetic susceptibility (Andrianov et al, 1974). Selected neutron (Petrov et al, 1986), electron (Ennen et al, 1983), and gamma irradiation (Kasatkin et al, 1981) experiments have been performed including numerous electron spin resonance (ESR) studies (Kasatkin et al, 1982; Masterov et al, 1983; Zakharenkov et al, 1985; Masterov et al, 1987; Baeumler et al 1987). Photoconductivity work has been done on InP (Berman et al, 1985) and Si (Bagraev et al, 1981) doped with rare-earth elements, and the electrical, galvanomagnetic, and thermomagnetic properties of rare-earth doped GaSb have been

investigated (Safaraliev et al, 1987). What follows is a survey of much of the luminescence (photo- and electro-) and optical studies of these systems including comments about electrical measurements. Ennen (1987) gave a similar overview recently. No cathodoluminescence data has been reported to date.

Luminescence

An important consideration in the study of rare-earth $4f^n$ -ions in solids is the spectral sharpness of the $4f$ -emissions, even at room temperature. This feature is a result of the shielding of the inner $4f$ -shell by the outer $5s^2$ and $5p^6$ orbitals. Emissions usually lie in the visible and infrared spectral region. The high solubility of the $4f$ -ions in insulating hosts led to their investigation as the gain media in externally pumped laser crystals such as YAG:Nd^{3+} and $\text{YAlO}_3:\text{Er}^{3+}$ (Dischler and Ennen, 1986). The possibility for their application in new types of optoelectronic devices led to their increased investigation recently in III-V semiconductors and silicon. Brief summaries on the recent investigations of the trivalent $4f^n$ -ions Yb^{3+} ($4f^{13}$), Er^{3+} ($4f^{11}$), Nd^{3+} ($4f^3$), and Pr^{3+} ($4f^2$) in the III-V semiconductors InP, GaP, and GaAs follow. Further discussions on these systems will be performed in the appropriate sections of the results and discussion to this document.

Ytterbium (Yb) in InP, GaP, and GaAs: First reports in

the open literature of 4f-emissions from Yb^{3+} was for Yb-doped GaP grown by the molten solution technique (Zakharenkov et al, 1981) and InP:Yb grown by the same technique (Kasatkin et al, 1981). These emissions were also reported for Yb-implanted InP, GaP, and GaAs samples after proper annealing (Ennen et al, 1983, Ennen et al, 1985). The growth of Yb-doped InP epitaxial layers by liquid phase epitaxy (LPE) was detailed by Haydl, et al, 1985; while Yb-doped InP by metal organic chemical vapor deposition (MOCVD) was demonstrated by Uwai, et al, 1987b. The observed transitions around 1.0 μm are a result of the internal 4f-4f transitions $^2\text{F}_{5/2} - ^2\text{F}_{7/2}$ of Yb^{3+} (4f^{13}). The fine structure results from the crystal field splitting of the spin-orbit levels. The excited states of the luminescent level in InP:Yb were determined by photoluminescent excitation spectroscopy (Wagner et al, 1984). Zeeman measurements (Aszodi et al, 1985) and optically detected magnetic resonance (ODMR) (Kallenbach et al, 1986) showed that the Yb^{3+} spectrum in InP arises entirely from only one type of cubic Yb^{3+} -center, which most likely is located on a substitutional cation site. Besides this dominant cubic (T_d) center, an Yb^{3+} center with trigonal symmetry was also identified (Ennen et al, 1985).

Erbium (Er) in InP, GaP, and GaAs: A band of sharp emissions around 1.54 μm has been observed in Er-implanted InP, GaP, and GaAs (Ennen et al, 1983, Pomrenke et al, 1986). These are due to the internal transition $^4\text{I}_{13/2} - ^4\text{I}_{15/2}$ of Er^{3+} (4f^{11}). Different annealing conditions result in the

creation of several kinds of Er^{3+} centers presumably due to Er^{3+} -complexes (Pomrenke et al, 1986; see also Fig. 2). This is especially evident in GaAs:Er; since in horizontal Bridgman grown GaAs:Er a luminescence spectrum was recorded with only a limited number of lines and with a spectrum somewhat different from that observed in Er-implanted samples (Ennen and Schneider, 1985). Er-doping during epitaxial growth of LPE (Stapor et al, 1986, Bantien et al, 1987) and MBE material (Smith et al, 1987) results also in quite different emission spectra of Er^{3+} around 1.54 μm . For MBE-grown GaAs:Er layers the structure of the luminescence spectrum depends on the substrate temperature during MBE growth (Ennen et al, 1987). The line-width of the main emission line at 1.542 μm is very small and amounts to 0.5 cm^{-1} (at 6 K). At room temperature the half-width is of the order of 10 cm^{-1} . The analysis of the temperature dependent photoluminescence measurements and photoluminescence excitation measurements (Ennen et al, 1987) indicates that the emissions arise from an Er^{3+} -complex with non-cubic symmetry. Zeeman measurements (Thonke, 1987) have shown that the Er^{3+} -center has C_{1h} symmetry. On the other hand Zeeman measurements on LPE-GaAs:Er reveals that this Er^{3+} -center has cubic symmetry (Bantien et al, 1987).

Neodymium (Nd) in GaP and GaAs: The following sharp emissions have been identified in Nd-implanted GaP, i.e. the intra-center transitions:

${}^4F_{3/2} \text{ --- } {}^4I_{9/2} \quad (\quad 900 \text{ nm })$

${}^4F_{3/2} \text{ --- } {}^4I_{11/2} \quad (\quad 1100 \text{ nm })$

${}^4F_{3/2} \text{ --- } {}^4I_{13/2} \quad (\quad 1400 \text{ nm })$

- Similar emissions have also been investigated in Nd-implanted GaAs. (Mueller et al, 1986) Isothermal and isochronal annealing studies and photoluminescence excitation measurements (Wagner et al, 1986) indicated that the multiplicity of the observed emission lines arises from different Nd^{3+} -centers with non-cubic symmetry.

Praseodymium (Pr) in GaP: A richly structured Pr-related emission spectrum from about 1.2 to 2.3 eV could be detected in Pr-doped GaP grown by molten solution. This intra 4f-shell transition of Pr^{3+} ($4f^2$) could only be observed (at 77K) after heat treatment of the sample (Kasatkin et al, 1981). If Pr was implanted in GaP and co-implanted with Li, different emission spectra were recorded presumably due to an association of Pr with lithium (Gippius et al, 1986).

Thulium (Tm) in GaAs: No 4f-spectra of Tm^{3+} have appeared in the literature; however, Ennen and Schneider mentioned a Tm-related transition at 1.2 μm (1985).

Samarium (Sm), Dysprosium (Dy), and Cerium (Ce) in GaP: The first report of 4f-luminescence in the open literature of a rare-earth element in a III-V semiconductor was by Pysnkin in 1975 for GaP:N:Sm; further data on Sm has not been reported. For Dy and Ce doped GaP only very broad, unstructured peaks have been reported (Kasatkin et al, 1978;

Kasatkin et al, 1979). No 4f-related emissions in III-V semiconductors have been reported for Pm, Eu, Gd, Tl, or Ho.

Actinides in Semiconductors: No luminescence data on actinides in III-V or Group IV semiconductors was found. Most spectroscopy data that is available on uranium may be dated to the Manhattan Project; in 1949 Dieke and Duncan tabulated these results on various uranium compounds. Another tabulation was published in 1964 by Rabinowitch and Belford on the spectroscopy and photochemistry of uranyl compounds. One of the more recent luminescent studies has been the investigations by Rurciman et al (1981) on uranium activated alkali fluorides.

Electroluminescence: Yb-doped InP layers grown by molten solution (Dmitriev et al, 1983) and LPE (Haydl et al, 1985; Koerber et al, 1986) have been used to prepare light emitting devices. It was shown that the internal 4f-4f transitions $^2F_{5/2} \rightarrow ^2F_{7/2}$ of Yb^{3+} at 1.0 μm could be excited electrically in these pn-diodes. Light emitting diodes prepared from MBE-GaAs:Er (Ennen et al, 1987) and MBE-Si:Er (Ennen et al, 1985) show emission spectra around 1.54 μm due to the internal 4f-4f transition $^4I_{13/2} \rightarrow ^4I_{15/2}$ of Er^{3+} ($4f^{11}$). The observed emissions around 1.54 μm are at a wavelength longer than that associated with the bandgap of the host material.

Electrical Measurements

Due to the possible application of rare-earth doped

semiconductors in the area of optoelectronics, it is important that some remarks are made about electrical measurements although this was not pursued in this investigation. One of the key interests in the investigation of rare-earths in semiconductors is whether the rare-earth atoms in the host material create electrically active states in the bandgap or whether they simply alter the electrical properties of the host materials producing neutral complexes through interaction with residual impurities. Most of the published work to date has been on the optical properties of rare-earth doped III-V compound semiconductors, only very limited work has been done on their electrical properties. Therefore, the effect of rare-earth ions on the electrical conduction process is as yet unknown.

The rare-earth ion may occupy one or both of two substitutional sites of the III-V compound semiconductor, or an interstitial site. If the trivalent rare-earth ions occupy cation sites substitutionally, then the trivalent ions become electrically neutral. However, if the divalent rare-earth ions occupy cation sites, then they would be electrically active as acceptors. In the interstitial sites, it is possible that the highly charged trivalent ions may associate with other impurities or defects and contribute to local charge compensation. Thus there are a multitude of variations possible for a rare-earth site based on whether the rare-earth occupies a cation, anion, or interstitial site.

No systematic study has been undertaken on the electrical activity of rare-earth dopants in III-V semiconductors and silicon. The limited recent electrical data that does exist is based on the measurements of Yb doped LPE layers of InP (Haydi et al, 1985), bulk doping of InP with Yb (Lambert et al, 1988) and with several rare-earth species (Zakharenkov et al, 1987), and LPE growth of GaAs:Er (Bantien et al, 1987). These preliminary studies indicate that some rare-earth elements in semiconductors behave as acceptor impurities. However, the majority of the rare-earth elements in III-V compound semiconductors may exist in electrically inactive states due to the tendency to form complexes with residual impurities and host atoms. The conclusion to be drawn, however, is that if such rare-earth doped semiconductors are to be used as injection driven optical emitters, one of the important aspects which must ultimately be understood are the electrical properties.

Results from LPE growth showed that several micrometer thick Yb layers deposited on n^+ InP substrates showed p-type conductivity and a net carrier concentration in the range 10^{16} - 10^{17} cm^{-3} (Haydi et al, 1985). Bantien et al, 1987, determined that the Er doped GaAs samples in LPE are p-type with concentrations ranging from 5×10^{14} to 1×10^{15} cm^{-3} . For Czochralski grown InP, doped with various rare-earths, Zakharenkov et al (1987) claim that no definitive values for the electron/hole density and mobility could be established;

a "purification" mechanism was hypothesized.

It is observed that electrical activity of rare-earth elements in III-V semiconductors can be of different origin (Ennen and Schneider, 1985). It was found by Bagraev et al, 1984, and by Benz and Koerber (Ennen and Schneider, 1985) that upon adding traces of Yb and Gd during LPE-growth of InP the mobility increased significantly. At 77 K mobilities in excess of $60000 \text{ cm}^2\text{V}^{-1}\text{sec}^{-1}$ could be achieved for lightly 4f-doped InP with an electron concentration of about $3 \times 10^{14} \text{ cm}^{-3}$. Without the 4f-dopants the mobilities were of only 1/3 to 1/2 of this value. Similar findings were also reported (Bagrev et al, 1984) for Gd-doping of the ternary compound $\text{In}_{0.53}\text{Ga}_{0.47}\text{As}$; 77 K mobilities in excess of $100,000 \text{ cm}^2\text{V}^{-1}\text{cm}^2\text{s}^{-1}$ were determined. The reason for these mobility enhancements as a result of doping semiconductors with 4f ions is not yet understood. It is proposed that the 4f-elements act as *scavenging agents* for intrinsic shallow donor impurities (Ennen and Schneider, 1985).

Excitation mechanism and lifetime measurements

Upon excitation of the rare-earth doped semiconductor, characteristic 4f-4f luminescence is observed. The rather sharp emission lines arise from the intra 4f-shell transitions. For ytterbium it has been shown that the 4f-4f transitions occur between the spin-orbit levels $^2\text{F}_{5/2}$ and $^2\text{F}_{7/2}$. These are split further by the crystalline electric field. The deconvolution of the rare-earth spectra has

required Zeeman analysis to determine that the spectrum arises from one dominant type of luminescent center on a cubic site (Aszodi et al, 1985, Ennen and Schneider, 1985). Thus, an Yb^{3+} ($4f^{13}$) ion (electrically neutral with respect to In^{3+}) residing on an unperturbed (T_d) indium site appears as the most likely candidate for the center in question, although a line associated with a trigonal center is also present.

From the outset of this research a major question has been over the mechanism which allows the excitation processes and the resulting recombination radiation to raise the impurity centers in the host to optically excited states. A study of the luminescence has revealed a resonant increase of $4f-4f$ luminescence at $h\nu = E_g - 7.5 \text{ meV}$, whereas the donor-acceptor pair recombination became suddenly weaker at that energy. The phenomena has been explained by the excitation of the Yb^{3+} ($4f^{13}$) center as a result of Auger recombination of Mott excitons localized at Yb atoms, with ytterbium f-electrons taking part. (Kasatkin and Savel'ev, 1984; Masterov, 1984, and references therein) Another mechanism involves the creation of "nonequilibrium carriers" which become localized at donor-acceptor pairs. Then an energy transfer occurs to an ytterbium center upon the non-radiative recombination of a donor-acceptor; this transfer raises the Yb center to the excited state $^2F_{5/2}$. (Kasatkin et al, 1985)

Countering the above models, has been the idea that the rare-earth, at least for the case of Yb, acts as an acceptor (Klein, 1987). It has been suggested (Ennen and Schneider, 1985) that for Yb the two weakly-bound 6s electrons are believed to participate in bonding, leaving a filled 4f shell, $4f^{14}$; thus, resulting in the Yb center behaving as an acceptor with a Yb^{2+} core. However, an inconsistency has resulted in that electrical measurements have reported p-type conductivity and EPR (Masterov et al, 1983) and excitation spectroscopy (Wagner et al, 1984) have indicated that the Yb ground state in InP is Yb^{3+} . A partial solution is suggested by Hemstreet (1986) as a result of cluster calculations. The calculations predict that the Yb ground state is a neutral acceptor, with an approximate 0.25 eV binding energy. The bound hole is found to reside partially on the core and partially on the bonds, as a result of hybridization (not found by EPR measurements) of the 4f orbitals with those of the host (Klein, 1987). Further insight into the recombination process was given recently by Klein (Klein, 1987; 1988) as a result of time resolved photoluminescence of Yb in InP.

A detailed investigation of the excitation and decay mechanism of Yb^{3+} in InP has been performed by Koerber and Hangleiter (1988). By examining both time-resolved photoluminescence and photoluminescence excitation spectroscopy, it was revealed that several decay processes are present and free carriers are required during the

excitation of Yb^{3+} in InP. The excited state lifetime of Yb^{3+} was established at 12.5 μs and corroborated by Klein (1988). Recently an excited state lifetime of Er^{3+} in various semiconductor hosts was established to be around 1 millisecond (Klein and Pomrenke, 1988).

E. Investigation Techniques and Physical Processes

Photoluminescence

Photoluminescence was the main investigating technique used in this study. It is a spectroscopic technique that allows the identification of various electronic states in the solid state. Photoluminescence in semiconductors occurs in general as the result of above bandgap excitation, with coherent or incoherent light, of the material and the subsequent recombination of electrons and holes with the simultaneous emission of photons. The recombination process can be in various stages involving both radiative and nonradiative recombinations, the latter resulting in thermal energy being released to the crystal (phonons). The resulting spectra provides information on impurity levels and crystal defects associated with energy levels within the bandgap. The impurities might be as a result of donors and acceptors intentionally or unintentionally added to the crystal. A schematic of selected recombination possibilities is given in Fig. 3. The energy of the emitted radiation in the case of the donor bound electron and acceptor bound hole (D^0A^0 or DA) is given

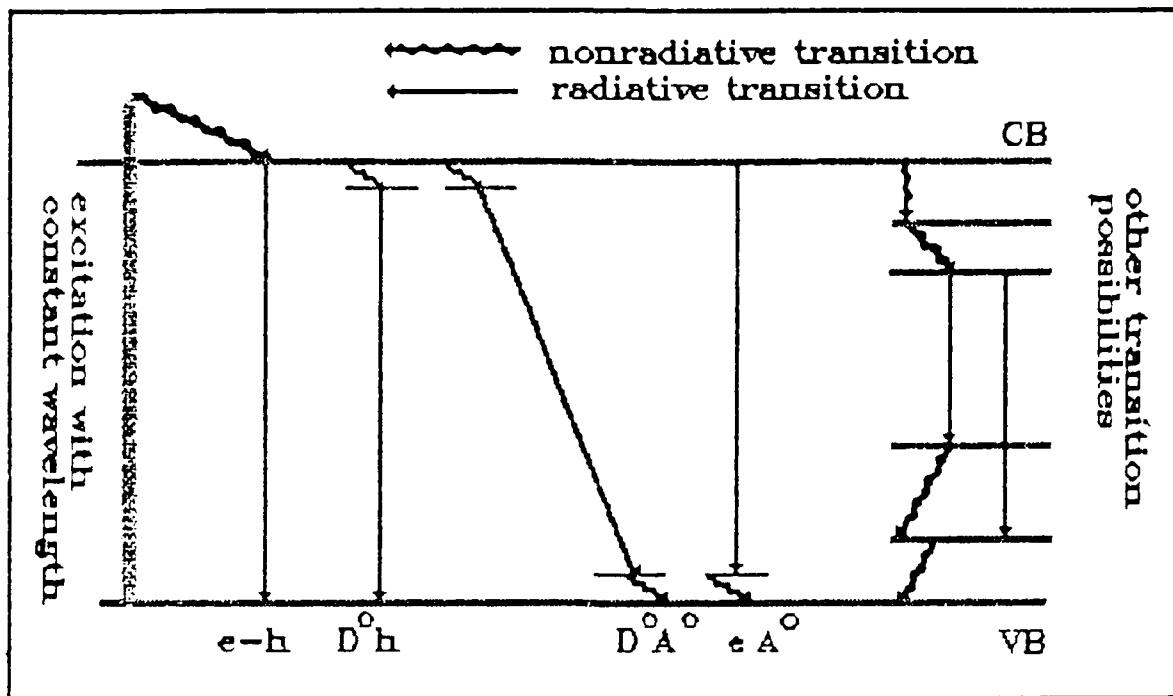


Figure 3. Recombination schemes in photoluminescence. Depicted is the recombination of a free electron and hole (e-h), donor bound electron with free hole (D^0h), donor bound electron and acceptor bound hole (D^0A^0), and free electron and acceptor bound hole, (eA^0).

by

$$E = E_g - (E_A + E_D) - nE_p + e^2/\epsilon r \quad (4)$$

where E_g is the bandgap energy; E_A and E_D are the acceptor and donor binding energies; nE_p represents the change in energy due to the simultaneous emission of $n = 0, 1, 2 \dots$ phonons of energy E_p ; and the last term represents the Coulombic attraction between the hole and the electron located at an acceptor and a donor, respectively, where ϵ is the dielectric constant of the host material, e is the electric charge, and r the donor-acceptor pair separation.

The free electron and acceptor bound hole (eA^0 or eA) recombination emits photons of energy

$$E = E_g - E_A + kT - nE_p \quad \circ \quad (5)$$

where kT is the kinetic or thermal energy of the free electron. Numerous references are available for detailed descriptions of the various possible transitions (Dean, 1982; 1968; and Pankove, 1971).

Photoluminescence is a very sensitive technique and allows for the identification of donors and acceptors in very small concentration; however, it is somewhat limited in giving quantitative results about the concentration of the impurities. Dependent on the exciting wavelength, the technique is also superior to absorption measurements since it allows the probing of very thin layers such as VPE, LPE, MBE, MOCVD, and implanted material. The recombinations of the states from the semiconductor need to be considered as they are involved in the excitation mechanism which results in the 4f emission. The theoretical considerations of the luminescence process can essentially be seen in this case as the interaction of radiation with a physical system; numerous writings exist which address this problem (Di Bartolo, 1968; Smith and Sorokin, 1966).

Excitation Spectroscopy

Purely photoluminescence excitation spectroscopy (PLE) is a combination of absorption and photoluminescence

spectroscopy. As in absorption spectroscopy the crystal of interest is excited by a light source of a specific wavelength. However, it is not a change in the absorption that is observed but the intensity modulation of a desired emission line dependent on the exciting wavelength. If the intensity of the line which is monitored increases, then the exciting wavelength is in resonance with an excited state. In general if one excites with a specific wavelength such a resonant state, one usually only observes in the associated photoluminescence spectrum the transitions which belong to this specific excited state (intracenter excitation). This process allows one to assign both a specific defect state to a level and also determine the splitting of that level. Such information can normally not be gained with photoluminescence. This technique has been useful even in investigating implanted layers (Wagner et al, 1984). The technique has also been used with selective pair luminescence to provide additional verification of acceptor energy levels (Dean, 1982).

The technique is also used in monitoring one specific emission as the sample is continuously excited through specific wavelengths over a particular spectral region. In this study a somewhat modified approach was taken to excitation spectroscopy in that the semiconductor/RE system was excited at particular energies above, across, and below the bandgap with a recording of the associated photoluminescence spectra. This way an excitation spectra

could be plotted through particular data points from the spectra; i.e. the excitation spectra is discrete versus continuous.

Lifetime measurements

The kinetics of the semiconductor-impurity system and the associated recombination processes can be studied by performing time-dependent photoluminescence or luminescence decay measurements. This involves investigating the direct internal excitation, the charge capture, and the subsequent recombination. The most common method of performing such experiments involves monitoring the decay of the sample emission while exciting it with a pulsed or modulated excitation (Demas, 1983). As a result of such measurements models may be proposed which describe the system kinetics after the exciting pulse and also allows for the determination of the magnitude of important system parameters and the main processes occurring during the exciting pulse. Some of these processes may be further examined by performing temperature dependent measurements. A likely response to increase in temperature is the increasing decay rate as well as the decrease in the overall signal intensity due to the increased efficiency of nonradiative transitions. One may also monitor the growth in intensity of one process while monitoring the decay in another process. A change in decay time might indicate that the electron-capture process is slowing down or increasing with temperature. As the

temperature is changed one has to also consider the phonon capture processes. An excellent example of a time-dependent luminescent experiment of a semiconductor-impurity (InP:Fe) system, including proposed models and rate equations, has been given by Klein, Furneaux, and Henry (1984).

Due to the bandgap of the III-V semiconductors most of the rare earth emissions in these materials are in the infrared spectral region, similar to 3d transition elements incorporated into semiconductors (Guillot et al, 1984). Hence, just as for these transition elements it appears that it will be difficult to determine the excited state lifetimes of the RE^{3+} mainly due to a lack of very sensitive and fast infrared detectors. Nevertheless, certain systems may be examined with the S-1 PMT, fast Ge detector, InSb detector, and to a limited extend modified PbS detectors. The decay time measurement, especially at very low temperature, can determine the electronic lifetime t_R of the excited state which is related to the matrix element for electric-dipole transitions by

$$t_R^{-1} \approx | \langle f | \underline{r} | i \rangle |^2, \quad (6)$$

where $|f\rangle$ and $|i\rangle$ are the final and initial states of the ion, respectively, and \underline{r} is the position operator (Guillot et al, 1984). The solution to the lifetime depending on the number of levels in the system.

For the rare-earth/semiconductor an appropriate first order system to examine would be a three-level system (Di

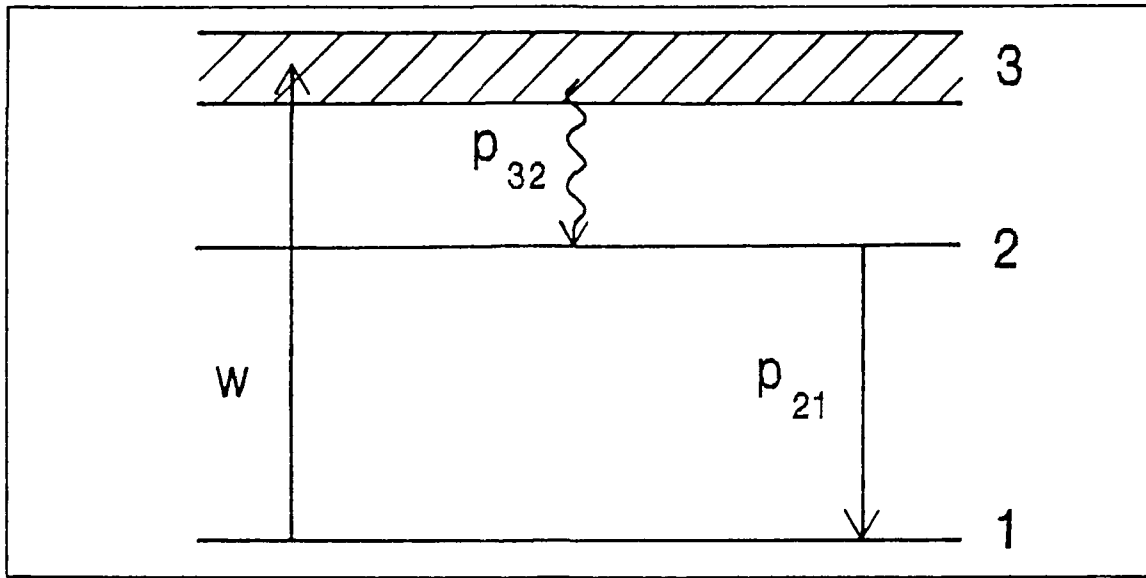


Figure 4. Three-level system with one luminescent level and a rapid decay process between level 3 and level 2.

Bartolo, 1968), depicted in Fig. 4, under pulsed excitation with one fluorescing level between level 2 and 1, and a rapid decay process between level 3 and 2. The quick process might represent the non-radiative energy transfer between the semiconductor host states and the internal rare earth states. The equations of the level populations are given by

$$N_3/dt = - (p_{31} + p_{32}) N_3 + w(t) (N_1 - N_3) \quad (7)$$

$$N_2/dt = p_{32}N_3 - p_{21}N_2 \quad (8)$$

$$N_1 + N_2 + N_3 = N_0 \quad (9)$$

with $N_2(0) = N_3(0) = 0$, N_0 is the total number of atoms in the system, N_i the number of atoms in the i -th state, the transition probability per unit time from level j to level i

is p_{ji} , and the probability per unit time that an ion undergoes a transition from the ground state to the broad band 3 is given by $w(t)$. Considering only the case where the decay time is long compared to the exciting pulse, $t > f$, the above governing equations become

$$dN_3/dt = -p_3 N_3 \quad (10)$$

$$dN_2/dt = p_{32} N_3 - p_{21} N_2 \quad (11)$$

where $p_3 = p_{31} + p_{32}$. The solutions of equations 10 and 11 are given by

$$N_3(t) = N_3(f) e^{-p_3 (t-f)} \quad (12)$$

$$N_2(t) = [N_2(f) + \frac{p_{32}}{p_3 - p_{12}} N_3(f)] e^{-p_{12} (t-f)} - \frac{p_{32} N_3(f)}{p_3 - p_{21}} e^{-p_3 (t-f)} \quad (13)$$

where $N_2(f)$ and $N_3(f)$ are solutions for the case $t < f$ which is considered elsewhere (Di Bartolo, 1968, pp 437-439). The luminescence or fluorescence of the three-level system follows the behavior for the $N_2(t)$ curve. After the end of the exciting pulse, this $N_2(t)$ curve consists of the two exponentials shown in equation 13. The decay behavior is such that in one case, pure exponential decay ($p_3 \gg p_{21}$) is shown with the decay time equal to p_{21}^{-1} . In the case of

fluorescence-rise, the decay behavior is such that if the exciting pulse is short enough, a maximum can occur for $N_2(t)$ some long time t_{\max} after the end of the pulse. In the final case if the behavior shows a double decay, it is evidence that level 2 is also pumped directly from some broad band above level 3 or from some other ion which transfers its exciting energy to the luminescing ion (Di Bartolo, 1968). The case considered in this investigation is essentially the single exponential decay and serves as in the majority of lifetime measurements as a good first-order or pseudo-first-order model for the kinetic process.

An interesting observation is that transition metal ions incorporated into solids emit luminescence from one excited level and upon pulsed excitation the many transitions from this level all exhibit the same decay rate; hence, the emissions are associated with the same center. Luminescence transitions from different centers will most likely have different decay rates; hence, decay measurements may be used to distinguish between different luminescence centers (Imbush, 1978). It should be possible to apply this observation to the case of the rare earths.

F. Ion Implantation and Annealing

The interaction of accelerated charged particles with solids has attracted considerable interest over the past two decades as ion implantation became a useful tool in producing microelectronic devices. Implantation offers such advantages

as the control over depth distribution of the implanted ion, control over the ion concentration, uniformity, reproducibility, lower annealing temperatures and different annealing techniques, a wide choice of dopants, control over lateral spreading, selective area implantation through masking, high yield at low cost, and the availability of numerous commercial implantation services. All the above reasons have made ion implantation a desired method of doping solids, specifically semiconductors. The impurity is initially ionized through various techniques and is then accelerated through a high potential. The various species in the beam are then separated by a magnetic field, and the desired ions are then directed to the target material through various beam-line optics.

The distribution of the ion in the solid is controlled through the mass of the implant ion, the potential field, and the implant time. The stopping of the ion is essentially through inelastic collisions with bound electrons, elastic scattering on the target atoms, and to a negligible extend inelastic scattering on the target atom (i.e. nuclear reactions). One can see that the complete understanding of the implant process requires an in-depth study of the energy loss mechanisms which control this distribution and the resulting radiation damage; therefore, for most practical applications, range-energy tables from the theory of Lindhard, Scharff, and Schiott (LSS) are utilized (Gibbons et al, 1975; Townsend, 1976). The tables essentially give

information on the total range (R) the impurity travels through the target in the form of the projected range (R_p) which is the projection of this distance, R, onto the direction of incidence. The theory addresses the differential energy losses through the following equation

$$- dE/dx = N [S_n(E) + S_e(E)] \quad (14)$$

where S_n and S_e are the nuclear and electronic stopping power, respectively, and N, the atomic density of the target. If S_e and S_n are known then the range, R, can be calculated through the integration of the above relation

$$R = \int_0^R dx = \frac{1}{N} \int_0^{E_0} \frac{dE}{[S_n(E) + S_e(E)]} \quad (15)$$

where E_0 is the implantation energy. As the stopping of the implanted ion is a statistical process, a straggling (ΔR_p) also needs to be determined; this has also been calculated by LSS theory and is available in tables. The impurity depth distribution developed from this theory can then be described by a Gaussian function

$$N(x_p) = \frac{\Phi}{\Delta R_p \sqrt{2\pi}} \exp \left(- \frac{(x_p - R_p)^2}{2 \Delta R_p^2} \right), \quad (16)$$

where Φ is the ion dose and x_p is a measured distance along the direction of the incident ion beam. The original LSS theory (1963) gave a set of formulae, graphs, and tables from which

the implant statistics could be determined. Over the years various sources have appeared which have improved and extended this original work, one relatively recent work being a set of implantation tables by Burenkov et al, 1986.

The implantation statistics used in this investigation were determined from source codes recently developed by either commercial vendors or through research organizations. One such code is the TRIM-88 computer programs developed by Ziegler, Biersack, and Littmark (IBM), 1985, to calculate the penetration of energetic ions into solids through Monte Carlo simulation techniques. The code and the associated text attempted to unify many of the past theoretical concepts and developments (including LSS) with existing experimental data; resulting in a sophisticated use of interpolation formulae to calculate the final distribution of the ions and also all kinetic phenomena associated with the ion's energy loss. A commercial software program from Implant Sciences (IS), which was also used, is basically developed from the Ziegler, Biersack, and Littmark transport theory. Numerous TRIM and IS source code runs were performed to produce Table 3 which lists the projected range and straggling for lanthanides and actinides implanted at various energies into semiconductors. This tabulation compiles all the implant statistics needed and used in this study. It should be mentioned that these statistics were not available from other sources such as tables or figures.

Table 3. Calculated Projected Ranges and Stragglings for Lanthanides and Actinides Implanted into Selected Semiconductors.

Implanted Ion	Target Material	Energy (keV)	Rp (Ångstrom)	ΔRp °
Er ¹⁶⁶	Al _{0.3} Ga _{0.7} As	1000	1847	638
Er		3000	5505	1326
		1000	1862	658
		350	716	230
		150	366	126
Er	GaP	1000	2157	634
Er	InP	1000	2172	739
Ho ¹⁶⁵	GaAs	1000	1947	679
		150	371	128
		100	258	98
Ho	GaP	1000	2247	674
Ho		500	1001	320
		400	825	271
		150	378	138
	InP	100	282	107
Ho		1000	2162	719
Ho		1000	3013	704
	Si	100	469	107
Pr ¹⁴¹	AlAs	1000	2971	908
Pr	GaAs	1000	2410	895
		380	957	387
Pr		1000	2718	861
	InP	380	1071	389
Pr		1000	2622	956
		380	1056	452
Pr	Si	1000	3748	918
Tm ¹⁶⁹	GaAs	390	781	248
Tm	GaP	390	894	244
Tm	InP	390	899	310
Tm	Si	390	1234	235
Th ²³²	GaAs	150	310	101
Th	Ge	150	340	111
Th	Si	150	584	115

Table 3 (continued)

U ²³⁸	GaAs	131	322	111
		139	345	115
		140	339	118
U	GaP	131	375	105
		139	381	111
U	InP	131	366	138
		139	403	146
U	Ge	140	323	105
U	Si	140	558	110
Yb ¹⁷³	AlAs	1000	2400	743
Yb	Al _{0.23} Ga _{0.77} As	1000	1846	498
Yb	GaAs	1000	1831	574
Yb	GaP	1000	2102	579
Yb	InP	1000	2086	684
		350	815	281
		140	454	163
		1000	2922	674
Yb	Si	350	1120	214

Finally, through the implantation process, damage occurs in the target substrate. In this study these are crystalline defects such as point defects (interstitials and vacancies), clusters of point defects, dislocations, and possibly dislocation loops. To remove the defects and to optically or electrically activate the implanted impurity, the implanted host is annealed. During this process the samples are heated to high temperatures through various techniques (e.g. conventional and rapid thermal annealing) so that the damaged layer may reorder itself and aid the impurity in moving into its proper sites. Due to volatile components of some compound semiconductors which may result in out-diffusion or surface decomposition, the implanted layers are sometimes encapsulated with various thin films (e.g. Si_3N_4 , SiO_2).

G. Secondary Ion Mass Spectrometry (SIMS)

A method which has shown a considerable success in material characterization is the surface analytical technique known as Secondary Ion Mass Spectrometry (SIMS); it has received considerable attention for more than a decade (McHugh, 1975; Katz and Newman, 1987; Wittmaack, 1982). The use of this technique in this study has been its application in profiling (Gauneau et al, 1982) implanted ions in material. The SIMS technique uses a focused ion beam to erode atoms from a specific sample region. A small percentage (a typical value of 1%) of the sputtered atoms undergo a charge exchange which results in their conversion to positive or negative secondary ions. However, it has been determined that the choice of the primary ions (the beam) has a considerable effect on the ionization efficiency and the uniformity of the secondary ion yield. A beam of positive O_2^+ ions (used in this study) is typically used for atoms with a low ionization energy and a cesium beam is used for those of high ionization energy. The secondary ions are removed by an electric field and passed into a mass analyzer. The technique has been shown to be able to detect ppm - ppb in the elemental range from hydrogen to uranium. The secondary ion signal (counts) of a specific element can be monitored as a function of time, resulting in a depth profile of the element. A depth profiling instrument may be used to measure the crater depth generated by the primary beam which allows the calculation of a constant sputtering rate. The depth

profile can then be converted from a time scale to an actual depth scale.

The SIMS data of the ion count can be calibrated in terms of concentration by integrating the area under the unannealed profile and setting it equal to the implanted dosage. This signal count (I) per unit time (Δt) is assumed to be proportional to the integral of the concentration over the sputtered depth

$$I / \Delta t \propto \int_A^B n(z) dz \quad (17)$$

where A and B represent the beginning and end of a specific sputtered layer and $n(z)$ is the concentration as a function of depth. Upon sputtering from the surface of the sample to some depth, Z, aside from a proportionality factor C, the relation may be written as follows:

$$C \sum_{\text{time}} \frac{I}{\Delta t} = \int_0^Z n(z) dz \quad (18)$$

$$C I_T = \int_0^Z n(z) dz \quad (19)$$

where I_T is the total count. For cases in which the implanted layer is relatively shallow and the sputtering is effectively past the implant region, the right hand side of the above equation is essentially the implant dosage, Φ ;

hence, the unknown proportionality factor, C, can be determined

$$C = \frac{\Phi}{I_T} \quad (20)$$

A constant depth sputtering rate can be calculated by dividing the measured crater depth, d, by the total sputtering time, T. Hence for a small subregion of the implant zone in which the concentration would vary little, one has the following approximation

$$\int_A^B n(z) dz \approx n(P) d/T \quad (21)$$

The concentration at some depth, B, can be determined by

$$n(B) = \frac{C}{d/T} \frac{I_B}{\Delta t} \quad (22)$$

where I_B are the counts at depth, B. Through iterative calculations the SIMS signal can be displayed as a profile which is a function of depth. Specific values for this study are given in the experimental section including a description of the equipment and procedures. SIMS investigations on rare earth or actinide implanted semiconductors have been essentially limited to two studies, one on Yb doped InP (Uwai et al, 1987b) and the other on 400 keV implanted Er in InP (Favennec et al, 1987).

III. Experiment

A. Overview

The investigations which were undertaken involved three experiments: photoluminescence, selective excitation luminescence, and lifetime measurements. The investigation also required the processing of a variety of samples which included cleaning, implanting, and annealing. A limited number of electrical measurements (by external agencies) and SIMS measurements were also performed. What follows are the details in conducting the study. Initially the experimental setups and procedures will be discussed followed by details on the sample properties and sample preparation, processing, and analysis.

Each of the three experiments consisted of a complete separate experimental setup located within the AFIT School of Engineering (Department of Engineering Physics). Time-dependent luminescence was used to make lifetime measurements on the rare earth emissions and the key elements included a boxcar averager and appropriate infrared detectors. The excitation luminescence used particular wavelengths of an Ar-ion laser pumped dye laser to excite the rare earth doped semiconductor above, at, and below the bandgap. The heart of the investigation was the low temperature photoluminescence setup which was used not only for specific luminescence studies but also to screen the samples for the other two experiments; it shall be discussed first.

B. Photoluminescence

A schematic of the luminescence setup is depicted in Fig. 5 and essentially includes an excitation source, sample chamber, and detector plus its associated electronics and data acquisition elements. The samples were contained in the innermost chamber of the cryostat and were excited by the light of one of three different lasers. The emitted luminescence was filtered and collected by a system of lenses; and if required the signal was modulated. After passing through the spectrometer the dispersed signal was detected by one of a series of detectors. These different detectors plus associated electronics and data taking (demarcated by the dashed box in Fig. 5 as 'acquisition subsystem') will be discussed separately.

Cryogenics and Evacuation

A Janis Research Company Model 10DT Super Varitemp cryostat served as the sample chamber; a schematic of which is depicted in Fig. 6. The dewar consisted of a stainless steel, cylindrical body housing an outer 8 liter reservoir filled with liquid nitrogen, LN_2 , and an inner 5 liter reservoir filled with liquid helium (LHe). The amount of LHe retained in the reservoir was sensed by an American Magnetics Inc. liquid helium level meter, Model 110A. Each of the reservoirs is surrounded by a vacuum jacket which needs to be evacuated before cooling the system down. A tail assembly with three sets of Suprasil quartz windows extended below the body and formed the lower section of the gas exchange column.

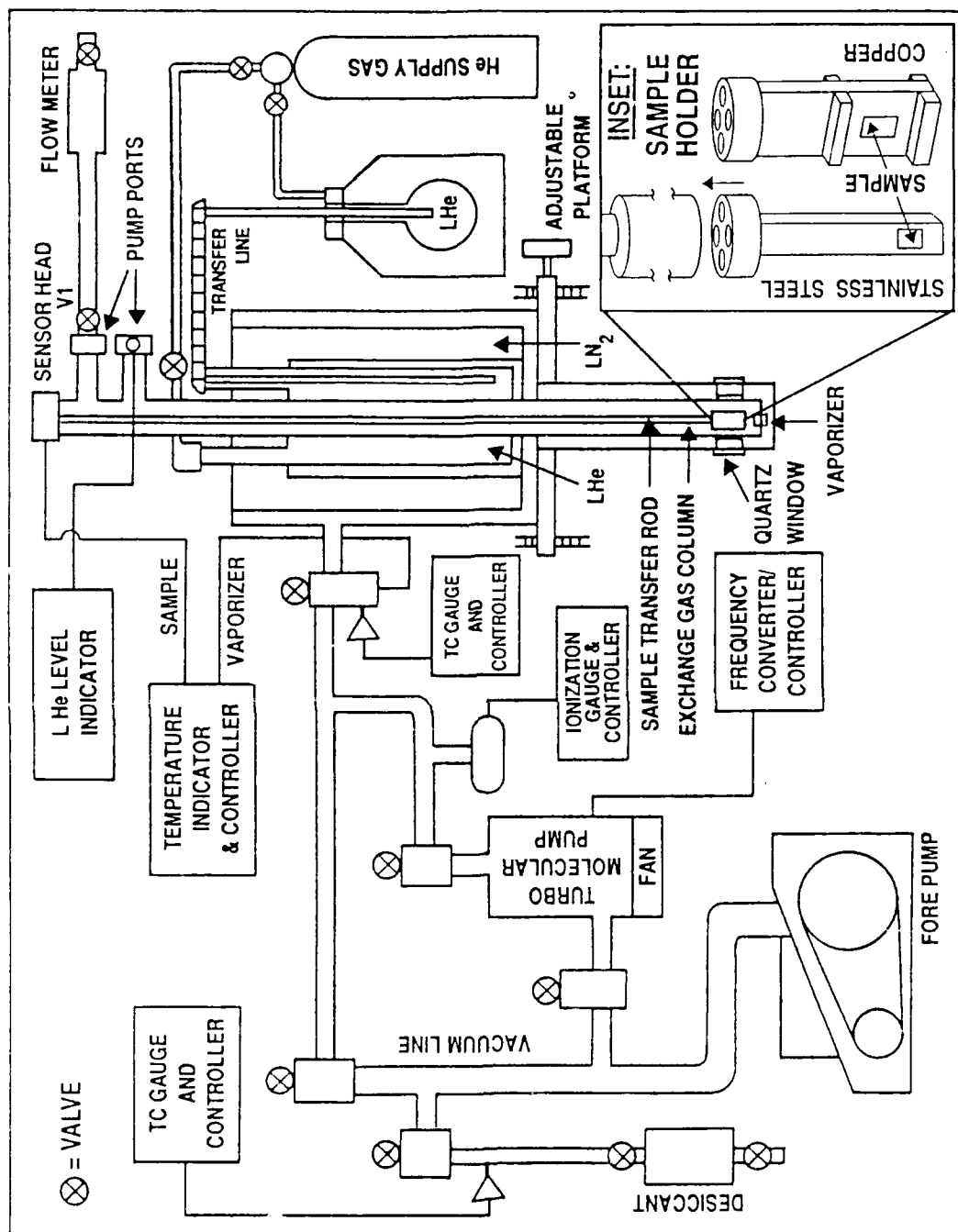


Figure 6. Schematic of the evacuation and cryogenic subsystem.

This column ran along the central axis of the system and housed the sample transfer rod. The cryostat's temperature could be varied from 4.2 K to room temperature and was not configured for lambda pumping. The liquid helium flowed into the column to cool the sample via a capillary tube by means of gravity-feed or back pressure. This flow was controlled by the valve operator, flowmeter, and/or flow valves (V1 in Fig. 6).

The approximately 5 mm X 5 mm samples were mounted on either the stainless steel or copper sample holder (see inset to Fig. 6) with standard rubber cement (silver paste mixed with vacuum grease was also used on a few occasions). As the cryostat works on the principle of cooling by flowing helium vapor, the quality of thermal conductivity between the sample and holder was not critical. The sample holder was attached with four screws to the copper cylinder at the end of the sample transfer rod. The copper cylinder contained one of the temperature sensors and above it was a 50 ohm wound wire heater. A second sensor and heater were located in the vaporizer assembly. The sensors from Lake Shore Cryotronics were silicon diodes, one calibrated (SN: D67352, Model: DT-470-CU-13) and one matched. Control and display of temperature and heater power was performed by a Lake Shore Cryotronics DRC 82C Temperature Controller.

Before the samples were inserted into the gas exchange column the column was flushed with helium gas for at least

10 minutes. Before cryogenics were added to the cryostat it needed to be evacuated using the setup shown in Fig. 6. This evacuation system which was built during the spring of 1988 allowed faster pump down time and easy access to the controls and valves. The forepump, a Sargent-Welch Model 1397, with a speed of 425 liter/min, evacuated the system down to a pressure of 20-30 microns (0.2 - 0.3 torr). The pressure was brought down further to 3×10^{-4} torr upon operating the air-cooled Leybold-Heraeus TMP/NT-150/360 turbomolecular (TM) pump and frequency converter; the Turbovac 360 TM pump had a specified throughput of 345 liter/sec. Hastings thermocouple (TC) type vacuum gauges with DV-6 and DV-5M gauge tubes monitored the pressure at points depicted in Fig. 6 while a CHA Industries IG100P ionization gauge monitored the pressure between the TM pump and cryostat. Liquid nitrogen was supplied to the outer reservoir upon reaching approximately 2 microns; the cryopumping from the LN₂ brought the pressure down to 4×10^{-5} torr. Upon transferring LHe from a supply dewar to the inner cryostat reservoir via a transfer line, the cryostat was isolated from the vacuum line and the evacuation system was shut off and brought to atmospheric pressure via the desiccant valves. As long as cryogenic fluids were in the cryostat no further evacuation was needed.

Excitation and Optics

After the samples reached the desired temperature, which was usually 6 - 8 K, they were optically excited with a Spectra Physics series Krypton-ion laser (Model 2020-11), a

Spectra-Physics air cooled argon-ion laser (Model 162A-07), or an Ion Laser Technology (ILT) Model 5490AWC air-cooled Ar-ion laser. The argon-ion lasers were necessary to excite the GaP semiconductors at above bandgap. The Ion Laser Technology laser was operated at a wavelength of 514.5 nm, typically at a power of 50 mW (65 mW maximum), while the Spectra Physics laser was operated with 15 mW also at 514.5 nm. The Kr-ion laser was typically operated at power settings of 50, 100, and 200 mW at the laser and at a wavelength of 647.1 nm (30 mW at 476.5 nm). The excitation of the many different semiconductor hosts required that the broad band mirror and output coupler to the laser cavity be changed to access the many other Kr laser lines (up to seven) as specified by the manufacturer. Unfortunately the limited output power at all but the 647.1 nm line prevented the laser from being a flexible and adaptable diagnostic tool. Under the most optimum achievable conditions none of the lines, besides the 647.1 nm line, ever achieved more than 50% of the manufacturer specified power output. To slow the rate of degradation of laser optics a laminar flow unit (Spectra Physics Model 2200) was installed. Furthermore, to insure continuous operation a heat exchanger and water pump were rebuilt to provide back-up for the Spectra Physics Model 314 water conditioner. The water conditioner is a closed cycle and self-filtering system which cools the laser tube.

As depicted in Fig. 5, to properly filter the excitation

source, the laser beam passed through an adjustable aperture stop of usually 3 to 4 mm in diameter and an infrared absorbing filter. This was followed by a narrowband or interference filter (typically 1.0 nm wide and 50% transmissive) depending on which excitation energy was used (i.e. 530.9, 514.5, 647.1 nm, etc.). The beam was then reflected from two mirrors of a periscope mirror (Kr laser lines) or one flat mirror (Ar laser lines) before being brought through the two 90% transmissive Suprasil quartz windows and onto the sample. Upon passing through the various optics, the 647.1 nm Kr line with a power of 200 mW at the laser drops to 52 mW at the sample; using a minimum 1.4 mm beam diameter (at $1/e^2$ points), this translates into an irradiance of 3.4 W/cm^2 . A typical irradiance value for the ILT 514.5 nm Ar line with 18 mW power at the sample was 4.7 W/cm^2 (0.7 mm beam diameter was used for both Ar-ion lasers). The irradiance values represent the maximum value attainable, without focusing, for the given beam diameter; actual beam size at sample is slightly larger. The laser beam was reflected from the sample at such an angle as to keep the beam within the cryostat.

The luminescence is collected by two lenses and filtered by a 90% transmissive long pass filter before passing into the spectrometer. Within the bounds of available equipment it was attempted to match the f-number of the collecting optics to the f-number of the spectrometer ($f/6.8$); however, the final design was chosen on the basis that the grating was

fully filled. The collimating lens had a focal length of 104 mm ($f/1.4$) and the focusing lens a focal length of 250 mm ($f/5$). The 76 mm diameter aperture between the lenses was mainly used to stop down scattered and reflected light from the sample chamber. A filter holder, to be attached to the spectrometer, was built to hold the 50 mm X 50 mm long-pass filters placed at the entrance window to reduce stray light, reflected laser light, or any above bandgap radiation that might be present.

A Spex 1702 3/4-m Czerny-Turner spectrometer was used to disperse the luminescence signal (linear dispersion was 1.1 nm/mm). Due to the wide spectral range covered in the investigation, three gratings were used: one with 1200 grooves/mm and blazed at 500 nm and used over the 500 to 1200 nm spectral range; one with 1000 gr/mm and blazed at 1000 nm and used from 800 to 1400 nm; and the most frequently used grating was one with 600 gr/mm and blazed at 1.6 μm operating in second order from 800 to 2000 nm. Due to signal-to-noise and the nature of the investigation most of the spectra were taken at relatively low resolution. Typically an entrance slit of 1000 μm and an exit slit of 2000 μm was chosen; however, higher resolution settings such as 100/200 μm (entrance/exit) slits were also used when applicable. Upon using the 600 gr/mm grating and 1000/2000 μm slits, the resolution at 1540 nm was found to be 3.4 meV (full width at half maximum, fwhm), with 200/400 μm slits it was found to

be 0.5 meV. Upon using the 1200 gr/mm grating blazed at 1.0 μm and using 1000/2000 μm slits, a resolution of 1.4 meV was achieved for a 1240 nm rare-earth emission, with 100/200 μm slits a resolution of 0.15 meV was observed. The above resolution results are from measurements on the sharp rare-earth emissions; better values are somewhat limited by the signal-to-noise ratio. The 500 nm blazed grating gave a resolution of 3.8 meV and 0.9 meV for slit settings of 2000/2000 μm and 300/300 μm , respectively, when using the 866.79 nm line from an Argon calibration lamp. The entrance slit height was either 10 mm or fully open to 50 mm, as was the case for the exit slit. The spectrometer scan rate was externally controlled by a stepper motor driver for which the settings were adjusted to cover a 569 nm or 142 nm range in approximately 13 minutes for the 600 gr/mm grating. This resulted in the recording of 4096 data points, only a small portion of which was used in the final analysis for most cases.

Ideally one would like to correct all spectra for system response by determining a correction function based on transmission losses, grating response, and detector response to a blackbody. However, since the investigation covered such a broad spectral region, employed up to eight different detectors, three different gratings, and a variety of filters, mirrors, and lenses; it would have made these corrections extremely time consuming and in the end not very enlightening or productive. In most cases the investigation

concentrated on making comparison studies over a relatively small wavelength region. The relatively sharp line spectra of the rare earths would not have been changed significantly in energy upon making such corrections.

The investigation did however attempt to minimize some transmission losses. The efficiency curve or response curve for the 1.6 μm blazed grating displayed a significant change in the response at 1230 nm such that it was considered a problem in the investigation of Tm^{3+} ; the 1.0 μm blazed grating was acquired to circumvent this problem and it was used for the 1100 - 1400 nm spectral region toward the latter part of the study. Atmospheric absorption interferes at various wavelengths at which rare earth emissions are seen or are expected to be seen. Figure 7 is presented to bring attention to these absorption bands (Wolfe and Zissis, 1978). To partially minimize this problem a liquid nitrogen dewar was attached to the spectrometer (see Fig. 5) such that the spectrometer could remain flushed with evaporating nitrogen gas; hence, reducing the amount of absorption at particular wavelengths. The transmission curve for the crown glass lenses was relatively flat from 400 to 1900 nm as can be referenced in any optics catalog of a lens manufacturer or supplier. The Suprasil dewar windows appear to have a 5 - 10% drop in transmission around 1.4 μm . The reflectance curve for the spectrometer and detector housing mirrors were

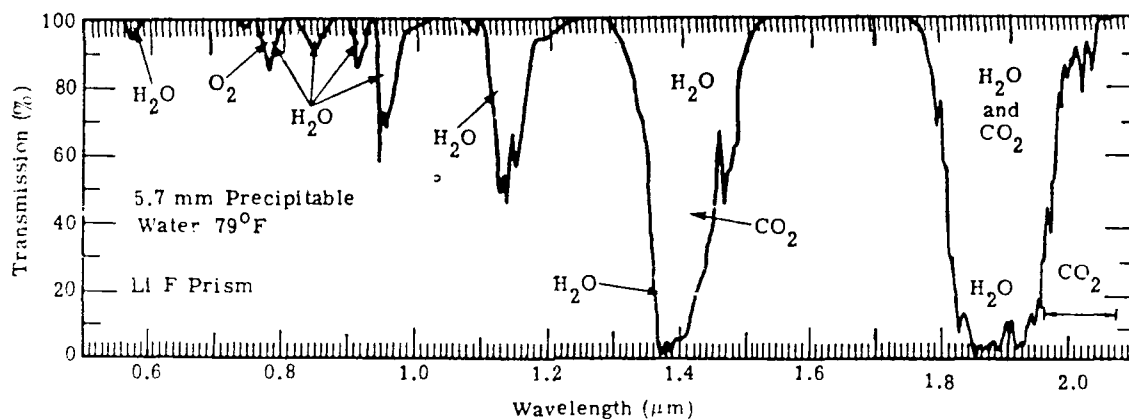


Figure 7. Atmospheric transmission at sea level over a 300 meter path. (after Wolfe and Zissis, 1978)

considered flat from 400 to 1900 nm as standard silica coated aluminum mirrors was assumed. A system response curve was generated using a standard Sylvania tungsten lamp (EKP/ENA, 80 W, 30 V, 28 HR) as an approximately 2850 K blackbody radiator or perhaps more correctly, as a greybody; it is depicted in Fig. 3. The configuration which produced the spectra consisted of the light from the tungsten lamp passing through the spectrometer loaded with the 1.6 μm blazed grating and then to a PBS detector. Slit settings were 100 μm and the spectrometer was purged with nitrogen gas. The change in intensity at 1227 nm is due to the grating response while the structure between 1347 and 1393 nm is due to atmospheric absorption.

Signal Detection and Processing

The entire spectral range covered in this investigation was detected by eight detectors were used. FIA

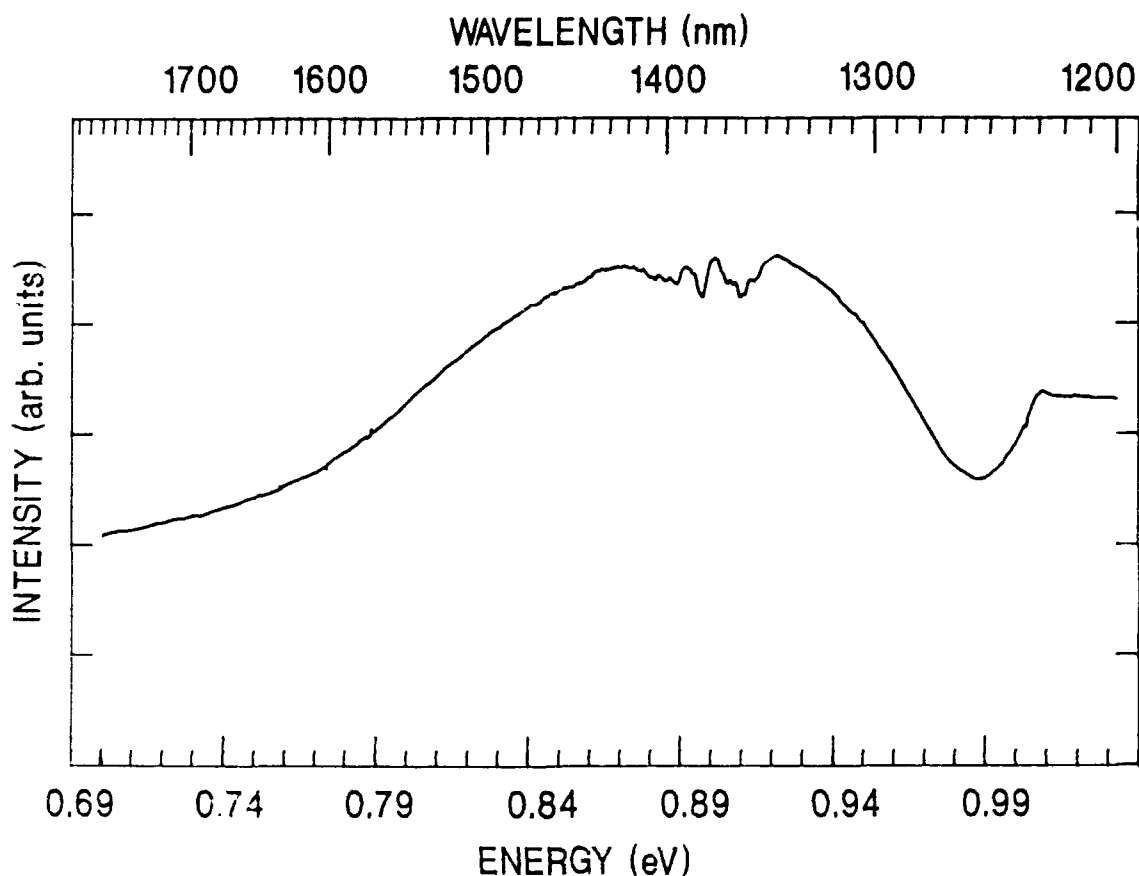


Figure 8. System response spectra.

7265 photomultiplier tube (PMT), EMI GENCOM 9808B PMT, Applied Detector Corporation Model 403L germanium photodetector, New England Photoconductor (NEP) dewar cooled lead sulfide (PbS) detector, Santa Barbara Research Corporation (SBRC) Type LTO PbS detector, thermo-electrically cooled Infrared Industries Model 2767 PbS detector, Judson J10D Series InSb detector, and a SBRC Model 40742 HgCdTe (PV) detector. Upon comparing detector sensitivity and detectivity the investigation relied almost entirely on the EMI GENCOM PMT, the germanium detector, and the NEP PbS

detector. These detection systems were generically depicted in Fig. 5 by the dashed box; the discussion of each of the three detectors plus electronics and data acquisition shall follow.

The detection electronics for the EMI 9808B PMT operated in a photon counting mode as illustrated in Fig. 9. This mode consisted of four elements including the photomultiplier tube, associated PMT housing, an amplifier-discriminator, and a photon counter. The PMT is a 46 mm diameter tube with borosilicate window material and a S-1 photocathode; the spectral response characteristic of a typical S-1 photocathode being illustrated in Fig. 9. The primary operating voltage was -1900 V (3000 V max). The PMT was located in a Products for Research LN₂ cooled Model TE-176-RF housing and cooled to temperatures between -70 to -90°C. As depicted in Fig. 9 the controller not only regulated the cold gas entering the housing but also the heater to the window of the housing. The PMT output went to a Princeton Applied Research (PAR) Model 1121A Amplifier-Discriminator (AD) which was located on top of the PMT housing. The noise threshold is set at the AD controller unit which operated in single threshold level mode and which also housed the high voltage supply to the PMT.

The FAST NIM output of the AD control unit is compatible with the TTL logic of the multi-channel analyzer (MCA); hence, the pulse amplifier box inverted, amplified, and stretched the -1 V, 15 ns short square pulse from the

FAST NIM to about 5 volts (minimum of 100ns duration) for TTL logic. The FAST NIM was also sent to a Princeton Applied Research Model 1112 Photon Counter/Processor where the real time digital output was used during alignment and S/N determinations. The output from the pulse amplifier went to a Canberra 8100/e Multi-Channel Analyzer (MCA) operated in the multichannel scaling (MCS) function mode. One of the major advantages to a MCA is its dynamic range.

The spectrometer stepper motor was controlled by an interface box (see Fig. 9) which also controlled the MCA channel advance by switch selectable motor speeds (frequency) and divider factors. Also influencing the channel advance was the gear ratio of the spectrometer. The combination of frequency, divider factor, and gear ratio produced a given number of Å/channel for a particular sampling time. Typical values included 0.6945, 0.8695, 1.389, and 1.739 Å/channel. The MCA continuously counted the amplified threshold pulses until a particular number of spectrometer wavelength steps had been taken after which the MCA advanced to the next channel and continued to count. When a scan of 1024 or 4096 channels was completed, the stored data was sent to a Zenith Z-100 microcomputer via a serial computer interface port on the back of the MCA. It was also possible to send the output directly to an x-y recorder via the J112 port of the MCA (see Fig. 9).

An alternate method of recording the signal generated by

the PMT was followed at various times as illustrated in the dashed inset to Fig. 9. The signal from the PMT went to a Keithley 417 Current Amplifier from which the output followed to a Keithley Model 840 Autoloc Amplifier. The reference signal originated from a 225 Hz mechanical chopper. The final output from the lock-in amplifier was recorded with an x-y recorder.

The PMT was the main detector for examining the Yb emissions, the remaining rare earth and actinide emissions were primarily investigated with the liquid nitrogen cooled Applied Detector Corporation (ADC) Model 403L germanium photodetector as depicted in Fig. 10. The 403L is considered to be equivalent to the North Coast EO-817L germanium detector which is a photovoltaic device based on a PIN structure fabricated from ultra high purity Ge material. To achieve a low NEP(1.36, 10-500, 1) value of $1 \times 10^{-15} \text{ WHz}^{-1/2}$ requires an optimized preamplifier integrated into the detector housing. Responsivity was specified to be on the order of $7 \times 10^9 \text{ V/W}$. The experimentally determined time constant was 6 msec, although the manufacturer stated a value of approximately 20 msec. The signal was modulated at 225 Hz, processed with a Keithley Model 840 Autoloc Amplifier, and digitized with the Hewlett-Packard (HP) Model 2212A bipolar voltage-to-frequency converter (VFC). (The VFC serves functionally as a type of analog-to-digital converter). The signal is stored in the Canberra MCA in the same manner as

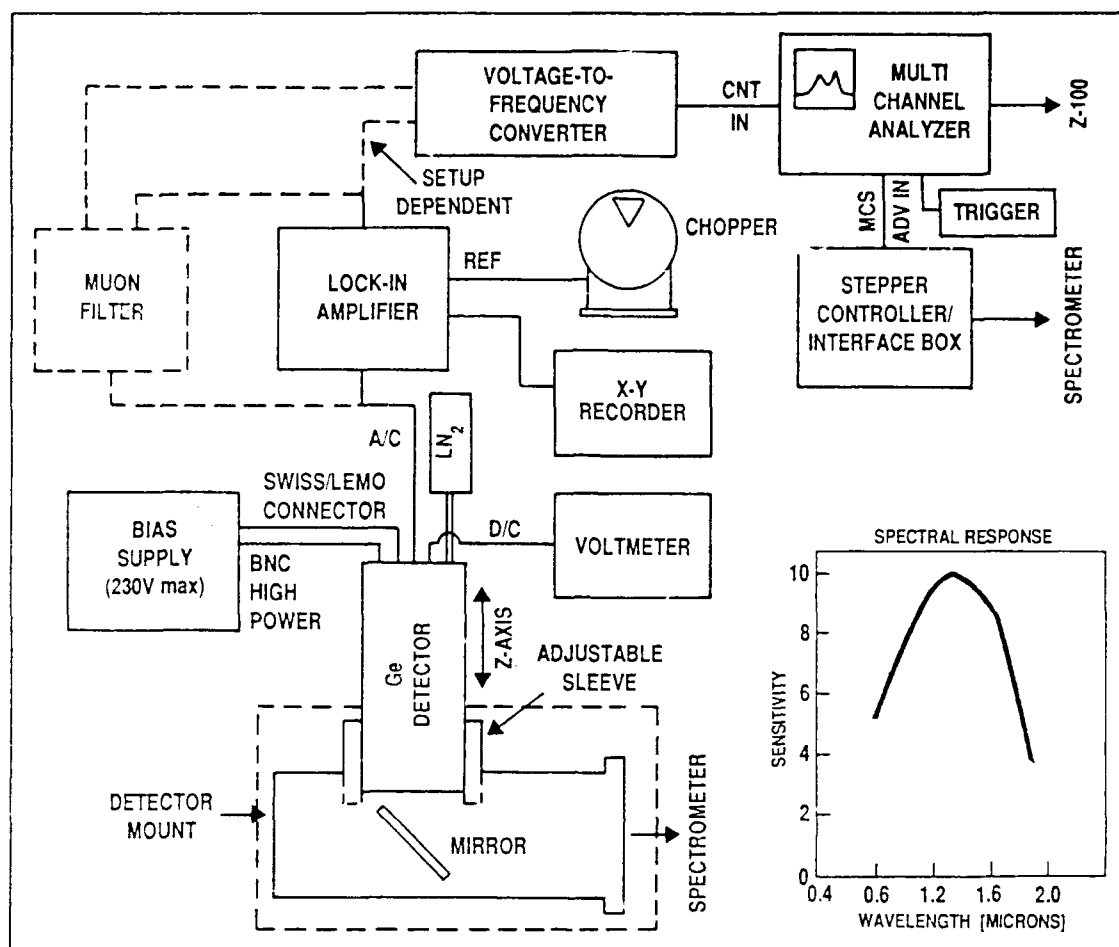


Figure 10. Experimental arrangement for germanium detector.

described earlier for photon counting. The data is then loaded to diskettes via the Z-100.

As seen within the dashed inset to Fig. 10 the Ge detector was inserted into an adjustable sleeve in the z-direction. The signal was focused onto the detector element with a spherical mirror ($f = 75 \text{ mm}$, $\varnothing = 88 \text{ mm}$). As depicted in Fig. 11, an additional detector mount was constructed for use with an off-axis parabolic mirror from Melles Griot ($f =$

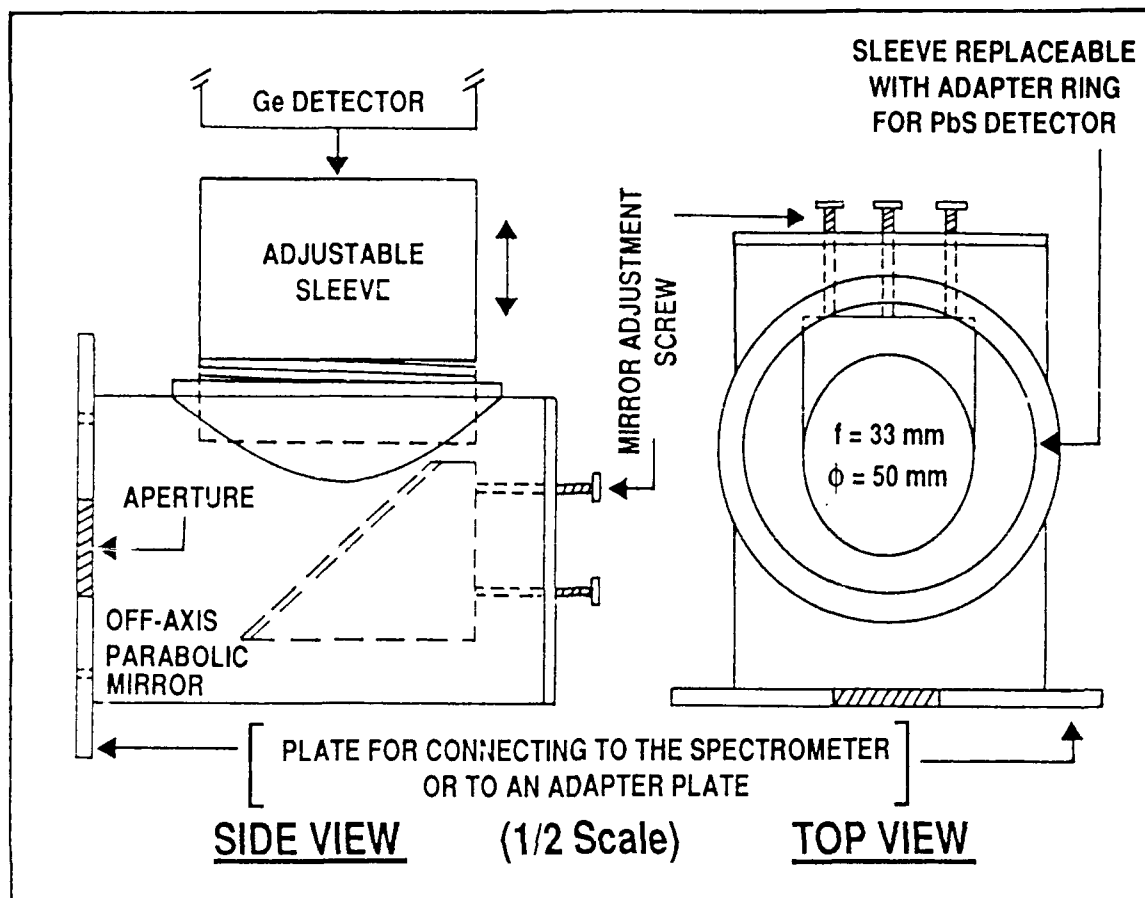


Figure 11. Germanium detector mount.

33 mm, $\phi = 50 \text{ mm}$). The spectra which were generated with the Ge detector show spikes which are generated by cosmic and other environmental ionizing radiation. Suppression of these spikes is possible upon integrating a North-Coast Model 829B moon filter and/or by building appropriate shielding around the detector system (see Mueller, 1986, for a detailed analysis of this problem).

In order to access the spectral region from 1.8 to

2.6 μm a PbS detector was used on occasion; the experimental setup of which is shown in Fig. 12. The New England Photoconductor Series EH lead sulfide detector, with an active $4 \times 4 \text{ mm}^2$ area, had the possibility to be either cooled with LN_2 or dry ice. The detectivity was near optimum with a chopping frequency of 225; typical spectral detectivity at different cooling temperatures is shown in Fig. 12 which shows an average D^* of $1 \times 10^{11} \text{ cm Hz}^{1/2}/\text{W}$ for the 1.8 to 2.6 μm region. Typical detection bias was 180 VDC and the load resistance was 5.65 Mohm. The modulated signal went to the Keithley Model 840 Autoloc Amplifier and was then typically recorded with a x-y recorder. Some digitized data was taken by using the setup shown in the dashed inset to Fig. 12. The output from the lock-in amplifier went to the HP VFC and then to the MCA from where the stored signal was sent to the Z-100 computer.

Since no acceptable mirror-based mount was available for the NEP PbS detector, the wooden mount depicted in Fig. 13 was constructed so that the signal from the spectrometer could be brought onto the active element of the detector. The support shelf carries the detector, 50 mm crown glass lens, and cover to the optical path. The detector and lens were both on runners which allowed adjusting the signal for optimum response. However, the Ge detector mount of Fig. 11 was modified to accept an adapter ring such that the parabolic mirror could be used with the PbS detector upon rotating the Ge detector mount assembly by 90° .

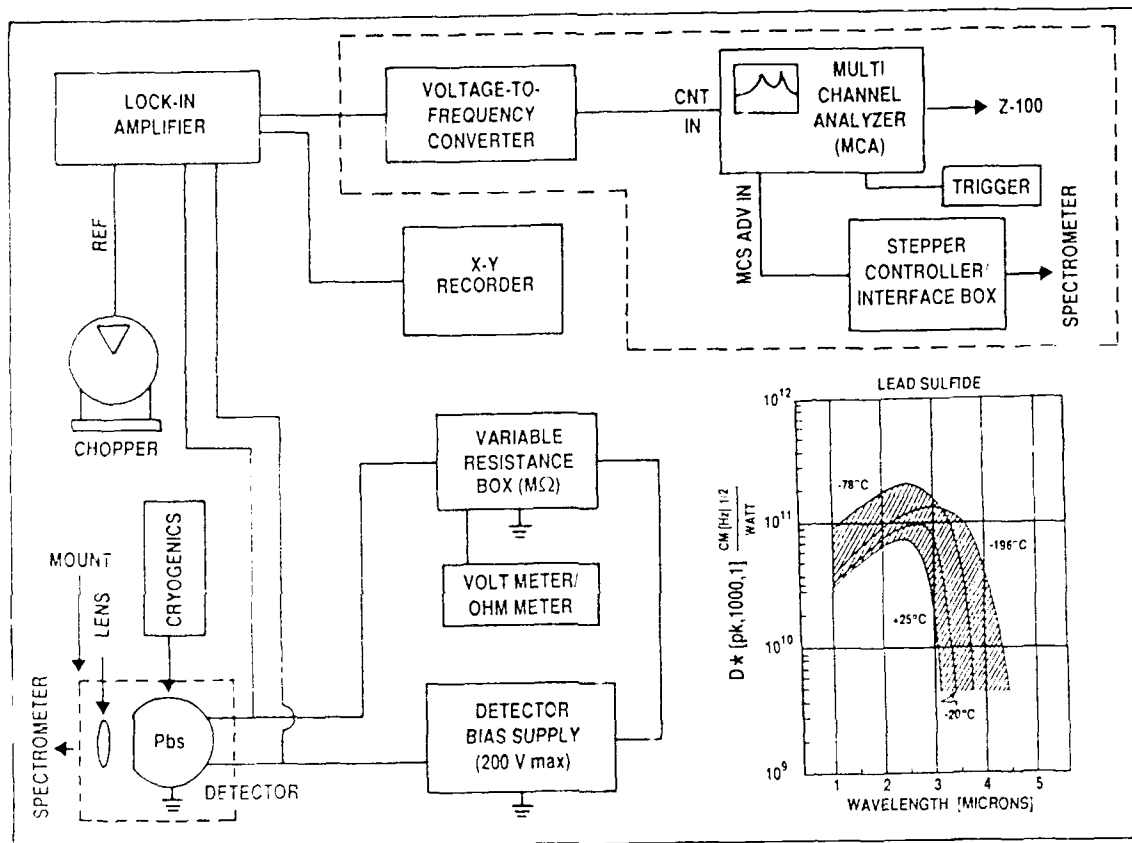


Figure 12. Experimental arrangement for the photoconductive detector (PbS).

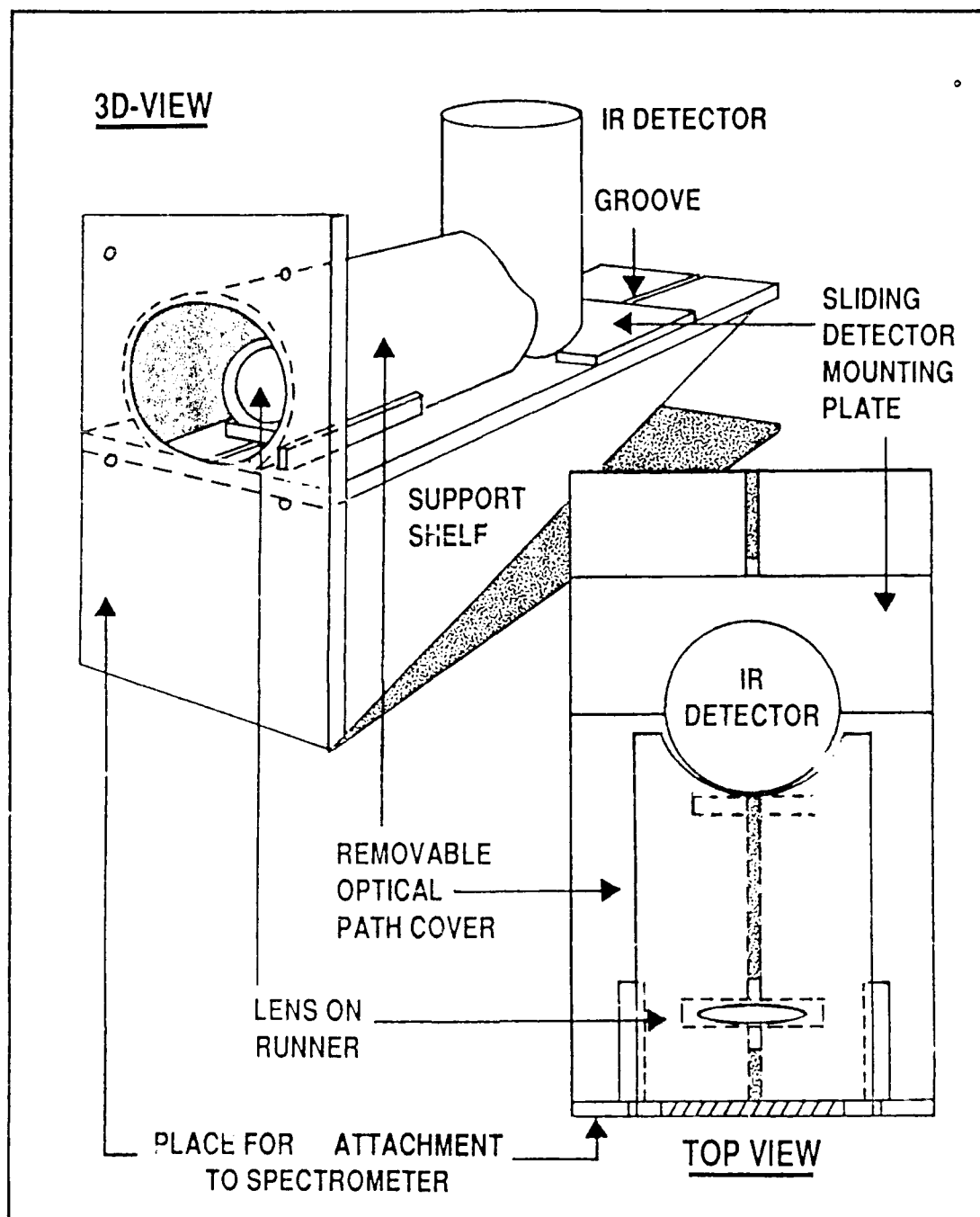


Figure 13. Infrared detector mount.

Data Processing

The digitized data from the various detectors was sent to the MS-DOS based Z-100 computer for storage on diskettes. The software to handle the hand-shaking between the computer and the instrumentation (MCA) plus the software to convert and analyze the data were developed at AFIT over many years but primarily by Capt. Jeffrey Cavins (Cavins, 1988) and Capt. Jamie Varni. The program CANPROG.BAS was used on the Z-100 to capture and store the data in ASCII files. Before analyzing the data, it was necessary through the program SPECCON.PAS to remove the file header of the MCA settings and channel markers. The data was then displayed and analyzed on a Zenith Z-248, IBM PC, or PC compatible through the program SPECPLOT.PAS. The program was menu driven and could produce a hard copy through a screen dump or generate a .PLT file for plotting the data to a Houston Instrument DMP-29 plotter using the program SETPLOT and PLOTTER on a Z-100.

C. Selective Excitation Luminescence

Overview

To investigate the excitation mechanism which allows for the 4f-4f transitions, selected excitation experiments were performed at 7 K on semi-insulating GaAs and InP implanted at an energy of 1 MeV with ytterbium and erbium, at 390 keV with thulium, and at 380 keV with praseodymium. The key instrument in this investigation was an Ar-ion laser pumped tunable dye laser in order to excite the samples above, at, and below the bandgap. Functionally the experiment parallels the photoluminescence setup discussed in the previous section but with the added feature of excitation wavelength tunability. Therefore one can discuss the setup again as basically existing of a sample chamber (with the associated cryogenics and evacuation), an excitation source, and detectors plus the associated electronics and data acquisition elements. Figure 14 depicts the setup for this experiment which could also be modified into a basic photoluminescence (PL) experiment (using above band excitation with the 514.5 nm line) by inserting a mirror between the argon ion laser and the dye laser and a second mirror to bring the beam down range through the optics. Further details on some of the discussion which will follow may be referenced elsewhere (Cavins, 1988).

Cryogenics and Evacuation

The dewar in which the samples were housed was a Janis model 6-5/8" DT variable temperature liquid helium cryostat

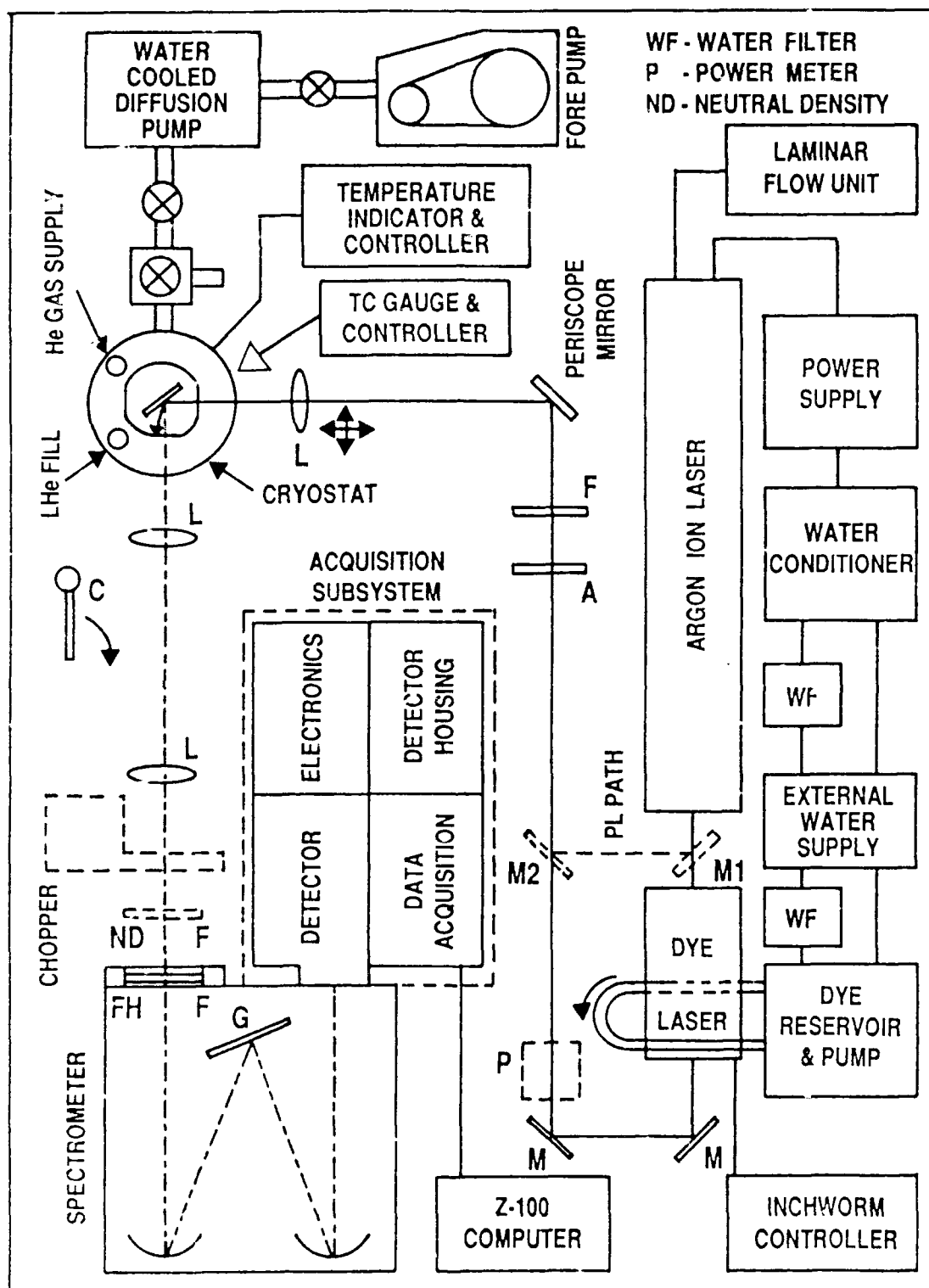


Figure 11. Setup for the selected excitation experiment.

constructed of a LN_2 outer jacket and a LHe inner jacket. Other details parallel the description outlined previously for the cryostat shown in Fig. C. The three fused silica optical windows in the detachable tail had a 19 mm clear aperture. The cryostat was evacuated with a Varian 100 l/s water cooled diffusion pump backed by a 5 cfm fore pump; pressure was maintained below 1 micron as monitored by a TC gauge. After the cryostat was again properly flushed and the sample rod added, the system was brought down to the 5-8 K range. Samples were mounted in a similar fashion as before; however, screw mounted masks were also used. The temperature of the sample was controlled by adjusting the capillary valve on the cryostat and using a Lakeshore Cryogenics Model DRC-80C digital temperature controller with a calibrated GaAs diode and three 3 W heaters imbedded in the cold finger.

Excitation and Optics

A Spectra Physics (SP) Model 171-19 Ar-ion laser was used as the pump laser for the tunable dye laser system and used as the 514.5 nm excitation source when the setup was used for photoluminescence (PL). The Ar-ion laser was cooled with a SP Model 314 closed cycle water conditioner and a laminar flow unit was used to protect the optics. In single line mode, power outputs of 300 mW and less were used for the 514.5 nm line. Spot size at the sample was approximately 3 mm in diameter. In PL mode after reflecting off of mirrors M1 and M2 (see Fig. 14) the 514.5 nm beam was brought through

a 4 to 5 mm diameter circular diaphragm, a 514.5 nm interference filter or a 470 nm long pass filter, reflected from two mirrors in a periscope arrangement, brought through a beam directing or focusing lens, and through the two cryostat windows and unto the sample. A typical irradiance value for a 40 mW laser power setting translated into 330 mW/cm² at the sample.

As indicated, the Model 171-17 Ar-ion laser was used to pump the Spectra Physics Model 375-50 dye laser. Depending on the condition of the Exciton LDS 821 dye, the Ar-pump laser was operated with the multiline optics and pump powers of 2 to 5 W (5.5 W was the maximum achievable). Dye laser output was usually at 40 mW after two mirror reflections; maximum attainable output was 160 mW. Although the dye laser system appeared to be relatively stable, the power was continuously monitored with a FND-100 silicon photodiode sensing the power of the beam back reflected from the cryostat windows. The optics were Spectra Physics standard dye optics for Styryl 9 (Exciton LDS 820) dye: a G3862-013 output coupler, two G3845-011 high reflectors, and a G3845-003 input mirror. Due to economy and similarity in results, LDS 821 dye was used instead of LDS 820. The LDS 821 dye was mixed in a 2 millimolar solution of 85% ethylene glycol and 15% propylene carbonate. The dye was circulated with a Spectra Physics Model 376 at a pressure of 80 psi.

A three plate birefringent filter assembly (Model 573) designed for LDS 751 or LDS 821 dye, was used to tune the dye

system to a particular wavelength. The tuning of the birefringent filter was by an inchworm controlled by a Burleigh Model PZ-550 Controller. A manual micrometer was also used at times for tuning. Figure 15 shows for a particular set of runs the experimentally generated bandwidth of the birefringent filter ranging from 800 to 859 nm. The top linear zone of the graph between 800 to 840 nm has a slope of 11.53 nm per unit inchworm setting. The filter has an approximate linewidth (fwhm) of 0.2 meV for this region. The lower or upper cut off could be shifted up or down in wavelength slightly (by about 5 nm), although the bandwidth would remain essentially unchanged. The dye laser output power when pumped at a continuous 3 W with the Ar-ion laser shows a somewhat flat performance region between 813 and 856 nm. Since the investigation also concentrated on InP, with a lower energy bandgap than GaAs, it was necessary to order and install optics for the extended wavelength coverage; this included two G3845-010 high reflectors, a G0230-010 output coupler, and a Model 573 birefringent filter for LDS 821 dye. Unfortunately, this extended the wavelength region only to 893 nm.

The output beam from the dye laser is turned by 180° with two flat mirrors. The beam which was tracked with a infrared viewer (FJW Industries) is then brought through the 1 to 5 mm diameter circular diaphragm and through a 780 nm longpass filter. After being reflected by the periscope

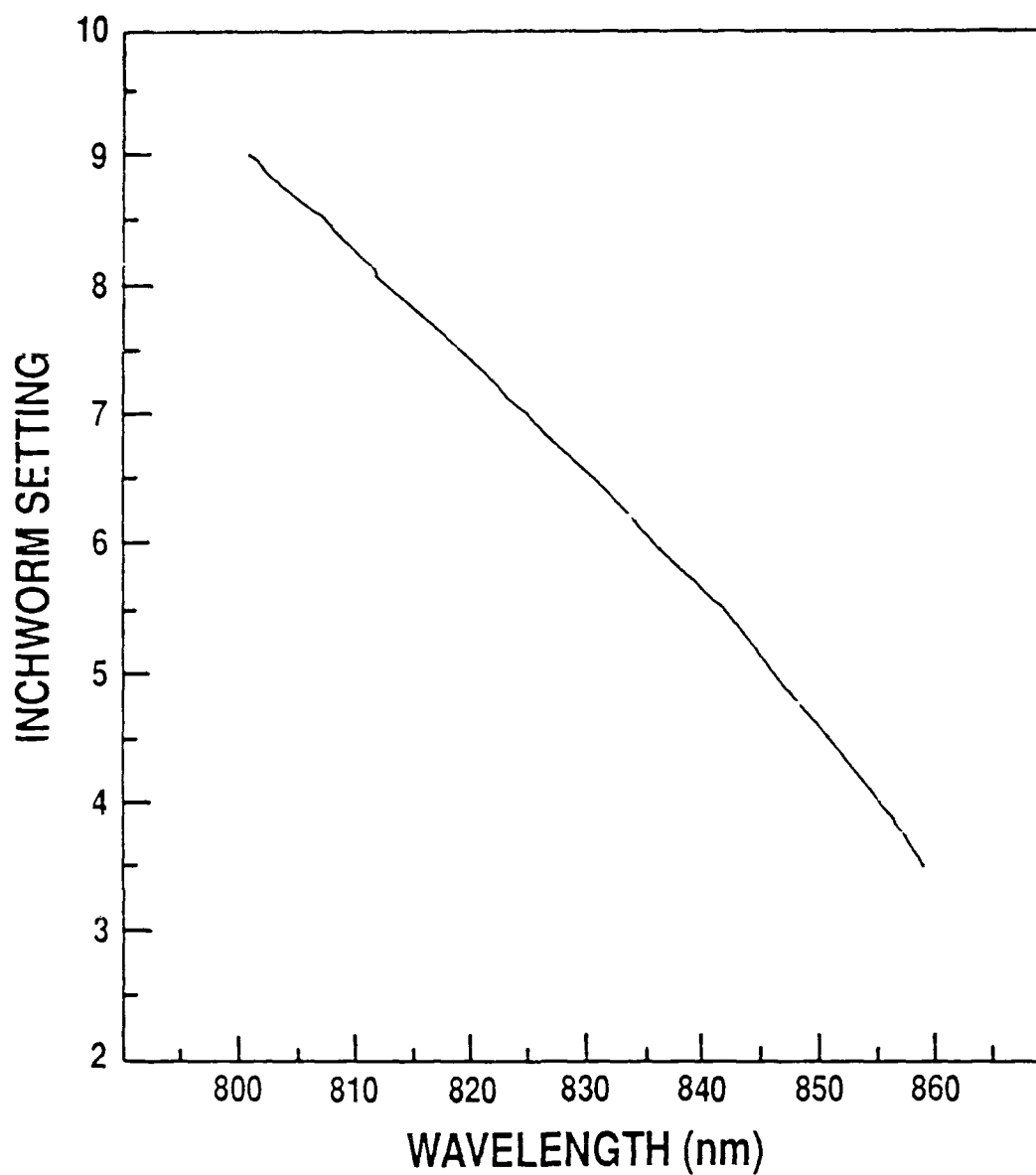


Figure 15. Bandwidth of birefringent filter (nonlinear behavior shown).

mirrors, the beam passes through the 'positioning' lens and through the two cryostat windows before passing to the sample.

As shown in Fig. 14 the luminescence from the sample was collected by a system of two biconvex lenses ($f = 105$

mm, $\phi = 47$ mm). Before entering the spectrometer the signal was filtered by a 695 or 780 nm long pass filter, and a neutral density (ND) filter was introduced if the first order dye laser line was recorded in the spectra. The spectrometer was a SPEX 1702, 3/4-m spectrometer with the same specifications as mentioned in the previous section. Either 500/1000 or 1000/2000 μ m entrance/exit slits were used with a slit height of 10 mm. Similar to the PL study, the signal was dispersed by either a 1200 gr/mm grating blazed at 500 nm or a 600 gr/mm grating blazed at 1.6 μ m. Transmission, reflectivity, and grating response characteristics of all optics were similar to those characteristics previously discussed.

Since the selective excitation experiment involved examining the Yb, Tm, Er, and Pr emissions which are located between 0.9 to 1.7 μ m, two different signal detection systems were used. As in the previous PL section, this involves the discussion of the 'acquisition subsystem' as depicted by the dashed box in Fig. 14. The S-1 PMT was used for Yb and the Ge detector was used to examine Tm, Er, and Pr. Functionally the acquisition subsystems are identical to those discussed in the PL section and depicted in Figs. 9 and 10. The S-1 detector was a Thorn EMI 9684B PMT with a spectral response as shown in Fig. 9 and operated at -1230 V and at a housing temperature of -80°C. The output from the tube was connected to an EG&G/PAR Model 1121A amplifier-discriminator and

control unit. The signal followed then from the control unit to a photon counter and separately through a pulse amplifier to the Tracor-Northern 1710A Optical Multichannel Analyzer (OMA) unit for signal storage. A Model 1710-30 signal-averaging/multichannel analyzer module was used with the OMA unit. The incoming count rate had to remain below 200 kHz and the dwell time of the module was set to 'external' to allow for channel advance through the stepper controller interface box.

The stepper-controller/interface was of slightly different design as compared to the PL study (Fig. 9). The wavelength advance of the SPEX 1702 spectrometer was controlled through a SPEX 1752-3 motor driver and a Wavetek square wave generator. A pulse divider synchronized the advance of the spectrometer with the advance of the OMA. Although settings on these units varied for some runs, typical settings included a 250 Å/min scan rate on the spectrometer, 70 Hz on the Wavetek, and a divide by 25 on the pulse divider which produced a 2048 channel data set covering a 178.2 nm wavelength region (using the second order grating) in approximately 11.6 minutes. This time was chosen as the mean time between failure of a system component of the selective excitation experiment appeared to be approximately 30 minutes.

Data Processing

The data which was stored in the OMA was sent to the Z-100 for storage on diskettes. The program TRACOMM.BAS was

used on the Z-100 to capture and store the data in ASCII files. As before, it was necessary to convert the data to a series of numbers in ASCII files which could be analyzed; this was performed with the program TRACONV.PAS. Further data manipulation and display of the recorded spectra was through the program SPECPLOT.PAS on a Z-248 or IBM PC compatible computer.

D. Lifetime Measurements

A schematic of the time-dependent luminescence or lifetime measurement experiment is shown in Fig. 16. Similar to the photoluminescence setup, it includes an excitation source, sample chamber and the associated evacuation and cryogenic subsystems, spectrometer, detector and the associated electronics, and the data acquisition elements such as the boxcar integrator and the Z-248 PC. Substantial use was also made of an oscilloscope which was used to directly sample the time varying signal from the detector. For the most part the sequence of events essentially involved the pulsed excitation of the cooled sample; the collection, dispersion, and detection of the signal at a fixed wavelength; and the gating and triggering of the boxcar integrator to allow the amplified signal to be recorded with a PC.

As shown in Fig. 17, the samples were located in a closed cycle cryogenic system which was evacuated below 10 microns of pressure with a fore-pump-backed and water-cooled Leybold-Heraeus NT220 turbo molecular pump. Two Granville-Phillips TC gauges and a Veeco ionization gauge were used to monitor the pressure. The cooling of the samples was with an Air Products LT-3-110A Heli-Tran system and the temperature control from room temperature down to 4 - 5 K was with an Air Products Digital Temperature Indicator/Controller which used an iron-doped chromel versus gold thermocouple. Since sample cooling was through conduction, the sample holder install-

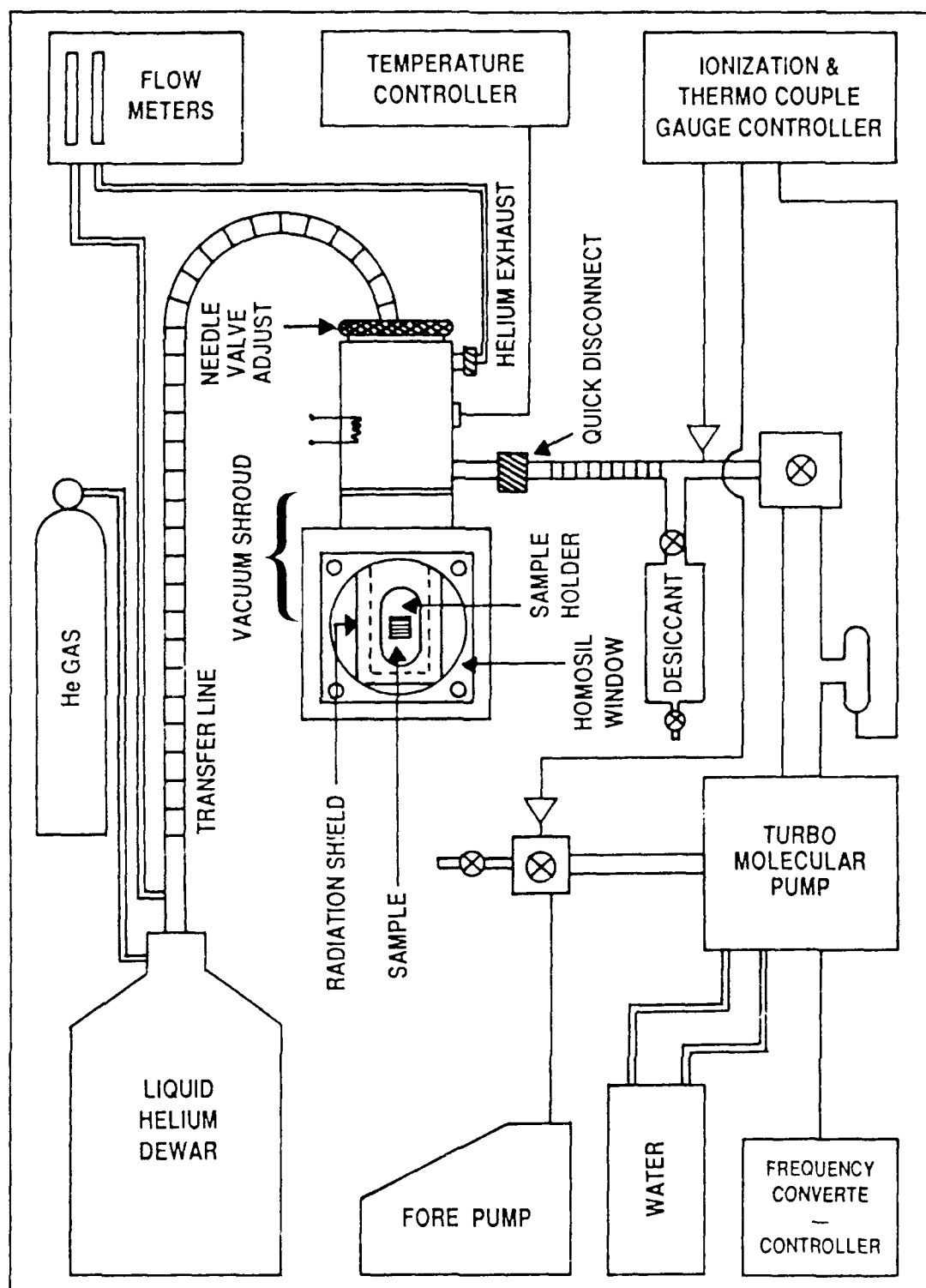


Figure 17. Sample environment and evacuation and cryogenic subsystems for the lifetime measurement setup.

ation and sample mounting was performed to maximize heat conduction. The sample temperature could be adjusted by either increasing the flow of helium through the transfer line by adjusting the needle valve, changing the back pressure on the liquid helium dewar, adjusting the flow meters, or changing the heater power on the controller. A typical cool down cycle from room temperature to 4 - 5 K was somewhat less than one hour. To reduce radiative heating a cylindrical copper shield with entrance and exit openings was designed to surround the sample (see Figs. 16 and 17).

The excitation of the sample was with the 570 - 610 nm dye laser output of a Laser Photonics DL14 tunable laser. This system, depicted in Fig. 16, was pumped with the 337.1 nm line of a Laser Photonics UV-24 nitrogen laser which was located within a grounded Faraday cage. (The electronic noise generated by the laser had to be given special attention). The nitrogen supply gas to the laser was either from a liquid nitrogen tank or from nitrogen gas bottles with appropriate filtering of the gas. A 21 l/min mechanical pump was used to remove the depleted nitrogen population. Dependent on the pulse frequency, the appropriate manufacturer suggested nitrogen pressure was used. The laser operating pressure was adjusted to 40 - 60 torr with the pressure and vacuum adjust controls. An oscilloscope or DSI Instruments frequency counter was used to adjust the pulse frequency of the laser to a typical value of 10 Hz.

As shown in Fig. 16, the dye laser was in tandem with nitrogen laser. As measured with a Scientech power meter the average dye laser output power was approximately 3 mW at a pump laser frequency of 10 Hz which was 15 times lower than the manufacturer's specifications; this resulted in a pulse energy of 0.3 millijoules per pulse and a peak power of 0.05 MW. The stated pulse width was between 5 to 7 ns and beam divergence was 0.3 - 0.5 mm. Spot size on the sample, which was controlled with a biconvex lens, was typically 3 to 4 mm in diameter. The active dye medium was Rhodamine 6G and showed peak output at around 579 nm. The dye was located in two quartz cuvettes and was magnetically stirred at the base.

Within the dye laser the UV beam was first separated with a 20 - 25% beam splitter. The first reflected beam went to the oscillator cell or the first cuvette located within the laser cavity. The remainder of the beam was diverted via a 98% beam splitter to the second cuvette or amplifier cell. The output wavelength was adjusted by rotating the diffraction grating which acted as the rear mirror of the laser cavity. The grating had 600 gr/mm and was blazed at 2.7 μ m; hence, for this dye, the laser was operated in fifth order.

The exit beam from the dye laser was brought onto the sample with a periscope mirror assembly and a convex lens. The fraction of the beam which was reflected from the single Homosil window of the vacuum shroud assembly was brought to a

pyroelectric detector from which the output acted as the trigger signal for the boxcar integrator and oscilloscope. The image of the optically excited sample was then focused unto the entrance slit of the spectrometer. Depending on the desired semiconductor emissions, an appropriate long-pass filter was used.

For most of the lifetime investigations, specifically InP:Yb, a 1/2-m Ebert type spectrometer (f/8.6) was used which contained a 590 gr/mm and 1.3 μ m blazed grating. Reciprocal linear dispersion was 3.2 nm/mm and vertical opening of the curved slits was 15 mm. During a particular run the wavelength settings of the spectrometer remained fixed on a particular emission wavelength. The maximum entrance and exit slit settings of 400 μ m turned out to be a limiting factor in this particular setup as the amount of signal passing through the spectrometer was reduced. Hence, for a certain number of investigations, such as AlGaAs:Yb, a Jarrell-Ash 1/4-m Ebert monochromator was used utilizing due to its improved throughput of f/3.8 and its improved input with interchangeable slits of up to 2 mm. However, its 500 nm blazed and 1180 gr/mm grating limited its use to below 1090 nm. After exiting the spectrometer, the signal entered an Al-lined cardboard box, which was later replaced with a metal housing, which contained a flat mirror from which the signal was refelected to the detector. The housing served as a light and electronic shield and as an adapter between the spectrometer and detector.

Signal detection was with either a S-1 type PMT (Thorn EMI 9684B) or a fast Ge detector (< 500 ns) with the setup and specifications very similar as described previously in the PL setup and depicted in Figs. 9 and 10. Details of this part of the setup can also be seen in Fig. 5 and the dashed inset to the figure. The response of the S-1 PMT was 9 ns, typical bias was from -1100 to -1400 V, and PMT housing temperature was between -80 to -50°C (see Fig. 5 for the response curve). The detector signal was brought to a Keithley Model 427 current amplifier with a minimum adjustable rise time setting of 10 μs (actual rise time was somewhat below this value). Due to gain and bandwidth arguments the amplifier also became a limiting element to the study. Total electronic system time response was determined to be 2.9 μs .

The amplifier output was brought to a sophisticated gated signal-recovery system, i.e. to an EG&G PARC Model 165 gated integrator module of channel A to the EG&G PARC Model 162 Boxcar Averager. The boxcar averager was used to improve the signal-to-noise ratio by averaging out a substantial amount of the random noise in the signal, and thus provided a higher signal resolution. The time-shifted boxcar signal was scanned and repetitively sampled to produce an output over many seconds (e.g. 100 or 1000 s). Baseline sampling was used with about a 5% initial delay. Typical system parameters were as following: scantime, 1000 s; aperture

delay range (ADR), 50 μ s; aperture duration (AD), 0.5 μ s; Model 165 gate time constant (GTC), 10 μ s; and signal processing time constant (SPTC), 10 ms. These were essentially established by using the procedures outlined in the EG&G Model 165 manual.

The smoothed output signal of the boxcar averager was sent with a coaxial cable to an interface box and then to the Z-248 computer as depicted in Fig. 16. The analog signal, with a maximum ± 10 VDC, was converted to a digital signal by an analog-to-digital converter board, specifically the QUA TECH SAC-12 12 Bit Signal Acquisition System. This input signal was controlled and manipulated with the CODAS (Computer-based Oscilloscope and Data Acquisition System) software by Dataq Instruments Inc. and the WSF-200 scroller board.

After the CODAS software system had stored the incoming analog boxcar output voltage to the hard disk files of the Z-248, the collected data was accessed and inspected and portions of the files were extracted and stored in the ASYSTANT+ format. (ASYSTANT+ is a software package for data acquisition and analysis by ASYST Software Technologies Inc., Rochester, NY.) Then the curve fit and graphics portions of this software package were used to evaluate and display the data. The decay data or lifetime measurements were modeled with a single exponential, $y = \exp(ax + b)$, as a first order approximation and as discussed in the background and theory section of this document. This approximation was also

supported by the reported near single exponential decay curves for InP:Yb (Koerber and Hangleiter, 1988; Klein, 1988).

Since the investigation also concerned itself with lifetime measurements for emissions between 1.1 and 1.7 μm , in the region with no S-1 PMT response, a 'fast' germanium detector was used. Upon the arrival of entrance and exit slits with settings of up to 2 mm for the 1/2-m spectrometer, the lifetime measurements were essentially setup with the modification shown in the dashed inset to Fig. 16. The 1/4-m spectrometer was not used due to the non-availability of a proper grating for this wavelength region. The detector was a North-Coast EO-817P Germanium Detection system with switch selectable time constants of 200 and 400 ns, which were experimentally confirmed. The responsivity of 10^6 V/W was approximately two orders of magnitude lower than for the APL Ge detector previously discussed. Output from the detector went straight to a 1 Megohm and 20 pF input of an oscilloscope; the displayed data was photographed. Some investigations utilized the higher response of the previously described APL Ge detector which was limited however by the experimentally determined 7 ± 1 ms lifetime.

Besides constraints on the availability of the proper equipment due to funding and acquisition problems, space-limitations produced various design, alignment, and adjustment shortcomings. Further information and procedural

details may also be referenced elsewhere (Bumgarner, 1988).

•

E. Sample Processing

Introduction

In this section details are presented on the semiconductor substrate material which was used in the course of the investigation, the pre-implantation treatment of the samples, the implantation conditions, post-implantation treatment, and the mounting of the samples. Also experimental details are given for the SIMS analysis.

Sample Information

The InP, GaP, and GaAs substrates were already cut into wafers and polished on at least one side, only the undoped GaP crystal (MRC) had to be cut and polished locally. All samples were supplied at one time or another by a commercial vendor. Many of substrates which were used for the implantation of the rare earth ions were semi-insulating and grown in the $\langle 100 \rangle$ direction as shown in Table 4. The substrates were of varying quality with the residual impurity content being acceptable, if only marginally, for most of the samples which were eventually investigated. Many other substrates were used and implanted but the strong substrate emissions due to impurities and defects prevented an in-depth study of the rare earth emissions, and hence, are not included in this discussion and investigation. In the results and discussion part to this document, the substrates which were used for a particular study may be identified by the Identifier Code in Table 4. Table 4 gives the electrical data, growth and doping data, and the origin of the III-V

Table 4. III-V Semiconductor Substrate Information.

Semi-conductor	Identifier Code	conductivity Type	dopant	resistivity ohm-cm	mobility cm^2/Vsec	carrier concentration cm^{-3}	orientation	Vendor
InP	MR(354)	SI	Fe	1.6×10^7	1.5×10^3	$n = 2 \times 10^8$	100	MR
InP	MR(338)	SI	Fe	1.2×10^9	1.6×10^3	$n = 3 \times 10^6$	100	MR
InP	MR(346)	SI	Fe	7.5×10^8	1.5×10^3	$n = 6 \times 10^6$	100	MR
GaP	MPC	p	und	4.7×10^1	-	$p = 2 \times 10^{16}$	111	-
GaP	CAC	n	S	5×10^{-1}	-	$n = 1 \times 10^{17}$	100	-
GaP	PC	p	Zn	4.2×10^{-1}	-	$p = 1 \times 10^{17}$	100	-
GaAs	CS	SI	Cr	3×10^7	4.4×10^3	$n = 5 \times 10^7$	100	CS
GaAs	MA	SI	und	1.6×10^8	9.2×10^2	$n = 4 \times 10^7$	100	MR
GaAs	CO	SI	-	3×10^8	7×10^3	$n = 3 \times 10^6$	100	CO
GaAs	WA	SI	und	$> 10^7$	-	-	100	WA
GaAs	WA	n	Te	5×10^{17}	-	-	100	WA
GaAs	WA	p	Zn	$0.5 - 3 \times 10^{17}$	-	-	100	WA
GaAs	AC	n	Si	1.2×10^{-1}	2.8×10^3	$n = 2 \times 10^{16}$	100	AC
GaAs	AC	p	Zn	-	-	$p = 4 \times 10^{18}$	100	AC
GaAs	LD	p	Zn	1.9×10^{-1}	-	-	100	LD

Crystal Grower or Vendor Identification:

MR - Metal Research (England)

CS - Crystal Specialties

MA - Micro Associates

WA - Wacker Siltronic (FRG)

AC - Atomergic Chemetal

LD - Laser Diode

CO - Cominco

semiconductor substrates. As seen in the table by the 'dash' and 'question' mark, some of the information is not known or not known for certain; due to the lack of data it is assumed that most of the crystals were grown either by the liquid encapsulated Czochralski (LEC) or by the horizontal Bridgman method. The electrical data was determined through Hall measurements by different investigators or through vendor specifications.

Table 5 gives various data on the AlGaAs layers which

Table 5. AlGaAs Sample Information.

Al _x Ga _{1-x} As x =	Identifier Code	AlGaAs layer			GaAs cap layer thick- ness μm	Vendor	Substrate
		thick- ness μm	dop- ing	Conduct- ivity & cc			
0.15	EPI-513	5	und	n = 1.2X10 ¹⁶	0.03	Epitronics	und SI LEC GaAs (Wacker)
0.30	EPI-514	6	und	p = 3.9X10 ¹⁶	0.02- 0.03	Epitronics	und SI LEC GaAs (Wacker)
0.23-0.25	MO-1719	4	und	-	0.03	Spire	LEC SI GaAs (Morgan)
0.10	EPI	5	und	n = 1X10 ¹⁶	<0.02	Epitronics	und SI LEC GaAs (Wacker)
0.20	EPI	5.5	und	n = ~ 10 ¹⁶			
0.30	EPI	5.0	und	n = 3X10 ¹⁶			
0.40	EPI	5.5	und	n = 0.8X10 ¹⁶			

were implanted with rare earth ions. All the layers were essentially undoped (und) with an approximate thickness of 5 μm and grown on top of a semi-insulating GaAs substrate; the AlGaAs layers were also covered with an approximate 25 nm thick protective layer of GaAs. The EPI-513 and -514 layers were essentially from test runs; as a result the material might not have been of as high quality as that of the EPI layers with an Al mole fraction of x = 0.1, 0.2, 0.3, and

0.4. The quality and sample data of the Spire Corporation samples (MO-1719) may possibly be questioned as the delivery of this product faced some controversy.

The study also used one² sample with a 3.7 μm AlAs layer; it was later implanted with erbium. The AlAs layer originated from a multi-structure which consisted of the following layers grown in order on top of a Si GaAs substrate: 30 nm GaAs, ten alternating layers of 3nm of GaAs and 3 nm of AlGaAs, 30 nm of GaAs, 3.7 μm of AlAs, and finally a 1.0 μm protective layer of GaAs. The MBE structure was grown by Dr. Rex Jones of the Avionics Lab, WPAFB, OH. Before implantation a 1:1:10 mixture of $\text{H}_2\text{SO}_4:\text{H}_2\text{O}_2:\text{H}_2\text{O}$ was used to etch the top protective GaAs layer for 9.8 minutes at an etch rate of 100 nm/min.

Sample Preparation

Before implantation the substrate wafer had to be cut, cleaned, etched, and again cleaned. One of the goals of the investigation was to implant the specific rare earth ions into all different substrate types which were available; however, due to cost and limits on the area (2 inch X 2 inch) which could be implanted, small sections had to be cut out of the different wafers which were then mounted on a 2 inch X 2 inch cut silicon wafer. This silicon wafer, which eventually became a mosaic of semiconductor crystals, was then loaded into the implantation machine. The cutting was performed with a diamond-tip scriber, a carbide-tip scriber, or with the diamond stylus of a manual dicer/cutter assembly.

After cutting, the samples were sequentially washed with a mild detergent solution, deionized water, trichloroethylene, acetone, methanol, and deionized water. Each wash was for 5 to 10 seconds and at the end, the samples were blown dry with nitrogen gas.

Just prior to mounting the samples on the Si wafer and prior to implantation, the samples were etched. First they were washed in acetone, methanol, de-ionized water, one minute in HF acid, and again in de-ionized water. This was followed by a continuously-slowly stirred etch of $\text{H}_2\text{SO}_4:30\%\text{H}_2\text{O}_2:\text{H}_2\text{O}$ in the proportion of 1:2:5 for 90 to 120 seconds. This removed approximately 0.1 to 0.4 μm of material from the semiconductor surface; removing layers which may contain oxides and limited residual damage due to mechanical polishing. The etchant was mixed in small quantities (< 100 ml) and kept at room temperature with a water bath. A faster etch with a 3:1:1 ratio proved to adversely affect the surface quality of some samples. The samples were then thoroughly washed in de-ionized water and dried with nitrogen gas. The samples were mounted with a small bead of rubber cement to the sample back surface in a manner to maximize the number of samples on the 2 inch by 2 inch Si wafer. Samples which were implanted by the Lawrence Berkeley Lab and the Implant Sciences Corporation did not require mounting on a 2 inch by 2 inch wafer.

Implantation

The actual implantation of rare earths into semiconductors became a research topic in itself since only one commercial service claimed to have implanted such ions and in that case, only one (Er). This was further complicated by the lack of gaseous rare-earth sources for the ion source during implantation; hence, considerable research and start-up time had to be invested before the actual implantation.

Four different services were used for the implantation. Dependent on the rare earth ion, a specific implantation system was utilized. Originally it was intended to implant all ions at a high energy of 1 MeV to maximize the depth of the impurity layer; however, due to cost considerations only a limited number of high energy implants could be accomplished. Due to the material handling problems associated with the actinides, a non-conventional method was used for the implantation of these materials. All implantations were carried out at room temperature.

Implant Sciences Corporation of Danvers, MA, implanted thulium (Tm^{169}), at an energy of 390 keV, doubly ionized, and a dosage of $5 \times 10^{13} \text{ cm}^{-2}$ ($\pm 5\%$). A high throughput Eaton Medium Current System was used with a completely cryopumped beam line and end station for contamination-free implantations. Prior to implantation the system was purged with argon. The actual thulium beam was generated by ionizing the TmCl_2 carrier gas. Chlorine gas flowed through a heated crucible containing 99.9% pure thulium shavings, the

resulting TmCl_2 product flowed to the arc chamber where it was ionized.

The ion stream was then accelerated, mass analyzed, shaped through beam line optics, and brought onto the samples seven degrees off from the $\langle 100 \rangle$ crystalline direction in order to inhibit channeling. Temperature of the implant block was considered to be well below 100°C due to the low dosage. The actual implantation time was on the order of minutes with an implant current of somewhat less than 15 microamps. System mass resolution was claimed to be 1 amu. After implantation the sample surface had a metallic and mirror like finish which was easily differentiated from the unimplanted semiconductor substrate (especially for GaP); upon annealing this metallic surface disappeared. The size of the implanted ion, the shallow depth to which it is implanted, and the resulting lattice damage are sufficient in this case to change the optical property of the implanted semiconductor layer.

The high energy implants at 1 MeV were performed at Universal Energy Systems (UES), Dayton, OH. The implants included Yb, Ho, Pr, and Er; however, the implantation of Pr was unsuccessful. Most of the attempts included a trial or test run of a 1 cm X 1 cm sample to see if a RE ion beam could be generated. The UES implantation system was a Tandatron accelerator by General Ionex Corporation. This is essentially a negative ion beam system versus a positive ion

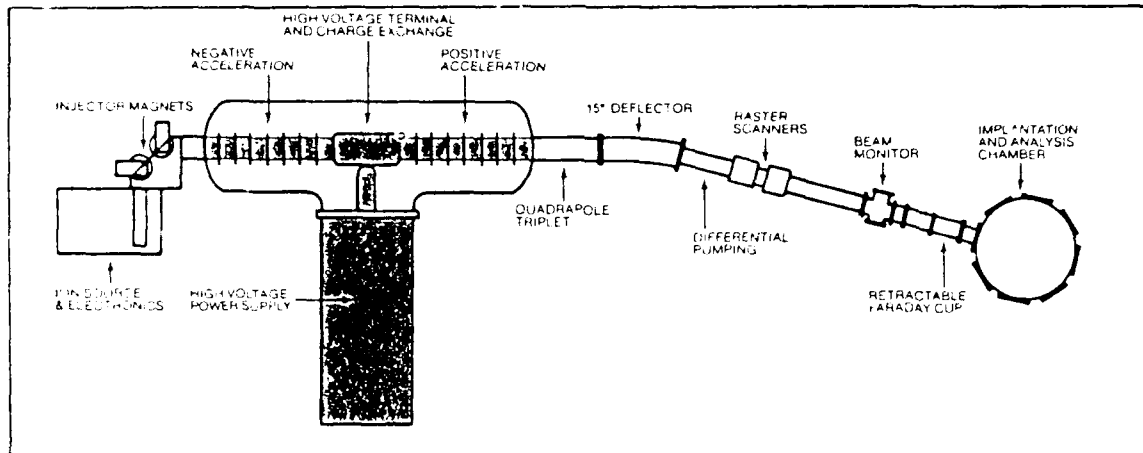


Figure 18. High energy ion beam accelerator. (from UES advertisement)

beam system used by most commercial implantation services which implant at lower energy.

As seen in Fig. 18 the system consists of a negative ion injector, an accelerator system, and a high energy analysis station. In this investigation a rare-earth oxide was pressed with small beads of Ag or Cu into an Al cylinder; this mixture of oxide and binding material was then sputtered with a 6 keV cesium beam to generate negative ions. The negative ions are mass analyzed and accelerated at 1 MeV toward the nitrogen stripper gas or charge exchanger in the center of the machine where the rare earth ion is separated from the oxygen. The rare earth ions were then accelerated at 1 MeV for a second time toward the target where an electrostatic analyzer helps in establishing further the purity of the implant. The 2 inch by 2 inch sample wafer was

mounted on an aluminum plate in the analysis chamber. The electrostatic steering devices scan the beam such that it is 7° off from the $\langle 100 \rangle$ crystalline direction to prevent channeling. Shortcomings of the system were the low mass resolution of 4 amu and the low beam current which resulted in up to 10 hour runs for dosages of up to $5 \times 10^{13} \text{ cm}^{-2}$. Furthermore, based on SIMS analysis, considerable surface sputtering appears to be occurring.

The rare earth oxide starting material (from either Alpha Products or Aesar) was of 99.999 % purity. Ytterbium oxide, Yb_2O_3 , was used to generate a 3×10^{-9} amp Yb beam; Pr_6O_{11} was used to supposedly generate a 10×10^{-9} amp Pr beam; erbium oxide, Er_2O_3 , was used to generate a $6-7 \times 10^{-9}$ amp Er beam; and holmium oxide, Ho_2O_3 was used to generate a $5-6 \times 10^{-9}$ amp Ho beam. The following dosages (in ions per cm^2) were generated for the 1 MeV rare earth ions: 5×10^{13} for the Yb test samples and 3×10^{13} for the Yb sample set; 5×10^{13} for the Pr sample set; 3×10^{13} for the Ho sample set; and 7.5×10^{13} for the Er test set and 5×10^{12} and 5×10^{13} for the Er sample sets. Unfortunately it was determined with both SIMS and photoluminescence that no Pr was implanted into the semiconductors. SIMS analysis indicated that silver (Ag) had been implanted instead of Pr; hence it was assumed that ionized silver oxide (AgO^+) was generated in the ion source region from the binder material which was eventually implanted versus praseodymium (the mass of Pr is 140.9 while

for AgO^- it is 139.8).

In order to achieve the implantation of praseodymium, the more conventional low energy implantation facility at UES was used which basically consisted of a Varian 20-1000 Implanter with a 190-200 keV capability (singly ionized). A hot cathode source filament was used to heat the high purity Pr metal and to produce the doubly ionized Pr which was mass analyzed and then accelerated at 190 keV, resulting in an effective implantation energy of 380 keV. The dosage was 5×10^{13} ions/cm² and the beam was brought onto the samples at seven degrees off from the $\langle 100 \rangle$ crystalline direction. Beam current was 1 microamp.

Implantation of the actinides thorium and uranium was performed with an unconventional implantation technique using a new kind of high current metal ion source (Brown et al, 1985; Brown, 1985; Brown et al, 1986). The technique was also tested on the rare-earth ions holmium and ytterbium. This Metal Vapor Vacuum Arc (MEVVA) ion source makes use of a dense metal plasma generated directly from the cathode material, as the medium from which ions are extracted. Regions of intense current concentration are formed at the cathode resulting in the vaporization and ionization of the cathode material into a dense, quasi-neutral plasma which plumes away from the cathode surface. The plasma plume is made to collide upon a set of extractor grids, and the ion beam is extracted from the streaming metal plasma. The resulting intense ion beam used for the implantation is then

composed of the cathode source material which in this case was U^{238} , Th, Ho, and Yb.

Although semiconductor implantation is a relatively well established technique, many systems are limited to the implantation of gaseous species, and limited in metallic ion beam intensity due to the conventional way of producing the plasma via ionization, evaporation, or sputtering, as was seen for the case of the 1 MeV implants. A multitude of metal ion beams have been produced with the MEVVA source, from Li to U, and this method can complement or even extend the range of metallic species implanted into semiconductors.

The MEVVA technique was applicable in this study to allow for the implantation of sufficiently deep layers such that the ions could be properly excited by the laser light. However, the technique is somewhat limited by the extraction energy which controls the depth of the implant. Also it is limited by the departure of the implanted depth profile from Gaussian because of the ion charge state distribution or structure, and hence, the energy structure of the incident ion beam. The spread of charge states results in a considerable uncertainty in the projected range and straggling. One can estimate for example for uranium the implant statistics by assuming the beam to be mono-energetic at the charge state distribution weighted mean energy of 131 keV. This energy is the product of a 50 keV extraction voltage and a mean charge state of 2.62 for uranium, based on

Table 6. MEVVA Implant Parameters
(after Brown et al, 1988)

Ion	Extraction Voltage (keV)	mean charge state (particle-current)	charge state distribution percentage				weighted mean energy (keV)
			1+	2+	3+	4+	
U	50	2.62	3	38	54	5	131
Th	50	2.92	3	15	70	12	146
Ho	50	1.93	15	76	9	0	97
Yb	-	-	-	-	-	-	140

particle current (Brown et al, 1988a). This information is given in Table 6 including the charge state distribution for all the implanted ions (most of this data was not available for Yb). The dosage for U, Th, and Ho was $7.5 \pm 2 \times 10^{13}$ ions/cm² and for Yb it was $5-10 \times 10^{13}$ ions/cm². The semiconductor targets, which were wafer pieces of different dimensions, were located at a distance of 45 cm from the ion source extractor and tilted off normal by about 10° to reduce channeling. The cryogenically pumped and oil free vacuum system maintained a main chamber pressure of 1×10^{-6} torr. Due to the low dosage, it was assumed that the samples were near room temperature during implantation.

Post-Implantation Sample Treatment

To remove the defects generated by the implantation process, the samples had to be annealed. First, the samples or wafer pieces were cut further to approximately 5 mm X 5 mm squares with the diamond stylus of a manual dicer/cutter assembly at the Avionics Lab, WPAFB, OH. A limited sample set was also encapsulated with Si₃N₄ prior to annealing. The

encapsulation, performed also at the Avionics Lab, was through plasma enhanced deposition and resulted in a 100 to 200 nm thick layer which remained stable up to a 750°C conventional annealing temperature after which it rapidly degraded.

Prior to encapsulation and annealing the samples were again cleaned with trichloroethylene, acetone, methanol, de-ionized water, and blow-dried with nitrogen gas. Annealing was through conventional furnace or rapid thermal annealing as depicted in Fig. 19. The majority of samples were annealed in a locally designed and constructed quartz tube positioned within a conventional annealing furnace (Lindberg oven) as shown in Fig. 19. A thermocouple (TC) was inserted into one end of the tube and sealed off with vacuum putty. The TC was connected to a Eurotherm controller where the anneal temperature was set and controlled. The gas 'inflow' was at the TC end while the gas 'outflow' was at the ball-and-socket end as seen in Fig. 19.

The conventional annealing procedure consisted of flushing the quartz tube with nitrogen while cutting a Si:P wafer to the size of the sample boat's dimensions and cleaning it with the same solvents as the samples themselves. The samples were set face-down onto the Si wafer in the sample boat. The clamp locked the ball-and-socket and the boat was initially kept out of the furnace. The flushing with nitrogen gas continued for 10 minutes before turning on

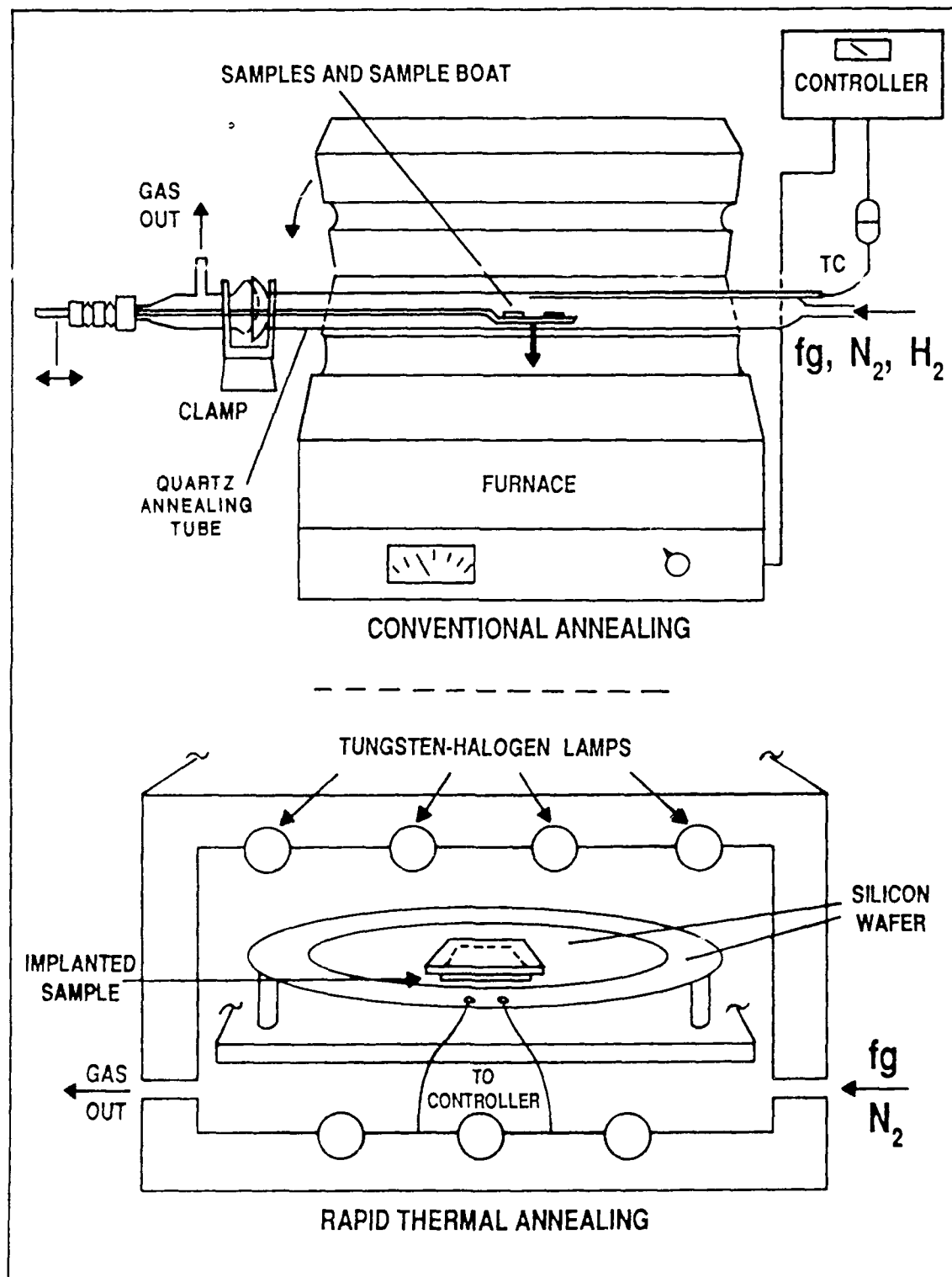


Figure 19. Sample annealing methods.

Anneal Furnace Characteristics

Anneal Time (min) vs. Temperature (C)

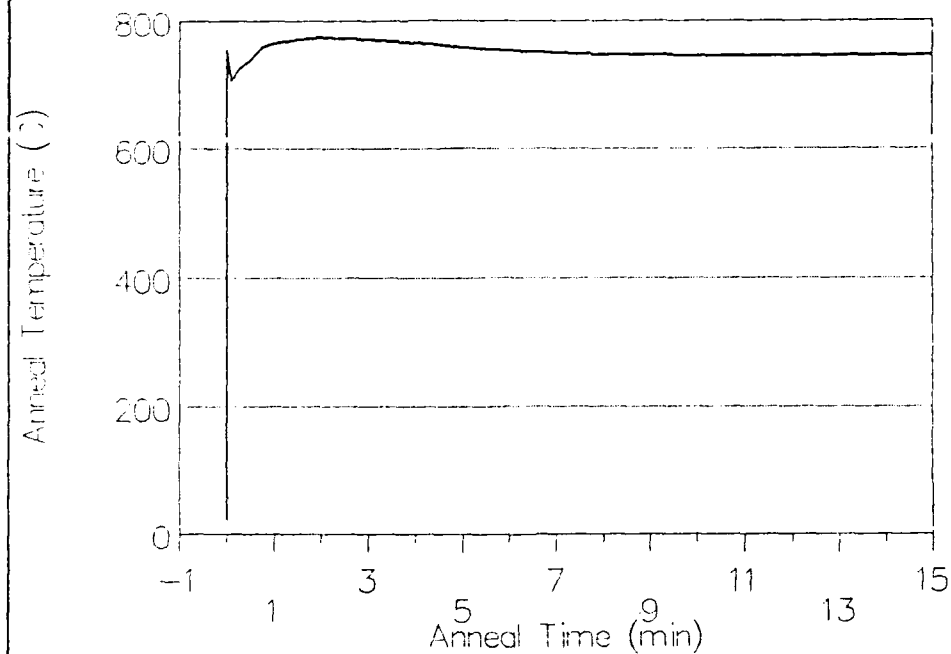


Figure 20. Conventional anneal furnace temperature profile for a 750°C anneal.

the forming gas or hydrogen (dependent on which was available, although forming gas was desired). After the furnace was turned on and the desired temperature was achieved, the sample boat was inserted into the center of the furnace for usually 10 or 15 minutes. After this time the boat was withdrawn, and the furnace was shut-off and allowed to cool to 450°C before turning off the forming gas or hydrogen and turning on the nitrogen. The samples were removed once a 250°C reading was reached at the TC. A

typical furnace temperature profile with time is shown in Fig. 20 for a 750°C anneal. As can be seen in the figure, once the boat is inserted the temperature drops, recovers past 750°C, and eventually stabilizes around the desired temperature.

A substantial number of the Yb implanted and incorrectly Pr implanted samples were annealed using the rapid thermal annealing technique. This method used a microprocessor controlled and water cooled AG Associates Heatpulse 210T system in which high-intensity, visible light produced by arrays of tungstens-halogen lamps was used to heat the samples (see Figure 19). The Heatpulse 210T was located in a class 100 clean room at the Avionics Lab and could only be accessed by suiting up with the proper clean room attire.

The implanted samples were placed face-down on an identical but unimplanted substrate sample which was sitting on top of a 2 inch diameter Si:P wafer. (This wafer was used only as a protective measure to guard against contaminants as the annealing system belonged to the Avionics Lab and not to AFIT). As seen in Fig. 19 this Si:P wafer was furthermore sitting on top of a 'master' Si wafer which was interfaced with the microprocessor such that the temperature could be monitored. After placing the samples on the Si wafers, the loading door was shut and sealed and the system was purged with flowing nitrogen. After a few minutes the forming gas (95% Ar, 5% H₂) was turned on and allowed to purge the system for a few minutes before programming the system to initiate

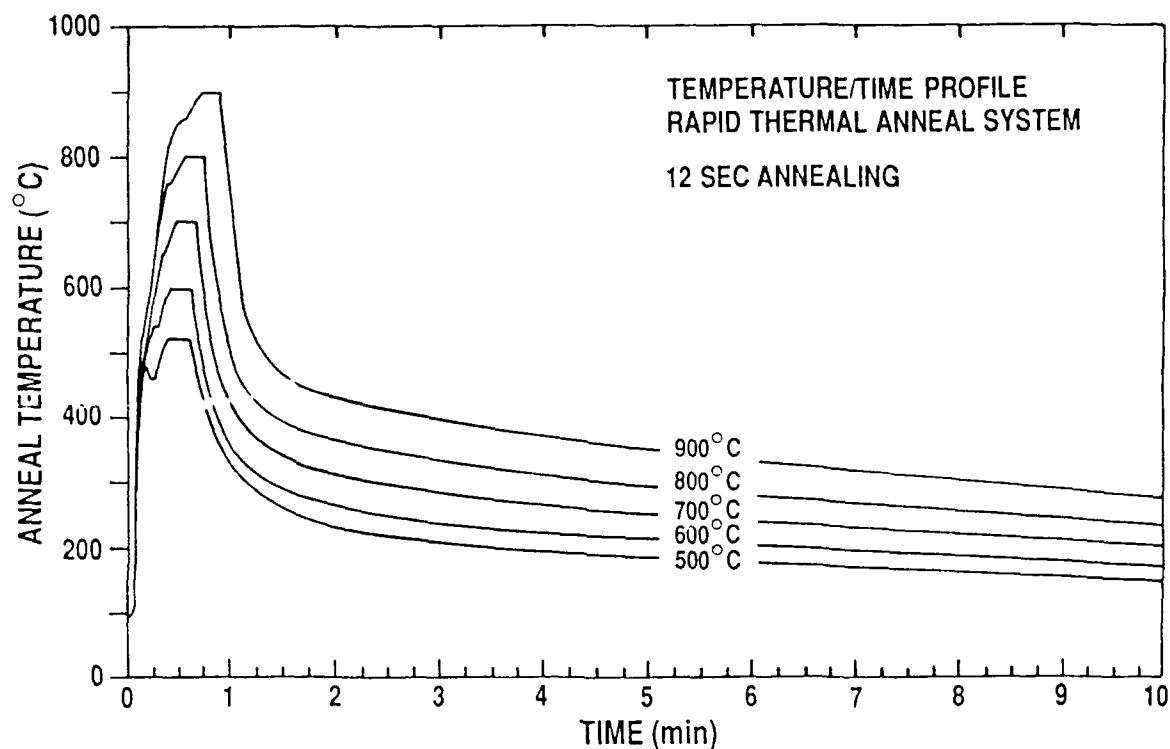


Figure 21. Temperature/time profile of the rapid thermal anneal system.

the annealing. Figure 21 shows the temperature versus time characteristics for five different annealing temperatures at 12 second anneal times. What must be recognized is that during the cool-down cycle, the samples continued to sit at elevated temperatures. Even when annealing at 700°C for 12 sec the cool-down cycle takes 25 minutes until 150°C is reached; the recommended sample withdrawal temperature. It must also be recognized that the temperature versus time profile is for the master Si wafer and not necessarily for the implanted sample. As conventional annealing also yielded satisfactory luminescence results, allowed a more 'user-controlled' operating environment, and had a faster turn-

around time, the conventional technique was chosen over the rapid thermal annealing. However, depending on future resources, some of the conventional anneal studies performed in this study should be repeated with rapid thermal anneal studies.

Sample Mounting

After processing, the 5 mm by 5 mm samples were mounted onto the sample holder of the cryostat or helitran in each particular experiment. The actual mounting appears to be more of an art than a science. For the photoluminescence experiment up to eight (5mm X 5 mm) samples could be mounted on the locally designed and constructed stainless steel sample holder; four samples were usually mounted on the copper holder. Background spectra with the laser line impinging on the holder were taken to determine if any non-sample related emissions were present.

For the photoluminescence experiment which used a gas-exchange cryostat, only standard rubber cement was used in the form of 2 to 3 mm diameter beads on the center of the backside to the sample. After the sample was cycled through the experiment the rubber cement was removed with acetone, trichloroethylene, and again acetone. Experience has it that small daps of vacuum grease could also be used, but it complicates the post-experiment cleaning; also small daps of dilute GE varnish could be used but it requires extended soaking of the sample in acetone to remove it from the sample

holder. The varnish also increases the probability that a sample will crack due to thermal stresses in cycling the samples through the cryostat.

In the selective excitation experiment, aside from fastening the samples with rubber cement, screw mounted copper masks were also used to hold the samples in place. Since the samples were located in a depression of the copper mounting block, extreme care had to be taken in removing them.

For lifetime measurements the samples were located on a solid copper mount screwed tightly into the stem of the Heli-tran system. To insure a good thermal contact the sample was mounted both with a small bead of eutectic mixture and a 2 to 3 mm diameter dab of a 1:1 mix of vacuum grease and silver paste. The eutectic mixture consisted of 63% gallium (donated by the Avionics Lab), 22 % indium, and 15% tin. The eutectic mixture was removed from the sample with HF, and the vacuum grease and silver paste was removed with rubbing and the organic solvents used in sample cleaning. The effects of stress due to mounting on the 4f-emissions is not ruled out; however, due to the somewhat low resolution used in recording most spectra, stress effects remain essentially unobserved.

SIMS

The secondary ion mass spectrometry (SIMS) on rare earth ions implanted into semiconductors was a collaborating effort with J. Solomon at the Material Lab on WPAFB, OH. The effort concentrated on rare earth implanted InP although some GaP

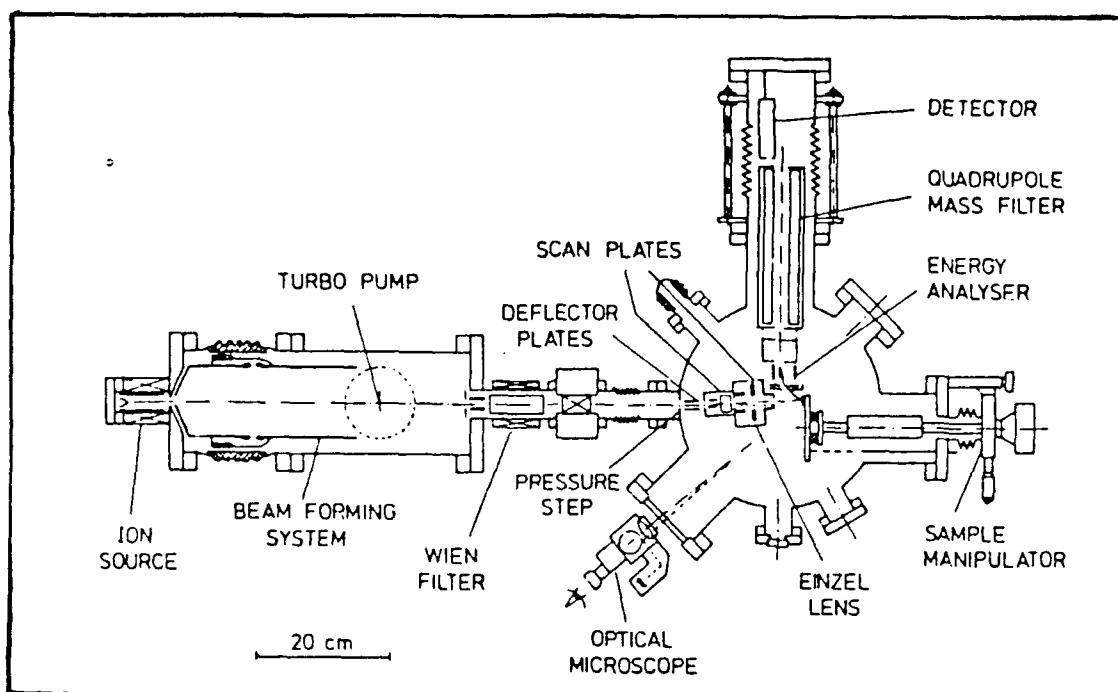


Figure 22. Cross-section of the DIDA ion microprobe (Wittmaack, 1982)

samples were also examined. The system was locally constructed out of equipment primarily from Atomika and Physical Electronics. The system is functionally and physically similar to the dynamic in-depth analyzer (DIDA) depicted in Fig. 22 (Wittmaack, 1982). The ion beam source was a mass-filtered, neutral-trapped model WF610 Atomika A-DIDA system which was operated with an oxygen beam potential of 12 kV at 2° to the surface normal of the sample. Typical beam current was on the order of 0.5 microamp which was measured on the metal sample holder. The secondary ion detector consisted of a parallel plate analyzer fitted to an Extrel C150 quadrupole mass spectrometer with an energy

resolution of 1 to 2 eV (Solomon, 1987). The system was typically brought to a base pressure of 1×10^{-9} torr.

After loading a single rare earth implanted sample and evacuating the system, the potentials to the various elements of the energy analyzer were set and the quadrupole analyzer was set for the mass of the particular rare earth which was to be investigated. The secondary ion current signal was electrically gated for 30% of the 0.13 mm^2 rastered area to minimize crater edge effects. The sputter yield with a 0.1 microamp beam was 2.4 atoms per ion. The samples were flooded with electrons from an electron gun during the analysis to prevent charging. Scan time was usually 5 seconds and 2 scans per ion peak were normally performed.

Prior to depth profiling many of the samples were initially sputtered by the oxygen beam to remove a 10 nm layer which could contain a substantial amount of oxides. A typical crater depth was determined to be 600 to 1000 nm deep as measured with a Dektak Surface Profiler; sputtering time for such craters was approximately 900 seconds. Typical sputter rates were 47 nm/min for GaP and 68 nm/min for InP.

The actual SIMS analysis and the resulting depth profiles (the first time such SIMS data reported for rare earth implanted semiconductors) will be appropriately presented in the results and discussion section to this document; however, the calculated (through the TRIM code) and measured projected range and straggling, plus the

Table 7. Calculated and Measured Implant Parameters in as-implanted InP

Ion	Z	Implant	Calculated		Measured		Implant	Peak
		Energy (keV)	Rp (nm)	ΔR_p (nm)	Rp (nm)	ΔR_p (nm)	Dosage (cm ⁻²)	Concentration (atoms/cm ³)
Pr	59	380	105.6	45.2	78	44	5X10 ¹³	1.8X10 ¹⁸
Ho	67	1000	220.9	77.0	221	98	3X10 ¹³	0.5X10 ¹⁸
Er	68	1000	216.0	75.6	245	105	5X10 ¹³	0.9X10 ¹⁸
Tm	69	390	89.9	31.0	98	90	5X10 ¹³	1.8X10 ¹⁸
Yb	70	1000	209.8	73.1	208	82	3X10 ¹³	0.6X10 ¹⁸
U	92	131	36.6	13.8	30	*	7±2X10 ¹³	8.0X10 ¹⁸

* not measured

measured peak concentration are presented in Table 7 for most of the rare-earth and semiconductor systems considered in the study.

Data collection and analysis was performed through various FORTRAN programs on an upgraded Z-100 computer system. The data was stored in standard ASCII files and may therefore be accessed by various commercial software. Finally, it should be reiterated that besides determining the rare earth depth profile and implant statistics, the SIMS analysis also performed the important service of verifying the implanted ion and determining the isotope distribution of the implanted rare earth.

IV. Results and Discussion

The luminescence investigations were divided into a series of three experiments which included photoluminescence, selective excitation studies, and lifetime measurements. What follows is a report and discussion of results for the various lanthanides and actinides which were analyzed with these three techniques. Due to the various factors which controlled the experiments a substantial part of the study concerns itself with the photoluminescence of the rare-earths (lanthanides) implanted into the III-V semiconductors.

A. Photoluminescence

This part of the study attempted to extend the present level of understanding of the rare-earth ions ytterbium and erbium in the III-V semiconductors, and for the first time investigate these lanthanides in the AlGaAs matrix. It was also attempted to investigate for the first time the rare-earth ions thulium and praseodymium, and compare the results with those of Yb and Er. Furthermore, the first luminescence investigations of actinides, specifically uranium and thorium, were undertaken. The photoluminescence investigations also served somewhat as a foundation for the selective excitation and lifetime measurements as the implanted semiconductors had to be characterized properly prior to using these techniques to understand the more dynamic processes.

Photoluminescence of Yb^{3+}

Among the investigations of rare earth ions in III-V semiconductors, ytterbium has received considerable and probably the most focused attention up to date. This study is concerned with further understanding the luminescence characteristics and processes of the 1.0 μm emission of Yb in the III-V semiconductors and AlGaAs. Ytterbium incorporated into InP is of special interest as it exhibits a very intense signal, the somewhat uncomplicated spectrum arises predominantly from one type of cubic Yb^{3+} center, and the system exhibits a simple electronic structure ($4f^{13}$, a single hole in the 4f-shell). Furthermore the interest in studying the InP:Yb system is enhanced by the availability of theoretical calculations, electrical data, and a series of in-depth studies on the luminescence and dynamic processes of InP:Yb.

Numerous studies have been performed on ytterbium incorporated into III-V semiconductors, specifically Yb in indium phosphide. The studies can be divided essentially into five areas: spectroscopy, electrical (Zakharenkov et al, 1987; Lambert et al, 1988; Whitney et al, 1988; and Raczynska et al, 1988), crystal synthesis or growth (Koerber et al, 1986; Nakagome et al, 1987; and Uwai et al, 1987b), theory (Hemstreet, 1986), and application (Haydl et al, 1985). This investigation shall only be concerned with the spectroscopic investigations, which in-themselves can be further subdivided into luminescence, excitation, and

lifetime measurements. The latter areas being discussed in the appropriate sections to this dissertation. As has been mentioned, investigations in the past of the rare earths have concentrated on ionic hosts (oxides and fluorides) and II_B-VI semiconductors; specifically relevant in this study is the work by Bryant and Nahum (1977) on the implantation of ytterbium into CdTe.

The 4f-intracenter emissions of Yb-implanted InP, GaP, and GaAs at 1.00 μm (1.24 eV) occur between the spin-orbit levels $^2F_{5/2} - ^2F_{7/2}$ of Yb^{3+} ($4f^{13}$) (Ennen et al 1985). First evidence of the 4f-emissions of Yb^{3+} in GaP was given by Kasatkin et al in 1981 for doped epitaxial films grown by molten solution. Spectra of Yb^{3+} in InP were reported by Zakharenkov et al (1981) from Yb doped InP layers also grown by molten solution. The characteristic sharp 4f-emissions at 1.00 μm were also observed in InP, GaAs, and GaP implanted with Yb at an energy of 350 keV (Ennen et al 1983). From the results of Zeeman measurements (Aszodi et al, 1985) and photoluminescence excitation spectroscopy on implanted InP:Yb (Wagner et al, 1984), it is concluded that the main Yb^{3+} center resides substitutionally on a cation site. For InP:Yb the dominant Yb^{3+} center has cubic symmetry (T_d); and a center with trigonal symmetry is sometimes also observed. The characteristic Yb^{3+} emission in InP was also observed in Yb-doped epitaxial InP layers grown by liquid phase epitaxy (LPE) (Haydl et al 1985) and metal organic chemical vapour deposition (MOCVD) (Uwai et al 1987a).

As indicated the transitions between the crystal-field split spin-orbit levels $^2F_{5/2} - ^2F_{7/2}$ of Yb^{3+} have also been observed in GaP and GaAs, but detailed investigations such as for InP:Yb have not followed. Of interest is the attempted spectroscopic study by Stapor et al (1986) of GaAs doped with Yb through LPE. It is claimed that Yb suppresses donor related optical transitions due to the gettering activity of the rare earth; possible total cleaning action of the rare earth is suggested which effectively prevents the proper incorporation of Yb into the crystal matrix and hence preventing the characteristic 4f-emissions to be seen. Although this gettering activity certainly appears to occur, this investigator believes that the Cr from the GaAs:Cr substrate, known for its rapid diffusion, is most likely also a factor in reducing the Yb emission; the chromium forming an associate with ytterbium, or the Cr emission itself competing with Yb. (It appears that the GaAs:Yb system is an interesting problem for further future investigations.)

In furthering the understanding of the ytterbium/semiconductor system numerous areas were investigated with a more application oriented point of view in mind, for example, it was attempted to establish the conditions for an optimum Yb^{3+} signal which would allow for follow-on studies such as selective excitation and lifetime measurements. First the three different III-V semiconductors were implanted to determine the reproducibility of the Yb^{3+} emission and to

compare the signal between the different hosts. Substrates with different conductivities were implanted to determine which doped substrate would yield the optimum signal and which substrate would yield different centers. The implantation was performed at high energy (1 MeV) to maximize the thickness of the implanted layer and therefore maximize the rare earth signal, and furthermore, to determine if high energy implants produce centers different from low energy implants (350 keV or 140 keV). Although a limited isochronal anneal study was reported by Ennen et al (1985), a more systematic conventional and rapid thermal annealing study was performed to establish the optimum rare earth signal and to monitor the emission lines for changes in intensity and energy. An isothermal study was also performed. Finally, Yb implants into AlGaAs of different Al mole fractions were investigated for the first time in order to observe the Yb³⁺ emissions.

The III-V semiconductor and AlGaAs samples which were processed and investigated are listed in Table 8; further sample information may be referenced in the experimental section through the 'identifier' code. All but the MR(338) InP samples were implanted at an energy of 1 MeV and a dosage of 3×10^{13} ions/cm². After implantation some sample sets were annealed face down on the same substrate but without encapsulation in the conventional annealing furnace in a flowing hydrogen (H₂) atmosphere. Other sample sets were annealed through the rapid thermal annealing (RTA) technique

Table 8. Sample Information for the Ytterbium Implanted Semiconductors.

Semiconductor	Conductivity Type	Identifier
InP	SI	MR(346)
	SI	MR(338)
GaAs	SI	CS
	SI	MA
	n	AC
	p	LD
GaP	n	GAC
	p	GPC
$Al_xGa_{1-x}As$	$x = 0.15$	EPI-513
	$x = 0.30$	EPI-514
	$x = 0.23$	MO-1719

with a high-intensity, visible light in flowing forming gas; annealing was also performed face down on the same unimplanted substrate and without encapsulation. Specific sample treatment conditions will be either given later in the text or referenced in a previous study (Colon, 1988). The (MR338) InP samples were implanted at low energy (140 keV) at a dosage of $5-10 \times 10^{13} \text{ cm}^{-2}$ through the new type of high current metal source. This Metal Vapor Vacuum Arc (MEVVA) ion source was originally developed to produce high current beams of metal ion species for synchrotron injection and is discussed in more detail in the experimental section and the section on actinides. SIMS analysis was performed on InP implanted with Yb to verify the rare earth impurity and to determine the depth profile parameters.

Shown in Figure 23 are the characteristic sharp 4f-

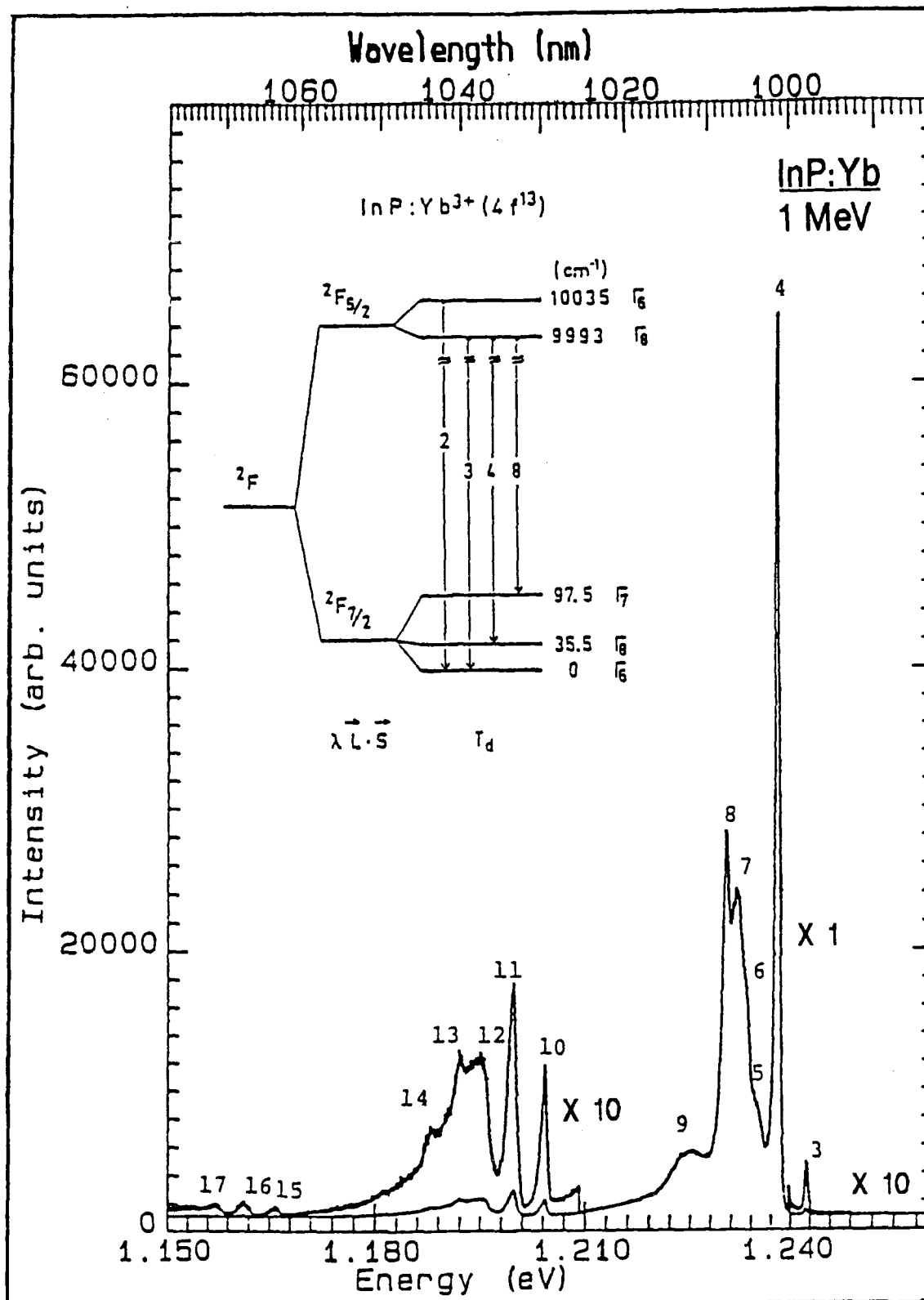


Figure 23. Luminescence spectra at 4.2 K and energy-level scheme for Yb³⁺ with T_d symmetry in InP.

emissions due to transitions at 1.00 μm between the spin-orbit levels $^2F_{5/2} - ^2F_{7/2}$ of Yb^{3+} in InP. The sample was (MR346) InP implanted at an energy of 1 MeV and a dosage of 3×10^{13} ions/cm², subsequently annealed at 850°C for 15 sec with the RTA method. The 4.2 K photoluminescence spectra was generated upon exciting with the 647.1 nm line of a Kr-ion laser at a power of 80 mW at the laser; resolution was 0.8 meV. The numbering scheme of the numerous emission lines is that followed by Ennen et al (1985). The energy level scheme for Yb^{3+} in T_d symmetry in the inset to Fig. 23, after Ennen et al (1985) and Aszodi et al (1985), identifies the transitions between the various crystal field states of the zero phonon lines (ZPL). Besides line 1 (not shown in the spectra of Fig. YB-1) which is associated with an Yb^{3+} center with trigonal symmetry, the remaining lines are phonon replicas or unassigned lines, but associated with the dominant cubic center. Table 9 tabulates and identifies the Yb^{3+} emission lines in Fig. 23; some of the phonon (ω) assignments relied on the study by Uwai et al (1987a). An averaged energy of 42 meV for longitudinal optical (LO) phonons was used, 39 meV for transverse optical (TO), and 7 and 8 meV for transverse acoustical (TA) phonons (Schulz and Weiss, 1981).

A high resolution spectra as shown in Fig. 24 was also taken for Yb implanted into InP at an energy of 140 keV with the MEVVA ion source. Sample excitation was with the 514.5

Table 9. Emission Line Assignment for Yb^{3+} in InP
(see Figure 23).

Line #	ZPL	phonon replica	peak wavelength (nm)	peak energy (eV)	center
1	ZPL		988.0	1.2549	trig
2	ZPL		993.0	1.2486	T_d
3	ZPL		997.8	1.2426	T_d
4	ZPL		1001.3	1.2382	T_d
5	?	? #3 - 1 w_{TA}	1003.8	1.2352	
6	?	? #3 - 1 w_{TA}	1005.0	1.2337	
7	?	?	1006.3	1.2321	
8	ZPL		1007.6	1.2305	T_d
9		? convolution of 1 w_{TA} phonons	1012.2	1.2249	
10		#3 - 1 w_{TO}	1029.3	1.2046	
11		#4 - 1 w_{TO} , or #3 - 1 w_{LO}	1033.3	1.1999	
12		#4 - 1 w_{LO}	1037.1	1.1955	
13		#8 - 1 w_{TO}	1040.0	1.1922	
14		#8 - 1 w_{LO}	1043.4	1.1883	
15		#3 - 2 w_{TO}	1063.3	1.1660	
16		#4 - 2 w_{TO}	1067.2	1.1618	
17		?	1071.4	1.1572	

nm line of the air-cooled Ar-ion laser with 50 mW at the laser; resolution was 0.5 meV using the 1.6 μm blazed grating with 600 gr/mm. When compared to the spectra of the 1 MeV implanted Yb into InP of Fig. 23, no significant changes are observed aside from the absence of line 3 (998.2 nm). Relative intensities remain unchanged. As suspected no new Yb centers appear to be generated with the low energy implant.

The somewhat limited spectral results for Yb-implanted GaAs and GaP do not allow for a good comparison spectra between the three III-V semiconductors. Hence, in Fig. 25 are the luminescence spectra of Yb-implanted and 750°C annealed GaP and GaAs after Ennen et al (1985). By comparing

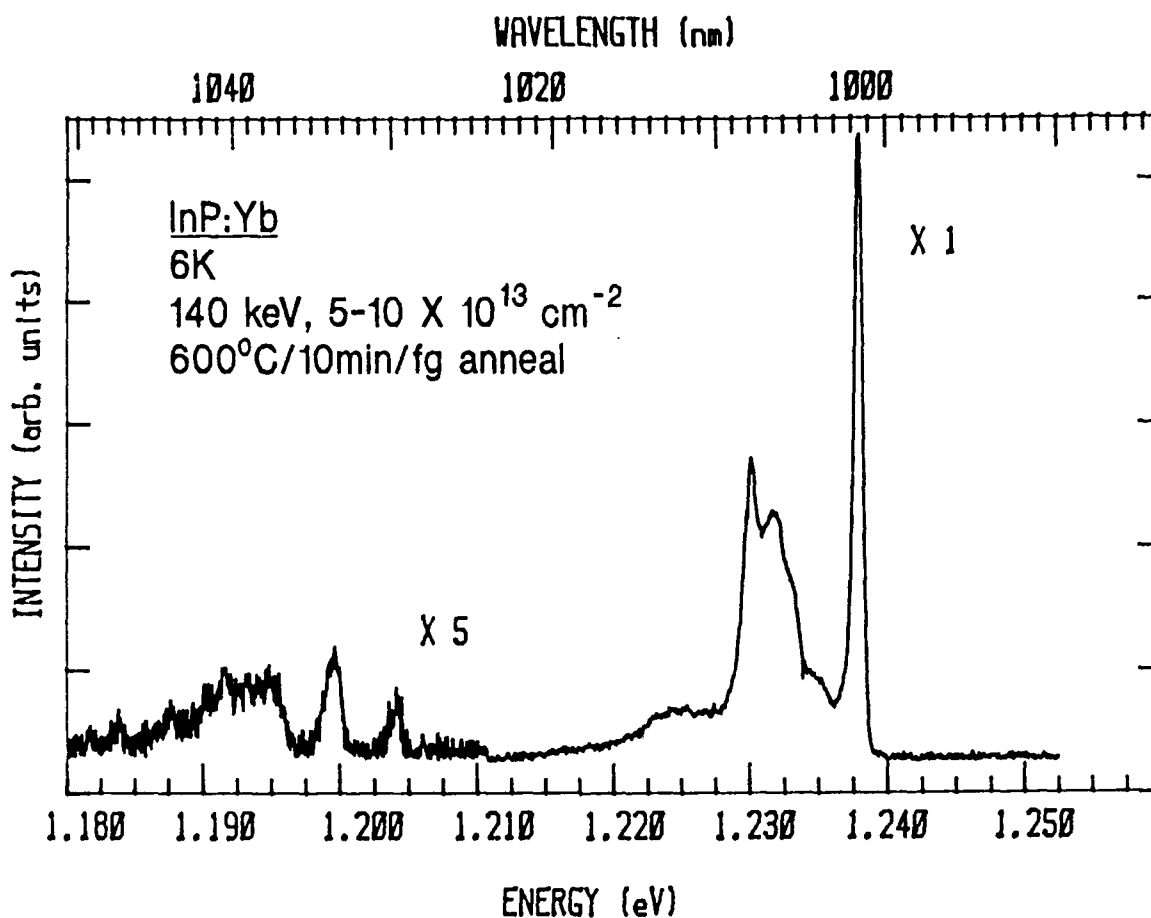


Figure 24. Photoluminescence spectra at 6 K of 140 keV Yb-implanted InP.

these spectra with the InP:Yb spectra of Fig. 23, it appears that the emission lines labeled 3, 4, and 8 in InP and GaP, have almost exactly the same energetic positions; but for GaAs:Yb a distinctly different Yb^{3+} spectrum is observed. It is concluded that the main Yb^{3+} center in InP, GaP, and GaAs is substitutional on a cation site (In or Ga).

As mentioned, one of the motivations for the study was to optimize the Yb signal in the III-V semiconductors through

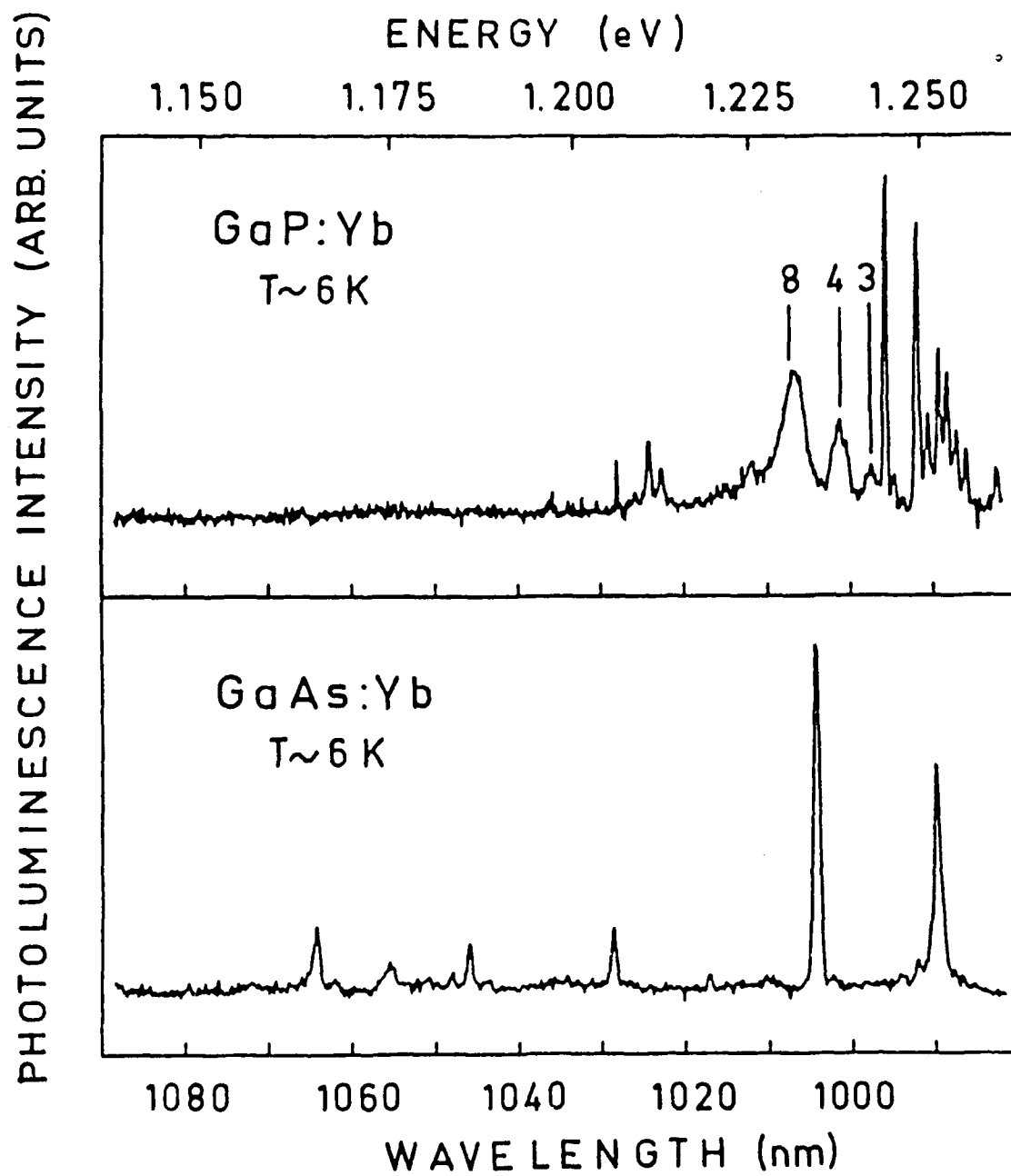


Figure 25. Photoluminescence spectra of Yb-implanted and 750°C annealed GaP and GaAs (after Ennen, Pomrenke, and Axmann, 1985).

isochronal and isothermal investigations. During these studies it was also the goal to monitor changes in the emissions as a result of the generation of new centers. Both isochronal and isothermal investigations were performed on InP implanted with Yb and subsequently annealed through RTA. Only isochronal studies were performed for the conventionally annealed 1 MeV and 140 keV implants. Figure 26 depicts the results of the isochronal studies by showing the integrated intensity of the 1001 nm (line 4, Fig. 23) emission as a function of anneal temperature. The excitation was with a 80 mW, 647.1 nm line of the Kr-ion laser; resolution was 2.7 meV. Four data sets were considered: 10 sec RTA of 1 MeV Yb implants, 15 sec RTA of 1 MeV Yb implants, 15 min conventional anneal of the 1 MeV Yb implant, and a 10 min conventional anneal of the 140 keV Yb implant. Immediately obvious is that the higher the anneal temperature the more optimum the Yb signal, which differs somewhat from previously reported results for isochronal anneal studies on erbium (Pomrenke et al, 1986). For Er implanted into III-V semiconductors the signal tends to decrease as one anneals past 750°C. The difference may be a result of multiple Er centers, whereas, at least for InP:Yb, there is only one dominant Yb center. Certainly Fig. 26 indicates that the optimum anneal condition is for the 875°C and 10 sec annealed sample using the RTA technique. However, little difference exists between the data sets at the specific anneal temper-

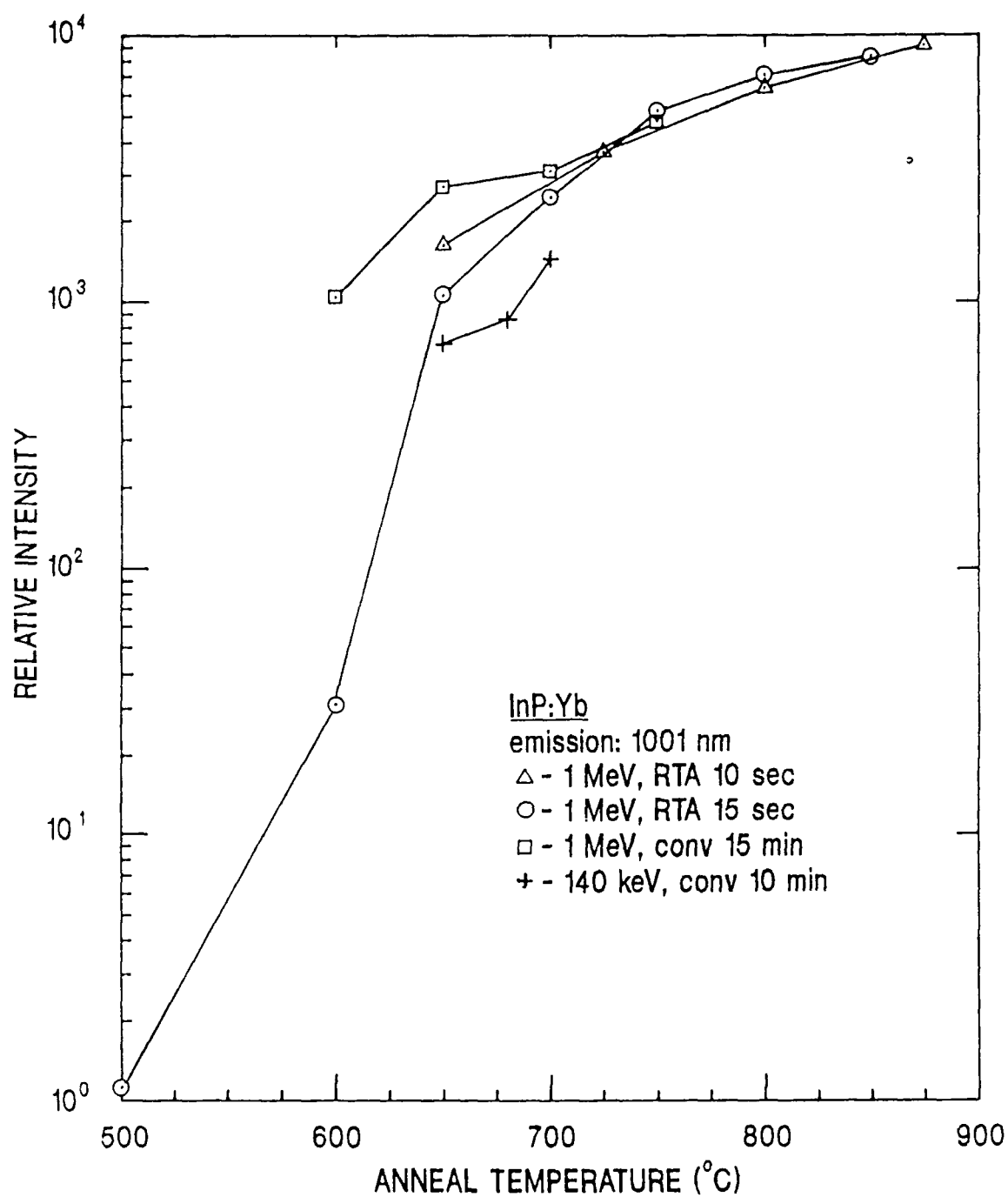


Figure 26. Isochronal anneal study at 6K of Yb implanted InP. The anneal temperature was varied from 650 to 875°C. The conventionally annealed samples were not annealed above 750°C since this temperature

represents the typical limit to which InP is annealed before severe surface degradation sets in due to outdiffusion of its constituents. Relatively good surface morphology was maintained up to 875°C upon using the RTA method.

A significant difference exists for the conventional versus the RTA anneals at temperatures below 650°C. The signal for the RTA drops precipitously after 650°C by almost two orders of magnitude whereas the Yb signal for the 600°C conventionally annealed sample has not changed by more than 25% from 650°C. This difference lies in the anneal time. It should be noted that the intensities between the low and high energy samples only vary between a factor of 2 to 3. Significant also is that Yb becomes optically activated already at 500°C; optical activation was not observed at 400°C. No changes in relative intensities and shifts in energies of the Yb-emissions were observed at the 2.7 meV resolution as the anneal temperature was changed.

An isothermal anneal study was performed on samples annealed at 850°C through rapid thermal annealing; the time was varied from 1 to 25 seconds. Figure 27 shows the integrated intensity of the 1001 nm line versus the anneal time and indicates that the optimum time is the longest time (25 sec). Since the 15 sec anneal did not vary significantly from the 25 sec anneal, it was chosen due to various practical factors in operating the RTA facility to be the

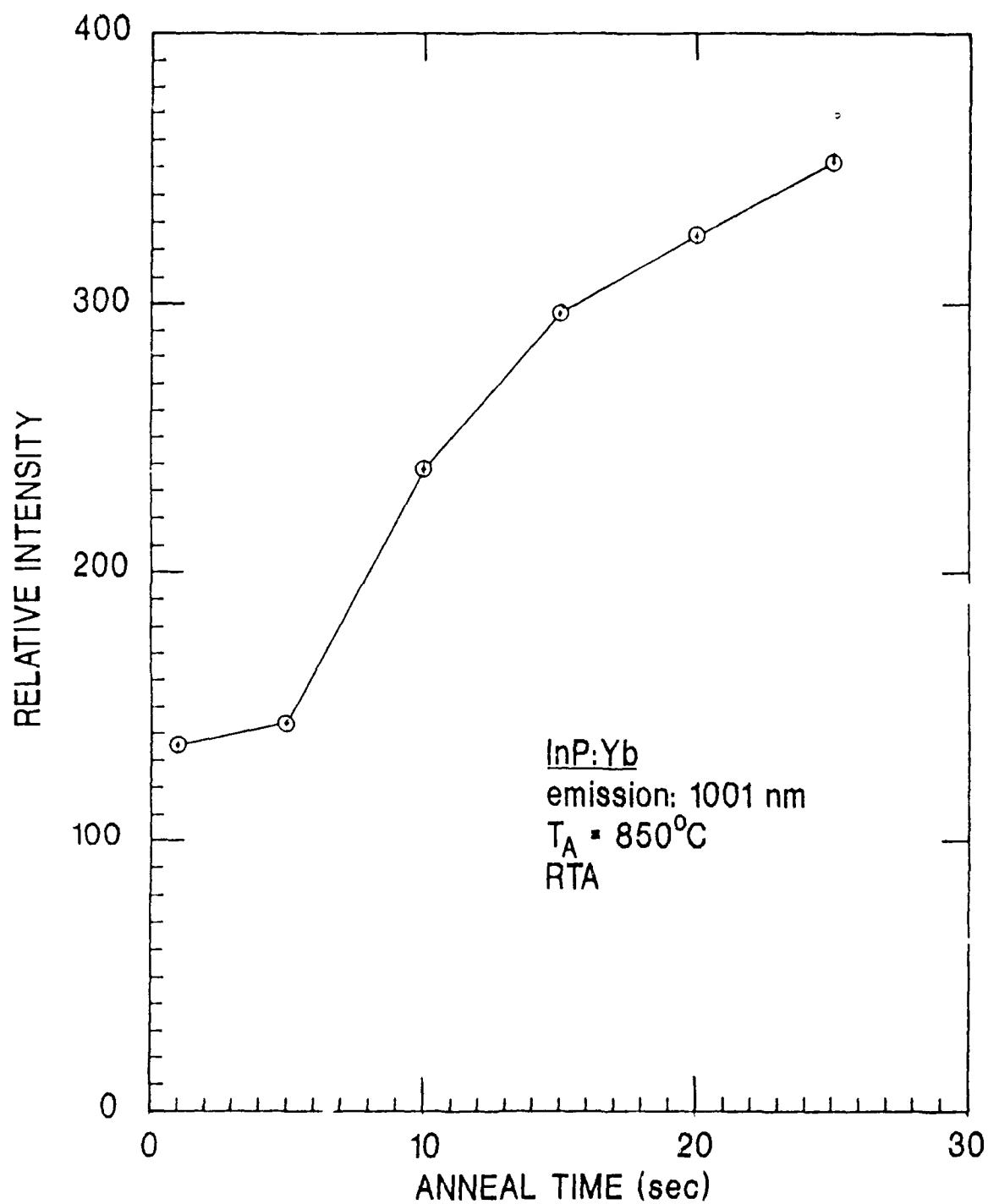


Figure 27. Isothermal anneal study at 6 K of InP implanted with Yb at an energy of 1 MeV.

anneal time for the main sample set in the isochronal anneal study. As for the anneal temperature dependent study, no significant changes were observed in energy or relative peak intensity of the emission spectra as the anneal time was varied.

The study was somewhat limited in making significant comparisons between Yb implanted InP, GaP, and GaAs, since the Yb^{3+} emissions in GaP were extremely weak and effectively unobservable in GaAs. Essentially only isochronal anneals were performed in these two materials, primarily aimed at observing a measurable signal instead of arriving at an optimum signal. As shown in Table 8 both n- and p-type GaP were implanted with Yb; post-implantation RTA annealing was at 600, 750, 800, and 850°C for 15 sec. Figure 28 shows the Yb^{3+} emissions in GaP(S):Yb for the isochronal anneal study; sample excitation was with the 50 mW, 514.5 nm line of the air cooled Ar-ion laser and resolution was 2 meV. The Yb becomes optically activated at 750°C and is maximized at 850°C. Three emissions (labeled A, B, C) evolve around 1.0 μm plus two weaker emissions at somewhat higher and lower wavelengths (D and E). By comparing the Yb^{3+} luminescence spectra of GaP(S):Yb and InP:Yb (Fig. 23) it is seen that the emission lines A, B, C and 3, 4, 8 have practically the same energetic positions. This can also be seen by comparing the GaP(S):Yb spectra with the GaP:Yb spectra in Fig. 25; the difference with GaAs:Yb should again be noted. Emissions D and E can be associated with low and high energy bands to

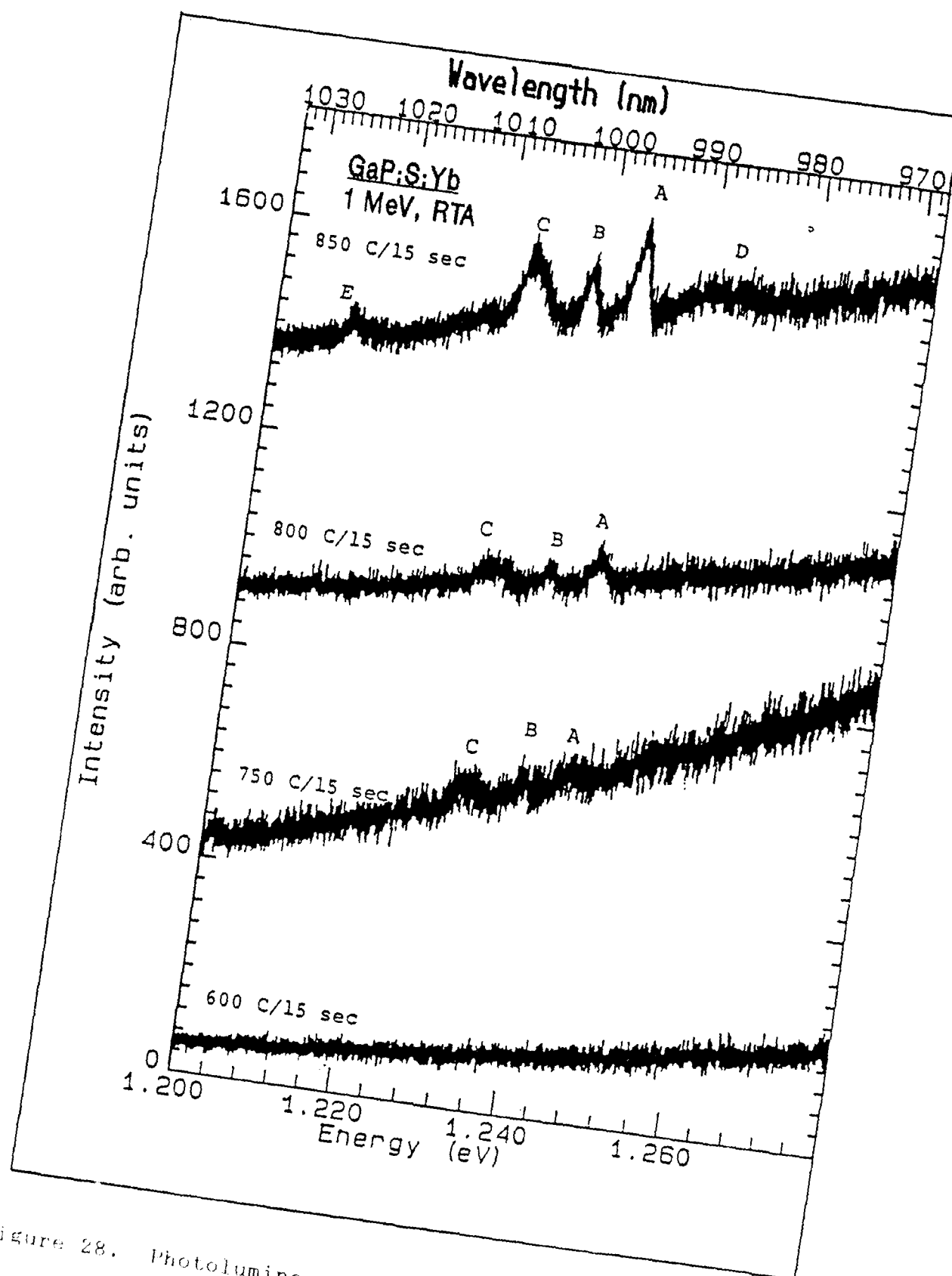


Figure 28. Photoluminescence at 6K of Yb^{3+} in n-type GaP.

3, 4, 8 in the GaP:Yb spectra of Fig. 25 and are most likely from a non-cubic Yb center. It is again concluded that the main Yb^{3+} center in InP, GaP, and GaAs is substitutional on a cation site (In or Ga).

Essentially no Yb^{3+} emissions were observable for p-type GaP (GaP:Zn). Aside from the fact that a broad background emission was present around 1.0 μm which might mask the signal, most likely the Yb^{3+} emission was not observed due to the high p-type conductivity of the host. As shall be discussed in a later section, free-carriers are associated with exciting the rare-earth. It should again be mentioned that the investigations by Ennen et al (1985) utilized n-type GaP (GaP doped with Te). The importance of choosing the proper substrate for implantation is stressed.

As shown in Table 8, semi-insulating, n-type, and p-type GaAs implanted with Yb was investigated. Post-implantation annealing temperatures, using both conventional and RTA annealing, varied from 600 to 975°C. Only extremely weak emissions were observable in two samples. For the 650°C and 15 min annealed SI-GaAs sample, limited evidence is given of Yb^{3+} emissions located at the same wavelengths as the two strongest emissions of GaAs:Yb in Fig. 25. For Yb implanted n-type GaAs, a weak emission is observed at 1.244 eV, which is located at the same energy as the main emission in the GaP:Yb spectra of Fig. 25. This is possible evidence of multiple Yb centers in GaAs. The fact that emissions are

observable again in n-type material versus p-type material emphasizes the importance in understanding the excitation mechanism and choosing the proper substrate material.

The investigations of AlGaAs were performed with RTA post-implantation annealing ranging from 500 to 975°C. First evidence of Yb³⁺ emissions in Al_xGa_{1-x}As of different Al mole fractions (x= 0.15, 0.23, and 0.30) is given in Figures 29, 30, and 31. The spectra for Al_{.15}Ga_{.85}As implanted with 1 MeV Yb is shown in Fig. 29 for 15 sec RTA anneals; two samples underwent single anneals while the other two samples underwent double anneals. For the double anneals the order of the temperatures indicates the anneal sequence, in other words, 600°C + 950°C means that the sample was first annealed at 600°C and then again at 950°C. Ytterbium becomes optically activated at 800°C and effectively only one emission is seen at 997 nm (1.244 eV), although a weak intensity, low energy peak appears to develop at 1008 nm with the 975 + 500°C anneal. The 996.7 nm emission is located at the same wavelength as that for the n-type GaAs:Yb case (not depicted). It should be noted that the 5 μm thick Al_{.15}Ga_{.85}As layer was measured by the vendor (Epitronics) to show an unintentional doped n-type conductivity.

The only evidence of Yb³⁺ emissions in Al_{.23}Ga_{.77}As is given in Fig. 30 for a 800°C and 15 sec RTA anneal. Samples were annealed from 600 to 975°C, including two double RTA

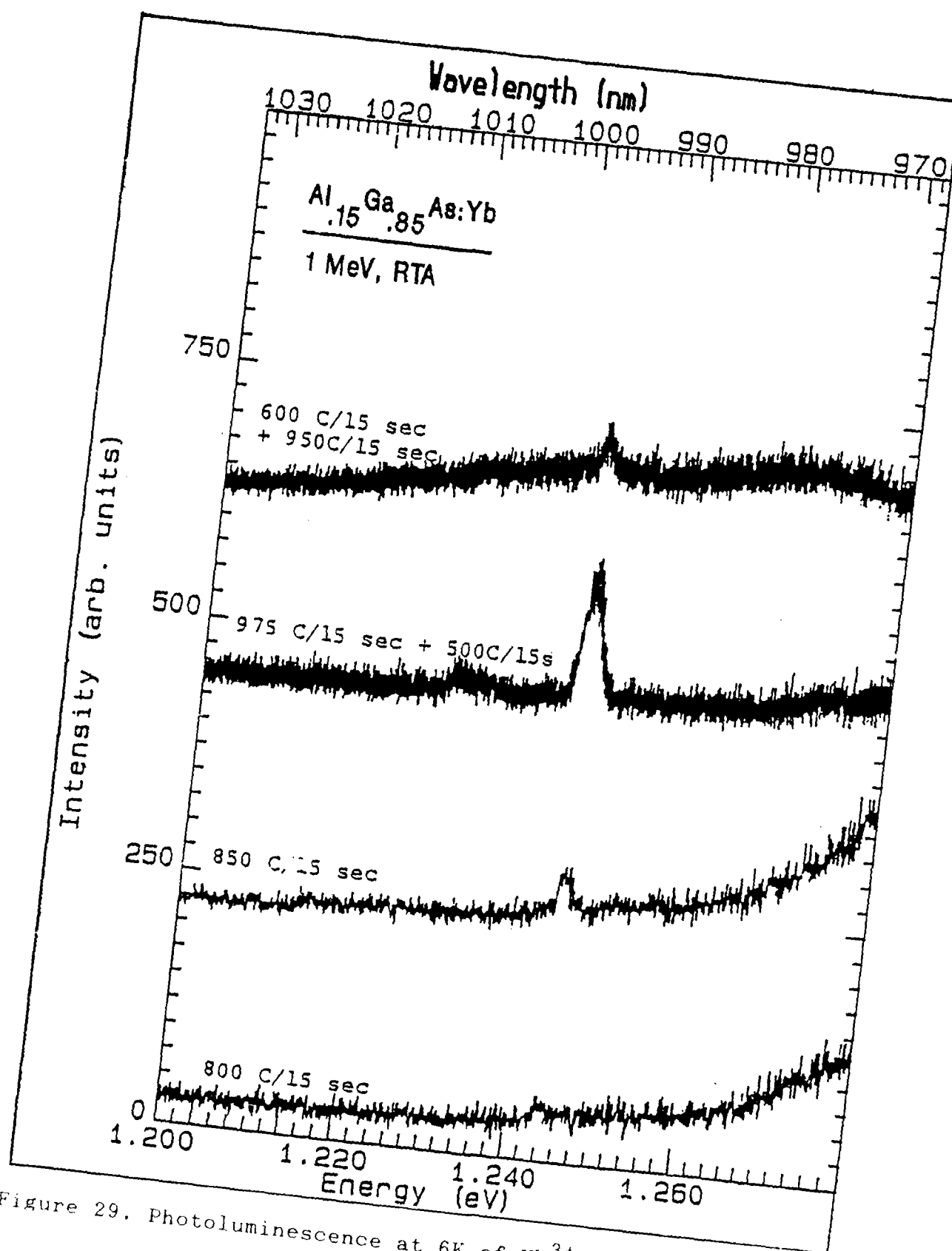


Figure 29. Photoluminescence at 6K of Yb^{3+} in $\text{Al}_{.15}\text{Ga}_{.85}\text{As}$.

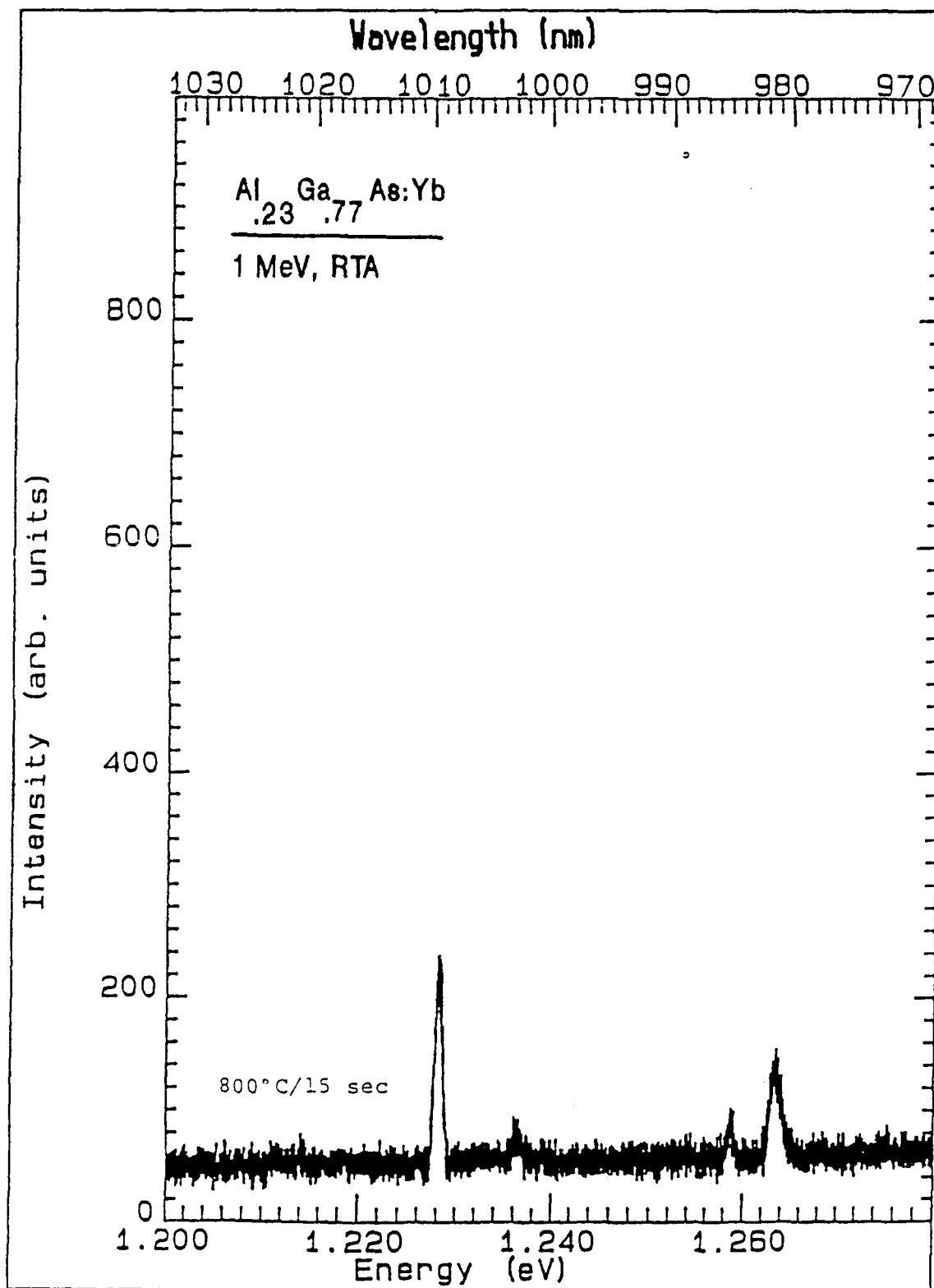


Figure 30. Photoluminescence at 6K of Yb^{3+} in $\text{Al}_{0.23}\text{Ga}_{0.77}\text{As}$.

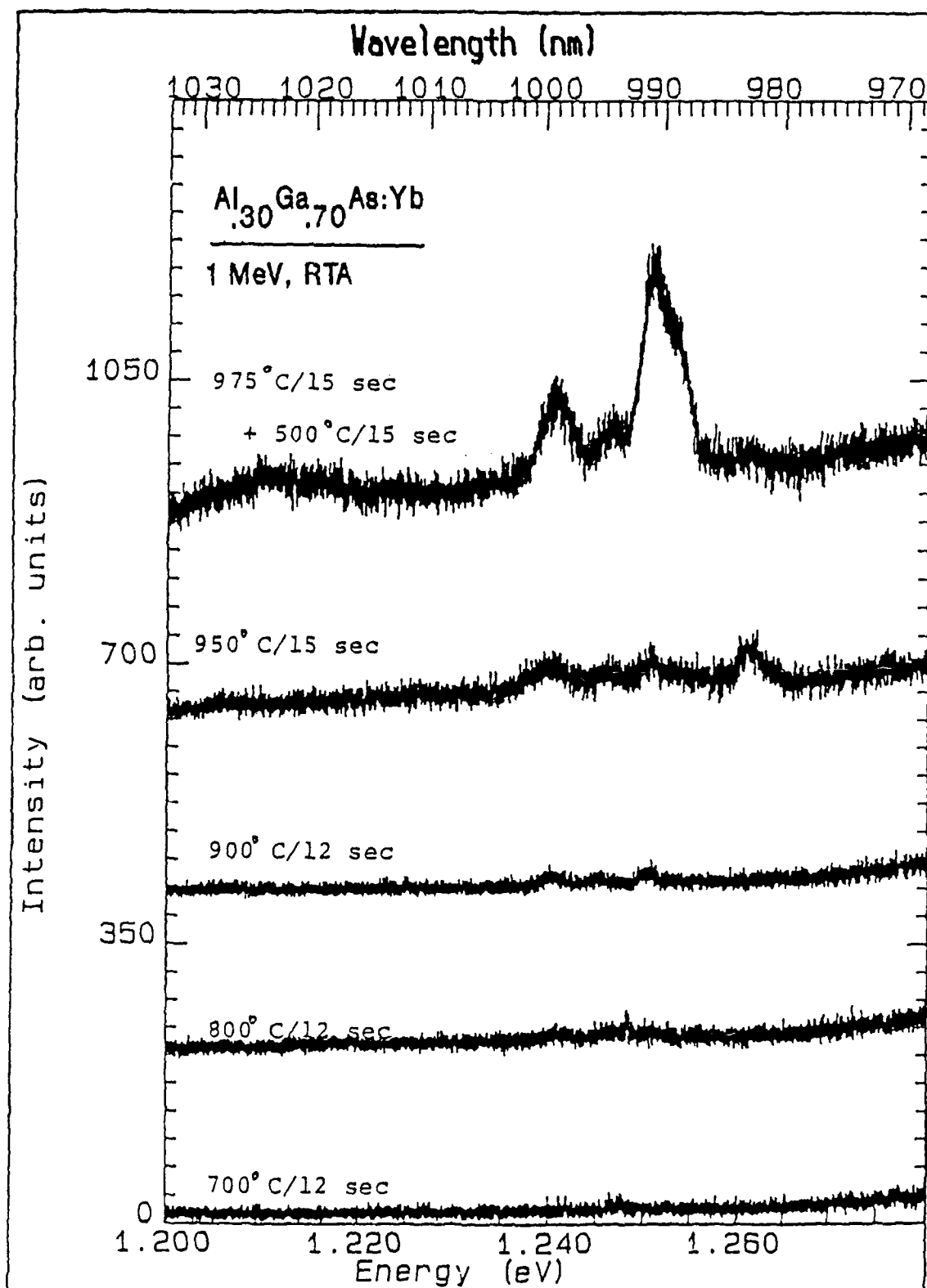


Figure 31. Photoluminescence at 6K of Yb^{3+} in $\text{Al}_{0.30}\text{Ga}_{0.70}\text{As}$.

anneals (600 + 950°C and 975 + 500°C). Besides the emissions pictured in Fig. 30, peaks were also seen at 1041.8 nm and 1044.5 nm. Apparent is the significant difference in energy position and shape from the Yb^{3+} emissions of $\text{Al}_{.15}\text{Ga}_{.85}\text{As}$ (Fig. 29). These differences cannot be explained at this time aside from the fact that the $\text{Al}_{.23}\text{Ga}_{.77}\text{As}$ layers were grown by a different vendor (Spire) resulting in material of possibly considerable difference in quality and residual impurity concentrations. The conductivity of the ternary layer is not known. (Although more Yb ions might be occupying Al sites, it is believed that this difference is not substantial enough to account for the difference in emission structure.)

The Yb^{3+} emissions in $\text{Al}_{.3}\text{Ga}_{.7}\text{As}$ are shown in Fig. 31 for different anneal conditions. RTA anneals were performed from 500 to 975°C for 12 or 15 sec anneal times. The ternary layer is 6 μm thick, unintentionally doped p-type conductivity, and grown by Epitronics. The Yb appears to become activated not until an anneal temperature of 900°C is used. Again the best anneal condition is achieved with a double anneal of 975°C/15 + 500°C/15 sec; however, more emissions are seen than for the case of $\text{Al}_{.15}\text{Ga}_{.85}\text{As}$. Emissions are located at 983.2, 991.9, 995.1, and 1000.7 nm; no overlap occurs with the 996.7 nm emission of $\text{Al}_{.15}\text{Ga}_{.85}\text{As}$. However, overlap does occur with the emissions of GaP(S):Yb . These differences can possibly be explained qualitatively by

assuming the main Yb^{3+} center as being substitutional on a cation site, Ga or Al. At the higher Al mole fraction ($x = 0.3$), the Yb ions located at cation sites after implantation and annealing can feel more effects of the presence of Al ions in their environment, and thus, the difference in the crystal-field generates the difference in the emissions.

Figure 32 shows the results of SIMS depth profile analysis on InP implanted with Yb. Depicted is the theoretical distribution (solid line) for the 1 MeV energy and $3 \times 10^{13} \text{ cm}^{-2}$ dosage Yb implants as determined from the R_p (209.8 nm) and ΔR_p (73.1 nm) calculated by the TRIM code (Ziegler et al, 1985). Also shown are the depth distributions of the Yb ion for implanted but untreated InP (as-implanted); for Yb implanted InP annealed conventionally (FA - furnace anneal) at 750°C for 15 min in forming gas; and for Yb implanted InP annealed through RTA at 750°C for 15 sec. The SIMS analysis verified the presence of the Yb ion in the InP matrix and allowed for the experimental determination of a projected range, R_p , of 208 nm and a straggling, ΔR_p , of 82 nm; this is in good agreement with the theoretically calculated values. As seen in the figure, Yb appears to diffuse 'into' the InP substrate after annealing instead of outdiffusing toward the surface. Depth distribution results are similar for both the conventional (FA) and RTA anneal case.

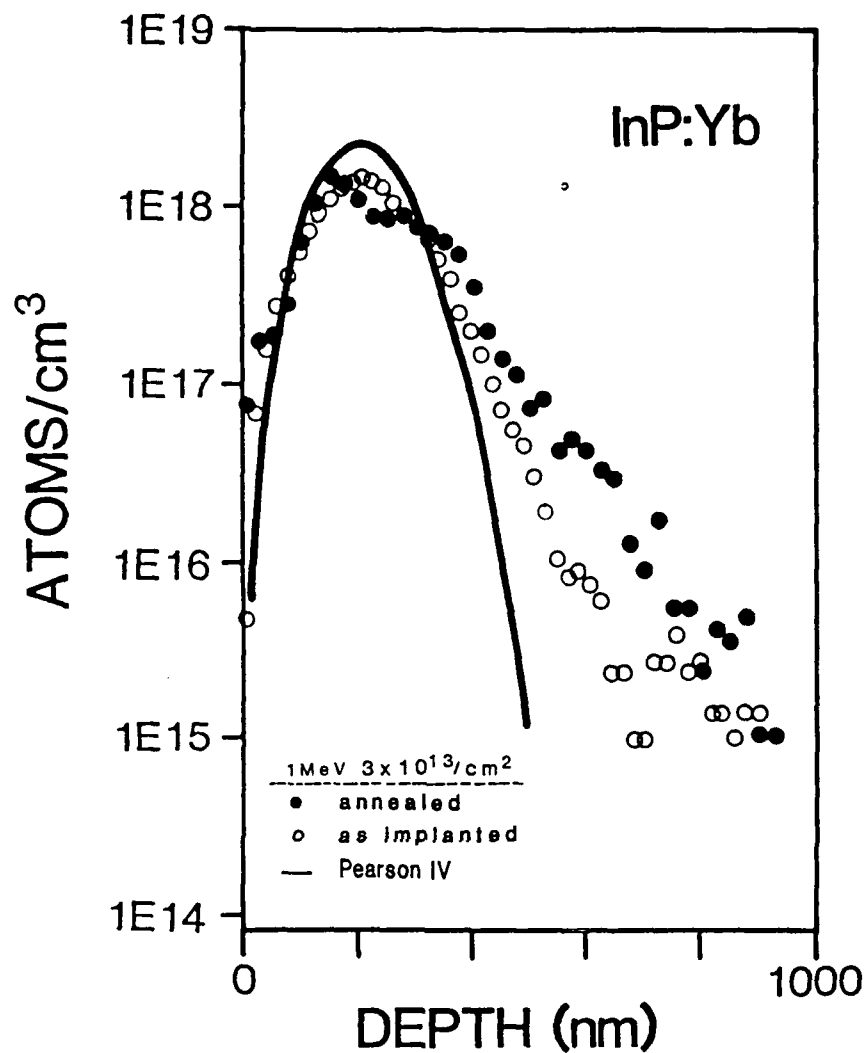


Figure 32. SIMS depth profile of Yb implanted InP.

In conclusion, very sharp and strong 1.0 μm Yb^{3+} emissions were seen in InP for the first time for 1 MeV and 140 keV implants. The emissions are assigned to transitions between the crystal-field split spin-orbit levels $^2F_{5/2} - ^2F_{7/2}$ of Yb^{3+} . Conventional annealing and rapid thermal annealing are viable techniques for post-implantation annealing in the 650 - 750°C and 650 - 875°C range,

respectively. Optimum optical activation for InP:Yb was obtained using RTA at 875°C for 10 sec but a 25 sec anneal will further increase the intensity as based on the isothermal study. The intensity of the InP:Yb emissions of the 140 keV implants were only 2 to 3 times weaker than those for the 1 MeV implants. The Yb implant and the associated depth distribution statistics were confirmed through SIMS.

In all semiconductors, except for InP, the Yb appears to have more than one center. The Yb^{3+} emissions for GaP, GaAs, and AlGaAs also appear to be considerably weaker in intensity than for the case of InP:Yb. It also appears that low doped n-type material is most likely the desirable host material for Yb implants; especially since no Yb-related emissions were seen in p-type GaAs and effectively no emissions in p-type GaP. The Yb^{3+} emissions were observed for the first time in $\text{Al}_x\text{Ga}_{1-x}\text{As}$ ($x = 0.15, 0.23, 0.30$), the structure of the emissions depending upon anneal conditions and the Al mole fraction.

It is concluded that the main Yb^{3+} center in InP, GaP, GaAs, and AlGaAs is substitutional on a cation site (In, Ga, or Al); the difference in the crystal field giving rise to the differences in the Yb^{3+} emission in the host. Finally, only the near-edge emissions of InP:Yb were studied and the FB and DA emissions effectively remained suppressed or weak for almost all Yb-doped samples; the study of near-edge emissions as well as deep emissions is suggested for future investigations.

Photoluminescence of Er^{3+}

Of the various rare earth ions which have been incorporated into the III-V semiconductors, erbium appears to have the greatest technological potential. As mentioned previously numerous sharp and strong emissions have been observed around $1.54\mu\text{m}$ for various erbium doped semiconductors; 4f-emissions have also been observed at room temperature. The $1.54\mu\text{m}$ wavelength corresponds to the minimum attenuation in silica based fiber optics. Since the initial investigations in 1982-83 (Ushakov et al, 1982; Ennen et al, 1983; 1983a), Er has been successfully introduced into the III-V semiconductors not only through implantation but also through growth by LPE into GaAs (Bantien et al, 1987), MOCVD into InP (Takahei et al, 1988), and MBE into GaAs (Smith et al, 1987). Also devices have been produced in the form of GaAs:Er pn-diodes (Whitney et al, 1988).

In this investigation it was intended to expand the study of Er^{3+} by examining high energy implants especially into AlGaAs and into various conductivity types of GaAs. Specifically, it was of interest to examine the more deeply implanted layers produced through 1 MeV energy erbium implants. These areas had not been previously studied. InP and GaP were also investigated, but the study essentially concentrated on n-type, p-type, and semi-insulating GaAs, and AlGaAs as a function of the Al mole fraction. First it was attempted to get an efficient Er^{3+} signal from the various materials; this would also support lifetime measurements and

excitation measurements. Second, it was of interest as to how the many emission lines, which had been reported in the past, changed with conductivity type in the case of GaAs and how they changed with Al mole fraction in the case of $\text{Al}_x\text{Ga}_{1-x}\text{As}$. Third, it was attempted to determine the change in the $1.54\mu\text{m}$ emission with semiconductor bandgap. Finally, it was desirable to determine which of the implanted samples would show the strongest Er^{3+} signal. Results from these considerations allow one to make certain conclusions about the centers responsible for the emissions, the recombination mechanisms, and technological applications. Secondary-ion mass spectrometry (SIMS) was used to verify the implanted ion species and to determine the ion distributions before and after annealing.

The samples were cleaned and mounted, as previously explained, and were then implanted with 1 MeV energy Er ions at dosages of 5×10^{12} and $5 \times 10^{13} \text{ cm}^{-2}$ and a small selected set at $7.5 \times 10^{13} \text{ cm}^{-2}$. Table 10 lists the samples and treatment conditions which were considered in this part of the study. After implantation the samples were annealed face down on a Si:P wafer in the conventional annealing furnace in a flowing forming gas (fg) atmosphere. Annealing temperatures were chosen to be close to the optimum annealing temperatures as previously established (Pomrenke et al, 1986). Unfortunately, upon performing SIMS analysis on InP:Er , it was determined that besides erbium, ytterbium was

Table 10. Sample Information for the 1 MeV Erbium Implanted Semiconductors

Semiconductor	Conductivity Type	Identifier	Dosage cm^{-2}	Anneal Condition $^{\circ}\text{C}/\text{min}/\text{gas}$
InP	SI	MR(338)	5×10^{13}	650/10/fg
	SI	MR(338)	7.5×10^{13}	650/10/fg
	SI	MR(338)	5×10^{13}	750/10/fg
GaP	p	GPC	7.5×10^{13}	650/10/fg
GaAs	SI	CS	5×10^{12}	650/10/fg
	SI	CS	5×10^{13}	650/10/fg
	SI	CS	7.5×10^{13}	650/10/fg
	SI	CS	5×10^{13}	680/10/fg
	SI	WA	5×10^{13}	680/10/fg
	n	WA	5×10^{13}	680/10/fg
	p	WA	5×10^{13}	680/10/fg
$\text{Al}_x\text{Ga}_{1-x}\text{As}$	x = 0.1	EPI	5×10^{13}	680/10/fg
	x = 0.2	EPI	5×10^{13}	680/10/fg
	x = 0.3	EPI	5×10^{13}	680/10/fg
	x = 0.4	EPI	5×10^{13}	680/10/fg

also accidentally implanted into the sample set with a dosage of $5 \times 10^{13} \text{ cm}^{-2}$. The source of Yb is unknown but is most likely from the impure Er_2O_3 starting material which is not properly mass separated due to the poor resolution of the 1 MeV implantation system. Since a relatively good Er^{3+} signal was seen and the Yb did not modify or substantially quench the Er-related emissions, the investigation of the samples was continued. The $7.5 \times 10^{13} \text{ cm}^{-2}$ dosage samples which were implanted at a different time did not show the Yb signal.

The photoluminescence setup used in this part of the study was essentially depicted in Figure 5 and 6. The excitation source was the air cooled argon ion laser at 514.5 nm (upon considering the $\text{Al}_x\text{Ga}_{1-x}\text{As}$ bandgap), dispersion with the 1600 nm grating, and signal detection with the Ge

detector.

Figure 33 depicts for the first time the photoluminescence spectra of Er implanted semi-insulating (SI) GaAs and AlAs plus $\text{Al}_x\text{Ga}_{1-x}\text{As}$ at different Al mole fractions; $x = 0.1, 0.2, 0.3,$ and 0.4 . The AlAs is actually from a multilayered structure from which appropriate layers were etched to allow for the implantation into the AlAs. Implantation was at an energy of 1 MeV and a dosage of $5 \times 10^{13} \text{ cm}^{-2}$ with subsequent proximity annealing at 680°C for 10 min in forming gas. The emission temperature is 7K; the resolution approximately 3 meV; and irradiance 600mW/cm^2 . The spectra depicted in Fig. 34 for GaAs of different conductivities are a result of the same experimental conditions as those for Fig. 33, and hence, the spectra of the two figures may be directly compared.

Seen in both figures are the characteristic Er^{3+} emission from 1.53 to 1.67 μm with the strongest signal occurring around 1.54 μm . The emissions are a result of the transitions between the weakly crystal-field-split spin-orbit levels $^4I_{13/2} - ^4I_{15/2}$ of Er^{3+} ($4f^{11}$). The near-edge emissions, FB and DA, were observed for several samples but not recorded. In Fig. 33 aside from AlAs, only minor variations occur in the Er emission from sample to sample which seems to indicate that the crystal-field has only a minor effect on Er^{3+} in these materials. The strongest signal is for $\text{Al}_{0.4}\text{Ga}_{0.6}\text{As}$ at 1.537 μm with a full-width at half-maximum of at least 0.4 meV at 7K upon adjusting the

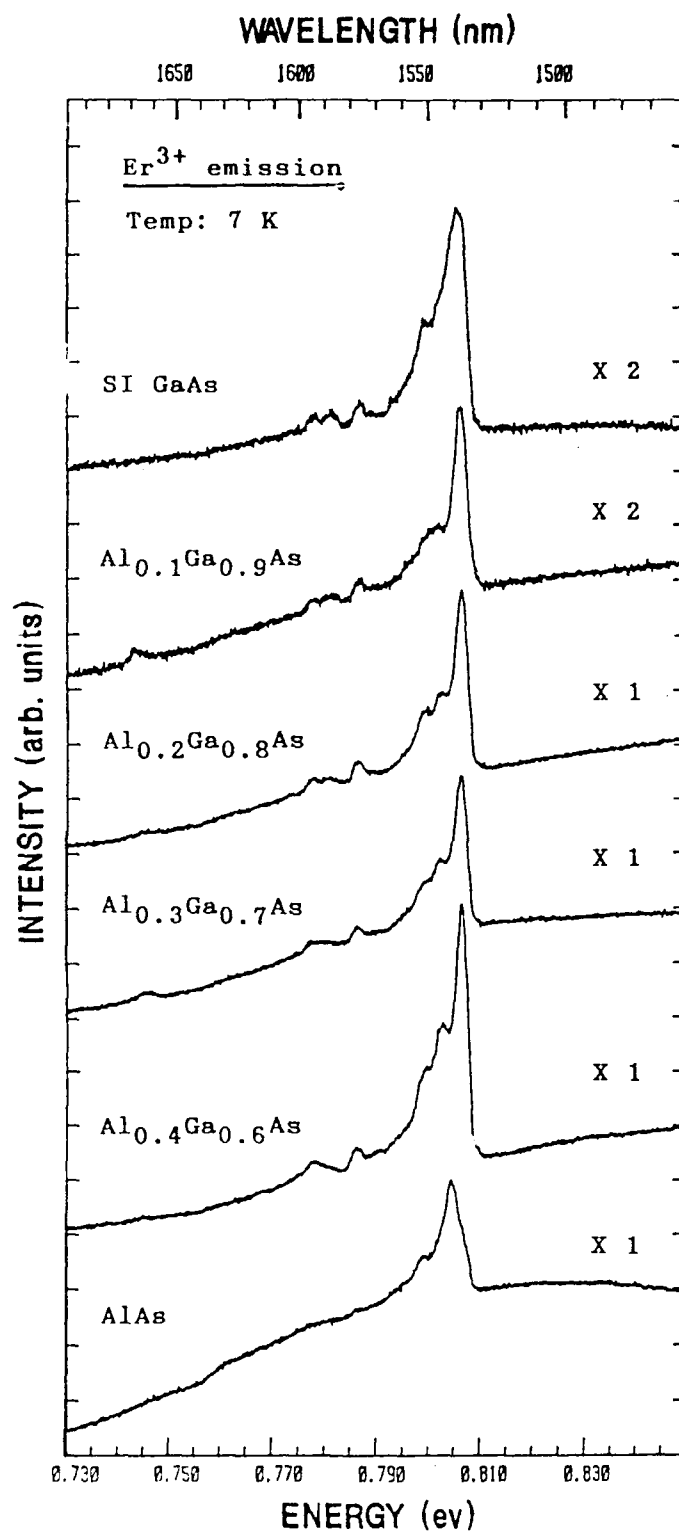


Figure 33. Photoluminescence spectra of erbium implanted into GaAs, AlAs, and AlGaAs with different Al mole fractions.

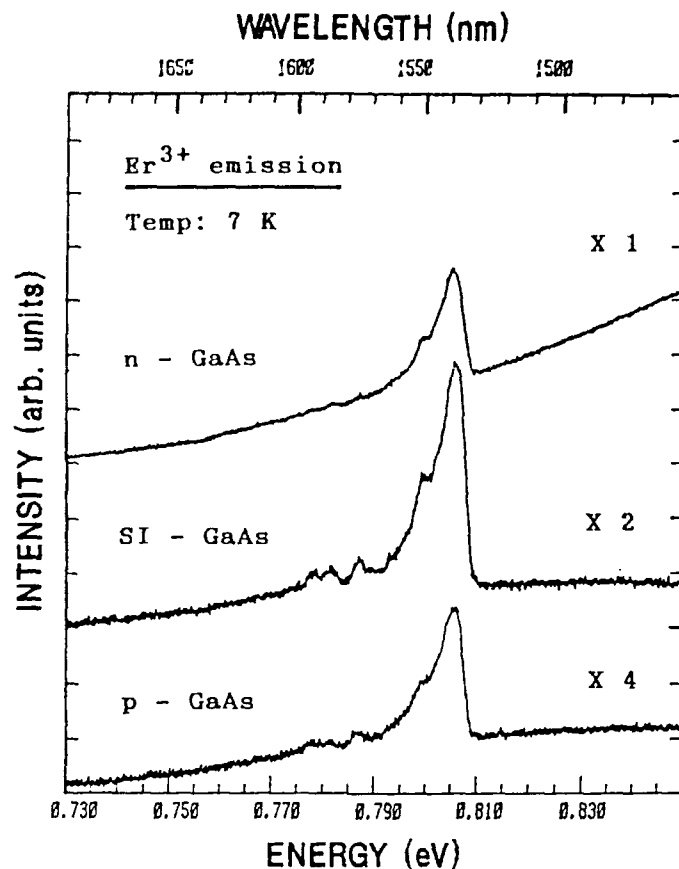


Figure 34. Photoluminescence spectra of erbium implanted into GaAs samples of different conductivity.

spectrometer slits to the improved resolution. However, this must be interpreted with caution as the penetration of the 514.5 nm may be most likely deeper in this material than in GaAs. The penetration depth at 514.5 nm in GaAs at 21K is approximately 132.2 nm (Seraphin et al, 1967). At least up to seven emission lines may be identified for each spectra at a resolution of 3 meV.

As determined in past investigations (Ennen et al, 1983;

1983a) and more recently by Rochaix et al (1988), there is no shift in energy or significant changes in the spectral characteristics of the Er^{3+} signal with variation of the semiconductor bandgap. It is of interest that the crystal-field imparts such small influence on the Er^{3+} center as compared to Yb^{3+} for instance.

Interesting results are also given in Fig. 34 for GaAs of different conductivity. The Er^{3+} emission for n- and SI GaAs is at least twice as intense as that for p-type material. Electrical measurements showed that SI-GaAs, although highly resistive, also had an electrical carrier concentration (n-type) of a low value of $4 \times 10^7 \text{ cm}^{-3}$. As will be discussed later, the recombination mechanism which allows the RE emission involves free carriers and $(e^- - h)$ pairs from the host semiconductor. Hence, one would expect at least a stronger Er^{3+} emission in n-type material versus p-type material. However, one must qualify this by stating that the extrinsic doping of the starting material should remain low, at least below $5 \times 10^{17} / \text{cm}^3$, otherwise deep levels associated with the n- or p- impurity might mask the RE emission.

From a technological point of view it is of interest that the Er-specific emission is seen near room temperature. Figure 35 shows for the first time the 4f-transitions for 1 MeV implanted $\text{Al}_{0.4}\text{Ga}_{0.6}\text{As}$ at 7K and 270K with a reduction in signal by a factor of ten at the higher temperature.

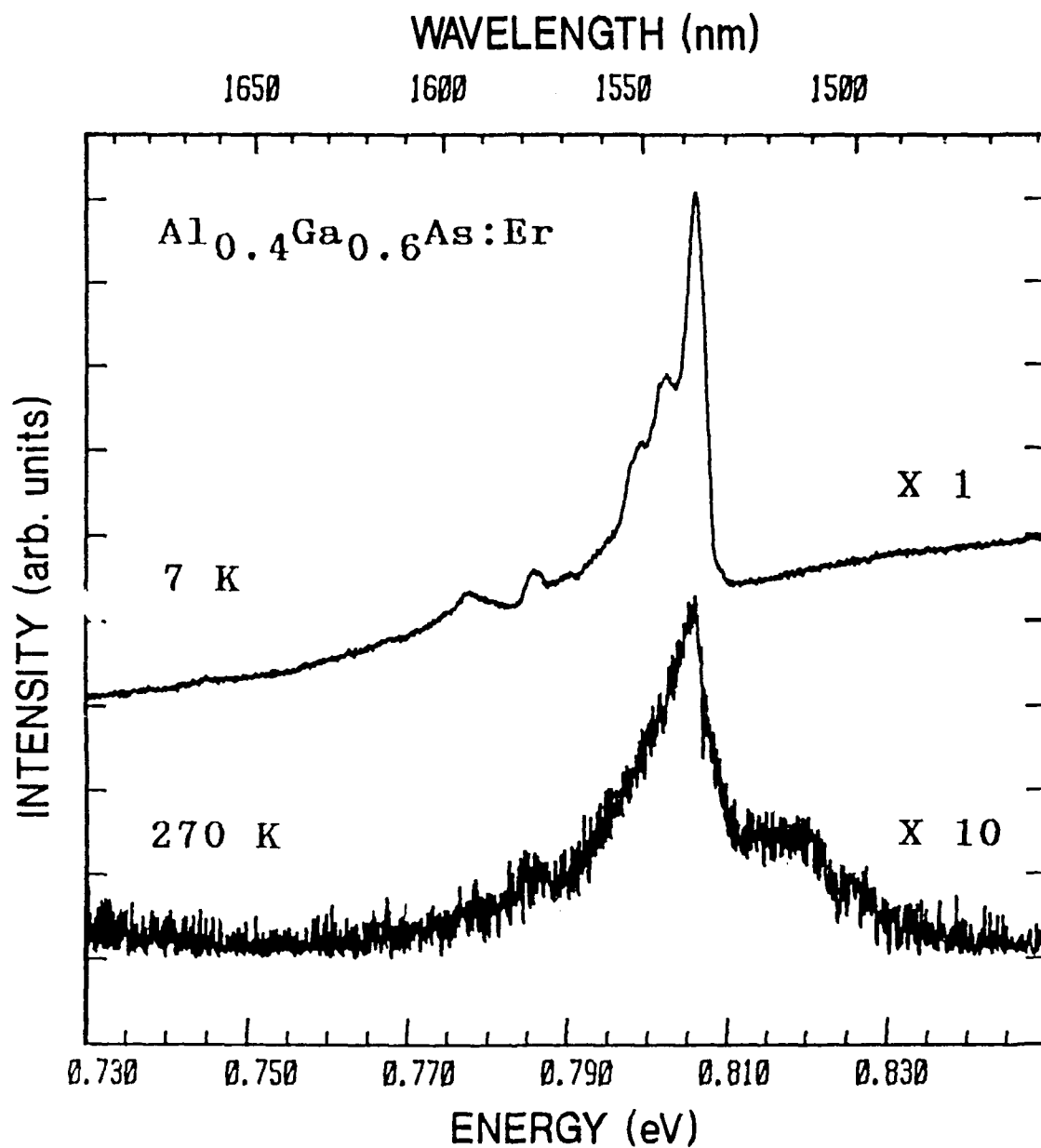


Figure 35. Temperature dependence of the Er-specific emission in $\text{Al}_{0.4}\text{Ga}_{0.6}\text{As}$.

Although not recorded the signal was also seen at room temperature (296K). The presence of a high energy shoulder

at 270K could be a result of the development of 'hot' lines at the higher temperatures.

Depicted in Fig. 36 is the implant dosage dependent study of Er implanted into (CS) semi-insulating GaAs. The implantation was at an energy of 1 MeV and at dosages of 0.5, 5, and $7.5 \times 10^{13} \text{ cm}^{-2}$. Subsequent annealing was in flowing forming gas at 650°C for 10 min. Laser excitation was 600 mW/cm^2 with the 514.5 nm line; spectral resolution was approximately 1.1 meV. Although the dosage was varied slightly over just one decade, no similar change occurred in the intensity as has been reported for Yb^{3+} in InP (Ennen et al, 1985). The integrated intensities between the low dose and high dose varies by not more than a factor of 2. Significant is the improved resolution of individual peaks at the $5 \times 10^{12} \text{ cm}^{-2}$ dosage as compared to the higher dosages. Most likely this is a result of fewer associates and complexes that can be formed between the rare earth and the defects generated by the implantation process. Peak positions and relative peak intensities show little variation between the spectra aside in the 1538-1548 nm region as marked in Fig. 36. As the Er^{3+} emission differs little from dosage to dosage indicates that most of the emissions are related to one center. Since the dosage spread was just over a decade, little can be said about concentration quenching, a phenomena observed in rare earth doped ionic crystals (Brown and Shand, 1970).

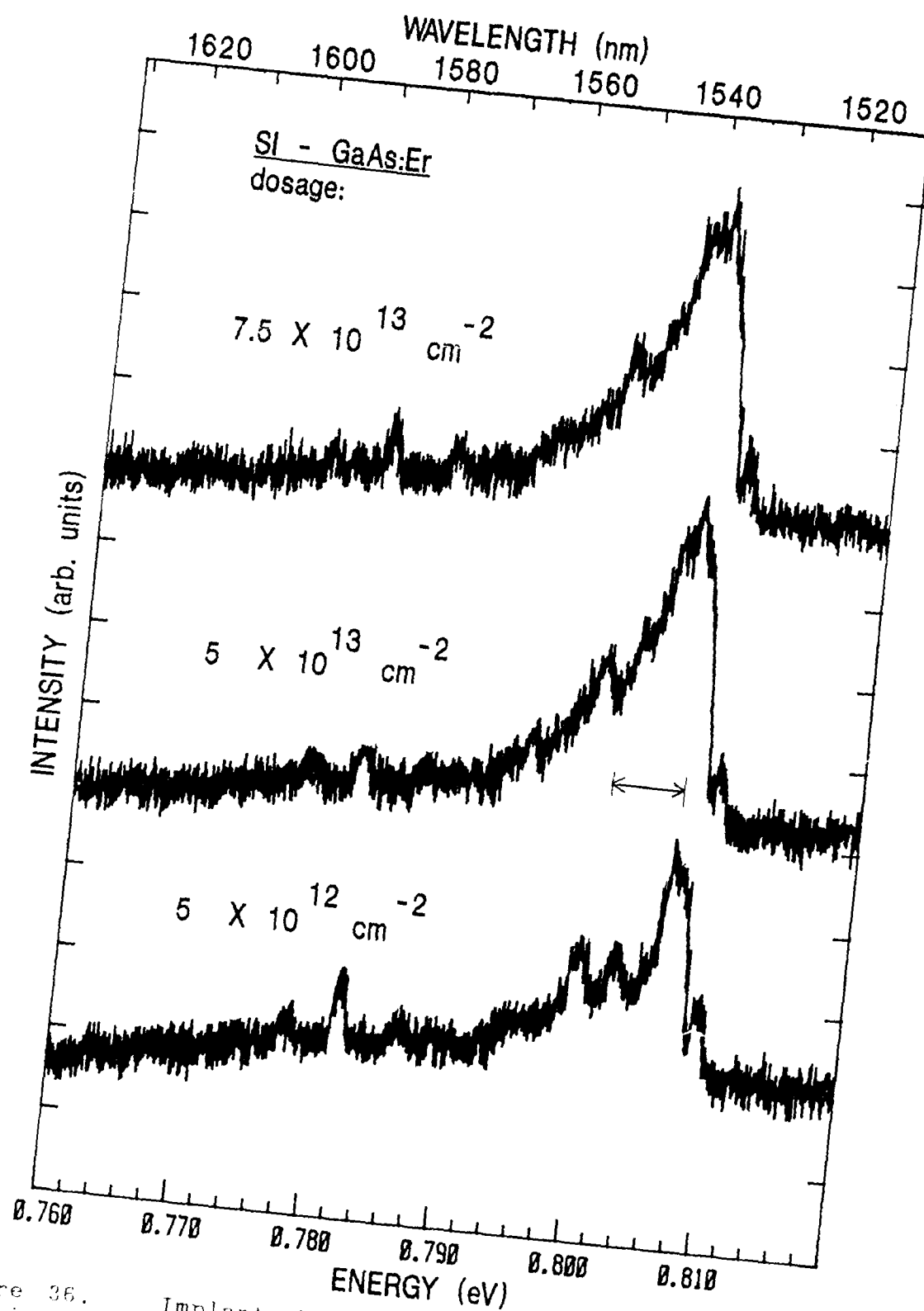


Figure 36. Implant dosage dependence of the Er-specific emissions of semi-insulating GaAs at 7K.

A high resolution (0.46 meV) spectra was taken of CS and WA GaAs:Er to determine the change in emission lines for two different semi-insulating samples implanted and treated under identical conditions.² Samples were implanted at an energy of 1 MeV and a dosage of $5 \times 10^{13} \text{ cm}^{-2}$ and annealed at 680°C for 10 min in forming gas. Little variation is seen in the spectra depicted in Fig. 37. However, differences do appear at less resolution ($>2.0 \text{ meV}$), where the CS sample shows a broad non-Er-related background upon which the Er emissions are positioned. Differences also exist in the NE region. As the resistivity and the residual impurity concentration are not the same between the samples, any differences in spectral features can be accounted for by different associates forming between the impurities or defects and the rare earth and the slight difference in the crystal-field splitting.

As mentioned, intensity comparisons between the different semiconductor materials must be done with caution due to the difference in absorption or penetration depth in these materials by the exciting line. Figure 38 depicts the spectra for the same sample (CS) under identical emission conditions but different probe or excitation beams (647.1 nm and 514.5 nm). Aside from changes in relative peak intensities and the appearance of peaks at lower energies, the spectra from the 647.1 nm excited layer is twice as intense. This is most likely a result of the difference in absorption depth of the probe beam, accessing more of the

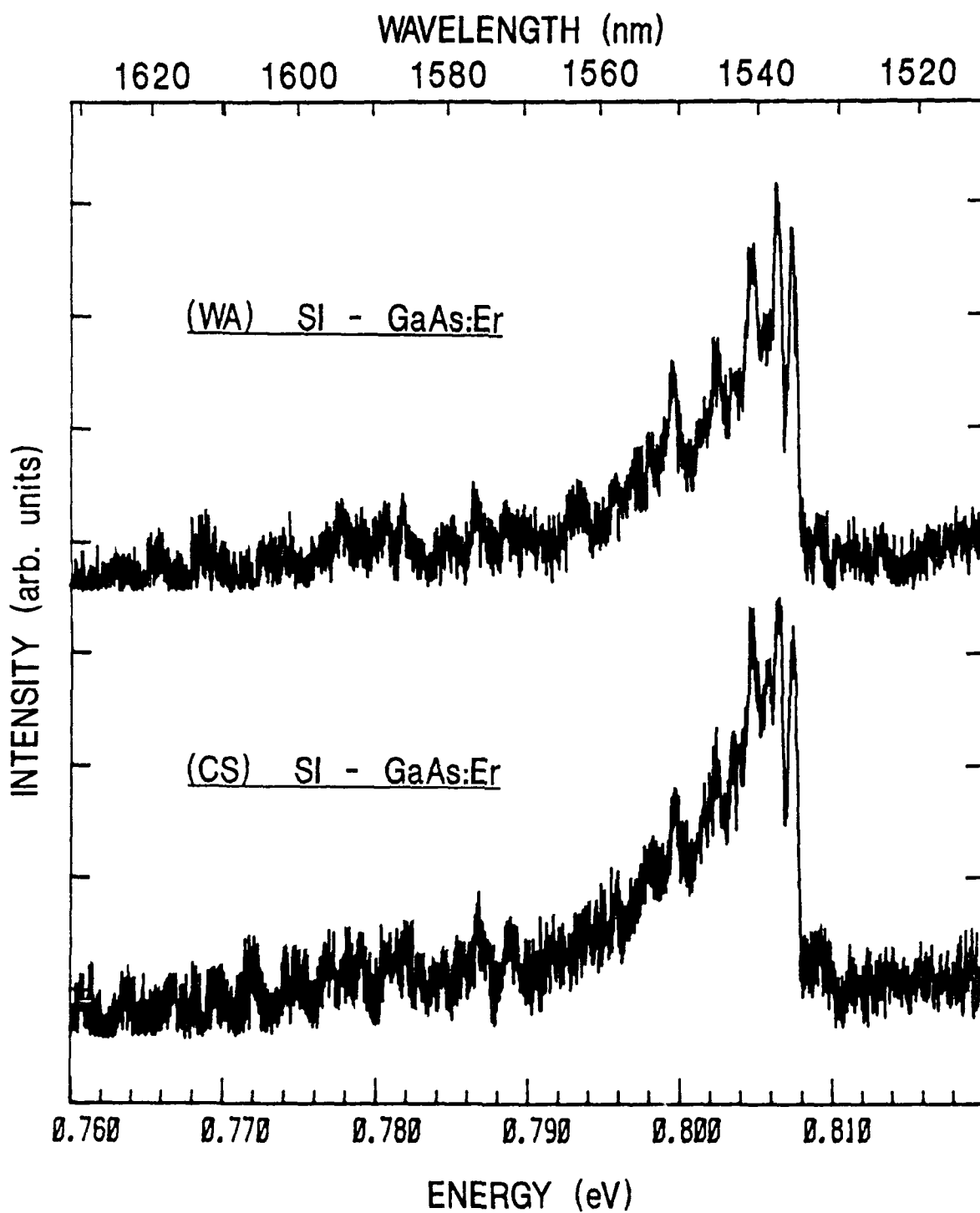


Figure 37. High resolution spectra at 7K of the Er^{3+} emission in two different but identically treated GaAs substrates.

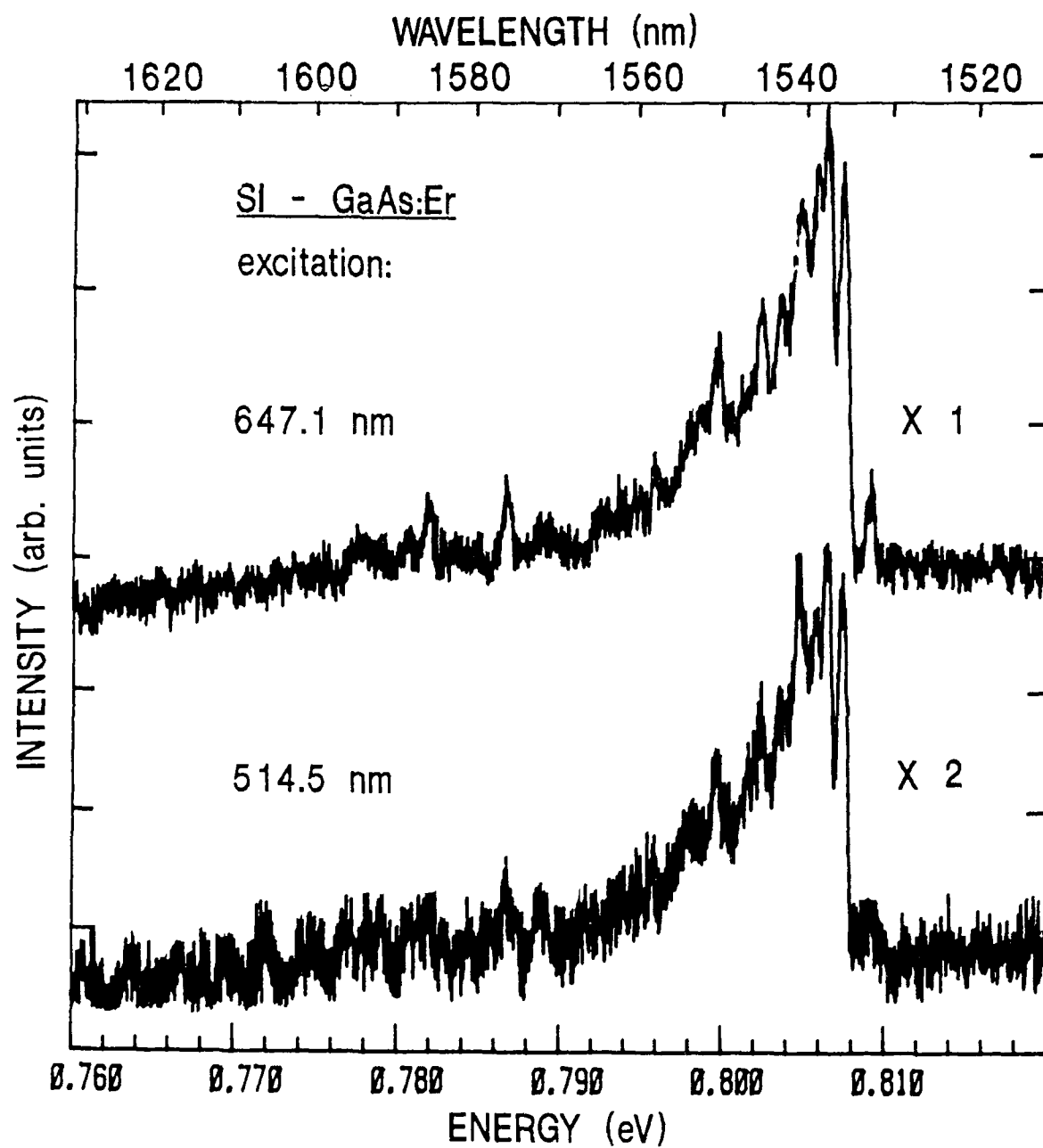


Figure 38. Photoluminescence at 7K of Er implanted (CS) semi-insulating GaAs excited by two different sources.

various Er centers of the implanted layers. This demonstrates the desirability of implanting at high energy, i.e. 1 MeV, to create more deeply doped layers.

The characteristic 4f-emission of Er-implanted InP is seen in Fig. 39; the SI GaAs:Er spectra from Fig. 34 is also shown for comparison. The semi-insulating InP substrate was implanted with Er at an energy of 1 MeV and a dosage of $5 \times 10^{13} \text{ cm}^{-2}$ and subsequent annealing was at 650°C for 10 min in flowing forming gas. Resolution was 2.4 meV and irradiance was 600 mW/cm^2 using the 514.5 nm laser line. The difference in spectral characteristics between the 4f-emissions of GaAs and InP are a result of different crystal-field splitting of the spin orbit $^4I_{13/2} - ^4I_{15/2}$ levels of Er^{3+} . The erbium center in GaAs and InP is assumed to be substitutional on Ga and In sites, respectively; this was confirmed recently for GaAs with electron spin resonance (ESR) measurements (Baeumler et al, 1987). The different ligands, As or P, are thought to be responsible for the difference of the crystal-field splitting. Very weak Er-related emissions were also seen for p-GaP but are not shown. The reason for the weak intensity is the intense, broad non-erbium related impurity level in the 1.0 to 1.6 μm region which dominates the recombination process.

SIMS depth profiling was performed to verify that the erbium ion was implanted and to determine the implant distribution. The measurements were performed on InP

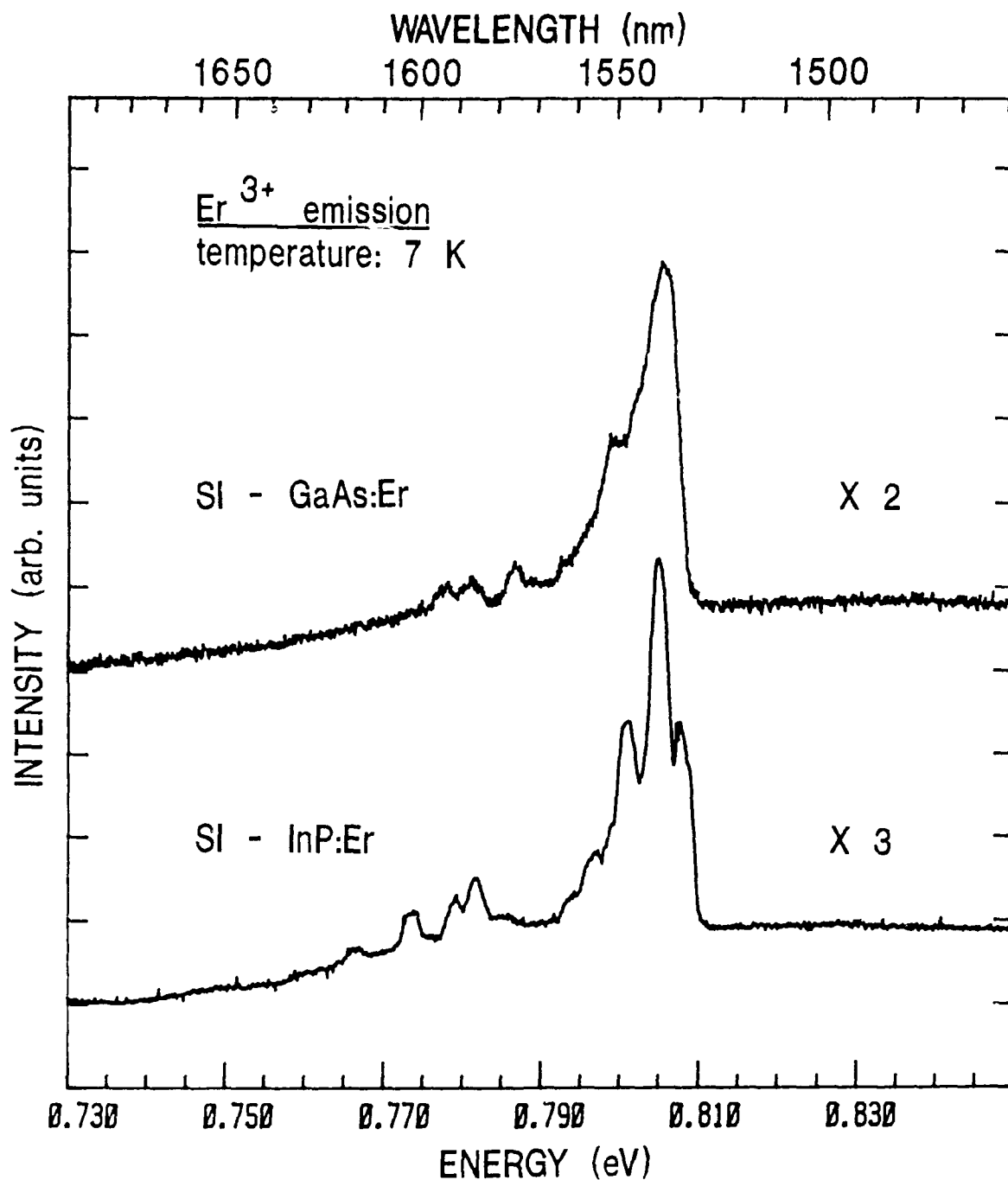


Figure 39. Comparison spectra of Er implanted semi-insulating InP and GaAs.

implanted with erbium at an energy of 1 MeV and a dosage of $5 \times 10^{13} \text{ cm}^{-2}$. Both as-implanted and post-implantation annealed samples were examined. The annealing was at 750°C for 10 min in forming gas; the 750°C temperature was chosen as the upper temperature at which one would conventionally anneal InP.

The measured and calculated profiles are shown in Fig. 40. The measured as-implanted profile has lower peak concentration than the calculated, also the peak depth is 245 nm compared to the 216 nm projected range, R_p , as calculated by the TRIM code. Some of the differences may be accounted for by a greater straggling than predicted due to implant induced damage in the semiconductor matrix; also, there is an error in the measured implantation current. The dosage determined by the implantation system is a result of the total current for a particular mass number or range of mass numbers. Thus if an impurity in the beam has the same mass number as the rare earth, it is then registered as part of the dosage. Finally, at least for the 750°C anneal case there is evidence of RE diffusion toward the surface. This is contrary to the results obtained by Favennec et al (1987) on the SIMS analysis of 600° annealed InP:Er. The discrepancy can probably be explained by the higher anneal temperature used in this study (750°C). The diffusion may be responsible for the poor luminescence signal at elevated anneal temperatures ($> 700^{\circ}\text{C}$) in InP.

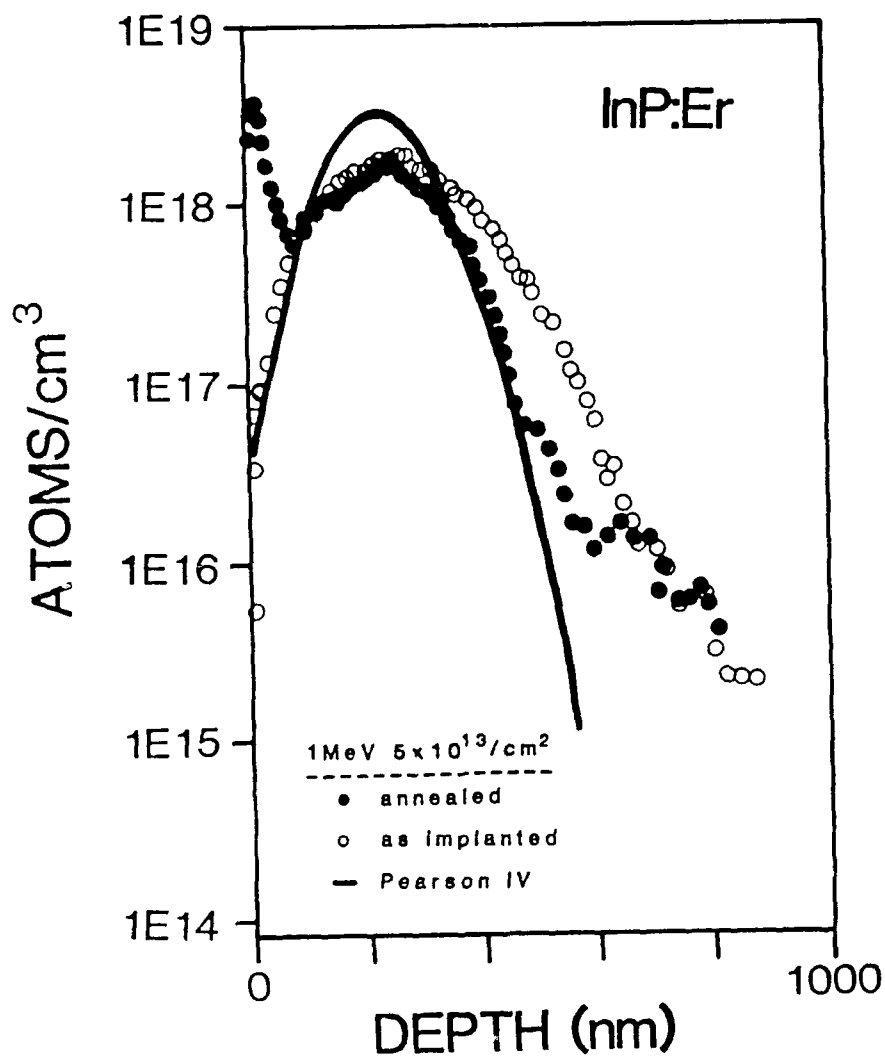


Figure 40. SIMS depth profile of Er implanted InP.

The characteristic 1.5 μm Er emissions have been demonstrated for the first time for AlAs and different Al mole fractions for $\text{Al}_x\text{Ga}_{1-x}\text{As}$ and also for different conductivity types of GaAs. This is also the first time that

Er had been implanted at a high energy of 1 MeV into a III-V semiconductor and confirmed with SIMS. The strongest signal was observed for $\text{Al}_{0.4}\text{Ga}_{0.6}\text{As}$. No significant shifts in energy occurred for the Er^{3+} emission as a result of the different crystal field environments from the various semiconductor hosts. The material which was examined had bandgaps ranging from 1.42 for InP to 2.24 eV for AlAs. Free electron rich material (i.e. n-type) appears to intensify the Er signal supporting the idea that free carriers are involved in the 4f-excitation process which allows for the rare earth emission. The Er emission can be activated in the III-V semiconductors with a post implantation anneal of 650 - 750°C for 10 min in a reducing or inert atmosphere. Finally, evidence of Er^{3+} emissions in the numerous semiconductors, emissions at room temperature, and the reported fabrication of Er-doped light-emitting diodes (Whitney et al, 1988; Rolland et al, 1988) support the idea that erbium doped semiconductors have substantial technological importance.

Photoluminescence of Tm^{3+}

The study of intracenter emissions from thulium implanted III-V semiconductors represents one of the first attempts to investigate rare earth emissions other than the relatively widely investigated ytterbium and erbium signals in these semiconductors. Aside from the fact that essentially no spectroscopic studies had been undertaken for thulium in the III-V semiconductors, there are various compelling reasons that lead to this particular study.

First, and rather basic, one could argue that thulium (Tm), which is located between Er and Yb in the periodic table, should not differ significantly in its chemical and physical properties which would preclude infrared emissions similar to Er and Yb seen at 1.5 and 1.0 μm , respectively. Second, if one examines the free ion energy levels of Tm^{3+} (see Appendix A), possible transitions between the three lowest excited states and the ground term ($^3\text{H}_6$) could lead to emissions around 0.8, 1.2, and 1.7 - 1.8 μm . Third, the lower energy terms of the free ion energy levels for Tm^{3+} are not significantly different from that of Er^{3+} . Furthermore, trivalent rare earth lasers have been reported for Tm^{3+} in calcium niobate (Ballmann et al, 1963), Tm^{3+} in CaWO_4 and ErF_2 (Johnson, 1963), and Tm^{3+} in $\text{Y}_3\text{Al}_5\text{O}_{12}$ (Johnson et al, 1965) with emissions between 1.9 and 2.0 μm due to the $^3\text{H}_4 - ^3\text{H}_6$ transition. Optical maser action was also reported for the divalent rare earth laser system $\text{CaF}_2:\text{Tm}^{2+}$ with emissions at 1.16 μm (Kiss et al, 1962). Furthermore, studies on

cross-pumped lasers using Tm^{3+} as either the sensitizer or activator ion have also been reported (DiBartolo, 1968). Finally, the idea of upconversion, changing infrared light into visible light, as reported for the two-photon upconversion process between Yb^{3+} and Tm^{3+} ions in the $\text{BaF}_2/\text{Th}_4\text{F}_4$ heavy metal fluoride glass (Yeh et al 1988) leads to speculations of possible similar phenomena for the rare-earth/semiconductor(III-V) systems.

Up to now only two references have appeared with respect to thulium-related emissions in III-V semiconductors. Although no spectra were presented, Ennen and Schneider (1985) reported in a review article that a 1.2 μm emission was observed for Tm^{3+} in GaAs and was associated with the $^3\text{H}_5 - ^3\text{H}_6$ transition. The earliest known work on the thulium-GaAs system was, however, investigated in 1964 by Casey et al, motivated by the system's potentially interesting magnetic and spectral properties. Using the relatively small atomic size of the rare-earth and a suitable radioactive isotope, ^{170}Tm , they determined the solubility and diffusion of Tm in GaAs. The maximum solubility was found to be $4 \times 10^{17} \text{ cm}^{-3}$ at 1150°C and was considered low due to the fact that the Tm atom is 25% larger than the Ga atom which it replaces substitutionally. Soviet investigations in 1979 (Fasatkin et al, 1981) report evidence of rare-earth-related emissions in GaP at approximately 1.27 eV for all rare earth ions including Tm; however, interpretation of their results

leads to the conclusion that the very broad 1.27 eV level is a defect or non-RE impurity and not associated with the intra-center transitions characterized by sharp and specific emissions. Finally, Masterov et al (1978) reported on the magnetic susceptibility of GaP doped with various RE ions, including Tm. It is stated that the rare-earth dopant which replaces the gallium atoms in GaP are in the trivalent state.

Reported here are the first relatively detailed investigations and spectra of the 1.22 - 1.33 μm 4f-intracenter transitions of Tm^{3+} in III-V semiconductors. The emissions are due to the transitions between the weakly crystal-field-split spin-orbit levels of Tm^{3+} ($4f^{12}$), $^3\text{H}_5$ - $^3\text{H}_6$. Anneal temperature and sample temperature dependent photoluminescence studies were performed for Tm implanted GaAs, InP, and GaP, to determine the nature and behavior of the Tm-related emissions and to determine the optimum emission conditions. Initial but unsuccessful investigations concentrated on finding in GaAs the 1.1 μm divalent Tm emission of $^2\text{F}_{5/2}(\text{E}_{5/2}) - ^2\text{F}_{7/2}(\text{E}_{5/2})$ (DiBartolo, 1968) using a S-1 PMT, and on finding the 1.9 - 2.0 μm $^3\text{H}_4 - ^3\text{H}_6$ emission using a PbS detector. That the 1.9 - 2.0 μm emissions were not seen is possibly due to a signal-to-noise problem; the emission is too weak and that the detectivity of the PbS detector is too low. Furthermore, the initial studies also concentrated on n-GaAs as it was believed that free electron-rich material would lead to stronger 4f-emissions.

The samples were implanted at an energy of 390 keV and a

Table 11. Sample Information for Tm Implanted GaAs

Substrate conductivity	Substrate identifier	Anneal condition °C/min/gas	encapsulated
SI	CS	575/10/fg	yes
SI	CS	600/10/fg	yes
SI	CS	625/10/fg	yes
SI	CS	675/10/fg	yes
SI	CS	725/10/fg	yes
SI	CS	750/10/fg	yes
SI	CS	600/10/N ₂	no
SI	CS	725/15/N ₂	no
SI	CS	775/15/N ₂	no
SI	CS	825/15/N ₂	no
SI	CO	725/15/N ₂	no
SI	CO	725/15/H ₂	no
SI	CO	775/15/N ₂	no
SI	CO	825/15/N ₂	no
n	AC	650/15/N ₂	no
n	AC	700/15/N ₂	no
n	AC	750/15/N ₂	no
n	AC	850/15/N ₂	no
n	AC	950/15/N ₂	no
p	AC	725/15/N ₂	no
p	AC	775/15/N ₂	no
p	AC	825/15/N ₂	no

dosage of $5 \times 10^{13} \text{ cm}^{-2}$ with ^{169}Tm as described in the experimental section. As shown in Tables 11, 12, and 13 different GaAs, InP, and GaP substrates were used, respectively, as identified also in the previously discussed experimental section (see 'identifier' code). Post implantation proximity annealing was performed in the conventional annealing furnace, face-down on a Si:P wafer, in either flowing forming gas (fg), nitrogen, or hydrogen; annealing times were either 10 or 15 minutes. The substrate and annealing conditions for all the samples which were

Table 12. Sample Information for Tm Implanted InP.

Substrate conductivity	Substrate identifier	Anneal condition °C/min/gas	encapsulated
SI	MR(338)	575/10/fg	yes
SI	MR(338)	600/10/fg	yes
SI	MR(338)	625/10/fg	yes
SI	MR(338)	675/10/fg	yes
SI	MR(338)	725/10/fg	yes
SI	MR(338)	750/10/fg	yes
SI	MR(338)	600/10/fg	no
SI	MR(338)	675/15/N ₂	no
SI	MR(338)	725/15/N ₂	no
SI	MR(338)	750/15/N ₂	no
SI	MR(338)	775/15/N ₂	no
SI	MR(346)	650/15/N ₂	no
SI	MR(346)	675/15/N ₂	no
SI	MR(346)	700/15/N ₂	no
SI	MR(346)	725/15/N ₂	no
SI	MR(346)	750/15/N ₂	no
SI	MR(346)	775/15/N ₂	no
SI	MR(354)	600/10/N ₂	no
SI	MR(354)	675/15/N ₂	no
SI	MR(354)	725/15/N ₂	no
SI	MR(354)	775/15/N ₂	no

investigated are tabulated in Tables 11, 12, and 13. Only limited sample sets were encapsulated prior to annealing.

The listing of the samples in the previously mentioned tables does not indicate that the 1.2 μm Tm³⁺ emission was seen in all the samples. As already indicated a considerable unsuccessful part of this study went into investigating possible Tm-related 1.1 μm and 1.9 ~ 2.0 μm emissions; during this part of the investigation the 1.2 μm emission was not investigated. Since the study essentially only discusses the successfully identified 1.2 μm Tm emission in (CS) GaAs,

Table 13. Sample Information for Tm Implanted GaP.

Substrate conductivity	Substrate identifier	Anneal condition °C/min/gas	encapsulated
p	GPC	625/10/fg	yes
p	GPC	675/10/fg	yes
p	GPC	725/10/fg	yes
p	GPC	750/10/fg	yes
p	GPC	600/10/N ₂	no
p	GPC	825/15/N ₂	no
p(und)	MRC	725/15/N ₂	no
p(und)	MRC	800/15/H ₂	no
p(und)	MRC	825/15/N ₂	no
n	GAC	725/15/N ₂	no
n	GAC	825/15/N ₂	no

(MR338) InP, and (GPC) GaP, it would appear that this emission is observable only for these samples. This is not the case; all other samples besides the CS, MR338, and GPC samples should be re-investigated in the proper spectral region. However, it is doubtful that a Tm³⁺ signal will be seen in n- and p-GaAs (AC) due to the very broad non-RE emissions in the 0.9 to 1.2 μm region as a result of heavy doping; however, n-type doping of the order of $< 5 \times 10^{16} \text{ cm}^{-3}$ could possibly yield a strong Tm³⁺ signal.

As shown in Figure 41, first evidence of the 4f-intracenter transitions of Tm³⁺ in III-V semiconductors was seen in (CS) GaAs:Tm annealed at 725°C for 15 min in N₂ and for (MR354) InP:Tm annealed at 600°C for 10 min also in N₂. Neither of the samples was encapsulated. The emission spectra are taken with the Ge detector at a sample tempera-

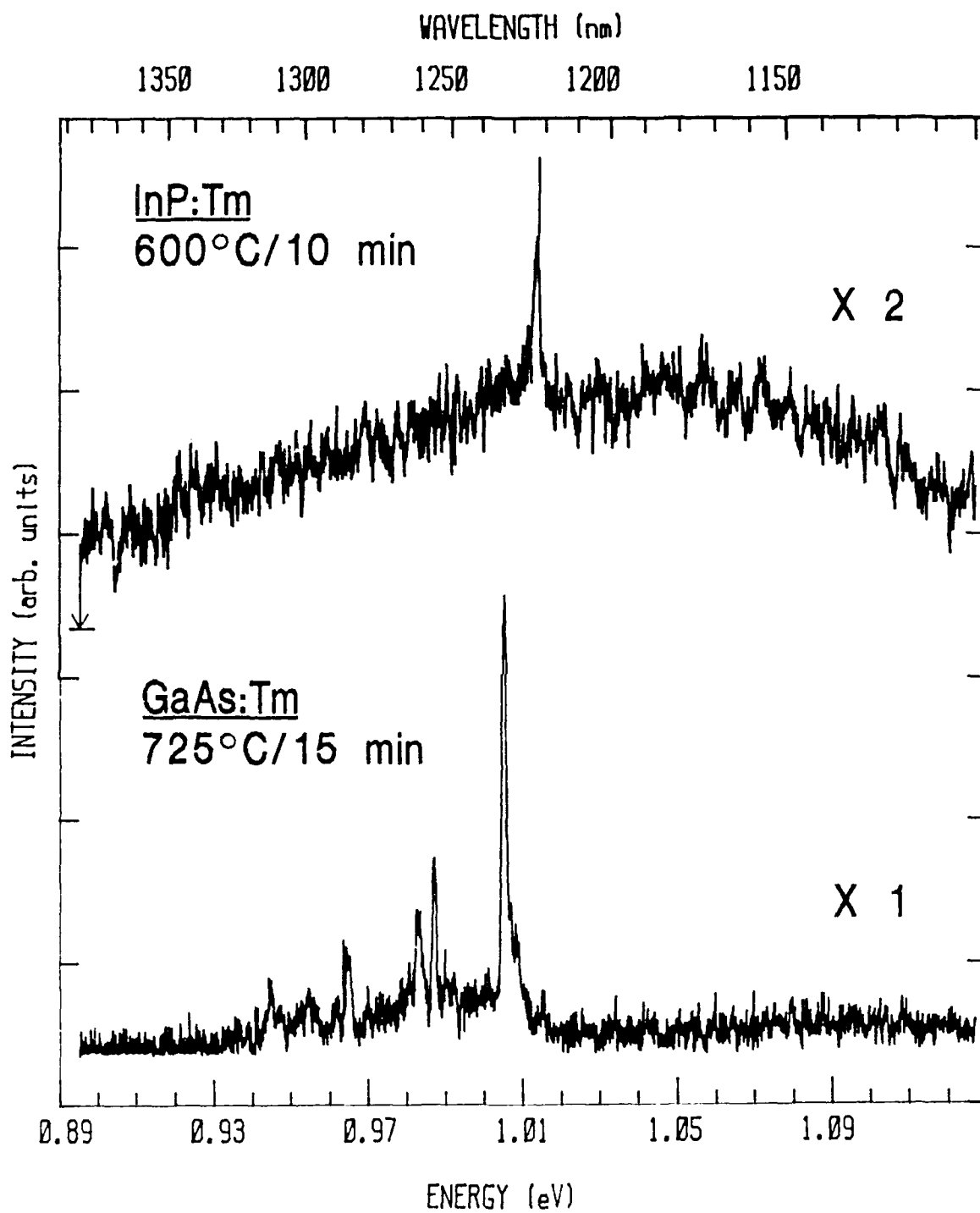


Figure 41. Comparison spectra of the Tm³⁺ emission in InP and GaAs.

ture of 6-7 K; laser excitation was with the 514.5 nm line at a power of 17 mW at the laser (see experimental section for further details). The spectra for both InP:Tm and GaAs:Tm in Fig. 41 are presented together for comparison and both show a dominant, sharp peak around 1.01 eV (approximately 1.22 μm) with some low energy structure for GaAs. The emissions are assigned to the transitions between the crystal-field-split spin-orbit levels $^3\text{H}_5 - ^3\text{H}_6$ of Tm^{3+} ($4f^{12}$). The difference in the emission structure between GaAs:Tm and InP:Tm is a result of a difference in the crystal field.

In order to improve the intensity of the signal, and hence the signal to noise ratio, improvements on the signal processing and sample annealing were considered. The spectra in Fig. 41 were taken with the 1.6 μm blazed grating and as seen in Fig. 13 for the system response to a 'graybody' or tungsten filament lamp, a substantial response change occurs at 1.23 μm due to this grating. The response drop was especially noticed for various GaAs:Tm and InP:Tm samples which exhibited a broad background emission in this spectral region. Replacement of the 1.6 μm grating by one blazed at 1.0 μm and with 1200 gr/mm not only gave a flat response it also improved resolution. To enhance the signal through the annealing process, a subset of the implanted samples was encapsulated with Si_3N_4 layers prior to the proximity annealing. Both improvements allowed for an increase in intensity such that a systematic study could be undertaken of the Tm^{3+} emissions as a function of anneal temperature and

emission temperature.

By performing isochronal anneal studies in conjunction with photoluminescence, several emission processes or phenomena may be examined. First, isochronal annealing helps to establish the optimum temperature at which the lattice recovers from the implantation damage. Second, the annealing allows the implanted impurity to move to its proper site upon which it becomes optically active (optimum optical activation is established). Located in the lattice are also residual impurities and point defects from the implantation; the annealing aids in activating or quenching the associated emission centers. During the process of annealing the thulium site location may convert from one type to another, for example, moving from an interstitial site to a substitutional site or vice versa (Bryant and Nahum, 1977). Furthermore, the point defects and/or residual impurities may actually interact with the rare earth impurity and form an optically active center (Gippius et al, 1986). It is seen that by monitoring the relative intensities of the emission lines of the Tm^{3+} spectra for the various anneal temperatures, it is possible to gain information, not only on the optimum emission signal, but also on a variety of centers which may be present in the implanted layer.

The characteristic 4f-emissions of Tm implanted (CS) GaAs were investigated as a function of anneal temperature. Shown in Fig. 42 are the spectra from encapsulated samples

annealed from as low as 575°C to as high as 750°C. Excitation was with the 200 mW, 647.1 nm line of the Kr-ion laser and signal processing was with the 1.0 μ m blazed grating and Ge detector. As in Fig. 41 the transitions are between the spin-orbit levels $^3H_5 - ^3H_6$ of Tm^{3+} . The main emission which appears in all the spectra is located at 1233 nm and shows a doublet structure with a resolution of 0.15 meV for each component. The optimum or most intense emissions occur at an anneal temperature of 725°C. There are no shifts in energy of the emission lines as the anneal temperature is changed. At temperatures above 600°C there are also no changes in the relative intensities of the emission lines, indicating that the Tm^{3+} emissions originate from the same center. However, at 600°C a separate center can possibly be identified as shown by the change in the relative intensities of peaks 'A' and 'B' of Fig. 42 upon annealing from 600°C to 625°C.

As for the encapsulated samples, a similar trend was observed for the spectra (see Fig. 43) of three non-encapsulated (CS) GaAs:Tm samples annealed at 600°C/10min, 725°C/15min, and 775°C/15min in nitrogen. The optimum signal also occurred at 725°C; however, the low energy satellite structure of the main 1233 nm peak was substantially quenched and changed in relative intensity. A similar trend was also previously observed for GaAs:Er; optimum annealing was established between 625 and 750°C and not at higher

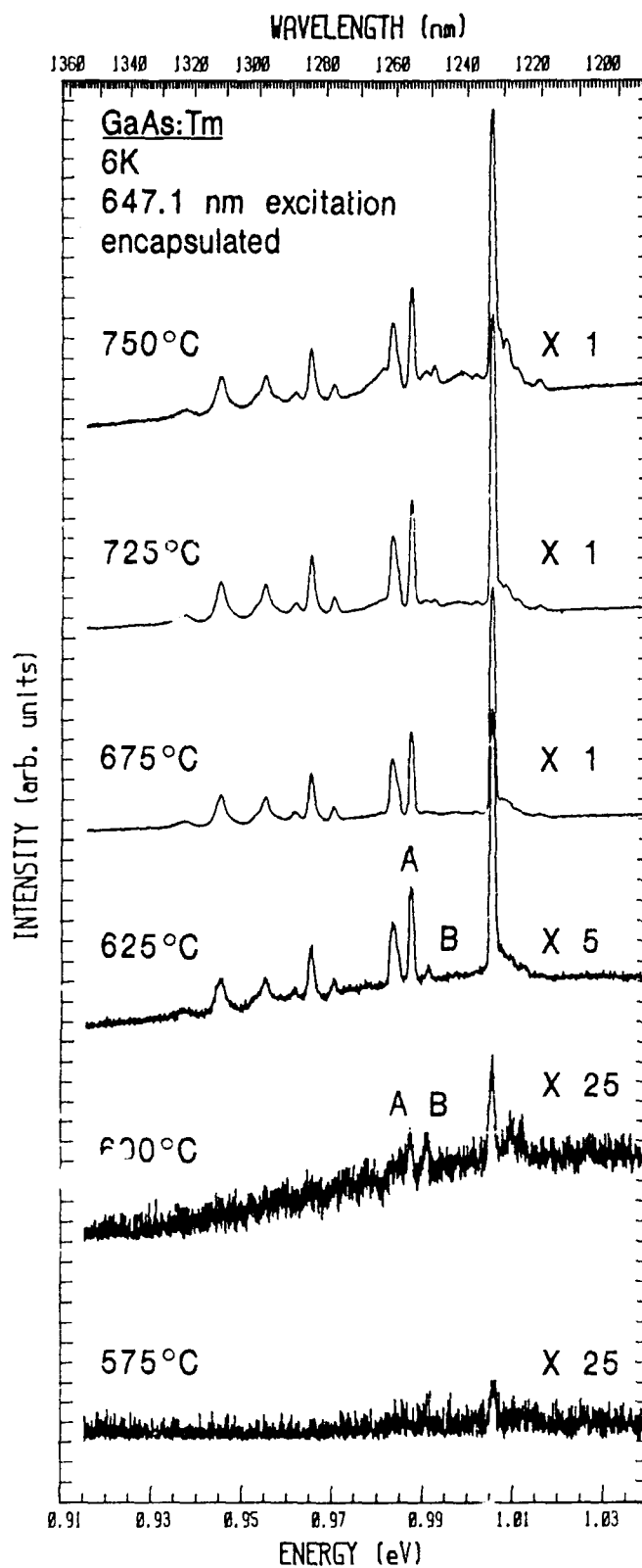


Figure 42. Photoluminescence of encapsulated GaAs:Tm as a function of anneal temperature.

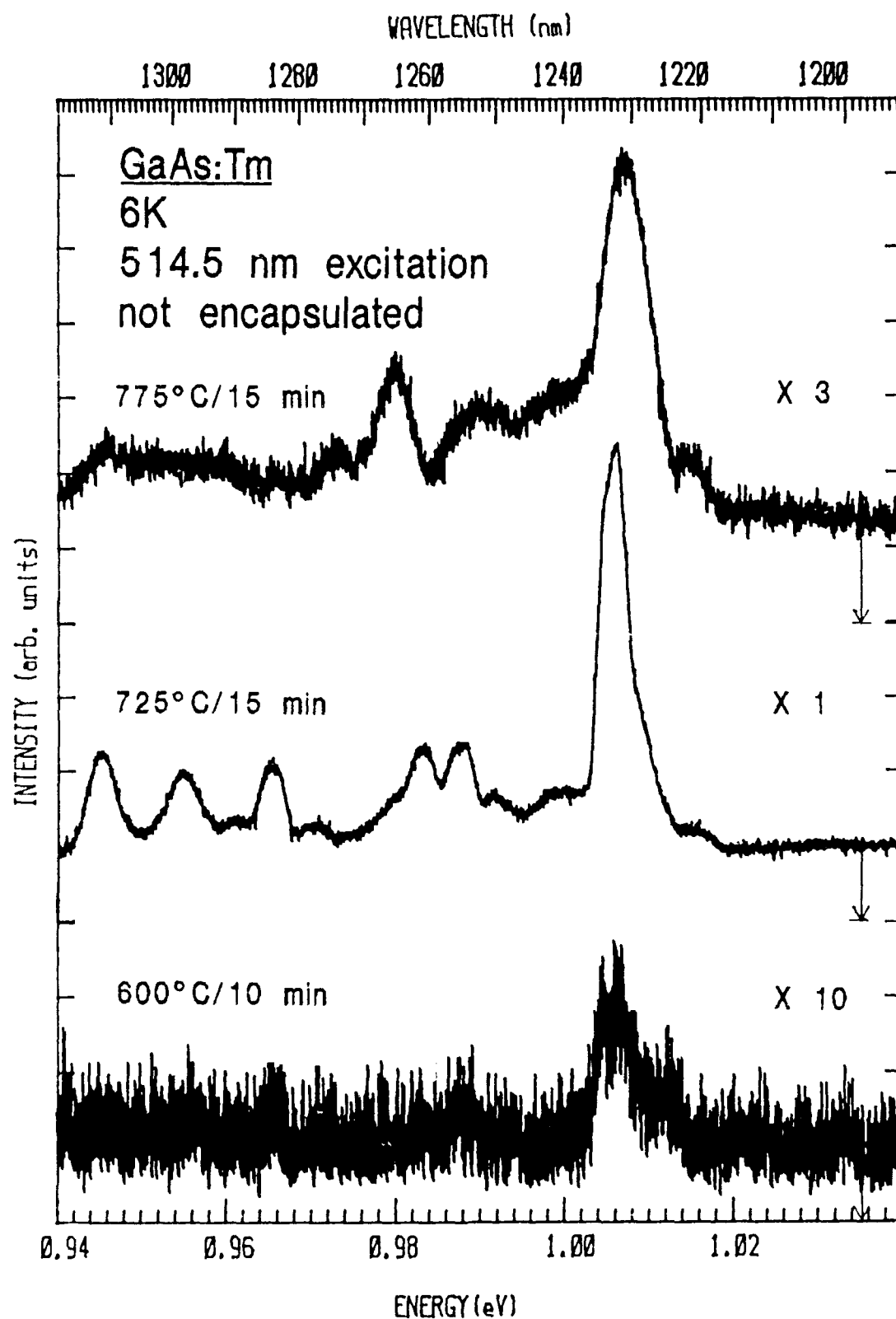


Figure 43. Photoluminescence of nonencapsulated GaAs:Tm as a function of anneal temperature.

temperatures as observed for shallow impurities (Pomrenke et al, 1986).

Two different processes are possibly occurring which might explain the previously discussed annealing results shown in Fig. 42. At temperatures of 600°C and less, the lattice damage has not fully recovered and a large number of the implanted rare earth ions are still located at interstitial sites. These interstitial sites (assume peak 'B') might be optically active at these temperatures, just as substitutional sites (assume peak 'A') are optically active. As the annealing temperature is increased from 600 to 750°C or to some critical temperature T_A , most of the interstitial rare earths move onto a substitutional site and increase the relative intensity of peak 'A'; consequently peak 'B' effectively disappears. However, at temperatures above 750°C, or above T_A , even though the rare earth ion remains relatively immobile at the substitutional site, residual impurities from the substrate do become more mobile and combine or associate with the rare earths and effectively quench the luminescence. This may explain the very weak peaks, labeled 'A' and 'B' in Fig. 42, for the non-encapsulated 775°C annealed sample. Besides for thulium it is believed that a similar scenario is followed by most of the implanted and annealed rare-earth/semiconductor systems.

The Tm^{3+} emissions in GaAs were also investigated as a function of emission or sample temperature. The effects of

temperature on emission lines or bands are known to affect band position, bandwidth, and band area (DiBartolo, 1968); and studying these effects enhances the understanding of the impurity/host system. In the investigation of shallow donor and acceptor impurities in III-V semiconductors, temperature dependent measurements allow for the measuring of characteristic activation energies of the impurity/host system and the determination of impurity state energies. However, it has been argued that the derivation of activation energies for transition metal impurities, and hence also rare earth impurities, might be impossible to derive by temperature dependent studies (Dean, 1982). Furthermore, the appearance of additional types of lines or bands can help identify the basic mechanisms responsible for the observed recombination processes (Dean, 1982). In this investigation the primary interest is to determine if additional lines develop, specifically 'hot' lines, and to determine the temperature effects that influence the more device oriented characteristics. From the technological point of view it is of interest to observe the rare earth emission at as high a temperature as possible (especially room temperature), to observe if spectral sharpness is maintained at the elevated temperature, and to observe if line position or energy varies with temperature.

Shown in Fig. 44 are the Tm^{3+} spectra in GaAs as the temperature was varied from 6 to 200 K. The sample was encapsulated and annealed at 750°C for 10 min in flowing

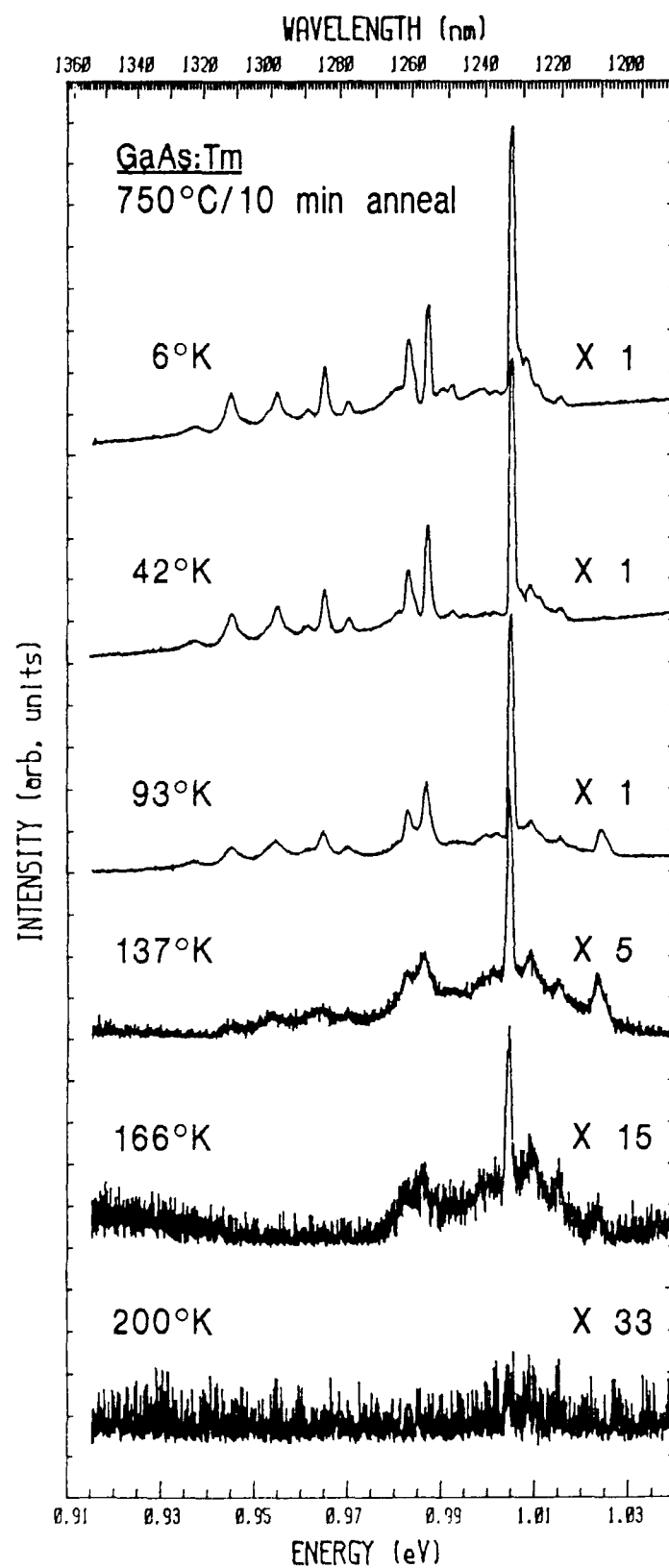


Figure 44. Tm^{3+} emissions in GaAs as a function of sample temperature.

fermium (ff) and laser excitation was with the 647.1 nm Kr-ion with a power of 200 mW at the laser. The Tm^{3+} emission is clearly seen up to 166 K after which the intensity falls off such that it shows only a very weak emission at 1211 nm. Higher emission temperatures might be possible with improved techniques of incorporating Tm into GaAs such as through MOCVD or MBE growth. Quite obvious is the development of a high energy hot line at 1211 nm with temperatures of above 42 K. This is due to thermal excitation involving the higher energy terms due to the crystal field splitting of the specific spin-orbit levels. At the same resolution settings, the sharpness (1.4 meV at fwhm) of the main 1233 nm emission is maintained up to 166 K.

The 4f-intracenter emissions of thulium in InP were also investigated as was shown previously in Fig. 41. The Tm^{3+} emissions for an isochronal anneal study from 575 to 750°C are depicted in Fig. 45 for (MR338) InP. Laser excitation was with the 647.1 nm line of the Kr-ion laser at a 200 mW power setting at the laser and signal processing was with the 1.0 μm blazed grating and Ge detector. The main but weak Tm^{3+} emission is located at 1223 nm. Obvious is the lower intensity and near absence of structure in the Tm^{3+} emissions of InP as compared to GaAs:Tm shown in Fig. 42. Probably the primary cause for this is the intense and broad InP background signal upon which the 4f-emissions are superimposed. This background is a result of a broad (250

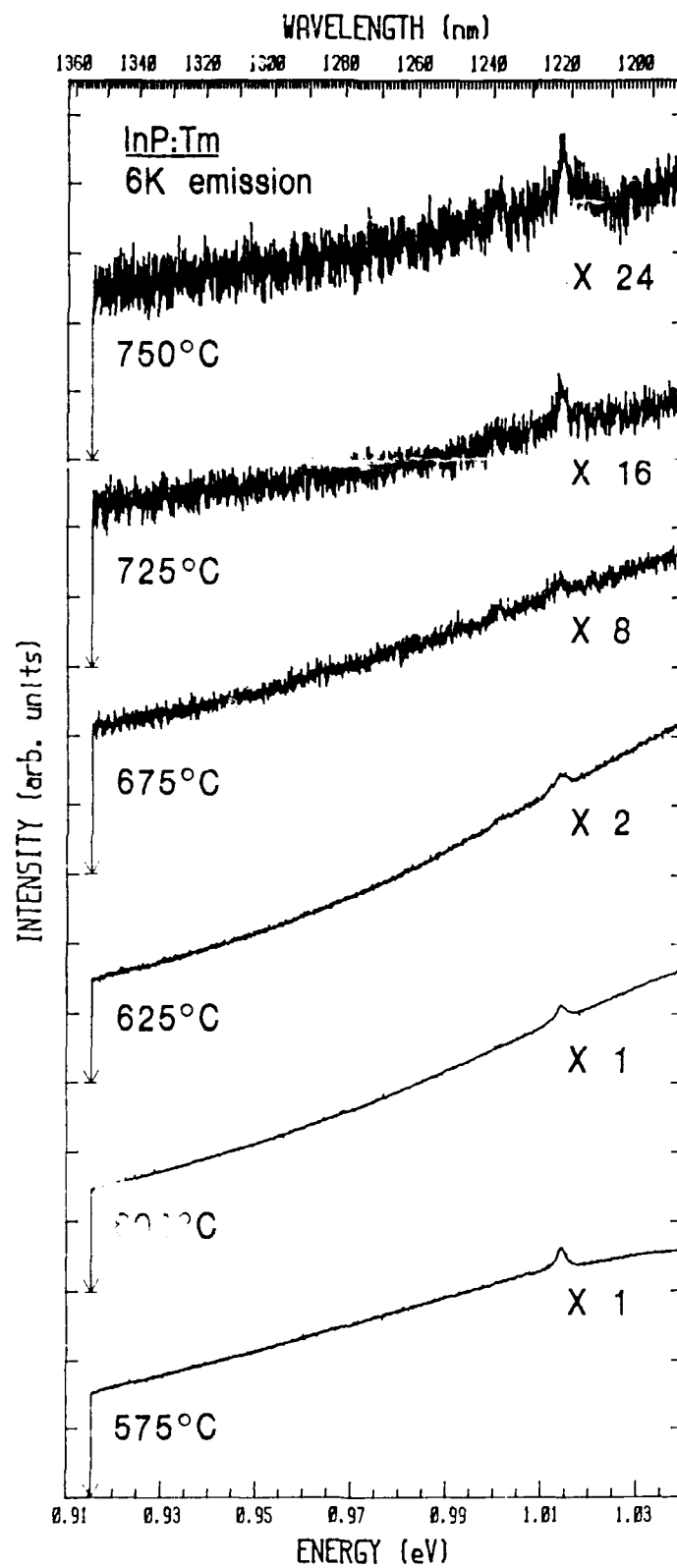


Figure 45. Isochronal anneal study of Tm implanted InP.

meV fwhm) band centered at 1.07 eV (1.16 μm) resulting from iron doped substrate and vacancies and complexes introduced through the implantation and annealing processes (Duhamel et al, 1983; Temkin et al, 1981 and 1982; Rao et al, 1983; and Eaves et al, 1982). The background is believed not to quench the 4f-emissions but to mask them.

The presence of the background emphasizes the importance of choosing the proper starting material before implanting the rare earth ions. Only limited experimental parameters were adjustable to intensify the Tm^{3+} signal; however, for the 675°C annealed sample it was observed that the background could be reduced by exciting with the green, 514.5 nm, line of the Ar-ion laser versus the red, 647.1 nm, line as shown in Fig. 46. The intensity of the Tm^{3+} signal was comparable even though the 514.5 nm line was set at 30 mW versus 200 mW for the 647.1 nm line. The signal differences are a result of the differences in the absorption coefficient of the excitation source in the semiconductor.

Due to the weak Tm^{3+} signal in InP, conclusions about the optimum annealing temperature for InP:Tm are somewhat unwarranted. However, it does appear that the signal in the 575 - 625°C temperature range is stronger when discounting the background. Also due to the weak signal, no Tm^{3+} emissions in InP were studied as a function of sample temperature. Finally, it should be mentioned that upon using a PbS detector, weak emissions were seen at 2003 nm and 2027

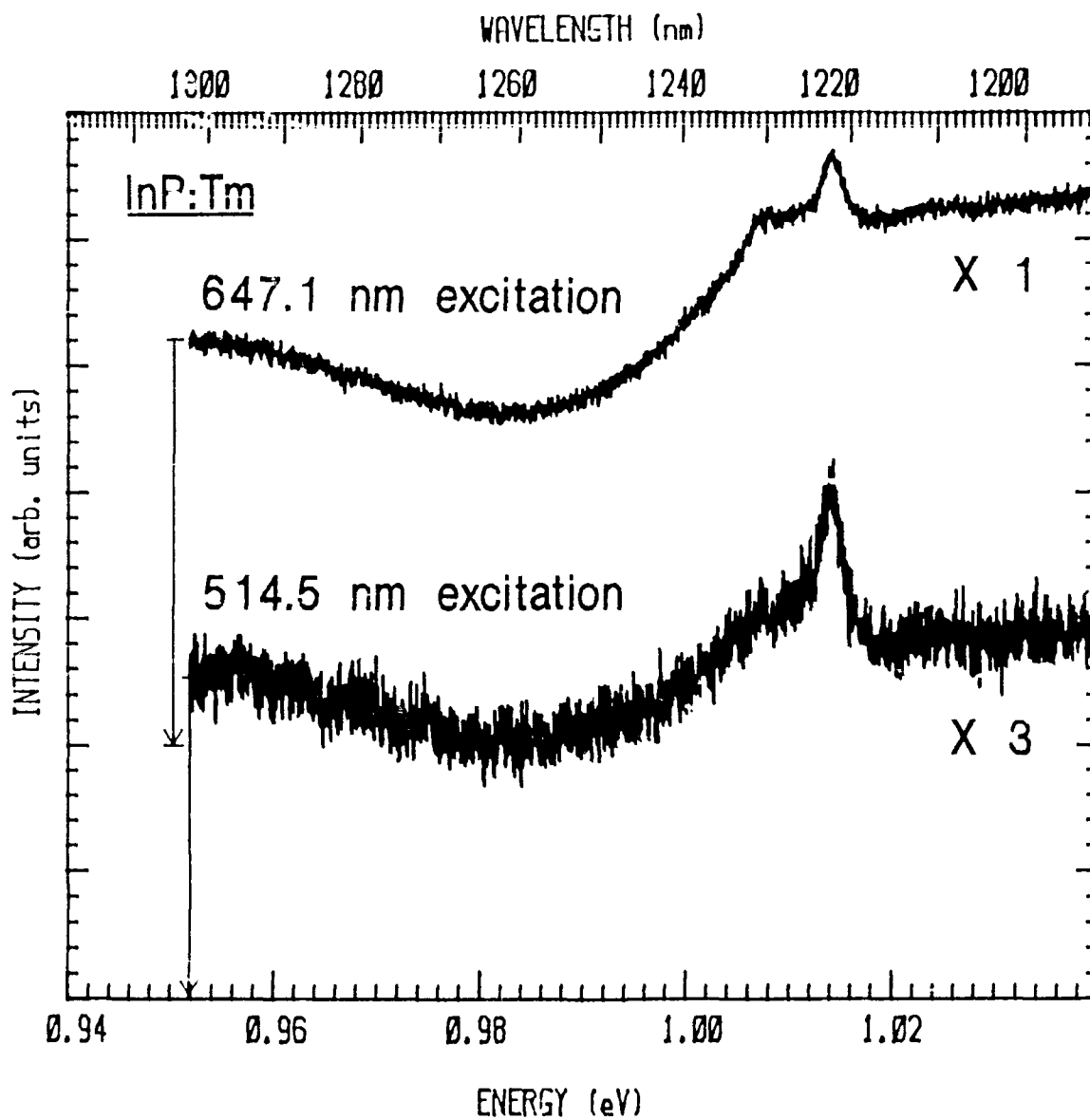


Figure 46. Photoluminescence of InP:Tm at two different laser excitations.

nm in InP:Tm annealed at 600°C for 10 min. This is possible evidence of transitions between the spin-orbit levels 3H_4 - 3H_6 of Tm^{3+} , observed as lasing transitions in the more ionic

crystals, and needs further systematic investigations.

As was shown in Table 13, numerous Tm implanted GaP samples were investigated in order to observe the 4f-intracenter emissions of Tm^{3+} . All investigations to observe a Tm-related emission at 1.1, 1.2, and 1.9 - 2.0 μm were unsuccessful. The primary causes for this were the dominating, broad-band emissions from the GaP substrate throughout the infrared (IR) region (0.9 - 2.0 μm) and the non-availability of a laser excitation source with a power capability of substantially greater than 30 mW for above bandgap excitation of GaP. The heavy doping of the substrate results in the broad IR bands which mask the 4f-emissions, that are most likely present. The importance of choosing the proper starting material for implantation is again emphasized.

Secondary ion mass spectrometry (SIMS) was performed on two of the InP samples implanted with thulium at an energy of 390 keV and a dosage of $5 \times 10^{13} \text{ cm}^{-2}$. As previously mentioned, in this part of the study it was attempted to verify the implanted thulium ion and to quantify and measure the associated depth distribution of the implant. The SIMS analysis, details of which were given in the experimental section, was performed on one sample which underwent no treatment after implantation (i.e. as-implanted) and one sample which was annealed at 750°C for 15 min in flowing nitrogen after implantation. The 750°C anneal was chosen not

that it represented the optimal anneal temperature for the rare earth implanted InP but that the temperature represented an upper limit to nondestructive annealing of InP samples (i.e. surface integrity is maintained).

Figure 47 shows the SIMS profile of thulium from as-implanted and annealed InP; also shown is the theoretical Tm-ion distribution based on the projected range ($R_p = 89.9$ nm) and straggling ($\Delta R_p = 31.0$ nm) as calculated by the TRIM code (Ziegler et al. 1985). As seen in Fig. 47, after annealing, the Tm appears to have diffused slightly toward the surface. The as-implanted profile seems to be broader than that predicted by the theory. As previously presented in the experimental section, the measured R_p of 98 nm is in good agreement with the calculated value. The straggling, ΔR_p , of 90 nm deviates considerably from the predicted value and may be a result of sputtering during implantation.

In conclusion, a photoluminescence investigation was performed on 390 keV implanted Tm into various substrate types of GaAs, InP, and GaP. The presence of thulium in the implanted layer was verified by SIMS. For GaAs and InP the characteristic sharp 4f-spectra are identified for the first time around 1.23 μm for transitions between the weakly crystal-field-split spin orbit levels $^3H_5 - ^3H_6$ of Tm^{3+} (4f¹²). The emissions which extend from 0.93 to 1.02 eV were best seen in semi-insulating GaAs and InP for samples which were encapsulated and then annealed. The main 1233 nm line in GaAs shows a doublet structure with the proper system

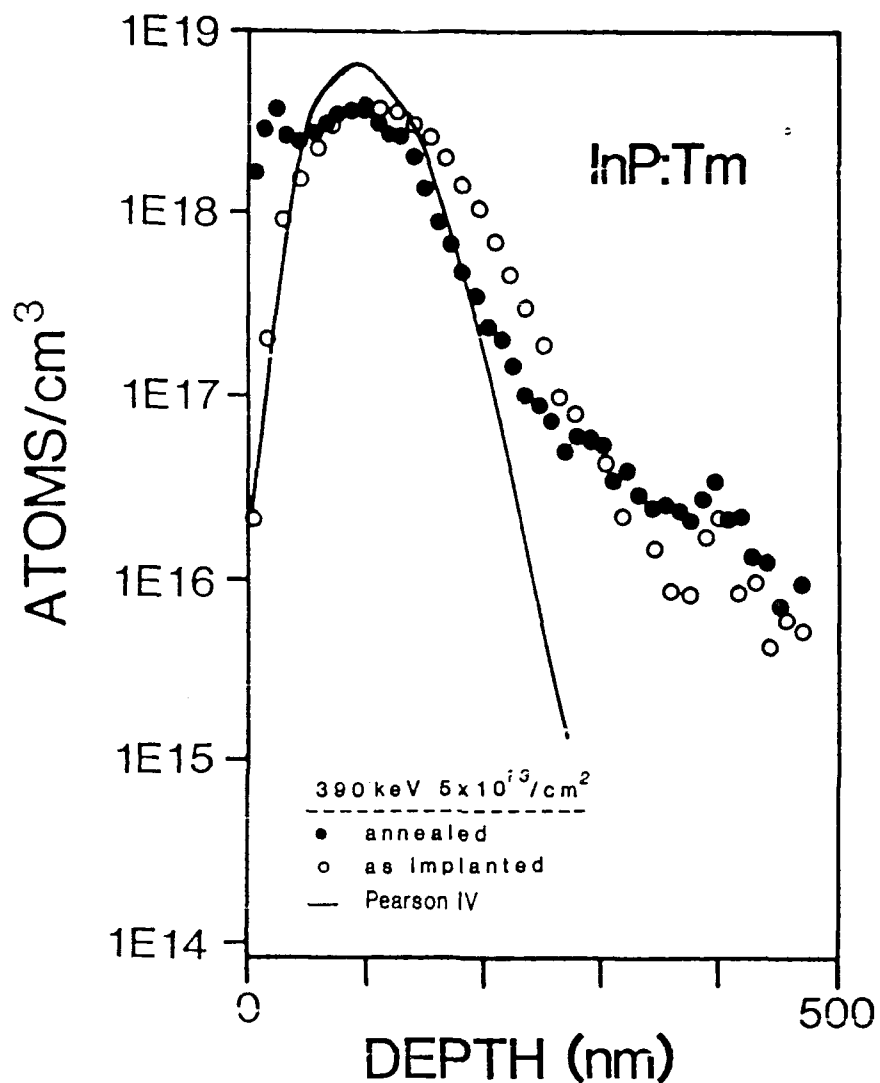


Figure 47. SIMS depth profile of Tm implanted into InP.

resolution, and each doublet component has a measured full-width at half-maximum of better than 0.15 meV. Limited evidence exists for a 2.0 μm emission in InP:Tm associated with transitions between the $^3\text{H}_4 - ^3\text{H}_6$ levels of Tm^{3+} .

Isochronal anneal studies established that the optimum

anneal temperature for 10-15 min anneals was 725°C for the GaAs:Tm system and most likely between 575°C and 625°C for the InP:Tm system. For GaAs:Tm evidence exists that the emissions originate from a second center at anneal temperatures below 625°C; however, with anneals between 625 to 750°C the emissions appear to originate from one dominant center. A model was proposed explaining the annealing behavior of rare-earth implanted semiconductors. Studies of the Tm^{3+} spectra in GaAs as a function of sample temperature show that the 4f-emissions may be seen up to a temperature of 200K without shifts in energy or relative intensity; however, 'hot' lines do develop.

The study made clear the importance of analyzing and choosing the proper starting material for implantation. Encapsulation prior to post-implantation annealing needs to be considered. Choosing a reflectance grating with a flat response in the 1.2 μm spectral region also becomes a consideration. Furthermore due to the shallow implanted layers the absorption depth of the exciting laser radiation becomes an important factor in being able to properly resolve the 4f-emissions, especially when background levels or signals are present.

Photoluminescence of Pr^{3+}

Praseodymium incorporated into semiconductors, specifically III-V semiconductors, has up until now remained essentially uninvestigated. Similar to the photoluminescence of thulium implanted in III-V semiconductors, this is the first investigation to report on the 4f-intracenter emissions of Pr in GaAs and InP. Only GaP doped and implanted with Pr has received prior attention. Some of the results from this investigation on the luminescence of Pr^{3+} in GaAs, InP, and GaP were recently presented (Pomrenke et al, 1989).

Trivalent praseodymium has an electronic configuration of $4f^3$ with a $^3\text{H}_4$ ground state. The free ion spectra of Pr^{3+} is given in Appendix A and shows that numerous infrared emissions may be observed as a result of the many spin-orbit levels. The emissions could range from 1 to 5 μm , a spectral range of interest to integrated optics, fiber optics, and various detectors. Aside from the fact that Pr^{3+} signals have been seen in GaP, infrared emissions at 0.9, 1.1, and 1.4 μm have been observed in GaAs and GaP from trivalent cerium, $Z=58$, (Mueller et al, 1986) a chemically and physically similar element to Pr ($Z=59$); this supports the idea that Pr^{3+} emissions may be observable also in GaAs and InP. An interesting characteristic of Pr is its melting point of 1224 K which is one of the lower values for the rare earths, allowing for possibly easier doping with this element during the epitaxial growth of III-V semiconductors.

Earliest reports of the luminescence of GaP doped with

Pr were by Kasatkin et al (1979) for 45-65 μm thick films grown from confined molten solution. The observed 1.96 eV band was assigned to FB or DA recombinations where the acceptor was possibly Pr; a 1.27 eV band was tentatively assigned to gallium vacancy and donor (Si, S) impurity complexes. No 4f-intracenter emissions of Pr^{3+} were reported. The photoluminescence studies of heat-treated (1300-1350 K) GaP doped with Pr, by Kasatkin et al in 1981, identify 4f-intracenter transitions of Pr^{3+} in GaP at 1.24-1.35, 1.68-1.75, 1.91-2.04, and 2.22-2.3 eV. The four series of emissions were characterized by the sharp lines typically associated with the rare earths. Infrared emissions other than the 1.24-1.35 eV emissions were not reported. A follow-up study on heat treated GaP:Pr by Kasatkin (1985) reports of the instability of the Pr^{3+} luminescence center, in which the Pr^{3+} signals decay over a long storage period.

A more recent study by Gippius et al (1986) addressed the implantation of Pr into GaP from the point of view of the interaction of the rare earth and other impurities and defects. The spectra of GaP implanted with 350 keV Pr and subsequently annealed at 700°C shows sharp emissions at 1.1 μm due to the intracenter transitions of Pr^{3+} . The co-implantation of Li results in changes in the 1.1 μm emissions plus the appearance of further sharp, structured emissions at 1.9 μm . This latter emission is attributed to Li-Pr complexes and it is pointed out that Li is considered an

important activator of rare earth luminescence.

Further studies on the Pr^{3+} emissions in III-V semiconductors have not been reported, however, Pr^{3+} emissions have been reported in the past in dominantly ionic crystals such as oxides and fluorides. Di Bartolo (1968) in his tabulation of trivalent rare earth lasers lists Pr^{3+} emissions in $\text{Ca}(\text{NbO}_3)_2$, CaWO_4 , LaF_3 , and SrMoO_4 . Tagiev et al (1987) reported on the photo- and electro-luminescence of GaS:Pr and discusses the excitation mechanism and the symmetry of the various Pr-centers. Of interest is also an article by Morgan et al (1986) addressing the quenching processes in $\text{LaF}_3:\text{Pr}^{3+}$ through lifetime studies.

The initial goal was to investigate high energy (1 MeV) implanted GaAs, InP, and GaP. As mentioned in the experimental section, the vendor performing the implantation was unsuccessful in this effort; implanting silver in the form of AgO_2 instead of Pr as confirmed by SIMS. Without knowing this fact, that is, prior to the SIMS analysis a multitude of samples were investigated through photoluminescence for the Pr-related emissions. Post implantation processing for most of the 1 MeV implanted samples was with rapid thermal annealing (RTA) as previously discussed. The samples included Si InP; Si, n-, and p-type GaAs; and n- and p-type GaP. The negative results did lead to the identification of defect related emissions as a result of the implantation. The implantation problem was rectified with the successful implantation of Pr at an energy of 380

Table 14. Sample Information for the 380 keV
Praseodymium Implanted Semiconductors.

Semiconductor	Substrate conductivity	Substrate identifier	Anneal Condition °C/min/gas
GaAs	SI	WA	600/10/fg
	SI	WA	675/10/fg
	SI	WA	725/10/fg
	SI	WA	750/10/fg
	SI	CO	750/10/fg
InP	SI	MR(338)	575/10/fg
	SI	MR(338)	625/10/fg
	SI	MR(338)	675/10/fg
	SI	MR(338)	750/10/fg
GaP	p	GPC	750/10/fg
	p(und)	MRC	750/10/fg

keV with a different implantation system.

Although numerous samples were implanted and processed, the semiconductor samples which were eventually investigated and which are discussed in this study are listed in Table 14. As indicated, they were implanted at an energy of 380 keV and a dosage of $5 \times 10^{13} \text{ cm}^{-2}$ into different semi-insulating (SI) GaAs substrates, SI-InP, and p-type GaP. After implantation the samples were not encapsulated and were annealed in the conventional annealing furnace face down on a Si:P wafer strip in flowing forming gas (fg). The annealing time was 10 minutes and the temperatures varied from 575 to 750°C. Excitation was with the 514.5 nm line of the air cooled Ar-ion laser, but primarily with the 647.1 nm line of the Kr-ion laser. Signal dispersion was with the 1.6 μm blazed grating; besides for the results reported in Fig. 53 for which the

1.0 μm blazed grating was used. Detection was with the Ge detector. Further details on the photoluminescence experiment are found in the experimental section.

The first evidence of 4f-intracenter emissions of Pr^{3+} in GaAs and InP is shown in Figure 48; no Pr-related emissions were seen in GaP. For both semiconductors the emissions due to transitions from the spin-orbit level $^1\text{G}_4$ to the level $^3\text{H}_5$ of Pr^{3+} ($4f^2$) are shown at around 1.35 μm . The GaAs:Pr spectrum also shows luminescence at around 1.6 μm due to transitions between the spin-orbit levels $^3\text{F}_3 - ^3\text{H}_4$ of Pr^{3+} . The difference in the structure of the 1.35 μm emission between the two semiconductors is a result of the difference in the crystal field. Laser excitation for both samples was with the 647.1 nm line and emission temperature was approximately 6 K. The (WA) GaAs:Pr sample underwent a 750°C anneal while the (MR338) InP sample was annealed at 675°C after implantation.

Further investigations were performed on Pr implanted (WA) GaAs which included isochronal anneal and sample temperature dependent studies. The upper spectrum in Fig. 49 shows evidence of another Pr^{3+} emission in GaAs around 1.05 μm ; this is a result of transitions between the spin-orbit levels $^1\text{G}_4$ and the ground state $^3\text{H}_4$ of Pr^{3+} . The lower spectra of Fig. 49 identifies the Pr^{3+} emission in GaAs as shown in Fig. 48. Hence, three sets of sharp lines are evident around 1.05, 1.35, and 1.6 μm in GaAs due to

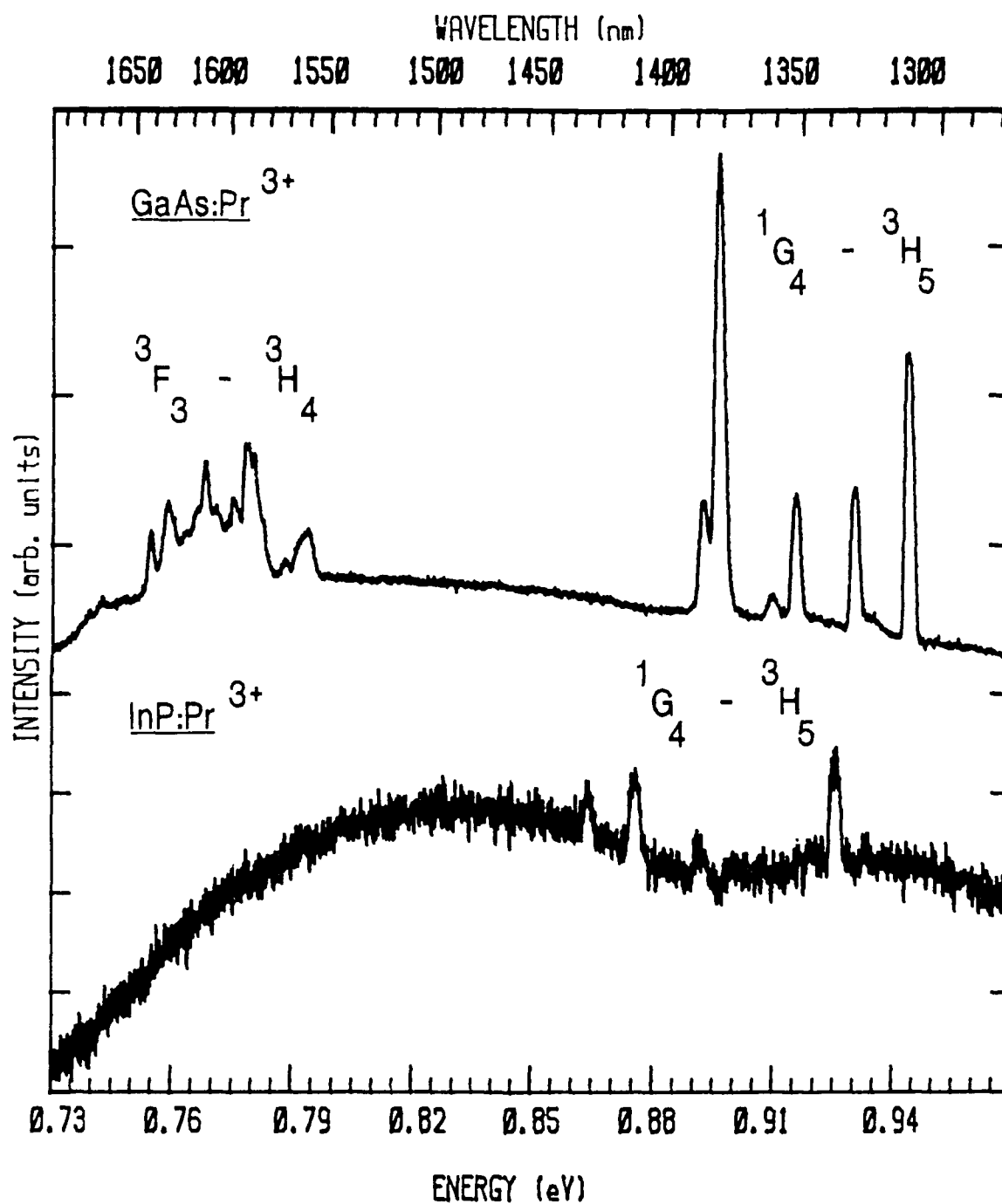


Figure 48. Comparison spectra of the Pr^{3+} emission at 6K in GaAs and InP.

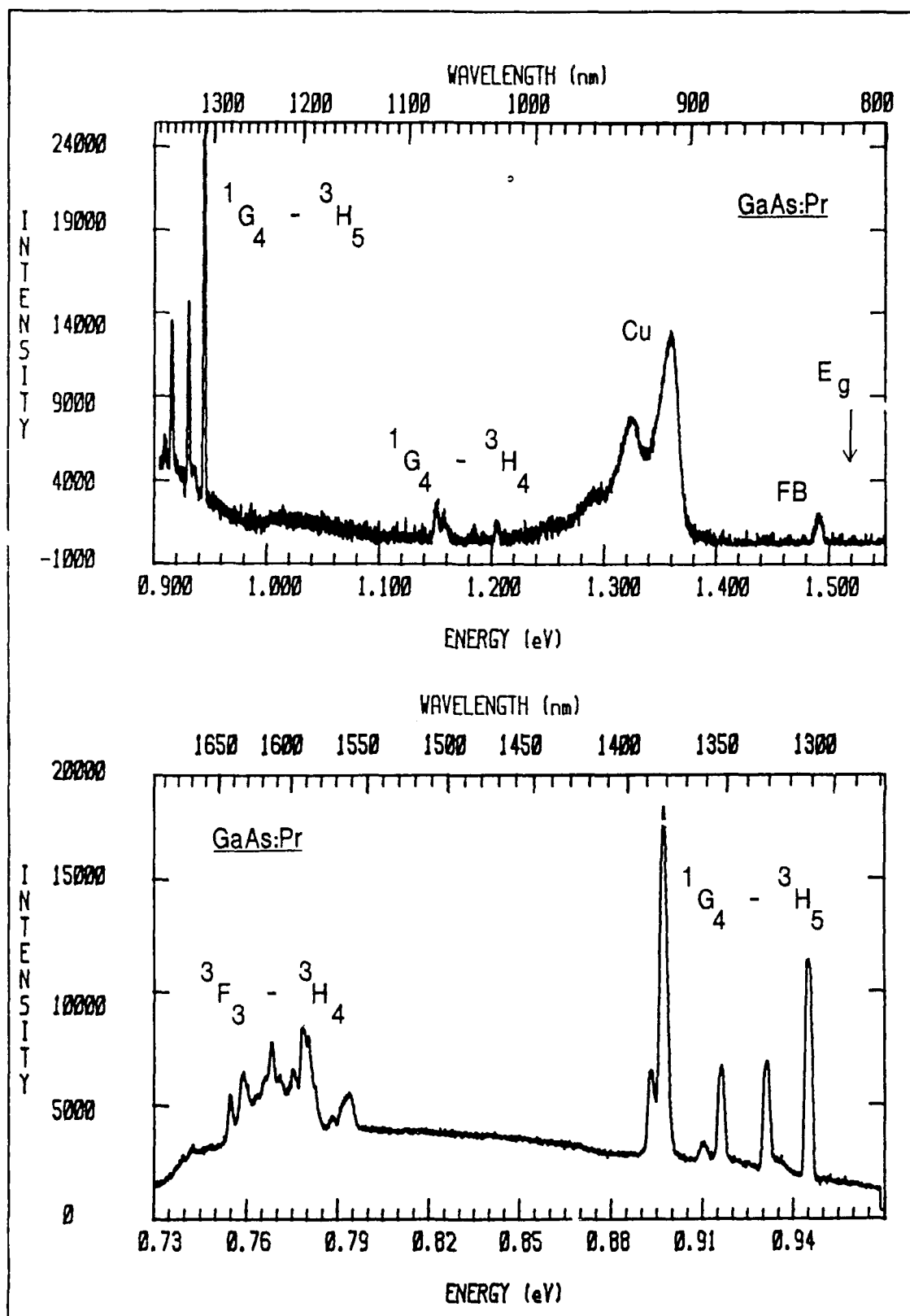


Figure 49. Transitions between three sets of spin-orbit levels of Pr^{3+} in implanted GaAs.

transitions between the crystal-field split spin-orbit levels $^1G_4 - ^3H_4$, $^1G_4 - ^3H_5$, and $^3F_3 - ^3H_4$, respectively. The $^1G_4 - ^3H_5$ transitions are the most intense. Figure 49 also identifies the free-to-bound (FB) near-edge emissions and a strong transition metal emission (i.e. Cu) at 1.36 eV plus its lower energy phonon replicas. It will be shown later that at lower anneal temperatures a Mn-related peak is also present around 1.40 eV. The spectra in Fig. 49 are from a 750°C annealed sample excited by the 647.1 nm Kr-ion laser line. Due to slightly different experimental conditions (power and long pass filter) the intensity of the $^1G_4 - ^3H_5$ emission is not at the same intensity for the two spectra of the top and bottom parts of the figure; however, this emission can be used to compare the relative intensities of all the emission lines in the 0.73 to 1.55 eV spectral range.

As discussed in the section on the photoluminescence of Tm^{3+} , various information about the emission processes may be gained by performing anneal temperature dependent studies. An isochronal anneal study from 600 to 750°C was performed on Pr implanted GaAs for the 0.73 to 0.96 eV and the 0.90 to 1.55 eV spectral region as shown in Figures 50 and 51, respectively. Although two different laser excitations were used for the spectra in these figures (647.1 nm at 200 mW and 514.5 nm at 50 mW), it appears that the maximum optical activation of Pr occurs for the sample annealed at the highest temperature (750°C). Based on investigations of

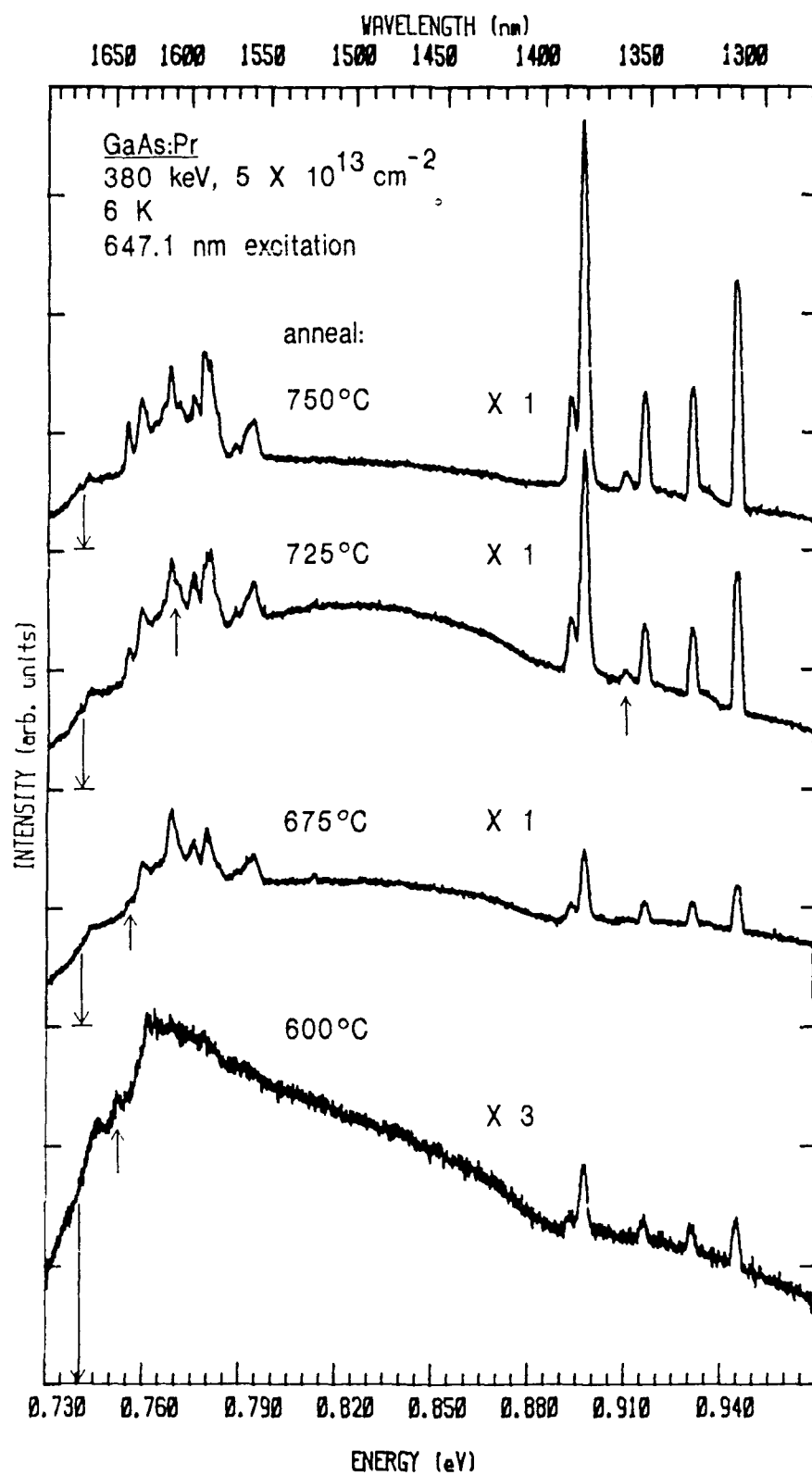


Figure 50. Isochronal anneal study of the GaAs:Pr emissions in the 0.73 - 0.96 eV spectral region.

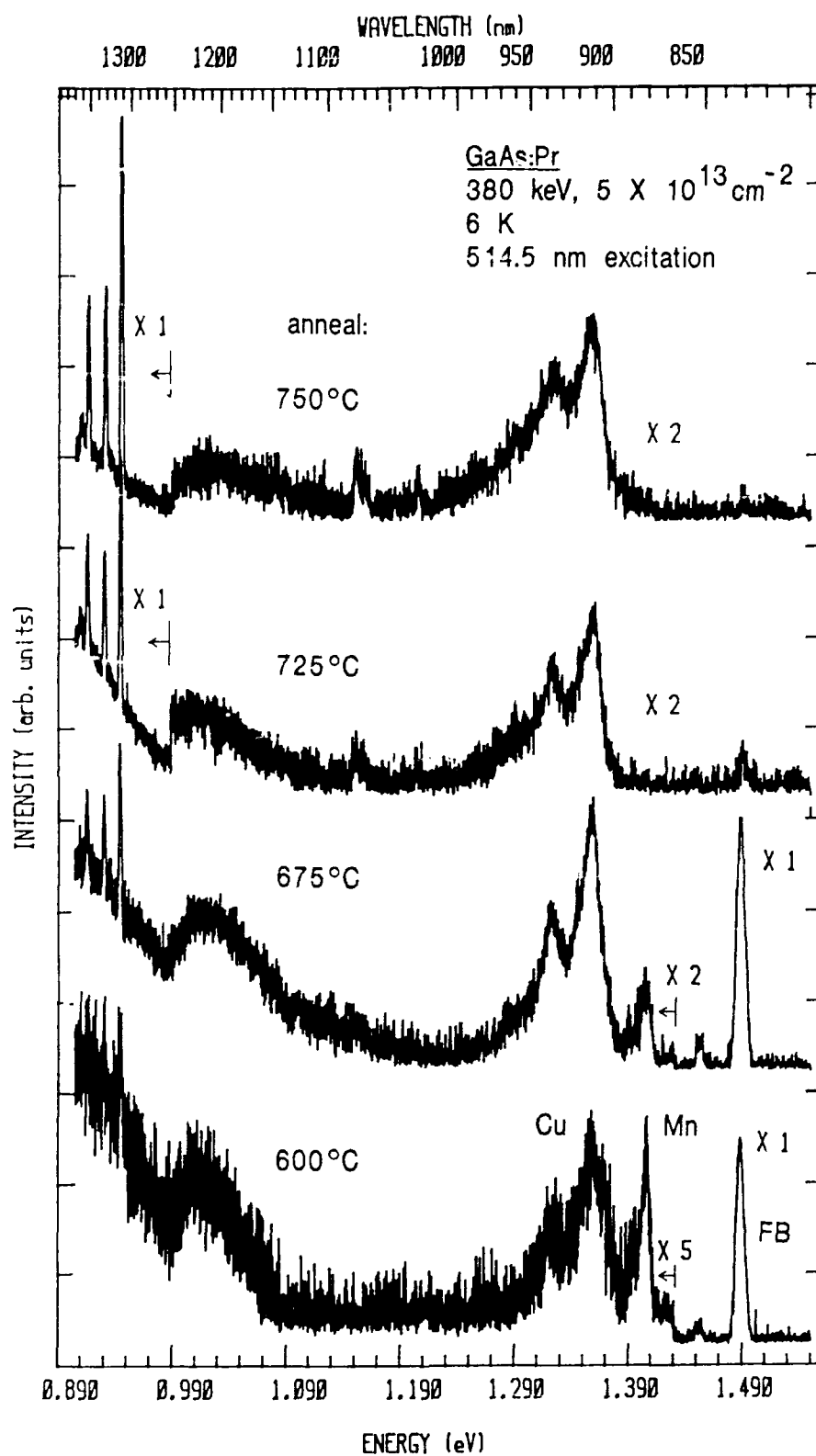


Figure 51. Isochronal anneal study of the GaAs:Pr emissions in the 0.90 - 1.55 eV spectral region.

other rare-earth/semiconductor systems it is believed that a higher anneal temperature would not necessarily lead to a more intense rare earth signal. The 750°C anneal represents most likely the optimum annealing temperature at an anneal time of 10 minutes for Pr implanted GaAs. However, investigations at higher anneal temperatures are certainly suggested for future study.

As seen in Fig. 50 and 51, both the 1.35 and 1.6 μm emissions are activated already at the lowest anneal temperature. However, evidence of the optical activation of the 1.05 μm Pr^{3+} emission does not appear until an anneal temperature of 725°C. It appears that the 1.35 and 1.6 μm emissions originate from one dominant center as evident by effectively no changes in the relative intensities of the main emission lines upon annealing from 600 to 750°C. However, some small changes do occur as noted by the 'up-pointing' arrows in Fig. 50, giving evidence of additional centers. As in the study on Nd-implanted GaP and GaAs (Mueller et al, 1986), isothermal investigations might be used to further characterize the behavior and nature of the different centers.

The spectra of the 4f-intracenter emissions of Pr^{3+} in GaAs show broad background bands centered around 1.0 eV and 0.80 - 0.83 eV. In past investigations such emissions have substantially masked or quenched the 4f-emissions; however, due to the quality (WA) GaAs substrate such problems were

minimized. The 1.0 eV band is associated with defect complexes as a result of implantation (Deveaud and Favennec, 1977); the high temperature annealing appears to reduce the intensity of the defect band. The 0.80 - 0.83 eV band is assigned to the 'EL2 Family' midgap levels in GaAs which have received much attention over the last decade (Ikoma and Mochizuki, 1985; Li and Wang, 1982). Controversy still surrounds the actual origin of the band, but the production of antisite arsenic (As_{Ga}) or As_{Ga} -related complexes and point defect clusters from both the substrate and the implantation process are not ruled out.

Of interest in Fig. 51 is the disappearance of the Mn-related and near-edge emissions as the Pr^{3+} emissions increase in intensity upon annealing to high temperatures. A competing process between the rare earth and these emissions appears to be involved. As will be discussed in a later section, free carriers are involved in the excitation of the rare earth. It appears that there is a greater probability for the free carriers to transfer energy to the rare earths, perhaps due to a greater capture cross-section, instead of recombining in the form of free-to-bound transitions. A similar behavior was noted for an isochronal anneal study of InP:Yb .

Sample temperature dependent studies as shown in Fig. 52 indicate that the 1.35 μm Pr^{3+} emissions essentially disappear around 107 K and the 1.6 μm Pr^{3+} emissions become

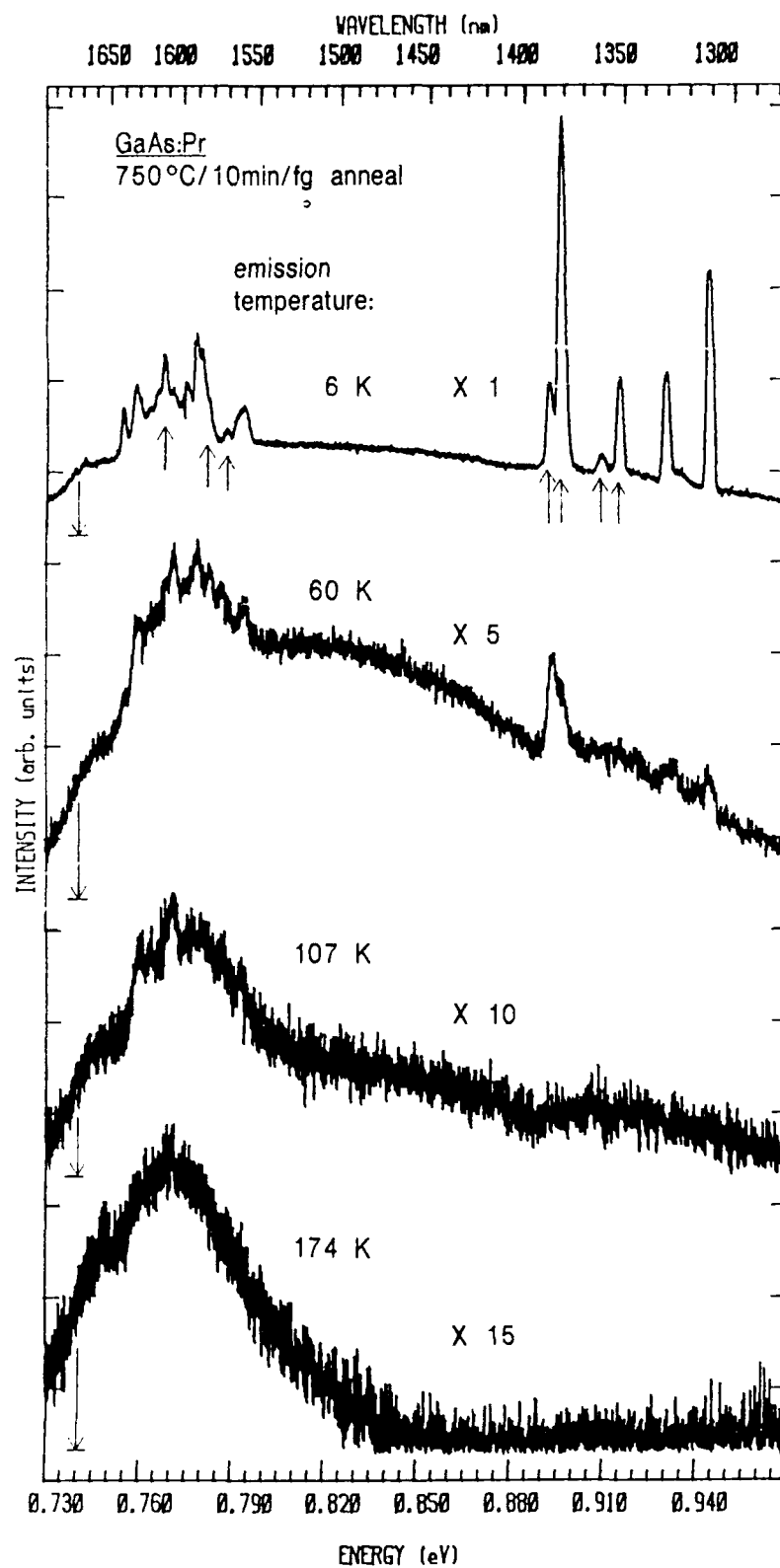


Figure 52. Intracenter emissions of Pr^{3+} in GaAs as a function of sample temperature.

quenched around 174 K. Due to the low intensity of the 1.05 μm emission, temperature dependent studies were not performed. Aside from the differences in the above mentioned temperature dependence between the 1.35 and 1.6 μm emissions, the relative intensities of various emission lines also change with temperature, specifically for those lines marked by 'up-pointing' arrows in Fig. 52. This supports the idea of multiple emission centers upon implanting Pr into the semiconductor lattice. Evidence of 'hot' lines was not seen. The spectra in Fig. 52 are a result of exciting the sample with the 647.1 nm line with a power of 200 mW at the laser.

High resolution investigations of the strongest Pr^{3+} emission at 1382 nm show the full-width at half-maximum to be less than 0.9 meV. The effects of incorporating the praseodymium into a different GaAs substrate were also examined. Figure 53 represents the 1.35 μm Pr^{3+} emissions from (WA) GaAs and (CO) GaAs substrates, both of which were annealed at 750°C for 10 min in forming gas after implantation. Excitation wavelength and power were the same, only the diffraction gratings were different. Aside from the higher resolution of the (CO) GaAs:Pr spectrum, no changes in the emission lines were observed between the substrates even though residual impurity concentrations differ.

The investigation of Pr-related emissions in InP lead to the identification of the $^1\text{G}_4 - ^3\text{H}_5$ transitions of Pr^{3+} as

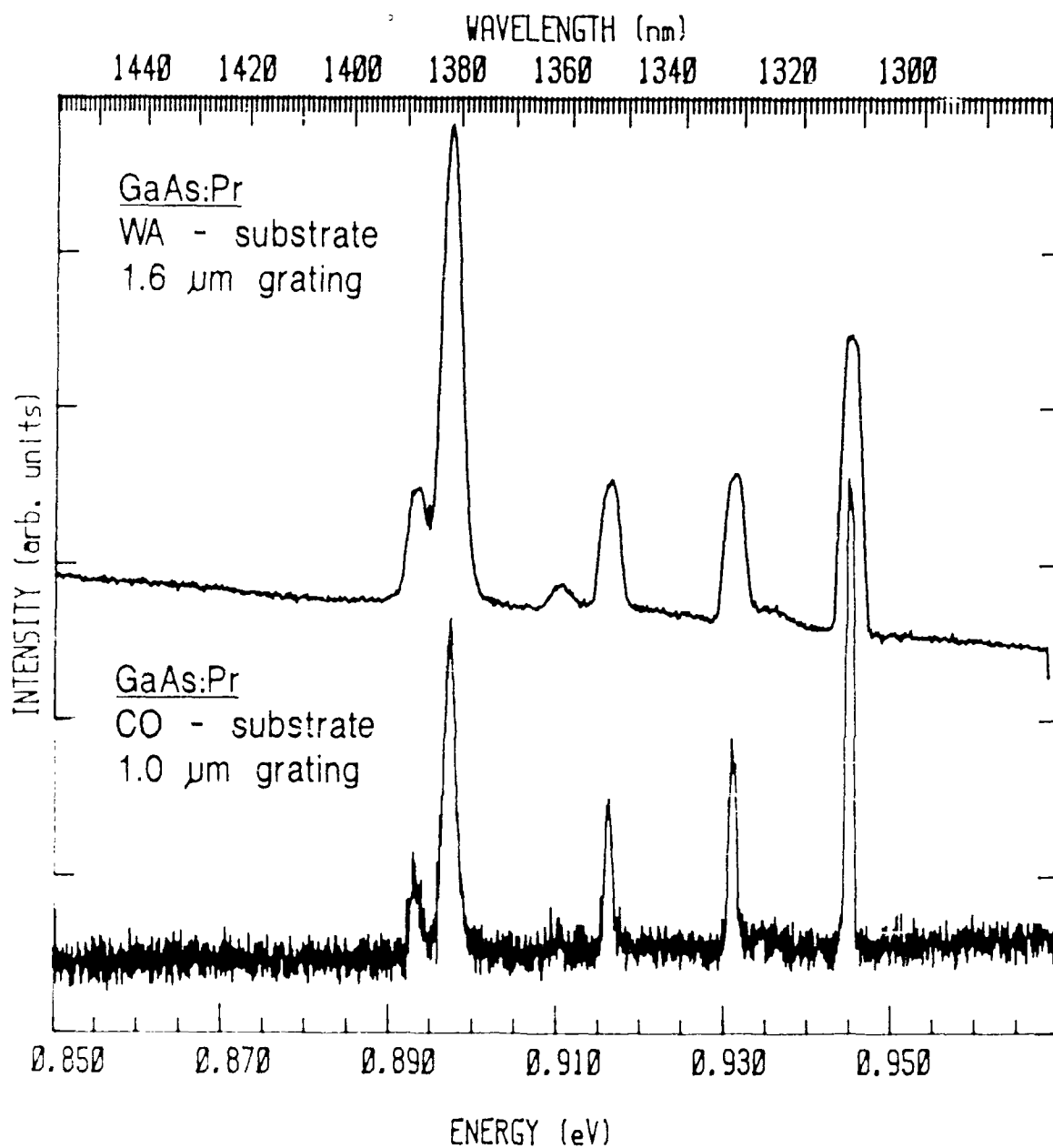


Figure 10. Photoluminescence spectra of Pr^{3+} implanted GaAs. From two different implantation conditions and substrate.

shown in Fig. 48. The excitation with different laser lines and isochronal anneal studies of InP:Er did not lead to evidence of the $^3F_3 - ^3H_4$ transition of Pr^{3+} at 1.6 μm or the $^1G_4 - ^3H_4$ transition of Pr^{3+} at 1.05 μm as seen in GaAs:Pr. This is most likely a result of the broad background peaks in the InP:Pr spectra as shown in the isochronal anneal studies of Figures 54 and 55. The intensity of the broad bands mask or even quench the Pr-related emissions such that they can effectively be seen only for the sample annealed at 675°C, which may be considered an optimum anneal temperature. Weak evidence of the 1.35 μm emission is seen for the 625°C annealed sample but the atmospheric absorption peaks ('abs', see Fig. 54) in this region interfere with the proper identification. (The 'L' in the figures represents the 647.1 nm laser line in second order.)

In Figure 54 two broad emission bands are seen centered around 0.83 eV and 0.94 eV. The former remains uninvestigated besides a reference to such a band around 0.77 eV as reported by Eaves et al (1982). The latter band (0.94 eV) is most likely not a band but an artifact as a result of the 1.6 μm grating; the actual peak being the very broad peak (220 meV) centered around 1.07 eV shown in Fig. 55. This emission has been attributed to a complex between either an indium vacancy and a phosphorous vacancy ($V_{In}V_{P}$) or a phosphorous interstitial and a phosphorus vacancy ($V_P P_i$) (Eaves et al, 1982). In Fig. 55 the less intense broad emission

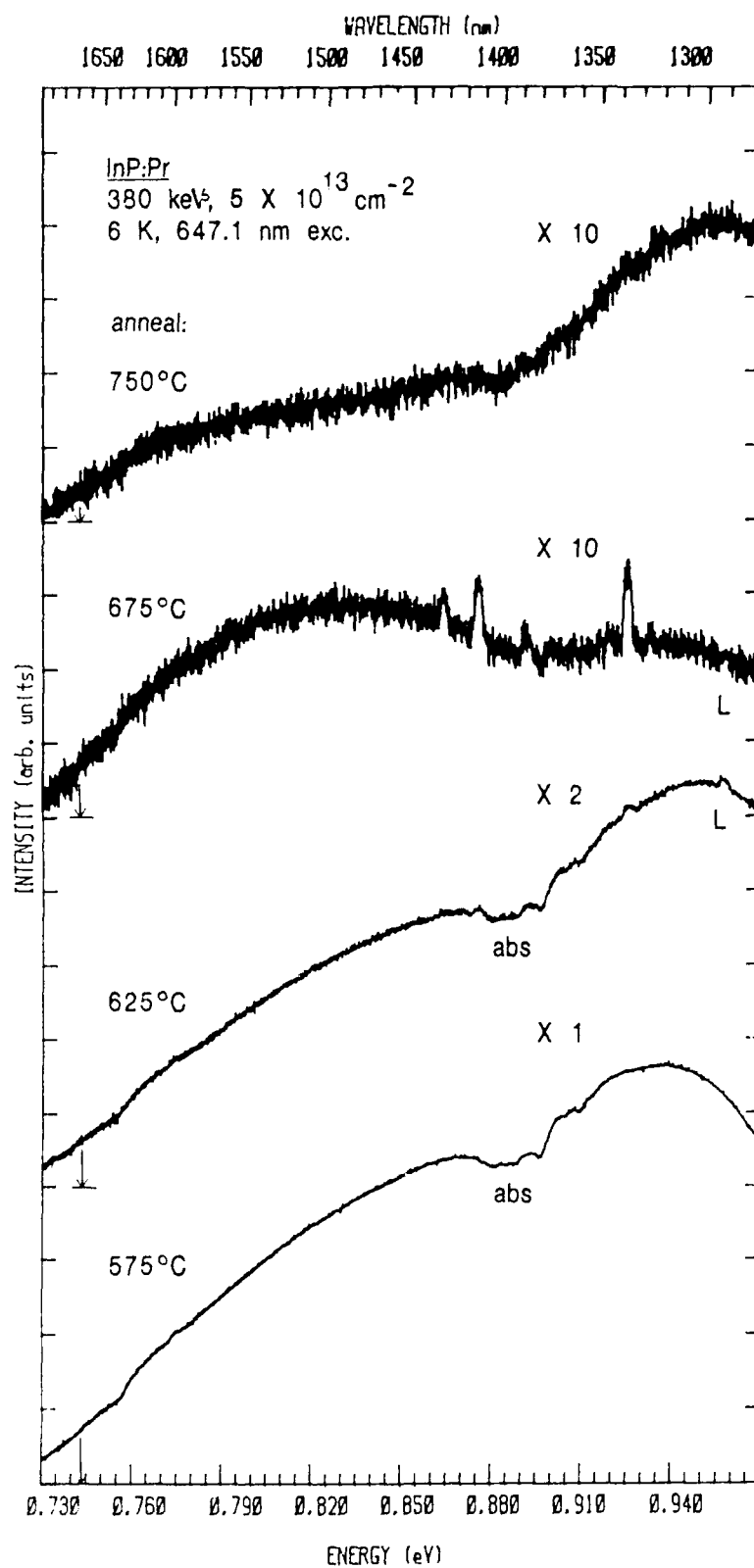


Figure 54. Isochronal anneal study of the Pr^{3+} emissions in InP for the 0.73 - 0.97 eV spectral region.

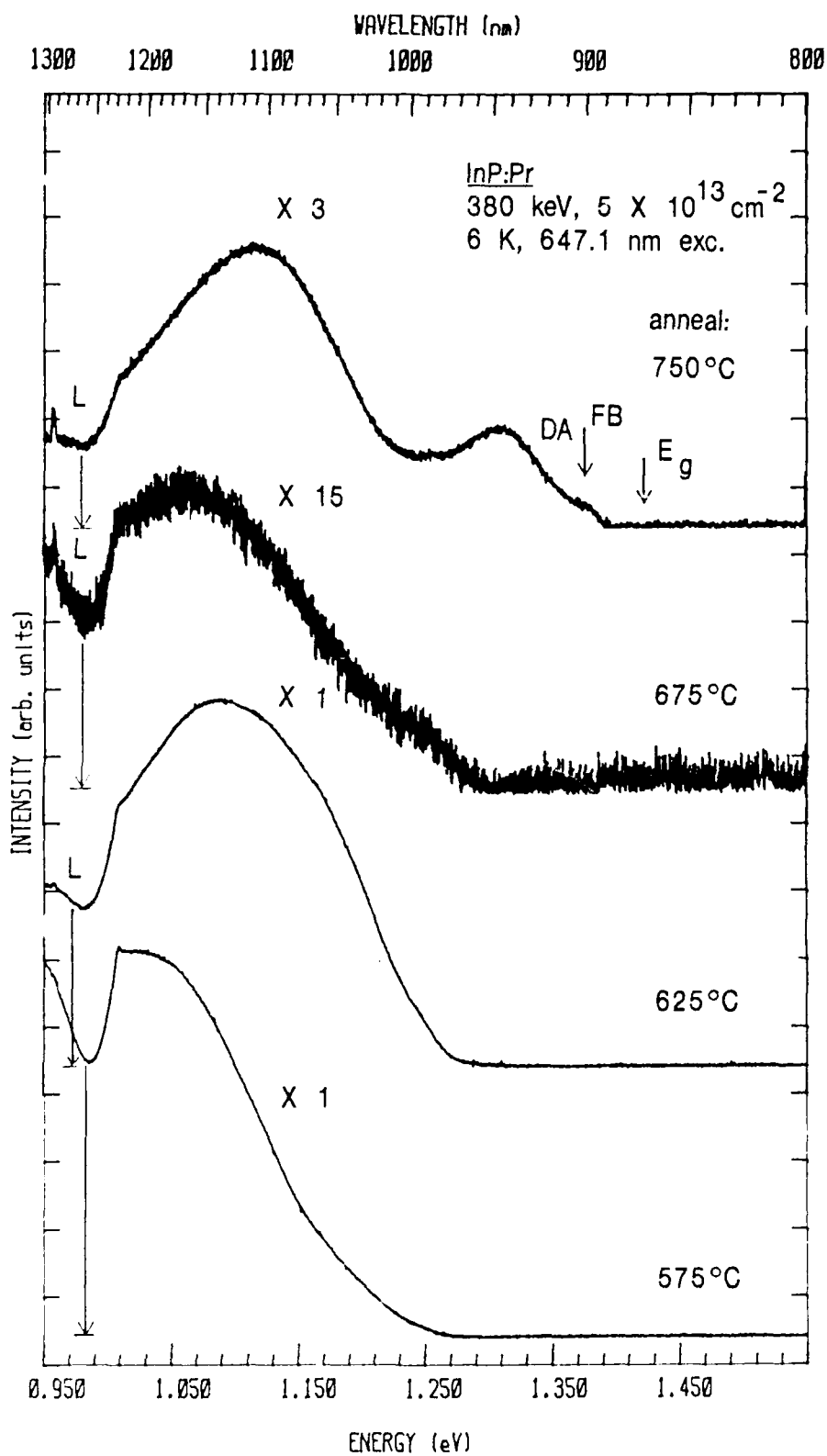


Figure 55. Isochronal anneal study of the Pr^{3+} emissions in InP for the 0.95 - 1.50 eV spectral region.

centered around 1.31 eV is most likely a defect complex associated with the implantation process; similar bands have been identified before in Mg implanted InP (Pomrenke et al, 1981).

Due to the weak Pr^{3+} emission around 1.35 μm in InP no sample temperature dependent studies were undertaken. Of interest in Fig. 55 is that essentially no near-edge emissions are seen even upon annealing the samples up to 750°C. The annealing conditions may not be satisfactory enough to fully recover the lattice from the implantation damage, perhaps as a result, the 1.07 eV vacancy peak has been intensified and might require a longer anneal time, different anneal atmospheres, and encapsulation to reduce the luminescence intensity of the defect accordingly. Another reason for the quenching of the near edge emissions might be a competing process as discussed for GaAs:Pr.

As mentioned no Pr-related emissions were seen in Pr implanted GaP; however, only p-type and undoped p-type GaP:Pr samples annealed at 750°C were examined (see Table 14) using the 514.5 nm excitation line. As in previous cases and as for InP:Pr, strong, broad background bands most likely masked or suppressed any evidence of Pr^{3+} emissions. Since free carriers are involved in the excitation process of rare earth implanted III-V semiconductors, p-type substrates are most likely not suitable hosts; however, heavily doped n-type GaP substrates also exhibit broad emission bands in the infrared

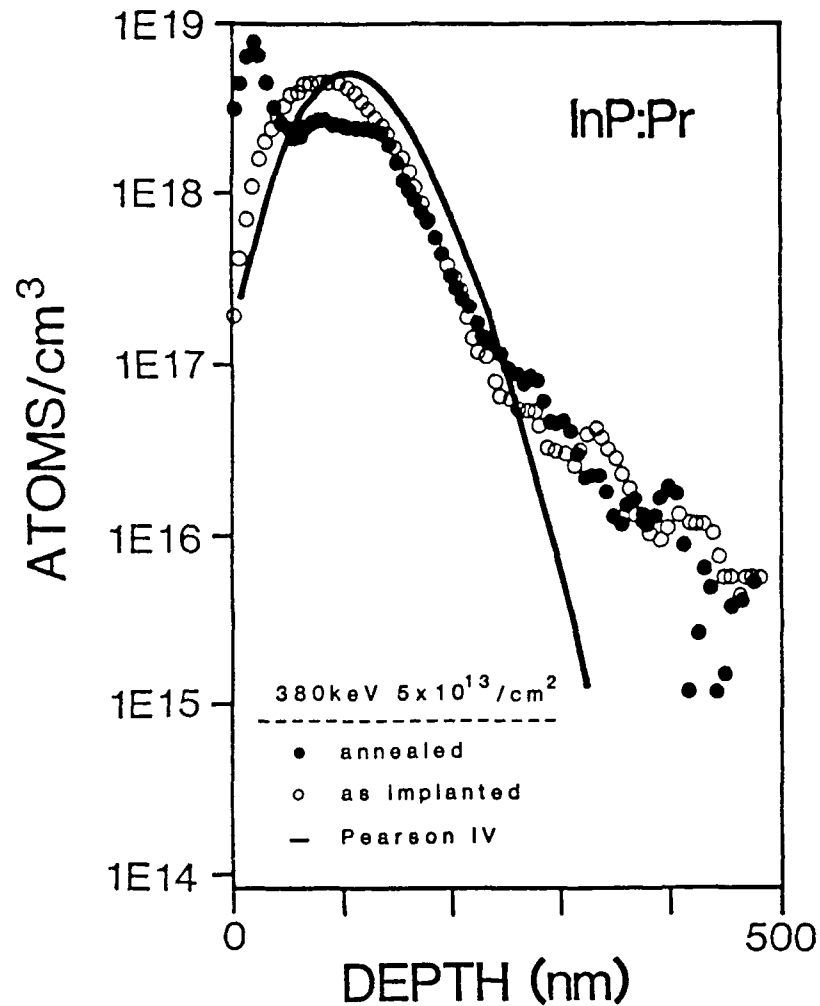


Figure 56. SIMS depth profile of Pr implanted InP.

spectral region. The importance of choosing the proper substrates prior to implantation is again emphasized; preferably, low concentration doped samples, $< 10^{16}$ carriers cm^{-3} . Past successful investigations by Soviet and German (FRG) researchers have concentrated on using GaP:Te substrate.

Figure 56 shows the results of a SIMS depth profile analysis on InP implanted with Pr. Depicted is the theoretical distribution for the 380 keV and $5 \times 10^{13} \text{ cm}^{-2}$

dosage Pr implants as determined from the R_p (105.6 nm) and ΔR_p (45.2 nm) calculated by the TRIM code (Ziegler et al, 1985); also shown are the depth distribution of the Pr ion for implanted but untreated InP (as-implanted) and for Pr implanted InP annealed at 750°C for 10 minutes in forming gas. The SIMS analysis verified the presence of the Pr ion in the InP matrix and allowed the experimental determination of a projected range, R_p , of 78 nm and a straggling, ΔR_p , of 44 nm. The somewhat poor agreement in the projected range may possibly be from the improper measurement of the implantation energy. The figure shows that Pr has diffused toward the surface upon annealing. This would support the idea of exciting the rare earth luminescence with excitation lines having a low absorption coefficient and performing a depth dependent luminescence study using layer removal techniques.

In conclusion evidence was given of Pr incorporated into GaAs and InP through spectroscopy and SIMS analysis. The characteristic intra 4f-shell luminescence spectra of Pr^{3+} ($4f^2$) were observed for the first time from praseodymium implanted GaAs and InP at an implant energy of 380 keV. Three sets of sharp (less than 0.9 meV, fwhm) emissions are apparent in GaAs due to transitions between the crystal-field split spin-orbit levels $^1G_4 - ^3H_4$, $^1G_4 - ^3H_5$, and $^3F_3 - ^3H_4$ of Pr^{3+} at 1.05, 1.35, and 1.6 μm , respectively. In InP only the transitions between the levels $^1G_4 - ^3H_5$ of Pr^{3+} are

observed. The 1.35 and 1.6 μm emissions have their own unique temperature dependent behavior; the highest temperature at which a sharp emission is observed is around 175 K.

Based on isochronal anneal studies and the sample temperature dependent studies for GaAs:Pr, the rare earth luminescent centers were found to occupy different lattice sites but one very dominant center is evident at anneal temperatures of 675°C to 750°C. The different centers are possibly due to the radiation damage from implantation. At an anneal time of 10 minutes, optimum anneal temperature for Pr implanted GaAs appears to be 750°C and for Pr implanted InP, 675°C. At and near the optimum anneal temperature for both GaAs and InP, there is essentially no evidence of near-edge emissions, hinting at possible competing processes that favor the excitation of the rare earths versus the free-to-bound or donor-acceptor recombinations.

The intense, broad background bands in InP prevented the further identification of Pr-related emissions. In GaP the background bands entirely masked the rare earth emissions; hence, preventing the verification of reports of 4f-intracenter emissions in GaP by Kasatkin et al (1981) and Gippius et al (1986). Finally, the successful identification of a total of three sets of lines from transitions from the luminescent levels of Pr^{3+} in GaAs for the 1.02 to 1.64 μm spectral range allows for potentially wide opto-electronic applications for this rare-earth/semiconductor system.

Photoluminescence of Actinides

It was possible to observe for the first time intracenter 5f-emissions of an actinide incorporated into different semiconductors. This leads to the possibility of fabricating pn-junction diodes and exciting the 5f luminescence via minority-carrier injection in a spectral region of interest to silica and nonsilica based fiber optics. Historically, the spectroscopy of the radioactive and artificial actinides have been limited due to the material handling problems associated with them, furthermore conventional doping of crystals is hampered by the affinity of actinides for oxygen and other impurities. Our success came as a result of implanting the long lived isotope of uranium (U) into GaAs, InP, and GaP with a new implantation technique. Thorium (Th) implanted III-V semiconductors were also examined to a very limited extent; however, since this trivalent ion ($5f^1$) would have most likely similar characteristics as cerium (Ce), which has only one excited state and an associated transition in the far infrared, no systematic study was pursued at this time. But if the valency of Th is 4+ one would expect changes in the F-B, D-A, or deep level emissions, and hence, one would want to pursue an appropriate investigation associated with these bands.

As to electro-optic applications, of special interest is the fabrication of devices for integration into third generation silica based fiber optics in the 1.5 to 1.6 μm region and into low loss nonsilica (for example, ZrF_4 and

As-S) based fibers (Miyashita et al, 1982) for the 2.5 μ m region. As mentioned in the introduction, the almost decade long interest in lanthanide or rare-earth doped semiconductors derives from a similar motivation to fabricate solid state lasers and light-emitting diodes (LEDs). The emission wavelengths in these 4f-doped materials are determined not through the host semiconductor bandgap, but from the transition energies within the 4f levels of the rare earth impurity. As mentioned in earlier sections, examples of 4f-shell luminescence in III-V semiconductors have been reported for Sm (Pyshkin, 1975), Yb (Zakharenkov et al, 1981; Kasatkin et al, 1980; Ennen et al, 1983; Ennen, 1987), Er (Ennen et al, 1983; Ennen, 1987; Ushakov et al, 1982), Nd (Mueller et al, 1986), Tm (Pomrenke et al, 1989), and Pr (Kasatkin et al, 1981; Pomrenke et al, 1989).

Similar to the lanthanides, actinides are good candidates as active ions in electro-optic materials due to the numerous sharp emissions covering a broad spectral region. Crystals of alkali fluorides, alkaline earth fluorides, and lanthanide fluoride doped with uranium have shown emission spectra containing many narrow lines and sharp bands associated with uranium centers (Goerlich et al, 1965; Runciman et al, 1981; Carnall et al, 1985). The sharpness of the emission and absorption spectra results from the 5f-shell being shielded from the crystal environment by filled 6s and 6p shells. Investigations have shown that uranium may be

incorporated into crystals with different valencies in the form of U^{3+} , U^{4+} , U^{5+} , and U^{6+} . Crystals doped with uranium show lasing properties in the 2.2 to 2.6 μm spectral region; the region of interest for nonsilica based infrared fibers. Studies on actinide solid state lasers go back to the early 1960's for $\text{BaF}_2:U^{3+}$, $\text{CaF}_2:U^{3+}$, and $\text{SrF}_2:U^{3+}$ (Porto et al, 1962a; Porto et al, 1962b; Boyd et al, 1962; DiBartolo, 1968).

The optical absorption spectra of uranium doped alkali and alkaline earth fluoride crystals are made up of components from trivalent uranium and tetravalent centers (Goerlich et al, 1965; Title et al, 1962). This becomes important when attempting to make valency assignments to particular emission centers. In the above case for laser activity, the emissions are assigned to the transitions between the $^4I_{11/2}$ manifold and the $^4I_{9/2}$ manifold of trivalent uranium. Title et al (1962) showed that the laser action at 2.24 μm observed by Porto et al (1962b) in CaF_2 samples was actually due to tetravalent uranium centers (U^{4+}) and was ascribed to transitions between the 3H_4 ground state and the excited state 3F_2 . This was later also confirmed by Porto and Yariv (Title et al, 1962), a fact which however has not been adopted by numerous review articles on laser crystals. It is noted that U^{4+} has a $5f^2$ configuration with a ground state of 3H_4 while U^{3+} has a $5f^3$ configuration with a $^4I_{9/2}$ ground state.

Crystals used in this study were grown in the $\langle 100 \rangle$

direction aside from the p-type GaP (MRC) which was grown in the $\langle 111 \rangle$ direction. Both (MA) GaAs and (Mk338) InP crystals were semi-insulating with resistivity ranging from $(0.1 - 1) \times 10^8$ ohm-cm. The GaP samples consisted of two different conductivity types, (GAC) GaP:S with a carrier concentration of $n = 1.0 \times 10^{17} \text{ cm}^{-3}$ and unintentionally doped p-type GaP with $p = 1.7 \times 10^{16} \text{ cm}^{-3}$. The samples were cleaned and etched before implantation at a mean energy of 131 keV. After implantation they were proximity annealed without encapsulation, face-down on a Si:P wafer, in a conventional annealing furnace. Nuclear activity measurements were made on the uranium implanted samples and activity was determined to be at or below background.

As explained before, implantation of the uranium was performed using an unconventional implantation technique with a new kind of high current metal ion source (Brown et al, 1985). This Metal Vapor Vacuum Arc (MEVVA) ion source was originally developed to produce high current beams of metal ion species for synchrotron injection. The MEVVA ion source makes use of a dense metal plasma generated directly from the cathode material, as the medium from which ions are extracted. The resulting intense ion beam is then composed of the cathode source material, which for our case was U^{238} .

Although suitable for this study, the technique is somewhat limited due to the departure of the implanted depth profile from Gaussian because of the ion charge state

distribution, and hence, the energy distribution of the incident ion beam. The spread of charge states (in this case U^{1+} , U^{2+} , U^{3+} , and U^{4+}) results in an uncertainty in the projected range, R_p , and straggling, ΔR_p . The high dose implantation of uranium into silicon has been experimentally demonstrated using the MEVVA ion source (Brown et al, 1988b).

In this investigation one of the main interests was to implant a sufficiently deep layer such that the U-ions may be properly excited by the laser light. One can estimate R_p and ΔR_p of the implant by assuming the beam to be mono-energetic at the charge state distribution-weighted mean energy of 131 keV and using the TRIM code which determines the various implantation statistics (Ziegler et al, 1985). This energy is the product of an extraction voltage of 50 kV and a mean charge state of 2.62 for uranium, based on particle current (Brown et al, 1988b). The R_p and ΔR_p for U^{238} in GaAs are calculated to be 32.2 and 11.1 nm; for InP they are 36.6 and 13.8 nm; and for GaP, 37.5 and 10.5 nm, respectively.

Secondary-ion mass spectrometry (SIMS) depth profiling was performed on as-implanted and 750°C annealed InP:U. As seen in Figure 57 the near-Gaussian distribution was skewed into the substrate for both samples; overall, a close correlation was observed for the depth distribution of the uranium as predicted by the TRIM code. Although low diffusivity is expected for uranium, we observed, at least for the 750°C anneal case, clear evidence of diffusion toward

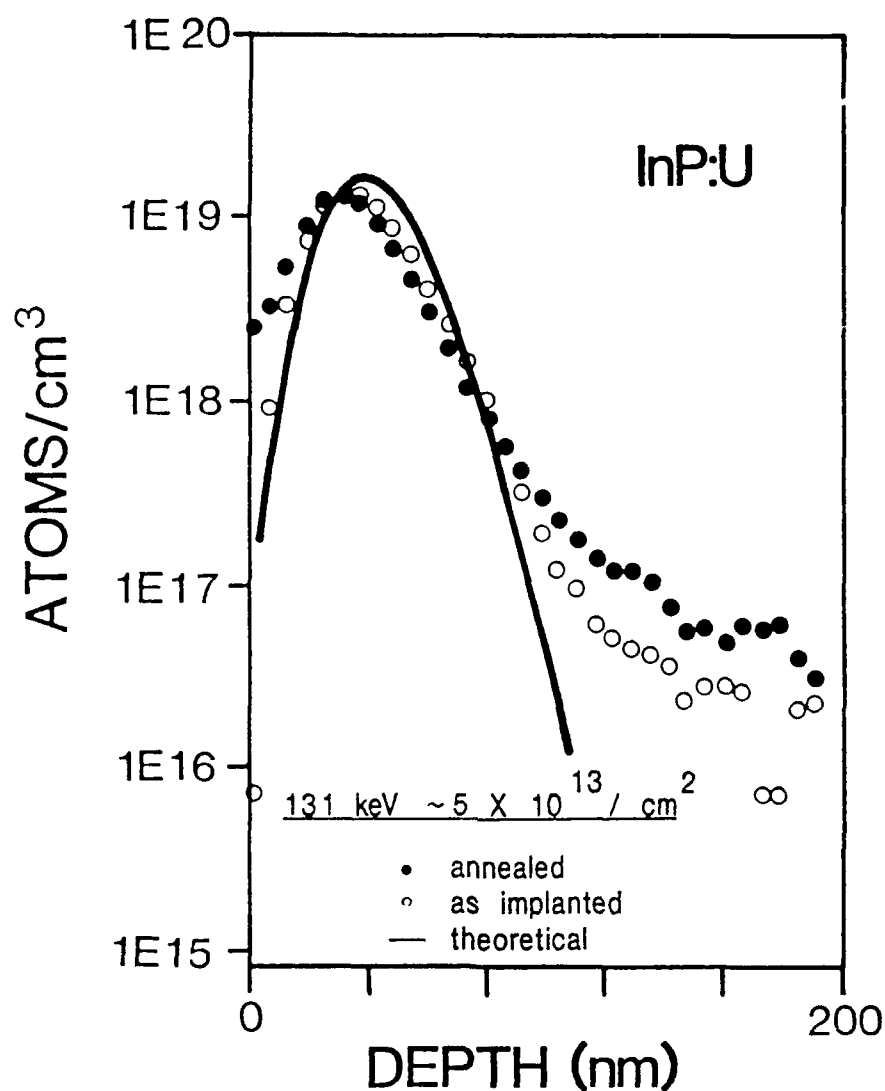


Figure 57. SIMS depth profiles of as-implanted and 750°C annealed InP implanted with uranium.

the surface. An implantation dosage of $\approx 4 \times 10^{13} \text{ cm}^{-2}$ was established using combined implantation and SIMS data. The SIMS instrument used in this study was described earlier and by Solomon (1987).

The low temperature (6K) and temperature dependent studies were performed in a gas exchange type of cryostat as depicted in Fig. 5 and 6. The photoluminescence was excited

by bringing a filtered 50 mW or 600 mW 514.5 nm beam from an air-cooled or water-cooled Ar-ion laser, respectively, unto the sample. The filtered signal was dispersed with a 3/4-m spectrometer and detected by a liquid nitrogen cooled Ge detector for the 0.8 to 1.8 μm region, or cooled (77K) PbS detector for the 1.8 to 2.6 μm spectral region. Typical irradiance at the lower power setting was 4.7 W/cm^2 and 8.5 W/cm^2 at the higher setting.

Figure 58 depicts the 1.6 μm photoluminescence spectra of the uranium implanted GaAs and InP. The emissions are a result of transitions from a specific excited state to the spin-orbit ground state of trivalent or tetravalent uranium. Although not depicted in Fig. 58, the 750°C annealed GaAs:U sample also showed an intense free-to-bound (FB) and donor-acceptor (DA) peak which appeared unaffected by the uranium implant, and the 1.36 eV copper related emission. The FB and DA levels were quenched for InP:U; however, the 210 meV broad and strong band, centered around 1.1 eV, which we have observed in rare earth implanted InP, was also present. The 1.1 eV level appears to be defect related due to the damage generated by implanting these heavy ions.

The GaAs:U spectra in Fig. 58 is a result of annealing the implanted sample at 750°C for 15 min in a flowing nitrogen environment. At a temperature of 6K and with a 514.5 nm excitation irradiance of 8.5 W/cm^2 , four main zero-phonon uranium emissions were observed for GaAs at 1601,

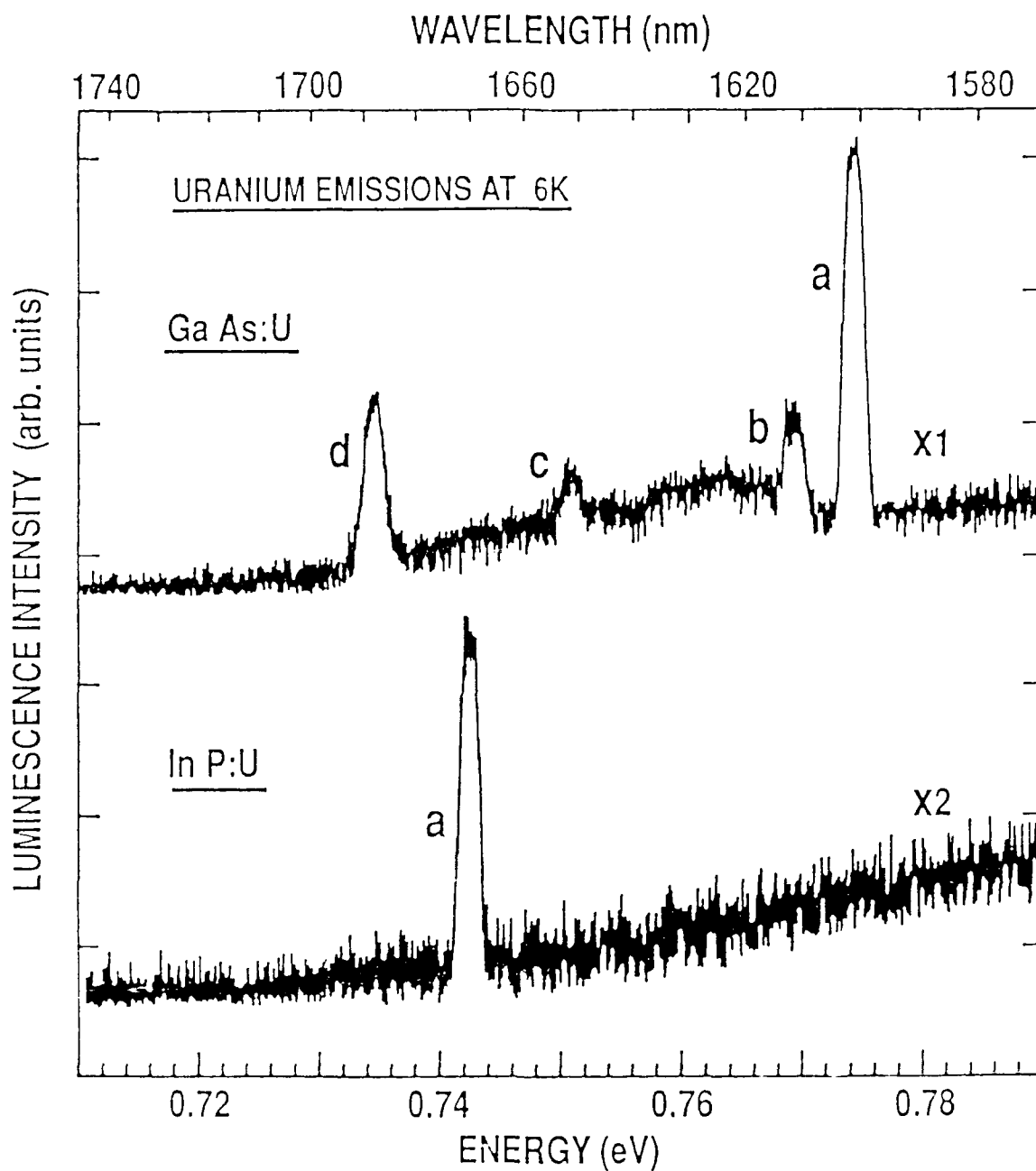


Figure 58. Photoluminescence spectra of GaAs and InP implanted with uranium at an average energy of 131 keV and subsequently annealed at 750°C for 15 min and 640°C for 10 min, respectively.

1612, 1651, and 1689 nm; these are labeled 'a' through 'd', respectively in Fig. 58. Evidence of two other very weak emissions is possibly seen at 1624 and 1633 nm. The only 5f emission seen in InP was at 1670 nm and is labeled with 'a' in Fig. 58. Higher resolution spectra of the main U-emission for GaAs and InP show a full-width at half-maximum of at least less than 0.46 meV at 6K.

For both GaAs and InP it was not possible to observe the 2.2 to 2.6 μm emissions from the lowest excited energy levels of U^{3+} or U^{4+} and associated with laser action in the alkaline earth fluorides. This is most likely not a problem based on the inherent physical processes, but a signal-to-noise problem associated with requiring a PbS detector for this spectral region versus a Ge detector. No U-specific emissions were observed for any of the GaP samples in the 0.5 to 1.8 μm region (a photomultiplier tube was used for the 500 to 800 nm spectral region). More specifically, the emissions are not seen in the 1.6 to 1.7 μm region due to the intense, broad none-uranium related impurity levels in this spectral region which dominate the recombination process. Under the proper residual impurity concentration the 5f-emissions should be observable in GaP.

The assignment of the observed 1.6 μm emission to transitions between specific spin orbit states is complicated by the possible presence of trivalent and tetravalent uranium centers in GaAs and InP. As previously indicated, the

absorption spectra of uranium doped CaF_2 and SrF_2 show emissions from two valency centers. The absorption spectra of $\text{CaF}_2:(100\% \text{U}^{3+})$ shows no evidence of absorption lines or bands between 1.35 and 1.75 μm (Boyd et al, 1962). However, samples of SrF_2 doped with 100% U^{4+} and CaF_2 doped with varying ratios of U^{3+} and U^{4+} show strong, sharp components between 1.55 and 1.70 μm (Title et al, 1962). Absorption spectra for $\text{LaCl}_3:\text{U}^{3+}$ show a relatively weak absorption band between 1.41 and 1.51 μm (Carnall et al, 1985) which is assigned to transitions between the crystal field split spin-orbit levels $^4\text{I}_{3/2} - ^4\text{I}_{9/2}$.

Although a possible argument could be made for the splitting of the $^4\text{I}_{3/2}$ and $^4\text{I}_{9/2}$ spin orbit levels by the semiconductor crystal field to allow for a trivalent 1.6 μm emission, this perturbation is most likely too small. The crystal-field splitting in actinides is roughly twice that for rare-earth ions which results in a Stark splitting of the order of 200 cm^{-1} or approximately 25 meV for actinides. In this case the splitting would have to be roughly twice this value for all emission lines to assign a trivalent center to the 1.6 μm emission.

This leads to a tentative conclusion that the 5f-emissions observed in GaAs and InP are due to tetravalent uranium centers. The 1.6 μm emission would therefore be assigned to the transition between an excited level and the ground state spin-orbit level $^3\text{H}_4$ of U^{4+} ($5f^2$). Variations in the spectral characteristics between the 5f-emissions of

GaAs and InP are a result of the different crystal field splitting of the spin-orbit levels as a result of the different ligands, for example, As or P, if uranium would enter GaAs and InP substitutionally on Ga or In sites, respectively.

If uranium would be found as a trivalent center and if the U^{3+} ion experiences a crystal field of cubic symmetry, the degeneracy of the $^4I_{3/2}$ level would not be split. The $^4I_{9/2}$ ground state of cubic (T_d) symmetry is split into three ($\Gamma_8 + \Gamma_8 + \Gamma_7$) states. Since only one 5f-emission (1670 nm) is observed in InP, one would then assume that U^{3+} experiences a crystal field of cubic symmetry in InP. The multiplicity of the 5f lines in GaAs suggests that the uranium center may experience non-cubic local crystalline fields in this material.

Depicted in Fig. 59 is the temperature dependence of the emission peak intensity of the 'a-d' lines for GaAs and the 'a' line for InP, as identified in Fig. 58. As the sample temperature is increased, the 5f emissions for GaAs and InP may be seen up to 100K after which they are rapidly quenched, only the two strongest U^{3+} in GaAs lines remaining slightly past 120K. The plotted intensity was determined from the area under the individual emission peaks. For all four 5f lines in GaAs the temperature dependence is very similar, indicating that they are associated with the same center. The center involved in the 1670 nm line of InP shows

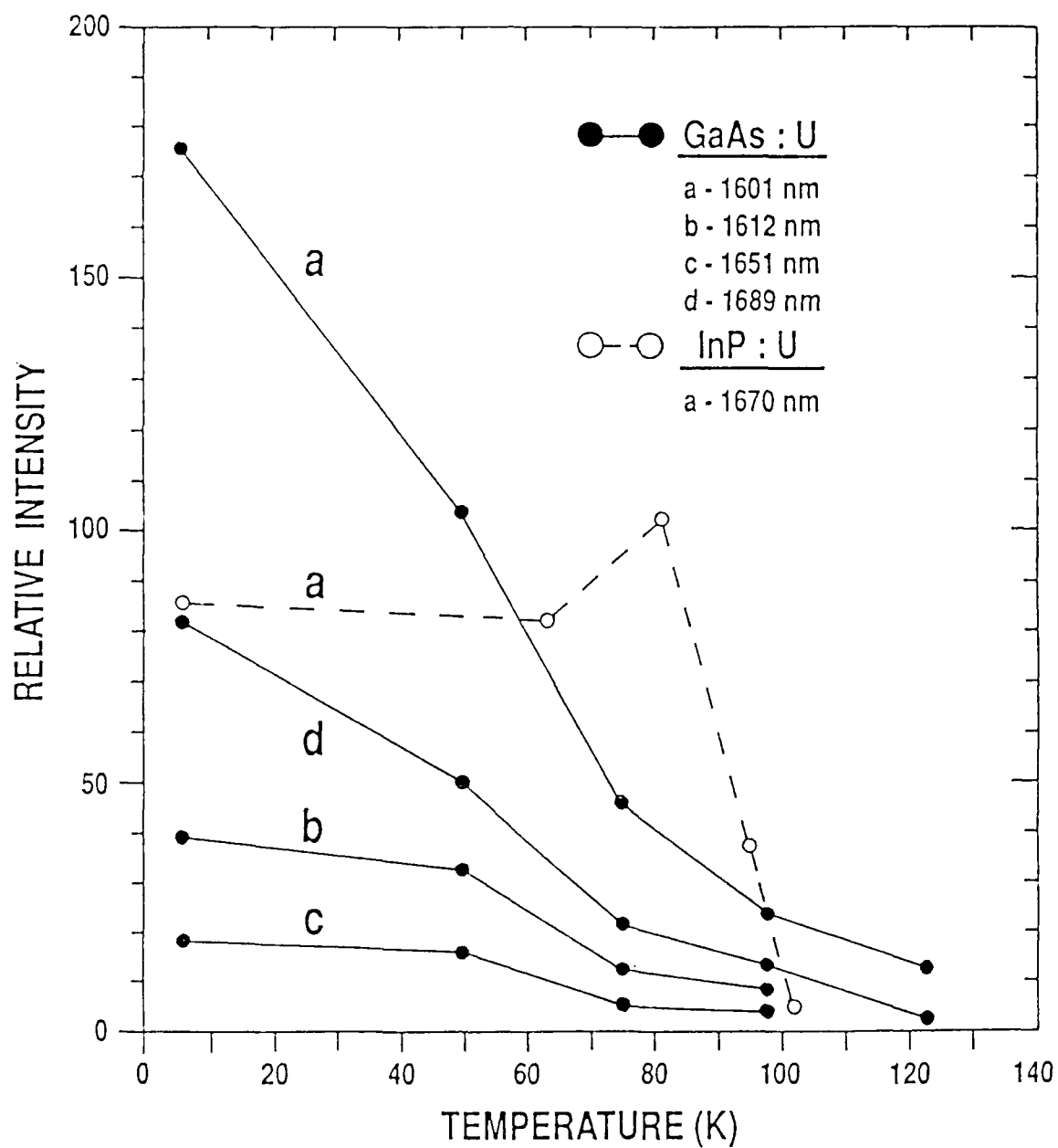


Figure 59. Temperature dependence of the luminescence intensities of the various 5f uranium emissions observed in GaAs and InP.

its own unique behavior by exhibiting a faster decline in intensity , once quenching started. There was no evidence of the development of a so called 'hot line' with increase in temperature as observed in 4f doped semiconductors. The 5f lines do not show any significant broadening or shift (less than 1.5 meV) in energy with temperature; however, the 1670 nm InP line broadens from 2.1 meV at 6 K to 3.4 meV at 81K, enough to be partially responsible for the increase in intensity at 81K as shown in Fig. 59.

The temperature dependent behavior in Fig. 59 may be partially due to a result of the energy transfer mechanism which may allow for the 5f transitions in the semiconductors. The behavior in Fig. 59 is similar to quenching processes observed for rare earth doped sulfides (Garcia et al, 1985). In these materials the 4f emission is excited through non-radiative transitions from a charge transfer state. Assuming the existence of such a charge transfer state, it is possible that the intensity degrades as a result of the thermal behavior of the transfer state, for example, and highly likely, the FB and DA transitions. The presence of impurity and defect states in the semiconductor would allow also for a 'killer' center (DiBartolo,1968); the thermal activation of this center quenching the 5f-luminescence by radiationless processes.

The temperature dependence of the intensity is sometimes used to determine an activation energy (E_a) for the

particular emission processes (Bimberg et al, 1971). An E_a of approximately 0.7 eV may be calculated for the 1601 nm line in GaAs by plotting peak intensity versus $1/T$ in a semi-logarithmic plot; however, this calculation is based on a very limited data set. This is very close to the internal $^4I_{3/2} - ^4I_{9/2}$ transition energy of U^{3+} . This suggests possibly that the main thermal quenching is associated with the actinide itself or possibly the deep level EL2 associated with GaAs which is located between 0.6 to 0.8 eV (Ikoma and Mochizuki, 1985). The data distribution and number of data points makes a calculation of E_a for InP meaningless. Based on this analysis, the U-specific emissions in GaAs and InP appear to be associated with one dominant center, and the decrease of the luminescence intensity is thermally activated. However, as mentioned previously in the text, it has been argued that the derivation of activation energies for transition metal impurities, and hence presumably rare earth impurities, might be impossible to derive by temperature dependent studies (Dean, 1982). The interpretation of the 0.7 eV activation energy must therefore be considered with caution.

In summary, it was possible to successfully incorporate uranium into III-V semiconductors through the new MEVVA ion source, which was confirmed by SIMS analysis. For the first time emissions in uranium implanted GaAs and InP are observed which are assigned tentatively to the internal 5f-transitions of tetravalent ($5f^2$) uranium. Based on temperature dependent

studies, the U-specific emissions in GaAs and InP appear to be associated with one dominant center and the quenching is thermally activated. Finally, for nonsilica based fiber optics applications, investigations to observe the 2.2 to 2.6 μm uranium emissions in III-V semiconductors are of importance. Paramagnetic resonance studies of bulk doped uranium are important to determine site location and the valency that uranium adopts when incorporated in the semiconductor crystal. Furthermore, as has been achieved for 4f doped GaAs (Whitney et al, 1988) and InP (Haydl et al, 1985 and Ennen, 1987), it is of interest to fabricate 5f doped light-emitting pn junction diodes, exciting the 5f luminescence via minority-carrier injection.

B. Selective Excitation

Introduction

The near infra-red spectroscopic investigations show that the emissions from the rare-earth/semiconductor systems are determined not by the host semiconductor bandgap but by the transition energies within the 4f levels of the rare earth impurity. As mentioned in earlier sections, the emissions are essentially characterized by their sharpness and their presence even at relatively high temperature, in some cases even at room temperature. The crystalline environment only weakly affects the 4f transitions due to the screening of the 4f states by the filled 5s and 5p shells. In spite of the present level of research and understanding of the optical characteristics after almost a decade of investigations, only a limited understanding exists of the interaction mechanism between the rare earth ion and the III-V semiconductor which leads to the 4f-4f transitions.

Investigations into the excitation and decay mechanisms of the 4f luminescent centers have been relatively recent and basically consider only the InP:Yb^{3+} system. Kasatkin et al (1984) investigated the excitation spectra of the 4f transitions of Yb^{3+} in GaP and InP, and concluded that the intracenter Yb luminescence occurred upon the Auger recombination of DA pairs and of excitons at the rare earth impurity. Time dependent electroluminescence of InP:Yb^{3+} was also performed by Kasatkin et al as reported in 1985. A more detailed investigation of the excitation and decay mechanism

of Yb^{3+} in InP has been performed by Koerber and Hangleiter (1988). By examining both time-resolved photoluminescence and photoluminescence excitation spectroscopy, it was revealed that several decay processes are present and free carriers are required during the excitation of Yb^{3+} . The time dependence of the internal 4f transitions of Yb^{3+} in InP as a function of temperature was also investigated by Klein (1988); a model was proposed linking experimental and theoretical calculations. Both of the latter studies address non-radiative decay mechanisms which limit the efficiency of the InP:Yb system. Aside from a report of the excited state lifetimes of the Er^{3+} emission in III-V semiconductors and Si (Klein and Pomrenke, 1988), studies addressing the interaction mechanism of the RE and the semiconductor host have remained limited.

In order to increase the understanding of the excitation mechanism which leads to the intra-center transitions, selective excitation photoluminescence experiments were carried out at 6-8 K on semi-insulating GaAs and InP implanted with ytterbium (Yb), thulium (Tm), erbium (Er), and praseodymium (Pr). Initial investigations were concerned with Yb and Er implanted at an energy of 1 MeV which represent the first investigations of such high energy implants in III-V semiconductors. Furthermore, to extend the level of understanding beyond these two most widely investigated rare earth ions, the investigations also report

for the first time the spectra of the 4f transitions associated with Tm and Pr in GaAs. Thulium was implanted at an energy of 390 keV while praseodymium was implanted at 380 keV. The observed rare earth emissions are seen around 1.0 μm for Yb, 1.5 μm for Er, 1.2 μm for Tm, and 1.1, 1.3, and 1.6 μm for Pr. Aside from taking for a few cases the standard excitation spectra for specific lines, the selected excitation studies essentially used a tunable dye laser set to pump the rare-earth/semiconductor system at particular wavelengths above, across, and below the bandgap. In this manner an extended spectral region could be observed for changes in the 4f emissions upon excitation.

Experimental

The GaAs and InP crystals used in the study were grown in the $\langle 100 \rangle$ direction. The Fe-doped InP was semi-insulating with a measured resistivity of 1.6×10^7 ohm-cm. The three different GaAs substrates were all semi-insulating, one of which (CS) was Cr-doped with a resistivity of 1×10^8 ohm-cm, the (WA) GaAs sample was undoped with a resistivity of $\geq 1 \times 10^8$ ohm-cm, and the (MA) GaAs sample was also undoped with a resistivity on the order of 10^8 ohm-cm. The samples were cleaned and etched before implantation. The Yb ion was implanted with a tandem accelerator machine at an energy of 1 MeV and a dosage of 3×10^{13} cm $^{-2}$ as shown in Table 15. Erbium was implanted at an energy of 1 MeV into (WA) GaAs at

Table 15. Sample Information for the Selective Excitation Study

semi-conductor: rare-earth	substrate conductivity type	ident- ifier	energy (keV)	implantation dosage (cm ⁻²)	anneal condition (°C/time/gas)
InP:Yb	SI	MR(346)	1000	3X10 ¹³	850/15s/fg
GaAs:Yb	SI	MA	1000	3X10 ¹³	640/10m/fg
	SI	MA	1000	3X10 ¹³	500/15s/fg & 640/10m/fg
GaAs:Tm	SI	CS	390	5X10 ¹³	600/10m/N ₂
GaAs:Er	SI	WA	1000	5X10 ¹³	680/10m/fg
	SI	CS	1000	7.5X10 ¹³	650/10m/fg
InP:Er	SI	MR(338)	1000	7.5X10 ¹³	650/10m/fg
GaAs:Pr	SI	WA	380	5X10 ¹³	750/10m/fg

a dosage of $5 \times 10^{13} \text{ cm}^{-2}$ and into (CS) GaAs and InP at a dosage of $7.5 \times 10^{13} \text{ cm}^{-2}$. The lower energy implants consisted of implanted (CS) GaAs with 390 keV Tm ions at a dosage of $5 \times 10^{13} \text{ cm}^{-2}$ while the Pr ions were implanted into (WA) GaAs at an energy of 380 keV and a dosage of $5 \times 10^{13} \text{ cm}^{-2}$.

After implantation the samples were proximity annealed without encapsulation, face down on a Si:P wafer, in a conventional anneal furnace or through rapid thermal annealing with a high-intensity, visible light, as detailed earlier in the experimental section to the dissertation. The annealing atmosphere was forming gas for all but the Tm implanted sample, for which it was N₂. The reported excitation results for Yb implanted InP are for an 850°C and 15 sec anneal, and for Yb implanted GaAs a 640°C and 10 min

anneal and a double anneal of 500°C/15 sec and 640°C/10 min. Thulium implanted GaAs was annealed at 600°C for 10 min while Pr implanted GaAs was annealed at 750°C also for 10 min. The Er implanted (WA) and (CS) GaAs included 680°C/10 min and 650°C/10 min anneals, respectively, while Er implanted InP was annealed at 650°C for 10 min. Specifics on the sample processing are tabulated in Table 15.

The rare earth emissions of Yb, Tm, Er, and Pr were investigated essentially with the selective photoluminescence technique, the experimental setup of which was detailed in an earlier section of this dissertation. The samples were located in a gas exchange type of cryostat and held at a temperature of 6-8 K and were optically excited with the filtered 514.5 nm line of an argon-ion laser or selected wavelengths from an argon ion-pumped tunable dye laser. The dye box was tuned using a three-plate birefringent filter assembly specifically for the LDS 821 dye which was used; the typical spectral range of 797 - 858 nm of the system was extended to the 835 - 895 range with the appropriate optics, tuning, and replenishment of the dye. The filter had a line-width of 40 GHz or 0.17 meV (0.00017 eV) at 830 nm. Typical excitation power ranged from 300 to 600 mW/cm². The filtered signal was dispersed with a 3/4 - m spectrometer and detected by a liquid nitrogen cooled Ge detector. The Yb signal was detected with a cooled S-1 type photomultiplier tube.

Results and Discussion

Ytterbium:

The observations of Koerber and Hangleiter (1988) for liquid phase epitaxial (LPE) layers, in studying the intra-4f transitions of Yb^{3+} in InP, imply that free carriers are needed to excite the Yb centers. This observation is not completely consistent with Kasatkin et al (1984) who suggested that the excitation essentially proceeds both via donor-acceptor (DA) pairs and excitons. The results reported here in principle support the former conclusion. It should be stated that the method of incorporating Yb into InP was not identified by Kasatkin et al (1984); however, the material is assumed to be either bulk-doped or LPE-doped InP based on their past investigations (Kasatkin et al, 1982; Kasatkin et al, 1981). The DA process is not completely excluded, but is considered of very low efficiency, at least for the case of implanted layers. Figure 60 depicts at different excitation energies the luminescence arising from the crystal field split spin-orbit levels $^2F_{5/2} - ^2F_{7/2}$ of Yb^{3+} in InP. The inset to Fig. 60 represents the excitation spectra of the 1007 nm line in the Yb^{3+} spectra of InP and is a result of continuously tuning the dye laser at constant power. The excitation spectra essentially duplicates the results of Koerber and Hangleiter (1988) as there was no significant evidence for the excitation of Yb^{3+} by below-gap states.

As the conventional excitation spectra in the inset to

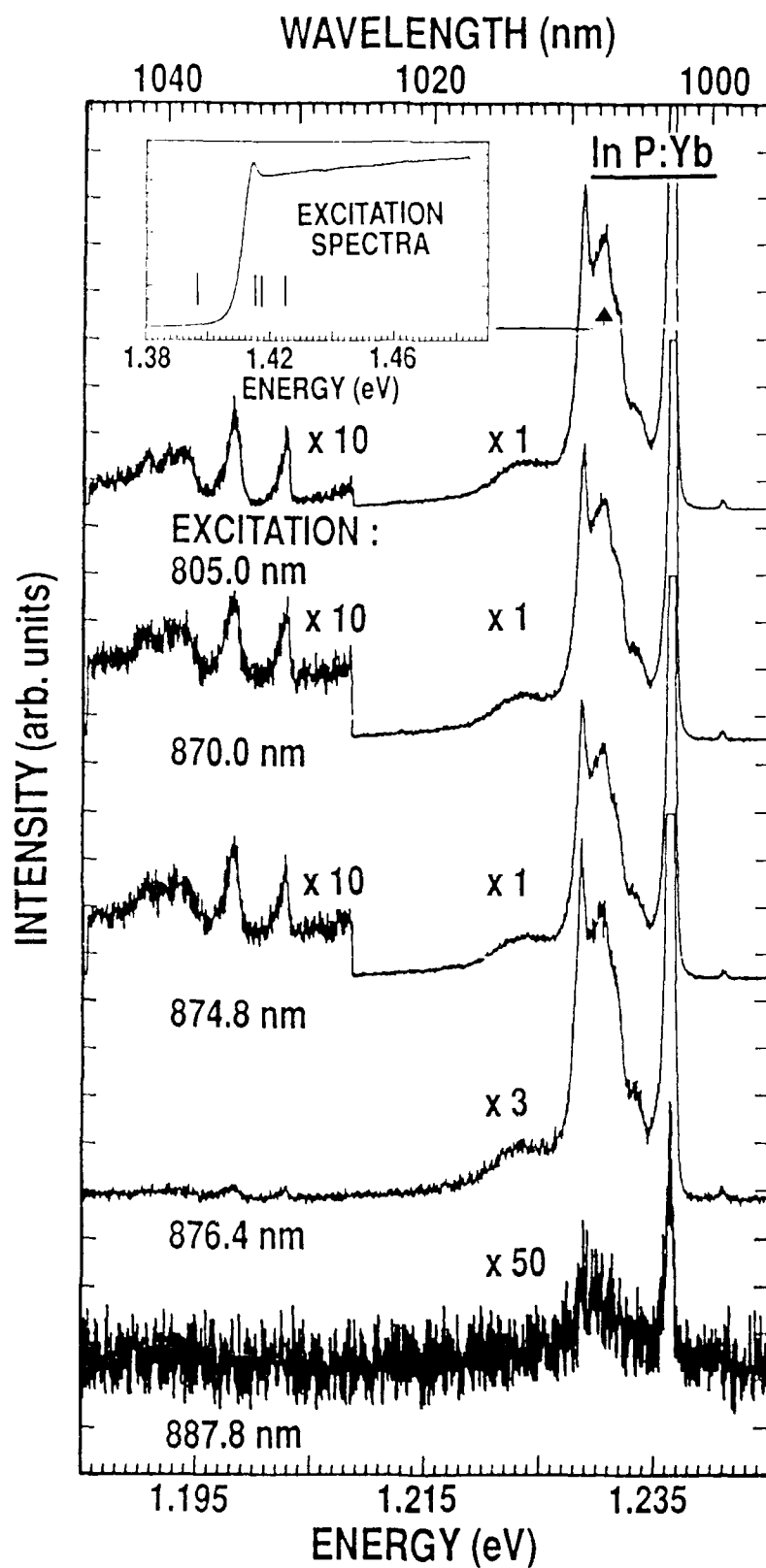


Figure 60. Yb^{3+} luminescence spectra at 7K of InP:Yb excited with different laser lines; inset shows excitation spectra of the 1007 nm Yb^{3+} emission.

Fig. 60 shows only results for one specific line, it is of interest to monitor the complete Yb^{3+} spectrum for energetic shifts and relative intensity changes of the emissions upon exciting across the bandgap. Aside from the spectra depicted in Fig. 60, emissions were also seen with excitation wavelengths of 514.5, 835.6, 856.8, and 882.7 nm. Furthermore, weak emissions were also seen at an excitation wavelength of 893.0 nm but only at considerable less resolution (i.e. spectrometer slits had to be set at 2mm). The energetic location with respect to the 1.4233 eV bandgap of InP of four of the excitation wavelengths in Fig. 60 may be seen by the four lines in the inset to the figure. As the energetic positions and relative intensities of the emissions do not change with different excitation, the Yb^{3+} spectrum is assigned to one center. As no substantial Yb^{3+} excitation occurred past 876.4 nm excitation, it allows one to conclude that the dominant excitation process requires free carriers. Although it was still possible to observe weak Yb^{3+} luminescence with excitation close to the DA states at 887.8nm and 893.0 nm (the latter, not depicted), this is possibly due to a resonant transfer from non-Yb related levels in the 1.2 eV region instead of Auger recombination of DA pairs. Investigations of some of these deep levels, especially around 1.0 μm or 1.2 eV, have been performed by Duhamel et al (1983), Eaves et al (1982), and Rao et al 1983. Kasatkin et al (1984) however argues against resonant

excitation based on results from absorption studies.

Unfortunately, the results for Yb^{3+} in GaAs are somewhat tenuous. The very weak Yb related emissions reported previously (Ennen et al 1985) between 1.10 and 1.28 eV are observed; however, upon exciting close to the GaAs bandgap a very strong and broad peak develops between 1.22 and 1.37 eV which masks the weak Yb^{3+} emission. Further investigations are necessary in order to improve the signal to noise ratio of Yb in GaAs and to identify the broad peak.

Thulium :

Similar results are observed for GaAs:Tm as for the selected excitation of InP:Yb. Shown in Fig. 61 are the first reported spectra of Tm implanted into the GaAs substrate which were recently presented (Pomrenke et al, 1989). The 1.2 μm emissions are assigned to the transitions from the spin-orbit state $^3\text{H}_5$ to the ground state $^3\text{H}_6$ of Tm^{3+} . Contrary to reports pertaining to the more ionic materials (DiBartolo, 1968), no Tm-related emissions were observed between 1.8 and 2.0 μm in using a PbS detector. The inset to Fig. 61 shows a plot of the intensity of the main emission at 1233 nm as the excitation wavelength was varied across the bandgap. The results are from the (CS) GaAs sample annealed in flowing N_2 at 600°C for 10 min (resolution was 3.4 meV). Subsequent photoluminescence studies allowed one to generate an improved luminescence spectra (bottom spectra of Fig. 61) for comparison upon annealing at 750°C and 10 min with an encapsulant; resolution was 1.4 meV.

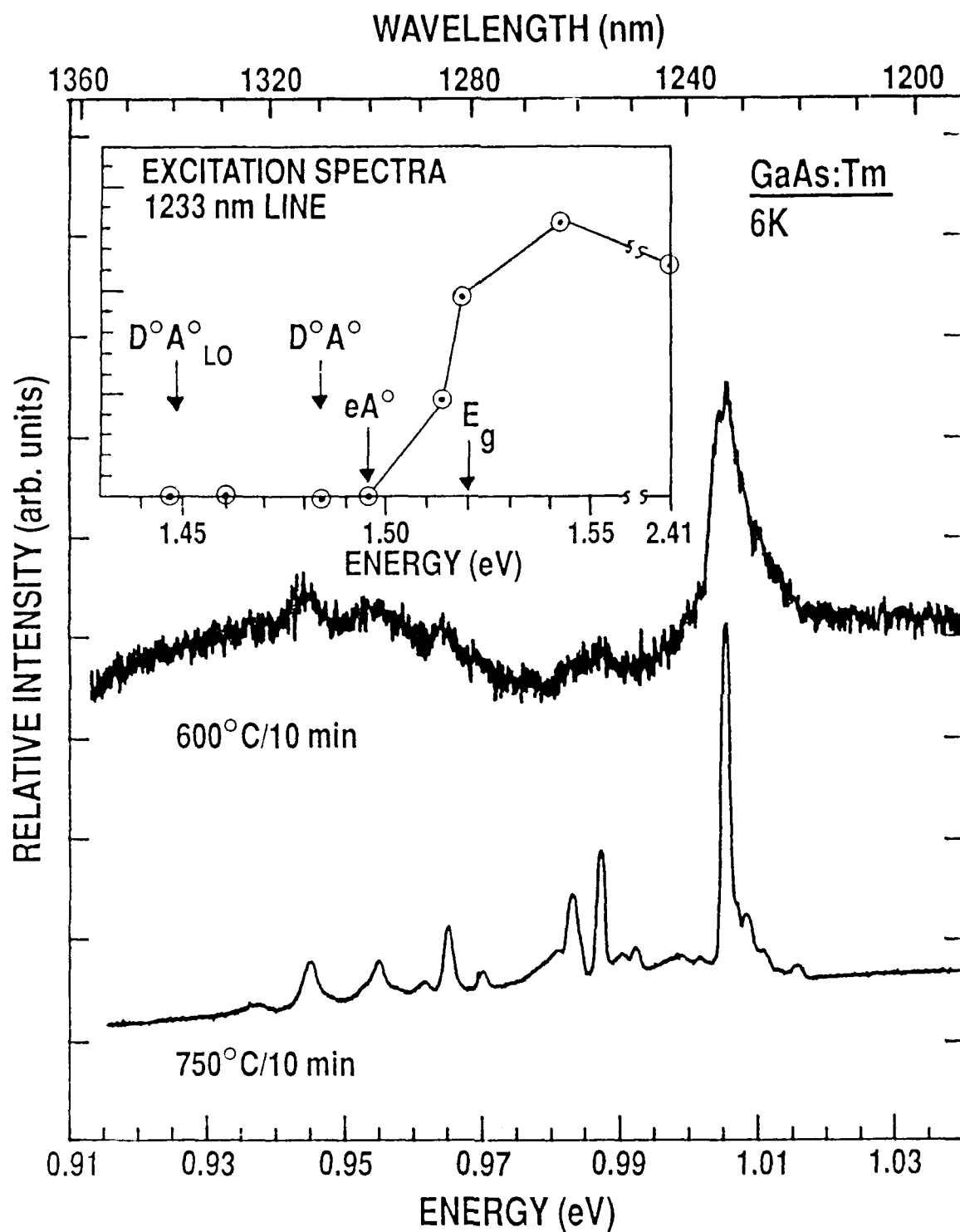


Figure 61. Tm^{3+} luminescence spectra of GaAs:Tm for two anneal temperatures; inset shows the excitation spectra of the dominant line for the 600°C/10min anneal.

Also, the 750°C spectra in Fig. 61 was generated with a 1.2 μm blazed grating versus a 1.6 μm grating for the 600°C spectra.

Important to note is that upon exciting below the bandgap a very broad (> 120 meV, fwhm - full width at half maximum) intense signal centered approximately at 1.0 eV is generated which partially masks the rare earth signal. As a consequence, the excitation spectra in the inset represents only the intensity of the Tm^{3+} signal with the background ignored. Investigations by Deveaud and Favenne (1977) reported of a 1.0 eV defect complex associated with As, O, and Ne implantation; it is believed a similar implant related defect is present in this case which is intensified upon pumping with below band gap excitation.

By taking selected photoluminescence spectra across the bandgap, allows one to get a more complete picture of the different radiative processes which are overlooked when taking the conventional excitation spectra of the integrated intensity at a particular wavelength. Although the Tm^{3+} signal might be masked or even quenched by defect levels, the results indicate that for at least these implanted layers no significant rare earth luminescence occurs upon exciting below the exciton levels of GaAs. The satellite emissions to the 1233 nm line were too weak to allow the plotting of an excitation spectra.

Erbium :

Considerably different from InP:Yb is the selected excitation of GaAs:Er. Shown in Fig. 62 are the Er^{3+} photoluminescence spectra at selected excitation wavelengths from the implanted but undoped (WA) GaAs substrate. (In Fig. 62 the 'L' identifies a peak associated with the 2nd order laser line). The energetic position of some of the excitation lines with respect to the GaAs band gap may be seen in Fig. 63. The emissions in Fig. 62 are due to the transitions between the weakly crystal-field-split spin-orbit levels $^4I_{13/2} - ^4I_{15/2}$ of Er^{3+} . As excitation energy is tuned across the bandgap of GaAs (1.5196 eV, 815.9 nm) the Er^{3+} luminescence continues to be observed upon exciting into the DA states (1.484 eV) and past the LO phonon replica of the DA states of the substrate. Effectively the intensity of the complete Er^{3+} spectra drops by only about 50% upon reducing the excitation energy from 1.540 to 1.445 eV. No substantial background luminescence was observed in the 1.5 - 1.6 μm region. The emission lines in Fig. 62 remain essentially unchanged in peak energy and relative intensity aside from the weak highest energy peak at 1.533 μm ; hence, the excitation is of the same Er centers and associated complexes and defects.

An interesting behavior was observed for the Er implanted (CS) GaAs substrate, as shown in Fig. 64. The Er^{3+} emission exhibited a substantial decrease in intensity when exciting at or close to the DA states (1.47 - 1.50 eV);

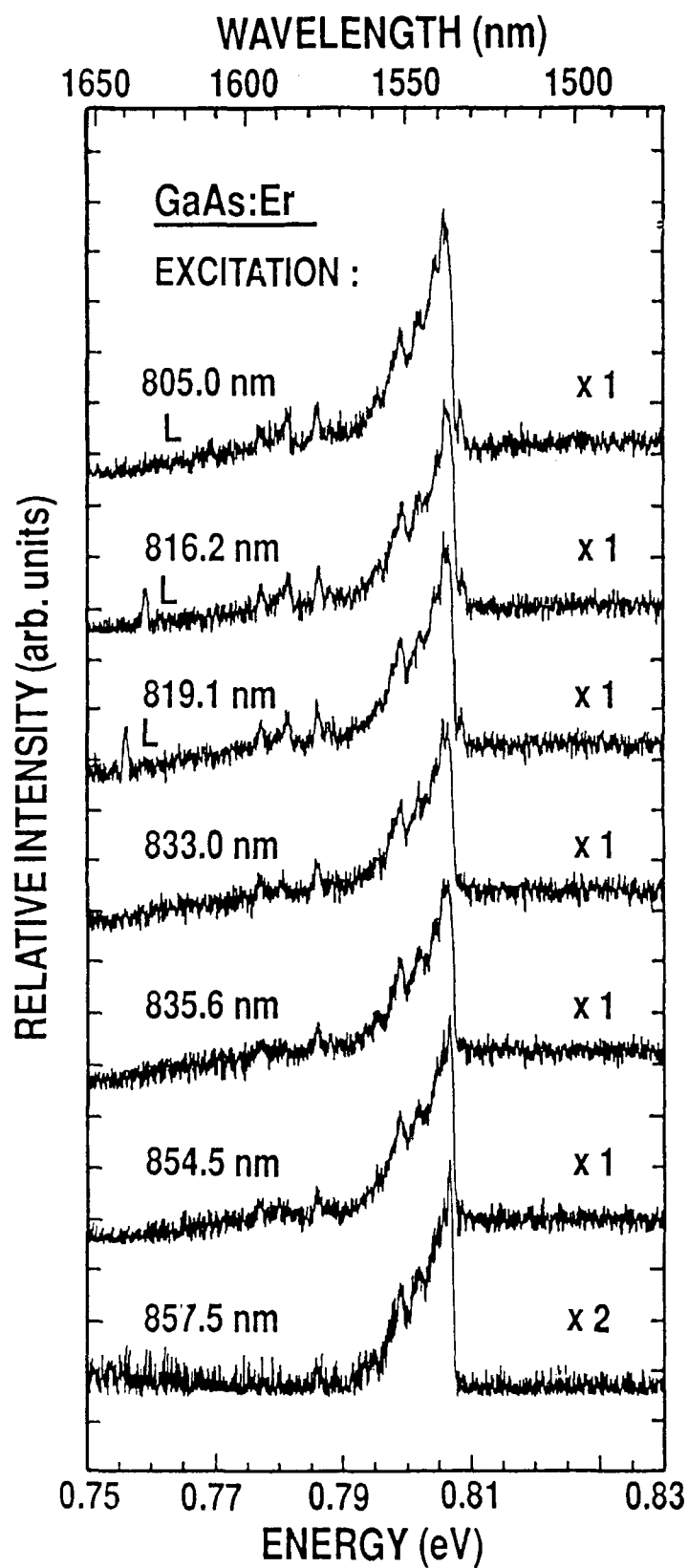


Figure 62. Er^{3+} luminescence spectra as a function of excitation energies for (WA) GaAs:Er.

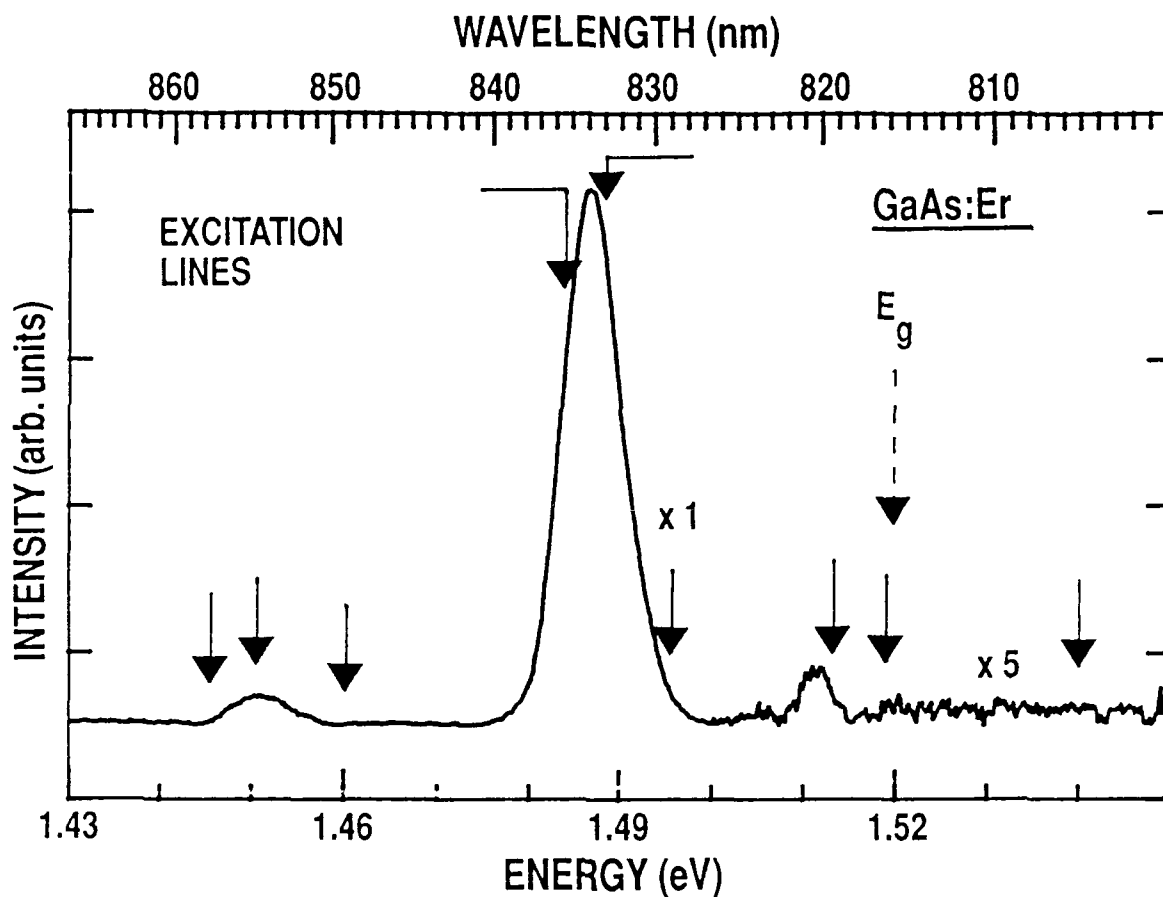


Figure 63. Position of laser excitation lines for GaAs:Er with respect to the near-edge emissions.

however, upon exciting below 1.47 eV the Er^{3+} signal recovered to the same intensity as at above bandgap excitation. It was determined that the decrease in the Er^{3+} signal was marked by a substantial increase in a broad (> 100 meV, fwhm) background signal centered approximately around 0.8 eV. (The relative intensity of the 1541 nm line and the background at 1541 nm as depicted in Fig. 64 are difficult to compare directly due to the difference in their structure, and thus, one should examine only the trend.) As the semi-

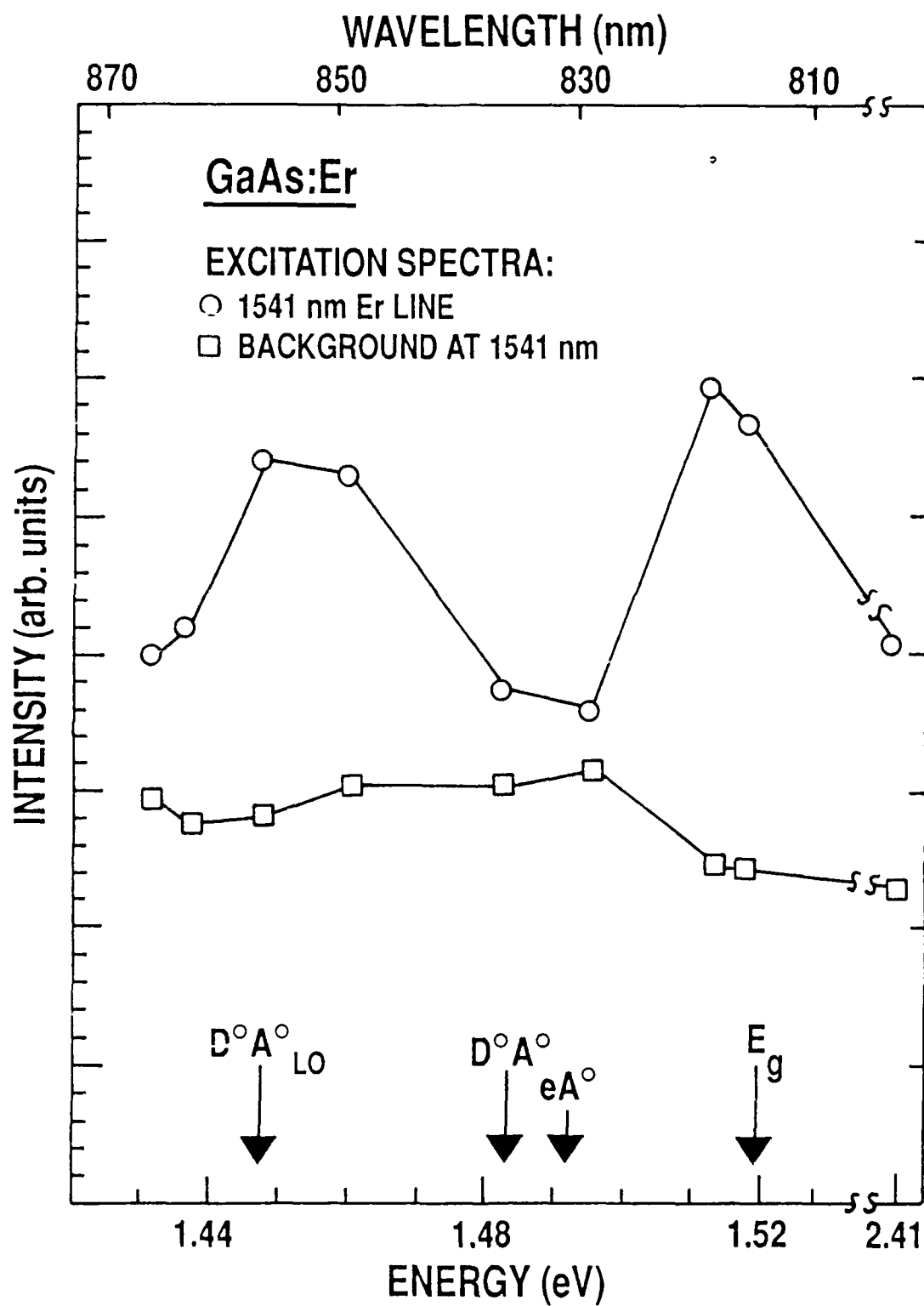


Figure 64. Excitation spectra of the dominant Er^{3+} emission and background at 1541 nm of (CS) GaAs:Er at 7K.

insulating sample was Cr-doped, the 0.8 eV level is believed to be associated with chromium on a gallium site as previously identified (Deveaud and Favennec, 1977). Upon pumping the DA states the Cr-related emissions become preferentially excited due to the greater penetration depth of the exciting laser light, resulting in masking the RE signal.

The excitation spectra for Er implanted into InP is shown in Fig. 65. Plotted is the emission intensity of the main erbium line at 1541 nm. The intensity decreases upon exciting below bandgap states, but a significant Er^{3+} signal is retained upon exciting close to the DA states. Unfortunately, the limitations of the dye laser system prevented the excitation at lower energy. Some background luminescence was observed at all excitation wavelengths but it remained relatively unchanged.

For the case of Er^{3+} it is established that not only do free carriers excite the rare earth ion, but also, other below gap states such as DA pairs and possibly the resonant transfer of energy from deeper lying levels. It has been established that Er luminescence can be observed in GaAs by exciting even at 1.4 μm (Klein, 1989); however, Bantien et al (1987) did not observe Er emissions in LPE GaAs:Er with 1.06 μm excitation.

Praseodymium:

Praseodymium in GaAs appears to show a complicated

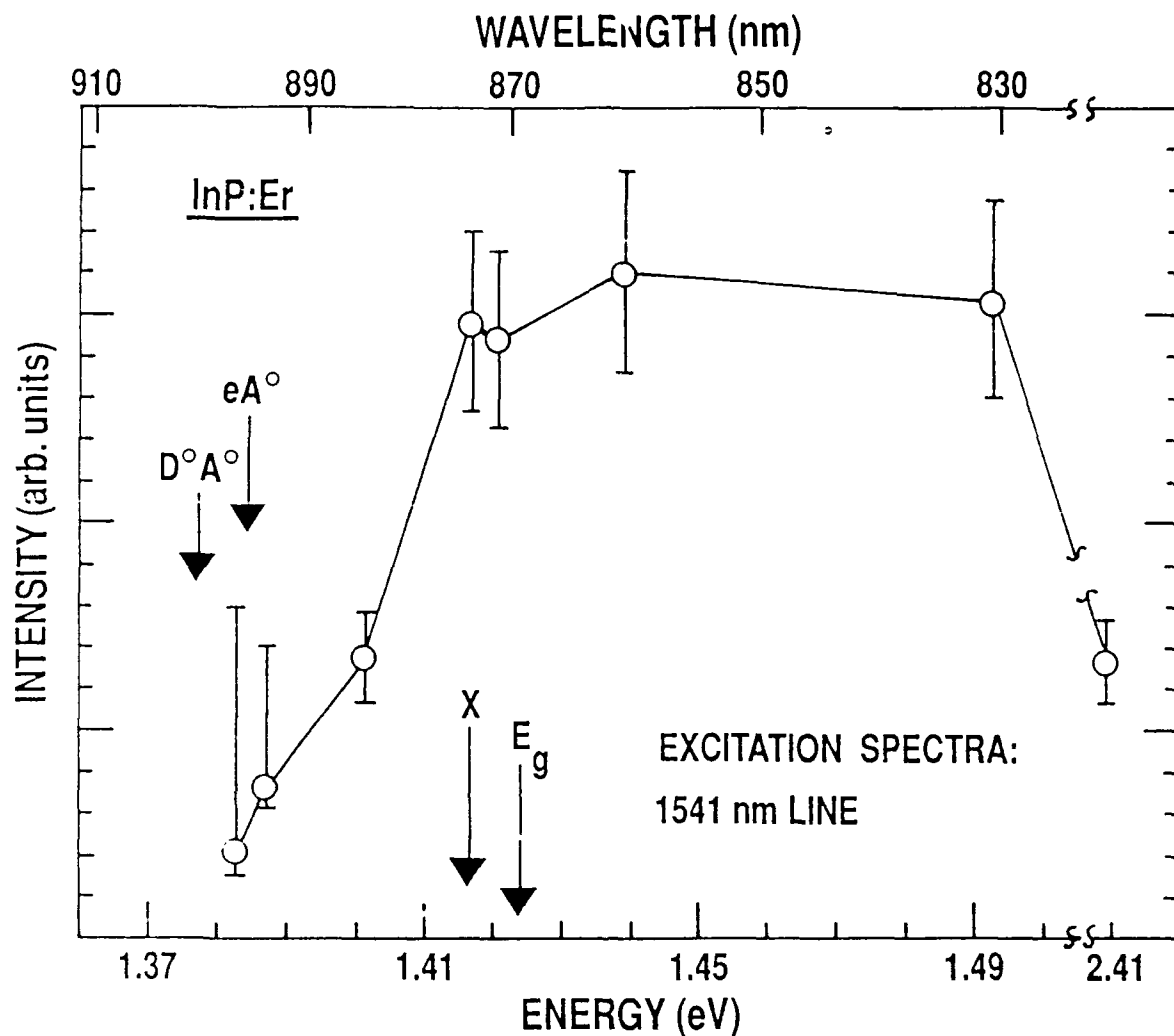


Figure 65. Excitation spectra of the dominant Er^{3+} emission of InP:Er at 7K.

excitation behavior. First evidence of Pr^{3+} specific emissions in GaAs is given in the top spectra of Fig. 66 upon optical excitation with the 514.5 nm line. These results were presented and reported recently (Pomrenke et al, 1989). Three sets of sharp lines are seen at 1.1, 1.3, and

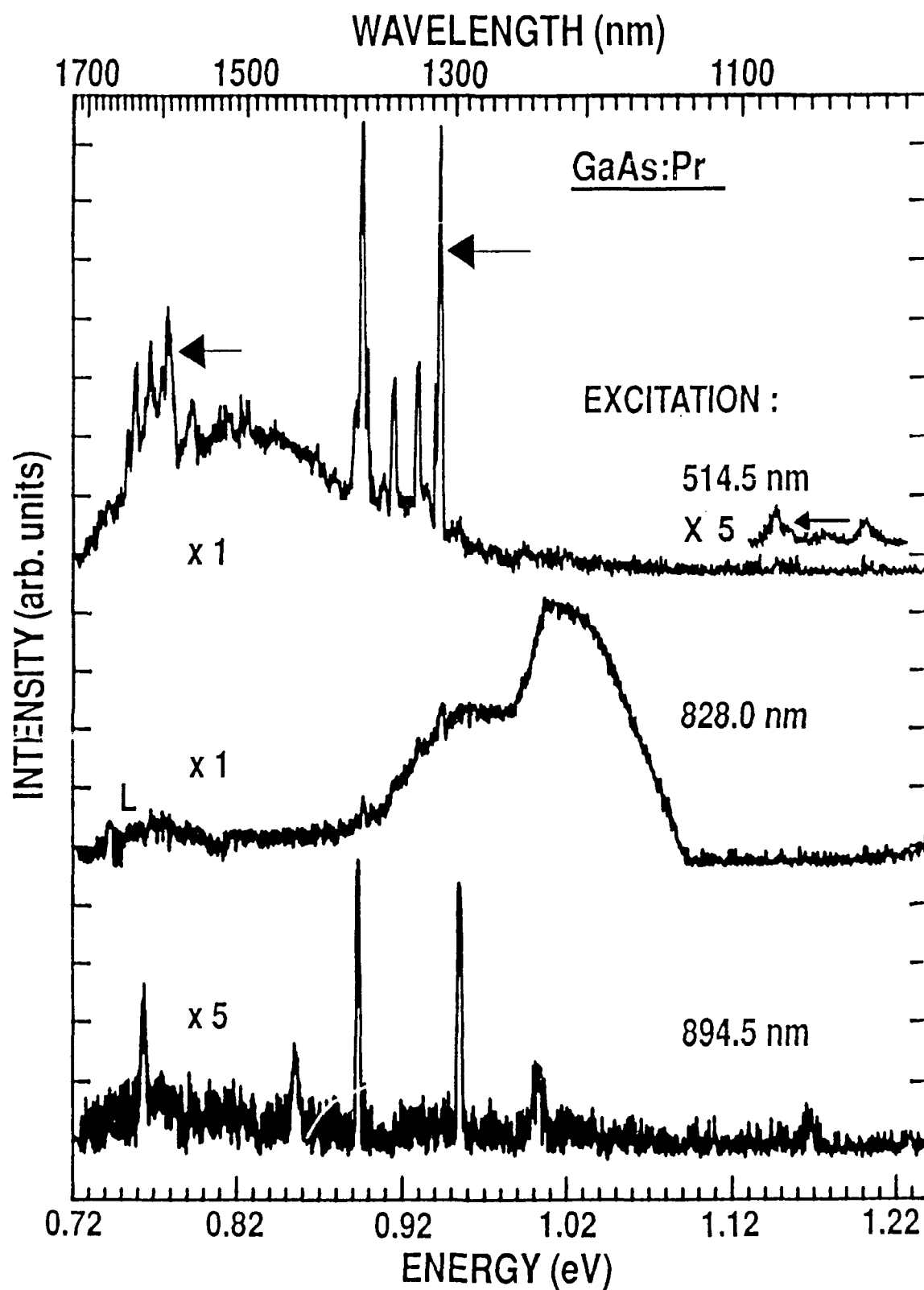


Figure 66. Luminescence spectra of GaAs:Pr upon pumping with three different excitation energies (arrows correspond to plotted lines in Figure 67).

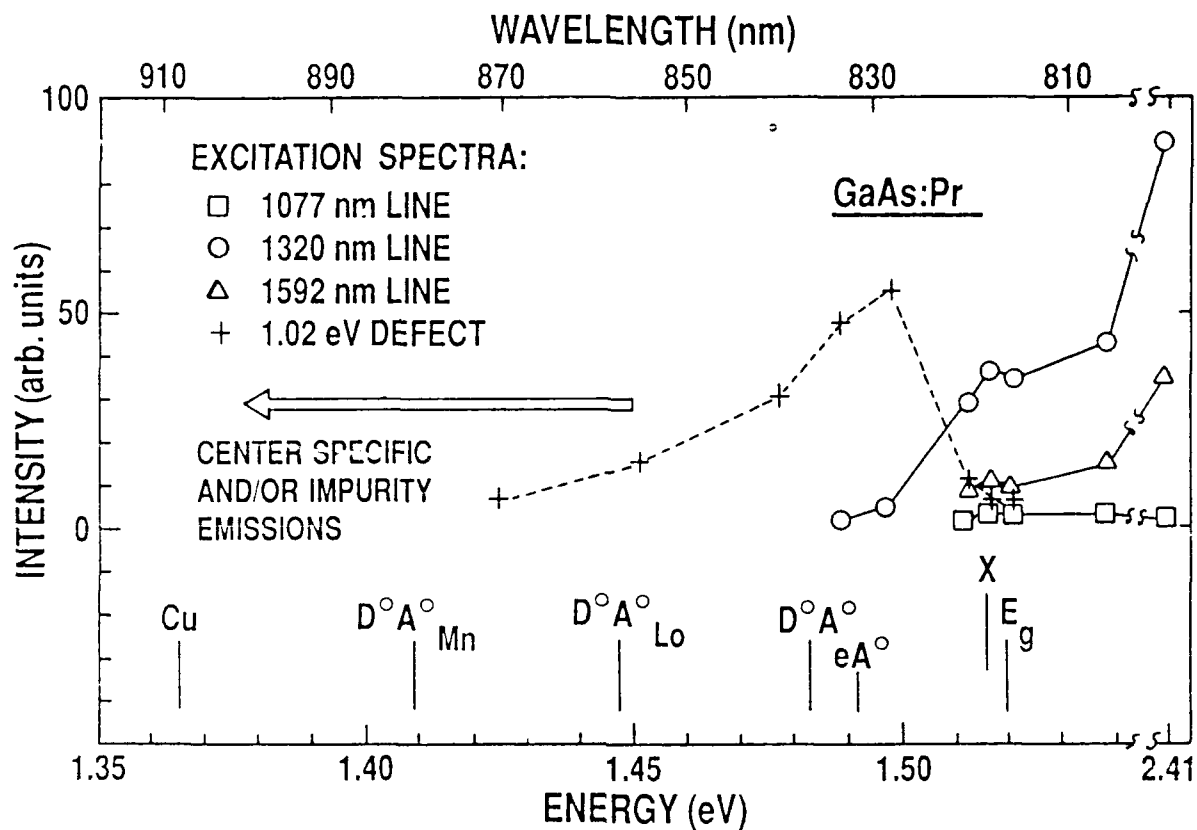


Figure 67. Excitation spectra of specific Pr^{3+} emissions of GaAs:Pr at 7K.

1.6 μm and are assigned to the intra 4f-shell transitions between the spin-orbit levels $^1\text{G}_4$ and the ground state $^3\text{H}_4$, between the level $^1\text{G}_4$ and the excited state $^3\text{H}_5$, and between the excited state $^3\text{F}_3$ and the ground state $^3\text{H}_4$, respectively. The weakest emission at 1.1 μm was multiplied by a factor of five.

The excitation spectra of GaAs:Pr in Fig. 67 shows the luminescence intensities of the strongest lines from each of the three sets of emissions as a function of excitation; they

are marked by arrows in the top spectra of Fig. 66. Also plotted in Fig. 67 is the behavior of the broad 1.02 eV defect level due to implantation as reported by Deveaud and Favanne (1977). As indicated by the number of data points plotted in Fig. 67, numerous spectra with different excitation were recorded. No significant excitation of the three Pr^{3+} emissions occurs through DA states or lower lying states. The 1.02 eV defect level dominates the spectra upon exciting below bandgap, especially into the DA states, until it essentially disappears upon exciting with lower than 1.42 eV energy. The structure or discontinuity in the center of the broad 1.02 eV defect level in Fig. 66 is an artifact from not correcting the spectra for system response.

Three emission spectra were taken in the 1.425 - 1.386 eV range upon exciting GaAs:Pr at 870.2, 890.6, and 894.5 nm (the latter depicted in Fig. 66) which resulted in an array of emissions different in energy and intensity from the original Pr^{3+} emission in Fig. 66 with above bandgap excitation. Preliminary evidence appears to indicate that by exciting in the 1.425 - 1.386 eV range one selectively excites two different Pr centers. However, as the (WA) GaAs substrate exhibits the presence of various transition metal impurities (i.e. Cu, Mn), it is not ruled out that below bandgap excitation shows the generation of new sharp lines from residual transition metal impurities, complexes between rare earth and transition elements, or other interaction

between the rare earth and impurity or defect (Gippius et al, 1986). For the case of GaAs:Pr evidence exists that the main excitation mechanism for the excitation of Pr^{3+} is through free carriers, but states at or well below the DA states are not excluded from the excitation process.

Conclusion

The rare earth emissions in GaAs and InP are due to the excitation of host-related states with subsequent energy transfer to RE centers. Specifically, it is established that the main mechanism needed to excite the rare earth centers is through free carriers in the case of the four implanted semiconductor-impurity systems that were investigated. As suggested by Koerber and Hangleiter (1988) the actual excitation might be through the direct capture of excitons or by impact excitation of hot carriers. That below bandgap states such as DA pairs are involved and possibly the resonant energy transfer from deep levels, was seen for Er and possibly Pr. The excitation from the Auger recombination of DA pairs as suggested by Kasatkin et al (1984) is responsible for the 4f luminescence to a lesser extent than free carriers. Future models concerning the excitation mechanism should consider both the 4f-4f deexcitation plus the three basic excitation mechanisms as outlined by Boyn (1988) for II-VI semiconductors: direct excitation of the 4f shell by the excitation source, the nonradiative energy transfer to the 4f shell by excitation of impurity states outside the 4f shell, and direct energy transfer to the 4f

shell through electron-hole pairs and/or excitons.

As was shown, residual impurities, defect levels, and complexes play a further role to complicate the excitation process in implanted layers in that they actually dominate the energy transfer process at particular excitation energies, quench or just mask the rare earth luminescence. Hence, the quality or characteristics of the substrate becomes extremely important in interpreting the results from the excitation experiment. Although selected excitation allowed examination of the implanted layers, there are obvious limitations (mainly associated with the absorption depth of the exciting line) in interpreting the results which can be only overcome by bulk doping or thick epitaxial layers. It should be reiterated that the results of Koerber and Hangleiter (1988) came from LPE layers while the results from Kasatkin et al (1984) most likely came from bulk doped material.

With Er centers in GaAs being excited over the widest range of states, combined with the observed room temperature luminescence, long lifetimes, and the technological importance of the 1.54 μm wavelength, allows one to conclude that the GaAs:Er system shows the greatest promise for electro-optic applications.

C. Lifetime Measurements

Introduction

In this part of the investigation the excited state lifetimes of various rare² earth doped semiconductors were studied. Specifically, it was attempted to determine the lifetimes of the Yb^{3+} emissions in InP and $\text{Al}_{.3}\text{Ga}_{.7}\text{As}$; of Er^{3+} in GaAs and $\text{Al}_{.4}\text{Ga}_{.6}\text{As}$; and of Tm^{3+} in GaAs. By investigating the time-dependent luminescence signal, allows one to probe for processes responsible for the specific excitation and recombination mechanisms, and thus allows one to propose models which describe the system kinetics after the pulsed excitation. Studies of the temperature dependence of these processes provides further information on the origins of the different mechanisms.

One might ask what happens after the exciting pulse, is there subsequent electron or hole capture, and what are the dynamics of the resulting radiative or non-radiative states? What are the capture cross sections of the excited states and the associated temperature dependence? Studies which lead to answers to such questions have been performed in the past for the internal transitions of 3d ions in III-V semiconductors (Klein et al, 1983; Klein and Weiser, 1982; Klein, 1984; Guillot et al, 1984). Studies which examine the radiative lifetimes of the donor and acceptor related emissions in III-V semiconductors go back at least two decades (Dingle et al, 1969; Thomas et al, 1965; Queisser, 1976, 1978, and 1980). This investigation concerns itself more with the former, the

kinetics of the internal transitions of impurities in semiconductors.

As explained and shown in the experimental section and the associated Figures 16 and 17, the lifetime measurements were performed by the pulsed excitation of the cryogenically cooled samples with a nitrogen-laser pumped dye-laser. The resulting luminescence was detected with a S-1 type PMT or Ge detector. For the majority of the investigations boxcar averaging was used.

Results and Discussion

InP:Yb

The initial investigations of excited state lifetimes were performed on the 1.0 μm emissions of Yb^{3+} in InP. The Yb^{3+} emissions in InP:Yb were shown in Fig. 23. This particular system was chosen because of the relative intense and sharp emissions in a spectral region easily accessible with a S-1 PMT. Furthermore it was chosen due to several careful optical studies concerning InP:Yb and recent publications addressing the dominant processes associated with the excitation and decay of the Yb^{3+} emissions. The results of these studies still allow for further interpretations of the dynamics leading to the Yb^{3+} decay. The different methods with which the rare earth is incorporated into the semiconductor host possibly leading to different experimental results and interpretations.

The lifetime at 20K of the Yb^{3+} emission in InP:Yb was

originally investigated by J. Windscheif and G. Pomrenke and reported at a 1983 Gordon Research Conference, with results indicating a lifetime of approximately 10 μ s. Subsequent investigations by Kasatkin et al (1985) established a lifetime of 9 μ s at 77K. Koerber et al (1988) and Koerber and Hangleiter (1988) reported a lifetime at 20K of 12.7 ± 0.4 μ s for all Yb^{3+} emission lines; Klein (1988) reported a lifetime of 12.5 μ s at 10K and a lifetime of approximately 3 μ s for a nonexponential component; and Takahei et al (1988) found a lifetime of about 12 μ s. These are short lifetimes when compared to the more radiative Yb^{3+} lifetimes of 1 ms in ionic hosts such as $\text{Y}_3\text{Al}_5\text{O}_{12}$ glass (DiBartolo, 1968). Since the 4f electrons are shielded through the 5s and 5p shells, the rare earth ion should be little affected by the environment, thus one would not expect the shorter lifetimes; hence, it is possible that a competing nonradiative process may be present, even at low temperature. Recently, investigations appear to indicate that the difference in lifetimes may be partially explained by the more covalent bonding of Yb^{3+} with its semiconductor host versus a more ionic bonding of Er^{3+} . The nonradiative decay associated with Yb^{3+} being an Auger process identified with covalent conducting materials in which the Yb^{3+} gives up energy directly to free electrons in the conduction band (Auzel et al, 1989).

Koerber and Hangleiter (1988) observed purely exponential decay for the strongest Yb^{3+} emission, contrary

to Klein (1988). Furthermore, the lifetimes were independent of the Yb concentration of their LPE InP:Yb layers, hence excluding the possibility of energy transfer between other centers. It was concluded that depending on temperature and doping levels, and also depending on results from Hall measurements and theoretical calculations (Hemstreet, 1986), bound-exciton-like Auger processes, energy transfer processes between excited Yb ions and ionized acceptors [i.e. between $(Yb^{3+})^*$ and $A^-(A^{2+})$], or thermal depopulation determine the lifetime of the excited state. It is believed that these are essentially valid arguments but must remain open for possible reinterpretation based on recent electrical measurements (Zakharenkov et al, 1987; Lambert et al, 1988; Whitney et al, 1988; and Raczynska et al, 1988).

Also based on these recent electrical measurements, some of Klein's results (1988) which are to some extent based on the theoretical work of Hemstreet (1986) may be open for reinterpretation. Klein's experimental results, although for implanted layers, are in general agreement with those of Koerber and Hangleiter (1988) aside from observing not only exponential but also non-exponential components to the decay curves. The dependence of the Yb^{3+} luminescence decay was also studied as a function of temperature. Differences do exist between Klein, and Koerber and Hangleiter in interpreting the dynamics which lead to the lifetime of Yb^{3+} . Klein concludes that the exponential components of the decay,

above 50K, is a result of hole emission processes from the neutral Yb acceptor. At low temperature the decay may be a result of weak coupling between the Yb excited state and resonant valence band^{*} states. The nonexponential decay is possibly due to the capture of nonequilibrium carriers by the neutral Yb acceptor. (The idea of Yb as an acceptor level is a result of past electrical measurements and the theoretical work by Hemstreet, 1986).

The lifetime of the 1002 nm Yb³⁺ emission was examined using the setup described in the experimental section. Lifetimes were calculated through curve fitting routines of the ASYSTAN analysis program. The initial results for the decay lifetime at 4.2K was 13.0 μ s for the 1 MeV Yb-implanted and 875°C/10s annealed sample, which agrees well with what is published. However, contrary to the literature, the lifetime remained approximately the same with increase in sample temperature until the signal was eventually lost at about 80K, i.e. it was independent of temperature. This discrepancy was solved upon building a Faraday cage around the nitrogen laser to reduce the electronic noise. The resulting decay curves at three different temperatures are presented in Fig. 68 and give the expected waveform. The trend in the figure was typical of all five samples. However, the decay times did vary somewhat for the differently annealed samples and this is graphically illustrated in Fig. 69 which also shows the rapid decrease in lifetimes in the temperature range of 50 to 90K. The low

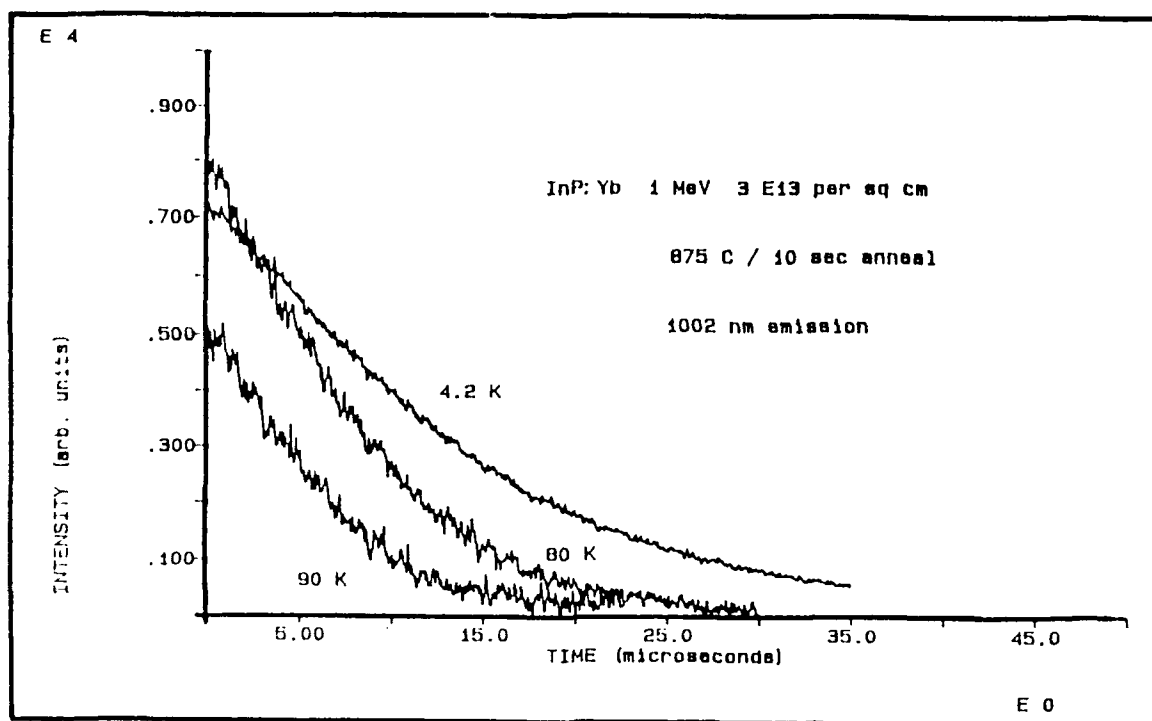


Figure 68. Decay curves for the Yb^{3+} emissions in InP:Yb at 4.2, 80, and 90 K.

temperature lifetimes for the samples which were rapid thermally annealed for 10 s at 650, 725, and 800°C and conventionally annealed at 750°C for 15 min were all clustered between 8.5 to 10.5 μs . These values are slightly lower than the reported values of 12.5 μs .

The curve in Fig. 70 was characteristic of the rise and decay waveform; however, a more precipitous rise was expected. The rise (2.9 μs) was indicative of a time constant that was too long for the aperture duration which was selected and resulted also in a type of 'plateau' region between the rise and decay. This so called low pass filter

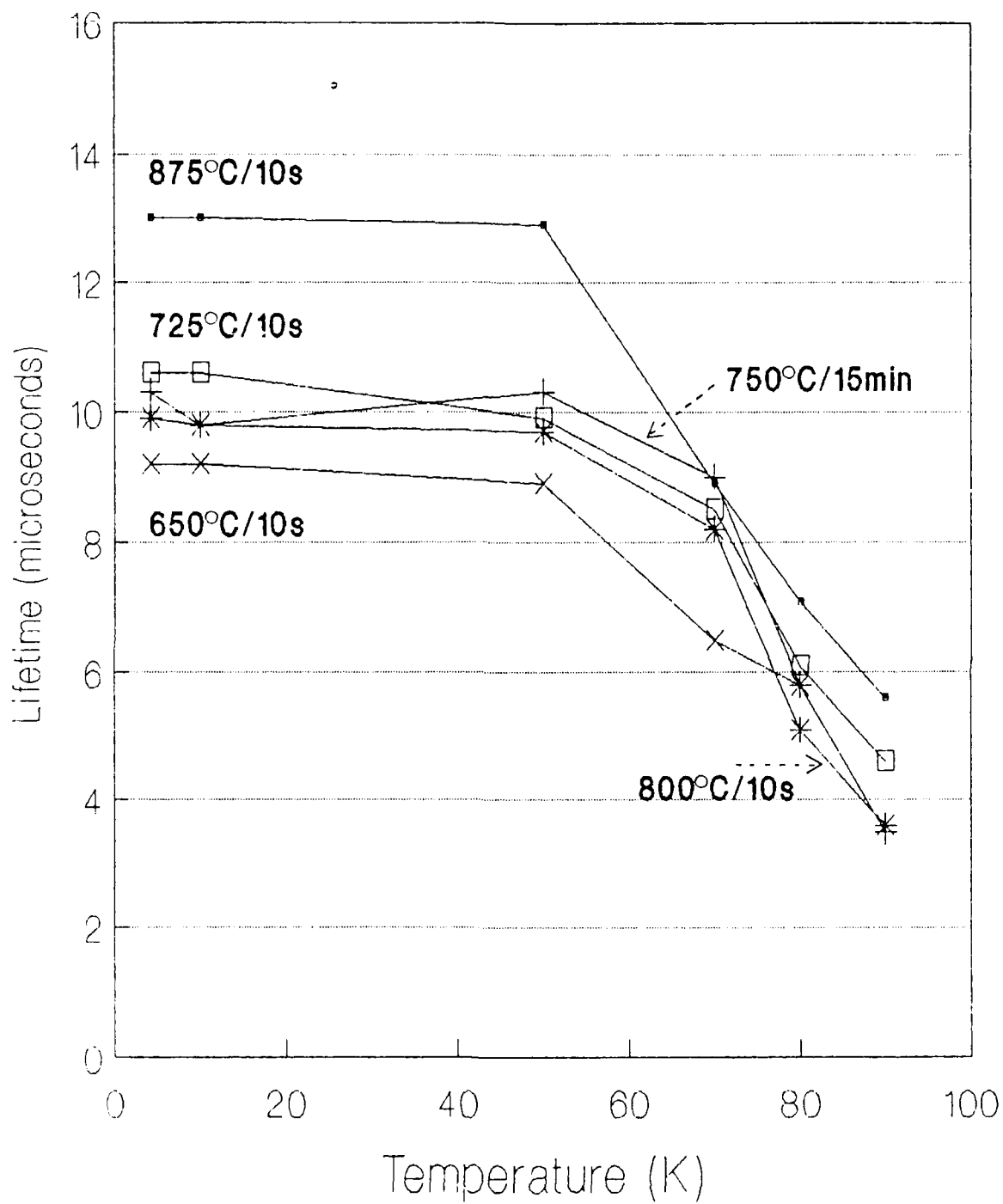


Figure 69 Anneal temperature dependence of the Yb^{3+} lifetimes in InP:Yb at 1002 nm.

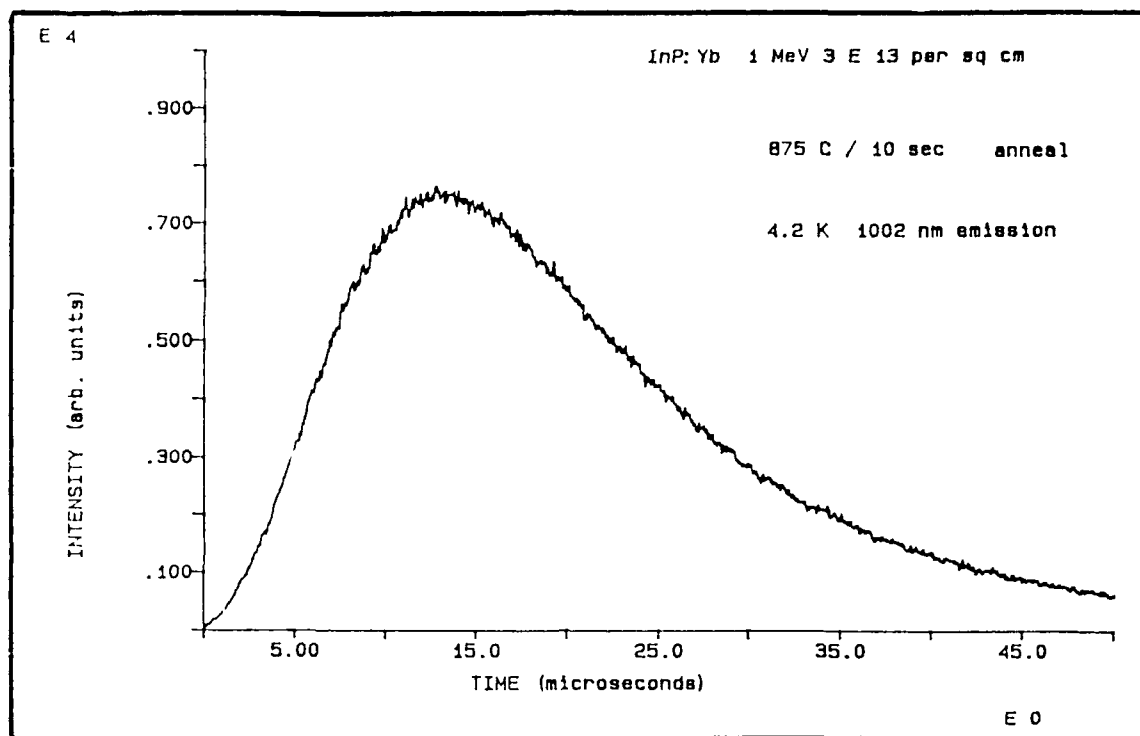


Figure 70. Example rise and decay waveform of the Yb^{3+} luminescence in InP:Yb (2.9 μs system time constant).

problem is a result of the system time constant and more specifically the current amplifier time constant. But since this filtering was noticed most where the voltage changed rapidly, the effect on the decay portion of the curve was much less. Hence, the values which were calculated were good first order approximations and were not expected to change significantly with a faster system time constant. (The decay curves of Fig. 68 were essentially taken from similar rise and decay waveforms, but only the decay portion was used in the analysis.)

Table 16. Corrected Decay Lifetimes (μ s) of Yb^{3+} in InP for a System Response Time Constant of 2.9 μ s.

Anneal Condition	Emission Temperature (K)						
	4.2	10	50	70	80	90	
650 C/10s	8.7	8.7	8.4	5.8	5.0	--	
725 C/10s	10.2	10.2	9.5	8.0	5.4	3.6	
800 C/10s	9.5	9.4	9.3	7.7	4.2	2.1	
875 C/10s	12.7	12.7	12.6	8.4	6.5	4.8	
750 C/15min	9.9	9.4	9.9	8.5	5.0	2.0	

To determine the error in the lifetime the system response was determined by eliminating the InP:Yb sample and bringing the laser pulse through the system. The electronic system decay response t_{sys} was determined to be 2.9 μ s, the same value determined from the waveform rise in Fig. 70. This value was used to correct the observed decay life time t_{obs} by the following expression (Valley and Wallman, 1948):

$$t^2 = t_{\text{obs}}^2 - t_{\text{sys}}^2 \quad (23)$$

The corrected decay lifetimes for different sample temperatures are listed in Table 16 for the five InP:Yb samples which were investigated. [Further details on these results for InP:Yb may be referenced (experimental section and Bumgarner, 1988).] The values listed in the table agree very well with what has been published (Klein, 1988; Koerber and Hangleiter, 1988); the sample that exhibited the

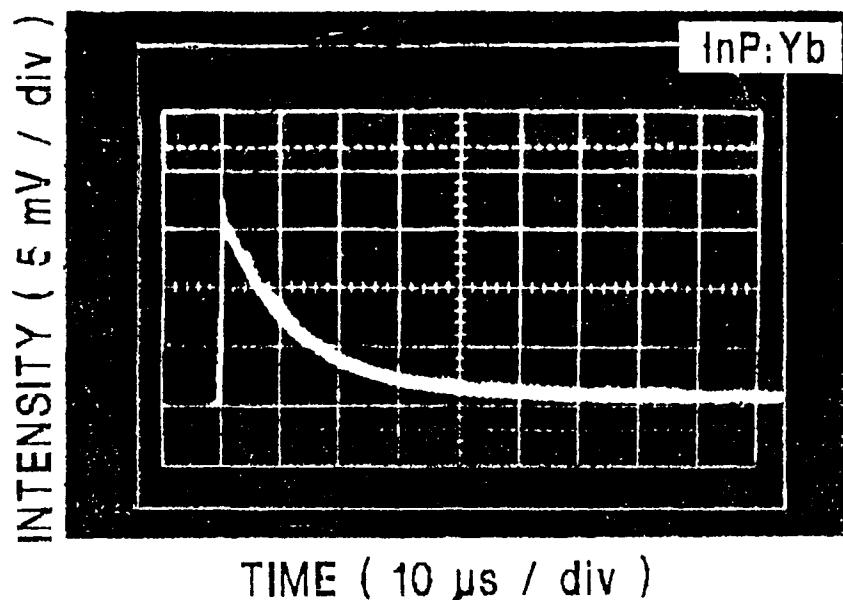


Figure 71. Luminescence rise and decay waveform of the Yb^{3+} 1006 nm emission in InP:Yb (fast Ge detector, 200 ns time constant).

strongest Yb^{3+} emission ($875^{\circ}\text{C}/10\text{s}$) showing the best agreement (12.7 μs). The lower lifetime values for the samples annealed below 875°C might indicate that not all the implantation damage is annealed away and more non-radiative processes are present.

To validate the corrected or improved results, the fast Ge detector was used at both the 200 ns and 400 ns time constant settings. The 1/2-m spectrometer with the 1.3 μm blazed grating was used including entrance and exit slit settings of 2 mm, respectively. The output to the detector went straight to the oscilloscope. Depicted in Fig. 71 is a copy of the oscilloscope display of the luminescence decay of

the Yb^{3+} 1006 nm emission (lines 7 and 8, Fig. 23) for InP implanted with Yb at an energy of 1 MeV and a dosage of $3 \times 10^{13} \text{ cm}^{-2}$ and post-implantation annealing of 725°C for 10s in fig. The detector setting was at the 200 ns time constant. Assuming an exponential decay, the time constant or lifetime was found from the following relationship:

$$t = \frac{(t_2 - t_1)}{\ln(A_1 / A_2)}, \quad (24)$$

where $t_{1,2}$ and $A_{1,2}$ represent time and relative amplitude values at two points on the decay curve in Fig. 71. The decay was calculated to be 8 μs which is in good first order agreement with the previously calculated value of 10.2 μs (Table 16) and published results. Rise time was less than 0.5 μs , contrary to the previous results using the current amplifier and S-1 PMT and the results by Kasatkin (1985), but in agreement with Klein (1988) and Koerber and Hangleiter (1988).

In conclusion lifetime measurements were achieved in high energy implanted, and rapid thermally and conventionally annealed InP:Yb. These are the first results for these deeper implanted layers of approximately 500 nm thickness. The study confirmed the published results for epitaxially doped and low energy implanted InP:Yb with reported lifetimes of 12.7 and 12.5 μs , respectively. The same lifetime was observed for the 1002 nm and 1005 nm emissions which agrees with Koerber and Hangleiter (1988). The investigation of the

lifetime as a function of sample anneal temperature gives shorter lifetimes below 875°C which might be indicative of the fact that all the damage is not annealed away and more non-radiative processes are present. A strong nonexponential component as seen by Klein (1988) was not observed. The multiple decay mechanism scheme proposed by Koerber and Hangleiter (1988) is supported.

AlGaAs:Yb

Lifetime measurements were attempted on the AlGaAs:Yb sample from the photoluminescence study which exhibited the strongest Yb³⁺ signal. The sample was Al_{0.30}Ga_{0.70}As implanted with Yb at an energy of 1 MeV and a dosage of $3 \times 10^{13} \text{ cm}^{-2}$ and post-implantation RTA double annealing at 975°C/15s and 500°C/15s in forming gas; the luminescence spectra was depicted in Fig. 31. The experimental setup was similar to that used for InP:Yb, in other words, a S-1 PMT and a 500 nm blazed grating was used; however, the 1/4-m spectrometer with 2 mm slits was used to increase the signal throughput and input. Figure 72 shows the decay of the 991 nm emission of Yb³⁺ in Al_{0.30}Ga_{0.70}As at 5K. Curve fitting analysis with the ASYSTAN software resulted in an excited state lifetime for Yb³⁺ of 15.5 μs , correcting for system response resulted in a value of 15.2 μs . This is a value very similar to that reported for InP:Yb. Lifetime measurements with the fast Ge detector were unsuccessful due to signal-to-noise problems.

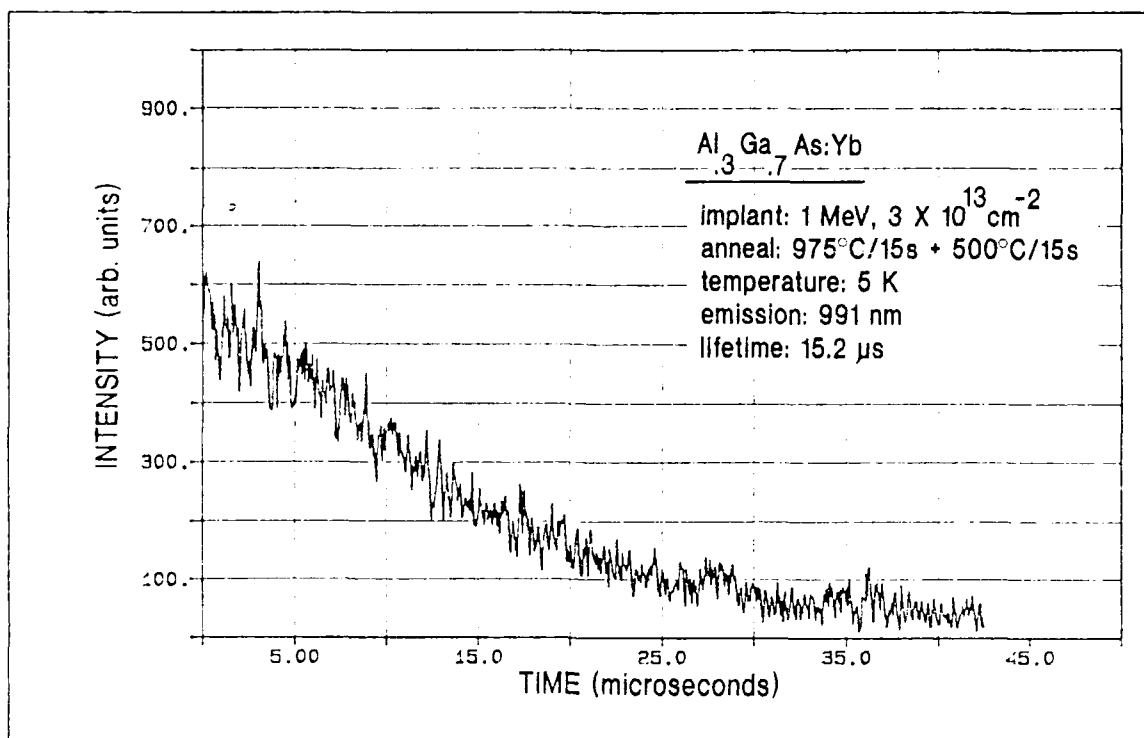


Figure 72. Decay curve for the Yb^{3+} emission in $\text{Al}_{0.3}\text{Ga}_{0.7}\text{As}:\text{Yb}$.

GaAs:Er and AlGaAs:Er

The determination of an excited state lifetime for Er^{3+} in GaAs and AlGaAs is especially important due to the technological importance of the 1.54 μm Er emission. Recently the luminescence lifetime of this emission was studied in a variety of Si and III-V semiconductor host materials (Klein and Pomrenke, 1988), but not AlGaAs. The approximately 1 ms lifetime which was observed in all hosts indicates that the Er emission is largely radiative, contrary to Yb, and therefore suggests that Er may be the rare earth dopant best suited for device applications. However, enough variance occurs with the different techniques used to

incorporate the rare earth into the host that further studies are needed to determine if there are Auger effects or defects which might be responsible for the non-radiative decay.

In this study it was attempted to verify the reported 1.2 ms lifetime in Er-implanted GaAs and furthermore to determine the lifetime for Er implanted into GaAs of different conductivity types. Furthermore, it was also attempted to establish for the first time the excited state lifetime of Er^{3+} in AlGaAs as a function of Al mole fraction.

Investigations of the excited state lifetimes of Er^{3+} were limited to the use of the Ge detectors due to the 1.54 μm wavelength of the Er emission. The 1/2-m spectrometer was used with a new variable slit housing with settings of up to 2 mm and a grating blazed for 1.3 μm (500 gr/mm). The output of the detector went straight to an oscilloscope. The semi-insulating GaAs and $\text{Al}_{0.4}\text{Ga}_{0.6}\text{As}$ samples were implanted with Er at an energy of 1 MeV and a dosage of $5 \times 10^{13} \text{ cm}^{-2}$ and subsequently annealed at 680°C for 10 min; the 7 K photoluminescence spectra of these samples were shown in Fig. 1. The attempts with the fast Ge detector were unsuccessful due to a high level of noise; however, the slow (APL) Ge detector was used in the attempt at three orders of magnitude increase in sensitivity. Signals were observed at 14 K for both $\text{Al}_{0.4}\text{Ga}_{0.6}\text{As}$ and for AlGaAs at 1550 nm, and for GaAs at 1560 nm. The relatively low temperature, however, was not sufficient to eliminate the fact that the lifetime of the Er^{3+} excited state is a function of temperature.

be 7 ± 1 ms. This prevented the determination of a lifetime for Er^{3+} in AlGaAs, or in GaAs where it has been established to be on the order of 1 millisecond.

GaAs:Tm

Due to the success in investigating for the first time the Tm^{3+} emission in GaAs at 1.2 μm , it was attempted to determine also the excited state lifetime of the strongest Tm^{3+} emission at 1233 nm as shown in fig. 42. The sample used for the study was semi-insulating (CS) GaAs implanted at an energy of 390 keV and a dosage of $5 \times 10^{13} \text{ cm}^{-2}$, encapsulated, and subsequently annealed at 725°C for 10 min in fig. The 1/2-m spectrometer was used with 2 mm slits and the 1.3 μm blazed grating. Both the fast and slow Ge detectors were used with the output going straight to the oscilloscope. Unfortunately, also due to signal-to-noise problems, the Tm^{3+} signal was not seen. Based on the results from the photoluminescence experiment and lifetime results from Yb^{3+} and Er^{3+} , it is suggested that the excited state lifetime for Tm^{3+} might possibly be on the order of 0.1 to 0.5 millisecond.

Conclusion

It was possible to determine lifetimes for the 1.0 μm In^{3+} emissions in high energy implanted and rapidly thermally annealed InAlGaAs. These are the first results for these deeper implanted impurities. The measured lifetime at 1.2 μm agrees very well with the published value of 12.5 μs . Lifetime dependent studies from 1.2 to 2.0 μm indicated that

for the 875°C/10s annealed sample the lifetimes drop from 12.7 to 4.8 μ s. Anneal dependent studies show smaller lifetimes at lower anneal temperatures. It was also possible for the first time to establish a lifetime of 15.5 μ s for $\text{Al}_{.3}\text{Ga}_{.7}\text{As}$. Although Er is proving technologically the most interesting rare earth ion, lifetime measurements were unsuccessful. It was also not possible to determine an excited state lifetime for Tm^{3+} in GaAs:Tm . Although signal-to-noise problems prevented the observation of these rare earth emissions, this problem can most likely be rectified with a high throughput 1/4-m monochromator with adjustable slits of at least up to 2 mm and the appropriate infrared grating. A slower Ge detector with higher detectivity and a PbS detector with a faster time constant needs to be considered. Finally, one of the important factors in affecting the data, both here and as reported in the literature, results from the method of incorporating the rare earth into the semiconductor host. Significant differences appear as a result of implanting the rare earth, growing doped epitaxial layers (LPE versus MOCVD), or growing bulk doped crystals. Due to the limitations of the experimental setup which led to time constant problems and signal-to-noise problems, no model is proposed as to the excitation mechanism associated with generating the 4f-emissions. However, the excitation processes as proposed by Klein (1988) and Koerber and Langhammer (1988) are in general supported based on their experimental spectrum.

V. Conclusion and Recommendations

This experimental investigation extended the current knowledge concerning rare-earth semiconductor systems and produced the first spectroscopic results for actinide and III-V semiconductor systems. It was shown that lanthanides or rare-earths, and also actinides, may be successfully introduced into binary and ternary III-V semiconductors through high, intermediate, or low energy implantation. The study supports the feasibility of producing infrared light emitting diodes, as has been shown for Er and Yb, for the 1.0 to 1.7 μm range. The possibility of producing laser structures (Tsang and Logan, 1986) and other electro-optic devices (Lozykowski, 1988) is encouraging. Based on this research and the energy levels of the free lanthanide and actinide atoms, devices for the 2 to 3 μm range are probable, but most likely of low efficiency. Besides the obvious spectroscopic characterization, these systems have lead to interesting results concerning physical questions about the excitation mechanism and decay kinetics. The fact that numerous rare-earth and semiconductor systems have been investigated allows for greater understanding through the comparison of the individual systems.

The lanthanides, ytterbium, erbium, thulium, and praseodymium, and the actinide, uranium, were successfully implanted into the binary III-V semiconductors (GaAs, InP, or GaSb) and GaAs hosts as verified also by SIMS analysis. This was possible through high energy (1 MeV), intermediate (300

and 390 keV), and low energy (140 keV) implantations with subsequent post-implantation annealing using both rapid thermal and conventional annealing. The resulting rare-earth and actinide emissions in the 0.9 to 1.7 μm spectral region were identified and characterized through photoluminescence. The characteristic sharp emissions are seen independent of host around 1.0 μm for Yb^{3+} ; 1.5 μm for Er^{3+} ; 1.2 μm for Tm^{3+} ; 1.1, 1.3, and 1.6 μm for Pr^{3+} ; and 1.6 to 1.7 μm for uranium. That the numerous REs and uranium can be incorporated into the different semiconductor hosts with little change in the emission energy shows how generally insensitive they are to the host lattice. This demonstrates how the 4f shell or 5f shell is shielded from the external environment by the filled 5s and 5p, or 6s and 6p, and only weakly affected by the crystal field. The observed transitions are between the weakly crystal-field-split spin-orbit levels of the trivalent rare-earths and possibly tri- or tetra-valent uranium.

The photoluminescence technique allowed for further analysis of the emission structure as studies were performed with different semiconductor substrates, and also various parameters were varied such as conductivity of the host, the laser excitation, sample temperature, anneal temperature, anneal time, and anneal technique. Selected excitation with a CO_2 laser of different systems was performed in order to determine the excitation mechanism between the semiconductor

host and the rare earth ion which leads to the 4f-intracenter emissions. Results indicate that the RE emissions are due to the excitation of host-related states with subsequent energy transfer to RE centers; specifically, free carriers appear to be involved in exciting the rare earth but below bandgap states may also play a role. Lifetime measurements with a nitrogen-laser pumped dye laser indicate that the Er^{3+} emissions are largely radiative (long lifetime) while mainly nonradiative processes dominate in the Yb^{3+} system (short lifetime).

Different approaches may be taken in summarizing the results to this study. Presented here are the combined photoluminescence, selected excitation, and lifetime measurement conclusions for each specific ion:

Ytterbium

The 4f-intra center emissions around 1.0 μm of Yb^{3+} were seen in semi-insulating (SI) InP, n-GaP, and for the first time AlGaAs; essentially no evidence of Yb^{3+} emissions in GaAs were observed. The emissions are due to transitions between the crystal-field split spin-orbit levels $^2\text{F}_{5/2} - ^2\text{F}_{7/2}$ of Yb^{3+} ($4f^{13}$). Very strong Yb^{3+} emissions were seen in InP for 1 MeV and 140 keV energy implants for the first time. Conventional and rapid thermal annealing were viable techniques for post-implantation annealing and optimum activation of Yb^{3+} in InP was achieved at 875°C and 10 seconds annealing. SIMS analysis shows that Yb ions diffuse into the InP host.

The Yb^{3+} emission in InP is considerably stronger than in n-GaP and AlGaAs, and it appears that low doped n-type material is most likely the desirable host material. The Yb^{3+} emission in $\text{Al}_x\text{Ga}_{1-x}\text{As}$ was seen at all three Al mole fractions of $x = 0.15$, 0.23 , and 0.50 ; and the spectra varied significantly with Al mole fraction. In all semiconductors except for InP, the Yb appears to have more than one center. It is concluded that the main Yb^{3+} center in InP, GaP, GaAs, and AlGaAs is substitutional on a cation site (In, Ga, or Al).

The selected excitation of InP:Yb with a tunable dye laser indicates that the dominant process in exciting Yb^{3+} is through free carriers. However, since weak excitation still occurred at 893.0 nm, an excitation process via donor-acceptor (DA) pairs is not ruled out but considered of low efficiency, at least for the case of implanted layers. Lifetimes at low temperature (4.2 - 15 K) of 12.5 and 15.5 μs for the Yb^{3+} decay in InP and for the first time $\text{Al}_{0.3}\text{Ga}_{0.7}\text{As}$, respectively, indicate that nonradiative processes limit the radiative efficiency of these RE-semiconductor systems. The excited state lifetimes of different Yb^{3+} emissions in InP are invariant, indicating that the emissions are from one center. Longer lifetimes at higher anneal temperatures seem to indicate that lifetime studies may be used as a measure of the quality of the implanted and annealed impurity layer.

Erbium

For erbium the characteristic sharp 4f-intracenter emissions around 1.54 μm were seen for the first time for AlAs, for $\text{Al}_x\text{Ga}_{1-x}\text{As}$ of different Al mole fractions ($x = 0.1, 0.2, 0.3, \text{ and } 0.4$), and for different conductivity types of GaAs (SI, n-, p-type). This technologically important emission was also seen in SI-InP and p-GaP. The emissions are a result of the transitions between the weakly crystal-field-split spin-orbit levels $^4\text{I}_{13/2} - ^4\text{I}_{15/2}$ of Er^{3+} (4f¹¹); only recently have there been reports of possible transitions between the spin-orbit levels $^4\text{I}_{11/2} - ^4\text{I}_{15/2}$ (Whitney et al, 1988). This is also the first time that Er had been implanted at a high energy of 1 MeV to create a relatively thick implanted RE layer. The strongest signal was observed for $\text{Al}_{.4}\text{Ga}_{.6}\text{As}$; however, taking into consideration photo-absorption, under the same experimental conditions, the emission intensity is roughly the same among the different semiconductors. No significant spectral changes occurred upon examining different vendor substrates of the same semiconductor. No significant shifts in energy occurred for the Er^{3+} emission in these implanted layers as a result of the different crystal field environments due to the various semiconductor hosts ranging in bandgap from 1.42 for InP to 2.24 for AlAs. This demonstrates how insensitive the erbium ion is, especially compared to other rare earth ions, to the external environment from which it is shielded by the 5s and 5p shells.

It appears that the erbium ion can be easily activated in the binary and ternary III-V semiconductors with 10 minute post-implantation annealing in the 650 to 750°C temperature range. Erbium appears to diffuse toward the surface as compared to into the host as shown for Yb upon performing SIMS analysis. The Er^{+3} emission was seen at room temperature. It should be noted that even though Er^{3+} is consistently similar in different hosts and under different treatment conditions for 'implanted' layers, significant spectral differences do occur when comparing these layers to those grown by MBE and MOCVD; indicating possibly the presence of numerous Er centers and associated complexes and/or defects. The understanding of these centers may be enhanced by performing a more detailed dosage dependent study as compared to the preliminary study performed in this study (0.5 to $7.5 \times 10^{13} \text{ cm}^{-2}$).

In the selected excitation of Er^{3+} in GaAs, as the excitation energy is tuned across the bandgap of GaAs the Er^{3+} luminescence continues to be observed upon exciting into the (DA) states and past the LO phonon replicas of the (DA) states of the substrate. For one specific GaAs substrate the intensity of the Er spectra drops by only about 50% upon reducing the excitation energy from 1.540 to 1.445 eV. For InP:Er a similar behavior is also observed in which a significant Er^{3+} signal is retained upon exciting from above the bandgap to close to the (DA) states. Free carriers are

needed to excite the erbium centers in GaAs and InP, but below bandgap states such as DA pairs and the resonant energy transfer from deep levels play also a role. Besides these excitation mechanisms one must also consider the de-excitation mechanism of the rare-earth itself in which energy is non-radiatively transferred from higher lying states (e.g. $^4I_{9/2}$ and $^4I_{11/2}$) to lower states (e.g. $^4I_{13/2}$) which would lead to transitions between the first excited and the ground state (e.g. $^4I_{13/2} - ^4I_{15/2}$ of Er^{3+}). The excitation of the erbium through free carriers is somewhat supported by the result that the Er^{3+} emission is more intense in n-type GaAs versus SI or p-type GaAs.

The exact measurement of excited state lifetimes for Er^{3+} in III-V semiconductors or AlGaAs was unachievable in this experiment due to signal-to-noise problems; however, 1 millisecond lifetimes have been reported for Er^{3+} in different semiconductor hosts (Klein and Pomrenke, 1988). This demonstrates that the Er emission is largely radiative. This fact plus room temperature observation, excitation over a wide range of states, spectral invariance in temperature and semiconductor host, and the technological importance of the 1.54 μm wavelength, allows one to conclude that Er is the RE dopant showing the greatest promise for electr-optic applications.

Thulium

For GaAs and InP the characteristic sharp 4f-emissions were identified for the first time at around 1.23 μm for

transitions between the weakly crystal-field-split spin-orbit levels $^3H_5 - ^3H_6$ of Tm^{3+} ($4f^{12}$). The main 1233 nm line in GaAs shows doublet structure and each doublet component has a resolution of better than 0.15 meV at fwhm. The emissions which extend from 0.93 to 1.02 eV were best seen in semi-insulating GaAs and InP for samples which were encapsulated during annealing. Post-implantation anneal studies of the 390 keV implanted samples established optimum annealing conditions for GaAs:Tm at 725°C for 10-15 min and for InP:Tm between 575 - 625°C also for 10-15 min. SIMS analysis indicates that the Tm ions diffuse toward the surface upon annealing.

Evidence exists that the Tm^{3+} emissions in GaAs for samples annealed between 625 and 750°C originate from one dominant center; a secondary center appears at low anneal temperatures ($< 625^\circ C$). As a result a model was proposed explaining the annealing process for some rare-earth implanted semiconductors. Sample temperature dependent studies show that the Tm^{3+} emission in GaAs may be seen up to 200 K without shifts in energy or relative intensity; evidence of 'hot' lines is also observed

Selected excitation studies of Tm^{3+} show that at least for these implanted layers no significant rare earth luminescence occurs upon exciting below the exciton levels of GaAs. The excitation mechanism is essentially through free carriers. Unfortunately an intense, broad signal centered

approximately at 1.0 eV partially masks the Tm^{3+} signal and prevents the results from being completely conclusive. Due to signal-to-noise problems no excited state lifetimes were established for Tm^{3+} .

Praseodymium

The characteristic 4f-intracenter emissions of Pr^{3+} ($4f^2$) were observed for the first time in GaAs and InP. Three sets of sharp emissions are seen in GaAs due to transitions between the crystal-field-split spin-orbit levels $^1\text{G}_4 - ^3\text{H}_4$, $^1\text{G}_4 - ^3\text{H}_5$, and $^3\text{F}_3 - ^3\text{H}_4$ of Pr^{3+} at 1.05, 1.35, and 1.6 μm , respectively. In InP only the transitions between the levels $^1\text{G}_4 - ^3\text{H}_5$ of Pr^{3+} are observed around 1.35 μm ; most likely the other sets of emissions being masked by broad, intense background emissions. The 1.05 μm emission in GaAs is the weakest. The 1.35 and 1.6 μm emissions have their own unique temperature dependence; the highest temperature at which a sharp 4f-emission is observed is around 175 K.

Post-implantation annealing of the 380 keV Pr implanted layers showed that for anneal times of 10 minutes, the optimum anneal temperature for GaAs was 750°C and for InP it was 675°C. At and near the optimum anneal temperatures for both GaAs and InP, there is essentially no evidence of near-edge emissions, indicating that recombination processes possibly favor the excitation of the rare-earth versus the near-edge emissions. Based on isochronal anneal studies and sample temperature dependent studies on GaAs:Pr, the Pr luminescent centers are found to possibly occupy different

lattice sites but one very dominant center is present at anneal temperatures of 675 to 750°C. The annealing appears to cause the Pr ions to diffuse toward the surface as determined by SIMS analysis.

Praseodymium in GaAs appears to show a complicated excitation behavior. Essentially free carriers are needed to excite the rare earth centers since no significant excitation of the three sets of Pr^{3+} emissions occurs through DA states or lower lying states. However, a 1.02 eV defect level appears to complicate this process by masking or quenching the Pr emissions and bringing to attention the photo-absorption problem between the implanted layers and the host. Upon exciting with lower than 1.42 eV energy, the broad 1.02 eV emission has essentially disappeared, and an array of sharp emissions results which are different in energy and intensity from the original set of three Pr^{3+} emissions seen with above bandgap excitation. Preliminary conclusions are that upon exciting in the 1.425 - 1.316 eV region one excites multiple Pr centers. Some of these centers might also be associated with residual transition element impurities (e.g. Cu, Mn) in the host, complexes between the RE and transition metals, or other interactions between the RE and impurity or defect.

Uranium

An actinide was successfully introduced into GaAs and InP for the first time. The implanted uranium ion gives rise

to relatively strong and sharp emissions between 1.60 to 1.69 μm in GaAs and at 1.37 μm in InP. The implantation was performed at an ion mean energy of 131 keV using a new type of high current metal ion source; the predicted depth profile of uranium plus very limited diffusion upon annealing was confirmed with SIMS. The emissions are a result of transitions between specific crystal-field-split spin-orbit levels of possibly U^{3+} ($^4\text{I}_{3/2} - ^4\text{I}_{9/2}$) but most likely tetravalent uranium ($^3\text{F}_3 - ^3\text{H}_4$). The full-width at half-maximum of the main 1601 nm line in GaAs and the 1670 nm line in InP is less than 0.46 meV at 6K. Temperature dependent studies indicate that the emissions are most likely associated with one center, and the luminescence is observed in GaAs and InP up to an temperature of 100 - 120 K after which it rapidly quenches.

The conclusions should also be summarized from the point of view of common parameters or experimental techniques shared among the various lanthanides and actinides incorporated in a solid. The sixteen generalized points which follow may also serve as ideas for future investigations.

(1) Elemental selection: In choosing an ion with emission energies at below semiconductor bandgap energy, one can be limitedly successful by examining the energy level diagrams of trivalent rare earths; however, comparison studies with glasses and II-VI semiconductors are desirable.

Superficially one may say that the RE ions of low atomic number (e.g. Nd, Pr) exhibit emissions from numerous spin-orbit levels while high atomic numbers (e.g. Er, Tm, Yb) exhibit emissions from only one set of spin-orbit levels. Also for the case of Tm which is positioned between Er and Yb in the periodic table, the sample temperature behavior of the emissions seems to exhibit characteristics somewhere between that of Er and Yb. The degree of nuclear activity of course is the primary selection factor for the actinides.

(2) Implantation: Lanthanides and actinides may be successfully implanted into semiconductors at high energy (1 MeV), intermediate (380, 390 keV), and low energy (140 keV). Both conventional and unconventional (MEVVA ion source) techniques may be used. Relatively thick implant layers may be generated with the 1 MeV implant. However, it was determined that the actual implantation process was for the vendor a research topic, as many unknowns existed as to what the best source material and technique was in producing the ion beam in the first place. The TRIM code established projected range and straggling parameters which were unavailable in the literature. A table was generated with these parameters for lanthanides and actinides implanted into selected semiconductors.

(3) Substrate selection: The semiconductor substrates need to be screened for intense and broad impurity and defect levels prior to implantation. These levels either mask or

possibly quench particular 4f emissions. Only low doped ($< 2 \times 10^{17} \text{ cm}^{-3}$) and semi-insulating samples are suggested. For GaP it appears that only Te doped substrates allow for the possible observation of RE or actinide emissions.

(4) Annealing and Processing Technology: Both rapid thermal and conventional annealing are successful in activating the samples; however, due to the clean room environment RTA was more time consuming inspite of the 'seconds' annealing time. Contamination of the RTA oven is also a concern when annealing material other than GaAs. Encapsulation of the sample is desired for annealing.

(5) Isochronal and Isothermal Studies: These studies were successful in determining optimum activation for InP:Yb, GaAs:Tm, InP:Tm, GaAs:Pr, and InP:Pr. They also told of the onset of the luminescence, possible competing processes with the near-edge emissions (e.g. InP:Yb, GaAs:Pr, InP:Pr), the presence of multiple centers, and the quality of the anneal. A model was proposed in the thulium luminescence section of this document which describes the sequence of events during annealing which might lead to multiple centers.

(6) Substrate Studies: By examining semiconductors of different conductivities (n-, p-type, SI), possible conclusions can be made about the excitation mechanism, such as involving free carriers as was seen for n-GaAs:Er and n-GaP:Yb. Similarly by varying the Al mole fraction for AlGaAs various conclusions can be arrived at pertaining to site location of the RE. By examining the many different

semiconductors, it is seen that the RE emissions are relatively insensitive to some of the hosts and that the perturbations by the crystal field are small.

(7) Above bandgap excitation: Different above bandgap excitations allow for varying depths of the implanted layer to be probed by the laser light due to the difference in the absorption coefficient of the material at the different wavelengths. Information on the luminescence structure, especially changes in intensity, may be gained as was seen for GaAs:Er and InP:Tm.

(8) Near-edge Emissions: It is important that as much of the spectral region below the bandgap be investigated in order that other emission processes may be monitored, associated or not associated with the implanted impurity. Of special interest are the (DA) and (FB) transitions since for the InP:Yb, GaAs:Pr, and InP:Pr systems it appears that competing processes between the near-edge and RE may be present; however, this phenomenon is most likely associated with the quality of the anneal.

(9) Temperature Dependence: The luminescence studies showed that the 4f-intracenter emissions of Yb^{3+} may be seen up to 90 K, the Er^{3+} emissions up to room temperature, the Tm^{3+} emissions up to 200 K, the Pr^{3+} emissions to 175 K, and the uranium related emissions up to 120 K. Aside from monitoring different centers, information was gained which would indicate that most likely Er and Tm show the greatest

possibility for technical application due to the presence of the emissions at higher temperature.

(10) Selected Excitation: For the four rare earth ions it was determined that free carriers are needed to excite the RE, but below bandgap states such as (DA) pairs and the resonant energy transfer from deep levels may also play a role. Furthermore, the de-excitation mechanism of the RE itself must be considered. The understanding of these mechanisms may be enhanced by examining similar phenomena observed in transition metal doped III-V semiconductors. Due to photo-absorption problems, limits exist in interpreting the data from the selected excitation of implanted layers.

(11) Lifetime Measurements: Although limited excited state lifetime information was gained from this study, it does appear that Er centers are more radiative than the Yb center. Different samples and system improvements should allow for future studies on the rare earth and semiconductor kinetics, although signal-to-noise problems will persist due to the limitations of the infrared detectors.

(12) Changing Emissions: Kravtsov (1985) and Ennen et al (1985) observed that the Yb^{3+} emissions appear to change with sample storage time. This is a possible explanation for the weak evidence of Yb^{3+} emissions in GaAs and GaP. It would be of interest to reinvestigate in the future some of the samples from this study.

(13) Defects: Aside from the different centers that the rare earth may occupy and the different associates it may

form between itself and the crystalline defects and complexes, the process of implanting the heavy ion into the host semiconductor appears to generate defect levels, seen especially in InP:RE in the 1.0 - 1.3 μm spectral region.

(14) SIMS: This analysis technique aided in verifying the presence of the ion from which the RE emissions were seen, and proved invaluable at times due to problems with the implantation. At least in InP it was determined that out of the four rare earths, all except ytterbium diffused toward the surface upon annealing; an explanation for this should allow for future investigations. One of the questions that could be answered is, if the RE signal intensity degrades as there is increased diffusion toward the surface.

(15) Limitations: As already alluded to in prior discussions and especially in conjunction with the selected excitation experiment, the photo-absorption problem associated with implanted layers limits some of the results and interpretations for all systems investigated. Bulk RE doped samples or RE doped LPE doped samples should be acquired for correlation studies. Further limitations were of course signal-to-noise problems associated with the infrared spectral region.

(16) Equipment: In general the Ge detector (7 millisecond time constant), the 1.0 and 1.6 μm blazed gratings, and the 514.5 nm line of the Ar-ion laser were crucial through many phases of the experiment.

One of the key interests in the investigation of rare earths incorporated into semiconductors is to understand the interaction or excitation mechanism between the semiconductor and the rare earth which leads to the characteristic 4f-emissions. For the systems which were investigated here a very general model is proposed that shows the transfer of energy from the states of the III-V semiconductor to the 4f-ion. Using diagrams of basic luminescence transitions and a type of configuration coordinate diagram for the 4f-impurity, Figure 73 illustrates the transfer of energy between the host and impurity. Upon either direct excitation from the exciting radiation or excitation from the nonradiative recombination of a free carrier, exciton, donor-acceptor, or deep levels of the host; the energy is carried to the RE^{3+} ion which is raised from the ground state to any of a number of available excited states. The resulting emission is then a radiative (or non-radiative) transition between two spin orbit states (e.g. $^4\text{I}_{13/2} - ^4\text{I}_{15/2}$) after relevant 4f-4f de-excitation mechanisms populated the particular states. Such de-excitation mechanisms, as listed in the figure, were recently tabulated by Boyn, 1988. Finally, it is believed that there is a considerable interaction between the RE and transition metal residual impurities (if present) that significantly affect all recombination mechanisms.

Finally, the overall significant contributions from this study was to support the idea of the feasibility of producing

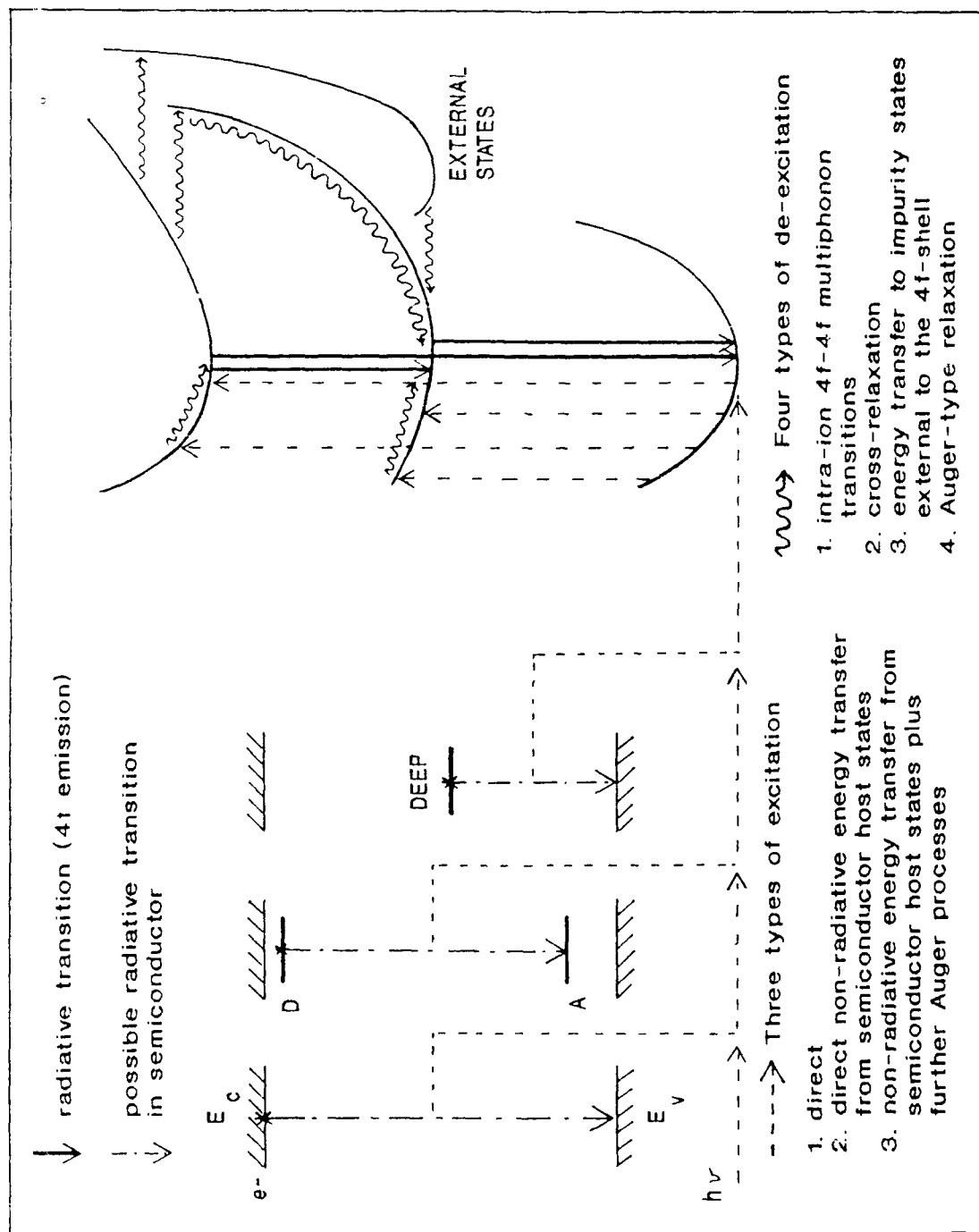


Figure 73. Model for possible energy transfer mechanisms in rare earth doped III-V semiconductors.

a family of infrared LEDs in the 1.0 to 1.7 μm range. The first observations were made of the 4f-intracenter transitions of Tm^{3+} and Pr^{3+} in III-V semiconductors. Rare earth emissions, specifically Er^{3+} and Yb^{3+} , were not only seen in binary III-V hosts but also for the first time in AlGaAs. The first investigations of actinides (U and Th) implanted in GaAs, InP, and GaP were undertaken resulting in uranium related emissions in GaAs and InP. Selected excitation studies indicate that free carriers are needed to excite the rare earth centers but other host-related states are not excluded from the excitation processes. Lifetime measurements show radiative and non-radiative nature in different rare earth doped semiconductors. The study of ytterbium continues to be an interesting physics problem as will most likely be the case of uranium in the III-V semiconductors. Praseodymium shows interest due to its set of three emissions and complicated excitation spectra. However, erbium shows the greatest technological promise as a result of room temperature luminescence, a broad range of excitation states, a long decay lifetime, and the technological importance of the 1.54 μm wavelength.

Numerous recommendations have been made throughout the text and the prospectus to the dissertation; what follows are some other areas for future research. Selected excitation experiments on uranium and praseodymium are highly

recommended including experiments on Er^{3+} in which the full 0.8 to 1.7 μm range is recorded for GaAs and InP. Studies and cooperative efforts are suggested to determine the valency of the uranium center and also studies to observe the possible 2.4 - 2.5 μm emission of U^{3+} . Also a systematic study needs to be pursued to identify Th-related emissions in the III-V hosts. The photoluminescence of holmium implanted into GaAs and InP at energies of 1 MeV and 100 keV should be performed and monitored for emissions at 0.91, 1.18, and 1.96 μm which correspond to transitions between specific spin-orbit levels (see Appendix E for the recent GaAs:Ho spectrum).

The problem of why Yb is so difficult to observe in GaAs should be pursued. Erbium introduced into GaAs of different levels of conductivity should be investigated. The systematic investigation of the electrical properties of rare earth implanted layers needs to be considered. Obvious cooperation should be initiated to produce rare earth and III-V semiconductor devices. Finally, continued attention needs to be given to equipment acquisition such as an Ar-ion laser for the photoluminescence lab, a Ge detector with an intermediate time constant, a fast PbS detector, further RF shielding for the lifetime measurement lab, and reconfiguration of the lifetime measurement system such that actual time-resolved spectra may be taken. A sapphire:Ti laser is recommended to replace the dye laser. Software

development for direct smoothing on the SPECPLLOT program is highly suggested.

Appendix A: Electronic Configuration of Lanthanide Ions
(Pappalardo, 1978)

Atomic Number	Element	Symbol	Electronic Configuration		Common Valence States
			Neutral Atom	Trivalent Ion	
58	Cerium	Ce	$4f^1 5d^1 6s^2 ({}^1G_4)$	$4f ({}^2F_{5/2})$	3,4
59	Praseodymium	Pr	$4f^3 6s^2 ({}^4I_{9/2})$	$4f^2 ({}^3H_4)$	3, (4)
60	Neodymium	Nd	$4f^4 6s^2 ({}^5I_4)$	$4f^3 ({}^4I_{9/2})$	3, (4)
61	Promethium	Pm	$4f^5 6s^2 ({}^6H_{5/2})$	$4f^4 ({}^5I_4)$	3
62	Samarium	Sm	$4f^6 6s^2 ({}^7F_0)$	$4f^5 ({}^6H_{5/2})$	3,2
63	Europium	Eu	$4f^7 6s^2 ({}^8S_{7/2})$	$4f^6 ({}^7F_0)$	3,2
64	Gadolinium	Gd	$4f^7 5d^1 6s^2 ({}^2D_{3/2})$	$4f^7 ({}^8S_{7/2})$	3
65	Terbium	Tb	$4f^9 6s^2 ({}^6H_{15/2})$	$4f^8 ({}^7F_6)$	3,4
66	Dysprosium	Dy	$4f^{10} 6s^2 ({}^5I_8)$	$4f^9 ({}^6H_{15/2})$	3
67	Holmium	Ho	$4f^{11} 6s^2 ({}^4I_{15/2})$	$4f^{10} ({}^5I_8)$	3
68	Erbium	Er	$4f^{12} 6s^2 ({}^3H_6)$	$4f^{11} ({}^4I_{15/2})$	3
69	Thulium	Tm	$4f^{13} 6s^2 ({}^2F_{7/2})$	$4f^{12} ({}^3H_6)$	3,2
70	Ytterbium	Yb	$4f^{14} 6s^2 ({}^1S_0)$	$4f^{13} ({}^2F_{7/2})$	3,2
71	Lutetium	Lu	$4f^{14} 5d^1 6s^2 ({}^2D_{3/2})$	$4f^{14} ({}^1S_0)$	3

Footnote: Electrons added to the Xenon core, namely to
 $1s^2 2s^2 2p^6 3s^2 3p^6 3d^{10} 4s^2 4p^6 4d^{10} 5s^2 5p^6$.

Appendix B: Electronic Configuration of Actinide Ions
(Pappalardo, 1978)

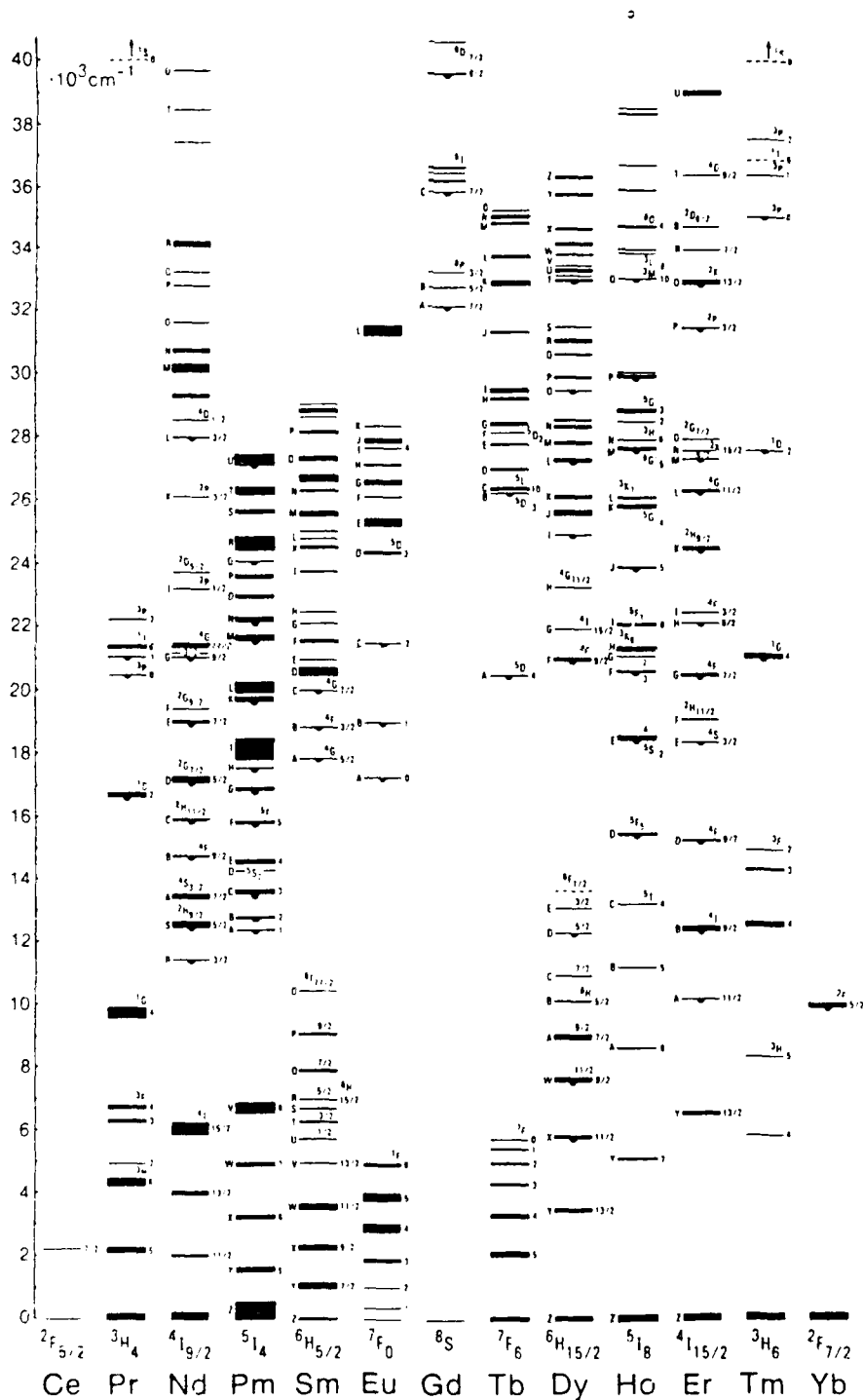
Atomic Number	Element	Symbol	Electronic Configuration		Common Valence States
			Neutral Atom	Trivalent Ion	
90	Thorium	Th	$6d^2 7s^2 ({}^3F_2)$	$5f ({}^2F_{5/2})$	4
91	Protactinium	Pa	$5f^2 6d 7s^2 (Jj)$	$5f^2 ({}^3H_4)$	5,3
92	Uranium	U	$5f^3 6d 7s^2 (Jj)$	$5f^3 ({}^4I_{9/2})$	3,4,5,6
93	Neptunium	Np	$5f^4 6d 7s^2 (Jj)$	$5f^4 ({}^5I_4)$	3,4,5,6,7
94	Plutonium	Pu	$5f^6 7s^2 ({}^7F_0)$	$5f^5 ({}^6H_{5/2})$	3,4,5,6,7
95	Americium	Am	$5f^7 7s^2 ({}^8S_{7/2})$	$5f^6 ({}^7F_0)$	3,4,5,6
96	Curium	Cm	$5f^7 6d 7s^2 (Jj)$	$5f^7 ({}^8S_{7/2})$	3,4
97	Berkelium	Bk	$5f^9 7s^2 ({}^6H_{15/2})$	$5f^8 ({}^7F_6)$	3,4
98	Californium	Cf	$5f^{10} 7s^2 ({}^5I_8)$	$5f^9 ({}^6H_{15/2})$	3,2
99	Einsteinium	Es	$5f^{11} 7s^2 ({}^4I_{15/2})$	$5f^{10} ({}^5I_8)$	3,2
100	Fermium	Fm	$5f^{12} 7s^2 ({}^3H_6)$	$5f^{11} ({}^4I_{15/2})^*$	3,2
101	Mendelevium	Md	$5f^{13} 7s^2 ({}^2F_{7/2})^*$	$5f^{12} ({}^3H_6)^*$	3,2,1
102	Nobelium	No	$5f^{14} 7s^2 ({}^1S_0)^*$	$5f^{13} ({}^2F_{7/2})^*$	
103	Lawrencium	Lr		$5f^{14} ({}^1S_0)^*$	

Footnote. Electrons added to the Radon core, namely to
 $1s^2 2s^2 2p^6 3s^2 3p^6 3d^{10} 4s^2 4p^6 4d^{10} 4f^{14} 5s^2 5p^6 5d^{10} 6s^2 6p^6$

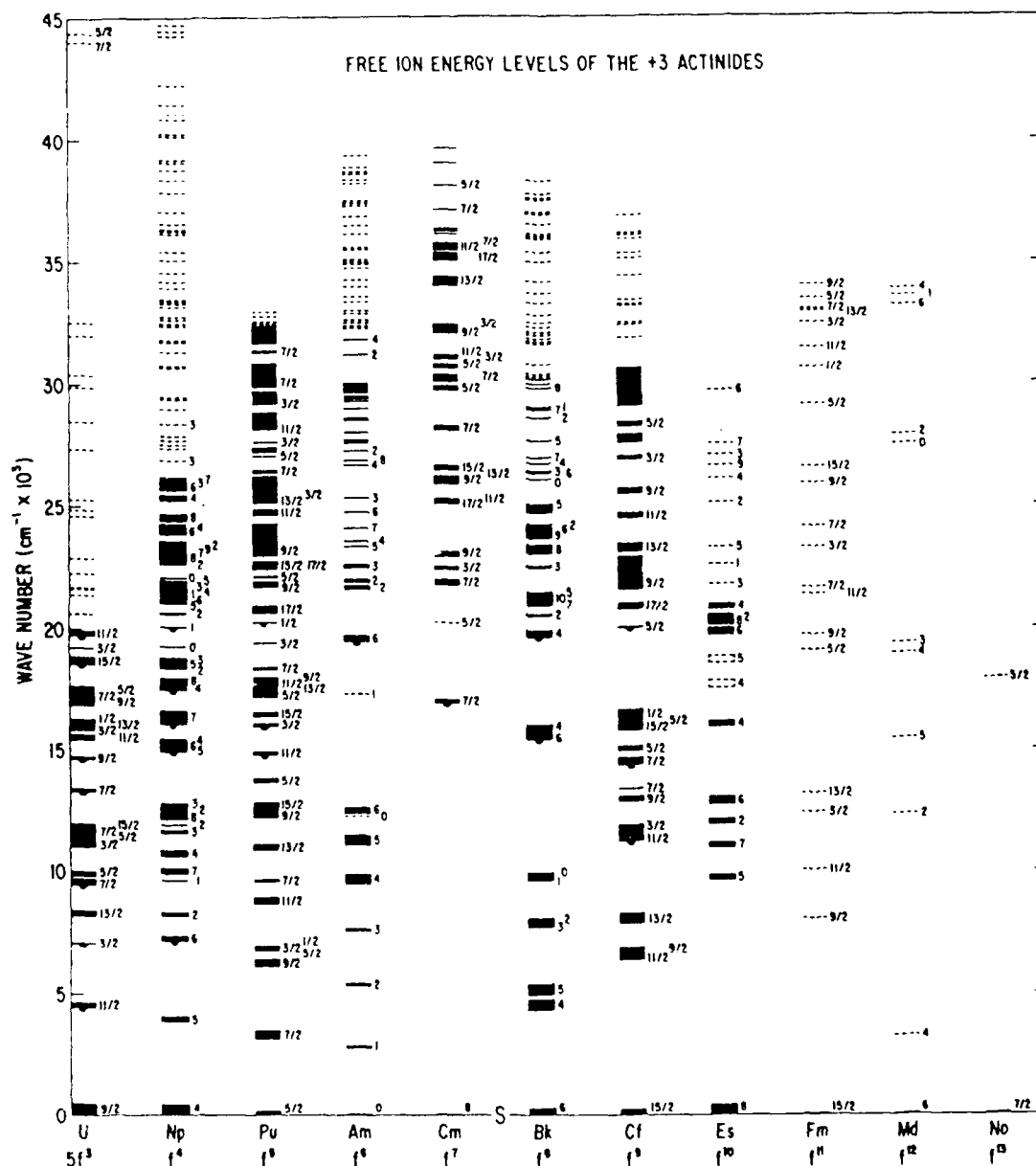
Jj: case of Jj-coupling.

* tentative assignment

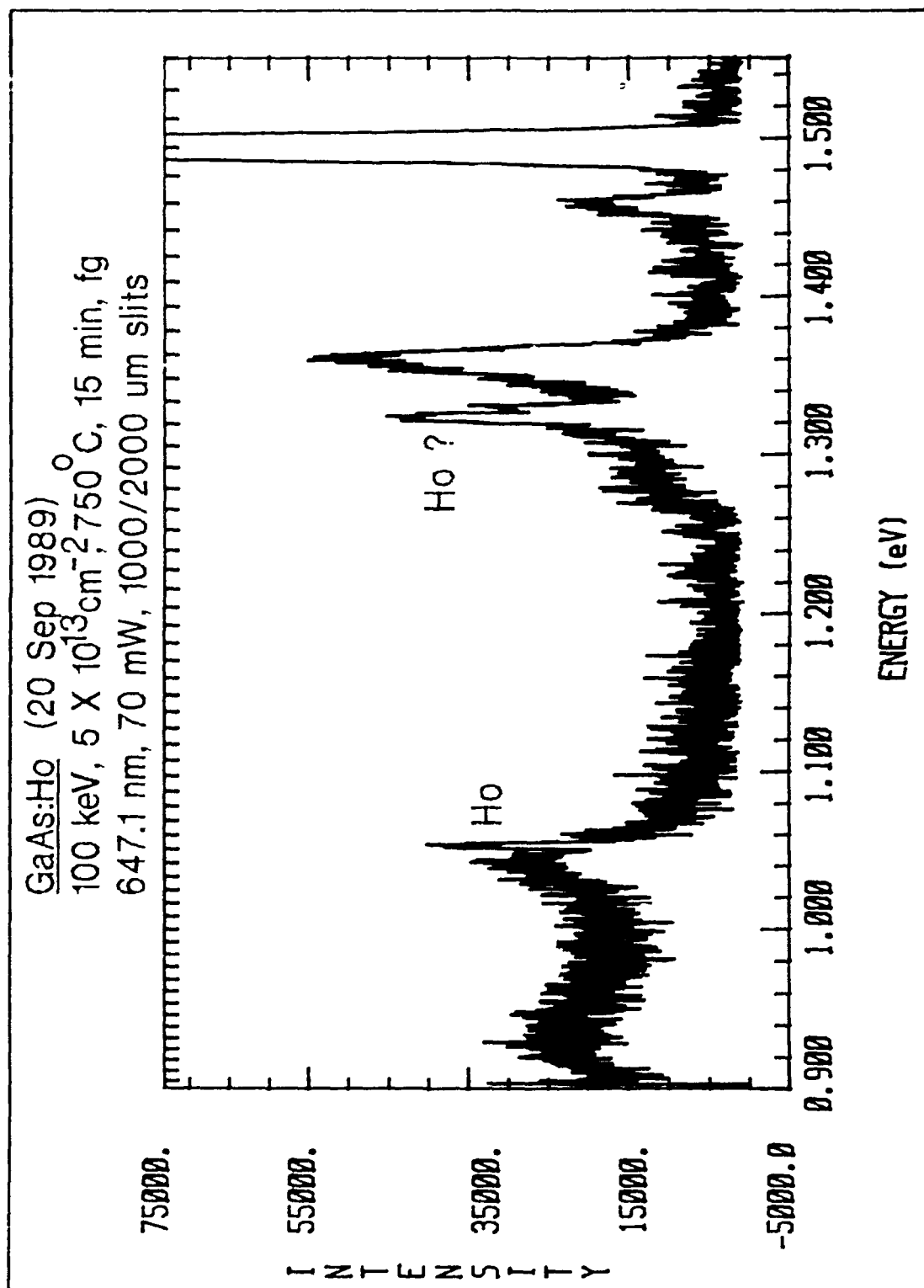
Appendix C: Energy Level Diagram for Lanthanides (RE^{3+})
 (after Macfarlane and Shelby, 1987, and references therein to Dieke, Crosswhite, and Carnall)



Appendix D: Energy Level Diagram for Actinides (An^{3+})
(after Carnall et al, 1985)



Appendix E: Photoluminescence of Ho^{3+} in GaAs



References

M. I. Aliev, G. I. Isakov, and S. A. Zeinalov, *Inorg. Mater.* (USSR) 14, 835 (1978).

D. G. Andrianov, E. P. Bochkarev, V. P. Grishin, Yu. A. Karpov, and A. S. Savel'ev, *Sov. Phys. Semicond.* 8, 320 (1974).

G. Aszodi, J. Weber, Ch. Uihlein, L. Pu-lin, H. Ennen, U. Kaufmann, J. Schneider, and J. Windscheif, *Phys. Rev. B* 31, 7767 (1985).

F. Auzel, A. M. Jean-Louis, and Y. Toudic, *J. Appl. Phys.* 66, 3952 (1989).

M. Baeumler, J. Schneider, K. Koehl, and E. Tomzig, *J. Phys. C*: 20, L963 (1987).

N. T. Bagraev and L. S. Vlasenko, *Sov. Tech. Phys. Lett.* 7, 413 (1981).

N. T. Bagrev, L. S. Vlasenko, K. A. Gatsoev, A. T. Gorelenok, A. V. Kamanin, V. V. Mamutin, B. V. Pushnyl, V. K. Tibilov, Yu. P. Tolparov, and A. E. Shubin, *Sov. Phys. Semicond.* 18, 49 (1984).

A. A. Ballmann, S. P. S. Porto, and A. Yariv, *J. Appl. Phys.* 34, 3155 (1963).

F. Bantien, E. Bauser, and J. Weber, *J. Appl. Phys.* 61, 2803 (1987).

R. L. Bell, *J. Appl. Phys.* 34, 1563 (1963).

L. V. Berman, A. T. Gorelenok, A. G. Zhukov, and V. V. Mamutin, *Sov. Phys. Semicond.* 19, 857 (1985).

H. Bethe, *Ann. Phys. (Leipzig)* 3, 133 (1929).

C. R. Betz, *Investigation and Study of Rare-Earth-Doped Silicon*, April 1964, Contract No. AF 19(628)2412 (AD-602031).

D. Bimberg, M. Sondergeld, and E. Grobe, *Phys. Rev. B* 4, 3451 (1971).

G. D. Boyd, R. J. Collins, S. P. S. Porto, and A. Yariv, *Phys. Rev. Lett.* 8, 269 (1962).

R. Boyn, *Phys. Status Solidi B*, 148, 11 (1988).

I. G. Brown, *IEEE Trans. Nucl. Sci.* NS-32, 1723 (1985).

M. R. Brown, A. F. J. Cox, W. A. Shand, and J. M. Williams, Advances in Quantum Electronics, ed. by D. W. Goodwin (Academic, New York, 1974) Vol. 2, 69.

I. G. Brown, J. E. Galvin, and R. A. MacGill, Appl. Phys. Lett. 47, 358 (1985).

I. G. Brown, J. E. Galvin, B. F. Gavin, and R. A. MacGill, Rev. Sci. Instrum. 57, 1069 (1986).

I. G. Brown, B. Feinberg, and J. E. Galvin, J. Appl. Phys. 63, 4889 (1988a).

I. G. Brown, J. E. Galvin, and K. M. Yu, Nucl. Instrum. and Methods B31, 558 (1988b).

M. R. Brown and W. A. Shand in Advances in Quantum Electronics Vol. 1, ed. by D. W. Goodwin (Academic Press, New York, 1970), pp. 1 - 76.

F. J. Bryant and J. Nahum, Radiat. Eff. 31, 107 (1977).

Bumgarner, Capt. Thad F., "Time Resolved Photoluminescence of Ytterbium in Indium Phosphide", MS thesis, AFIT/GEP/ENP/88D-1, School of Engineering, Air Force Institute of Technology (AU), Wright-Patterson AFB, OH, December 1988.

A. F. Burenkov, F. F. Komarov, M. A. Kumakhov, and M. M. Temkin, Tables of Ion Implantation Spatial Distributions (Gordon and Breach Science Publishers, New York, 1986).

W. T. Carnall, H. Crosswhite, and K. Rajnak, in Rare Earths Spectroscopy edited by B. Jezowska-Trzebiatowska, J. Legendziewicz, and W. Strek (World Scientific Pub. Co., Philadelphia, USA, 1985).

H. C. Casey, Jr. and G. L. Pearson, J. Appl. Phys. 35, 3401 (1964).

Cavins, Capt. Jeffrey R., Selective Pair Luminescence of Magnesium in Gallium Arsenide, PhD dissertation, AFIT/DS/ENP/88-2, School of Engineering, Air Force Institute of Technology (AU), Wright-Patterson AFB, OH, December 1988.

J.-W. Chen and A. G. Milnes, Ann. Rev. Mater. Sci. 10, 157 (1980).

Colon, 1Lt. Jose E., Low Temperature Photoluminescence Study of Ytterbium Implanted into III-V Semiconductors and AlGaAs, MS thesis, AFIT/GEP/88D, School of Engineering, Air Force Institute of Technology (AU), Wright-Patterson AFB, OH,

December 1988.

P. J. Dean, Trans. Metall. Soc. AIME, 242, 384 (1968).

P. J. Dean, Prog. Crystal Growth Charact. (Great Britain) 5, 89 (1982).

J. N. Demas, Excited State Lifetime Measurements, (Academic Press, New York, 1983).

B. Deveaud and P. N. Favennec, Solid State Commun. 24, 473 (1977).

B. DiBartolo, Optical Interactions in Solids (John Wiley & Sons, New York, 1968) and references therein.

G. H. Dieke and A. B. F. Duncan, Spectroscopic Properties of Uranium Compounds (McGraw-Hill Book Co., New York, 1949).

A. G. Dmitriev, L. F. Zakharenkov, V. A. Kasatkin, V. F. Masterov, and B. E. Samorukov, Sov. Phys. Semicond. 17, 1201 (1983).

R. Dingle, Phys. Rev. 184, 788 (1962).

B. Dischler and H. Ennen, J. Appl. Phys. 60, 376 (1986).

N. Duhamel, E. V. K. Rao, M. Gauneau, H. Thiberge, and A. Mircea, J. Cryst. Growth 64, 186 (1983).

L. Eaves, A. W. Smith, M. S. Skolnick, C. R. Whitehouse, and B. Cockayne, J. Appl. Phys. 53, 4955 (1982).

H. Ennen, U. Kaufmann, G. Pomrenke, J. Schneider, J. Windscheif, and A. Axmann, J. Cryst. Growth, 64, 165 (1983).

H. Ennen, J. Schneider, G. Pomrenke, and A. Axmann, Appl. Phys. Lett. 43, 943 (1983a).

H. Ennen, G. Pomrenke, and A. Axmann, J. Appl. Phys. 57, 2182 (1985).

H. Ennen and J. Schneider, J. Electron. Mater. 14A, 115 (1985).

H. Ennen, J. Wagner, H. D. Mueller, and R. S. Smith, J. Appl. Phys. 61, 4877 (1987).

H. Ennen, Extend. Abst. of the 19th Conf. on Solid St. Devices and Materials, Tokyo, Japan, 25 - 27 Aug 1987 (Tokyo, Japan Bus. Center Acad. Soc., Japan, 1987) pp. 83 - 86 and references therein.

P. N. Favennec, H. L'Haridon, A. LeCorre, M. Salvi, and M. Gauneau, *Electron. Lett.* 23, 684 (1987).

A. Garcia, R. Ibanez, and C. Fouassier, in Rare Earths Spectroscopy, edited by Jezowska-Trzebiatowska, J. Legendziewicz, and W. Strek (World Scientific Pub. Co., Philadelphia, USA, 1985).

M. Gauneau, A. Rupert, and P. N. Favennec, in Proceedings of the Third International Conference on Secondary Ion Mass Spectrometry (SIMS III), Budapest, Hungary, 1981, ed. by A. Benninghoven, J. Giber, J. Laszlo, M. Riedel, and H. W. Werner (Springer, New York, 1982).

J. F. Gibbons, J. L. Moll, and N. I. Meyer, *Nucl. Instrum. & Methods*, 38, 165 (1965).

J. F. Gibbons, W. S. Johnson, S. W. Mylorie, Projected Range Statistics, Semiconductors and Related Materials (Dowden Hutchinson, and Ross Inc., 1975).

A. A. Gippius, V. S. Vavilov, V. V. Ushakov, V. M. Konnov, N. A. Rzakuliev, S. A. Kazarian, A. A. Shirokov, and V. N. Jakimkin, Proc. of the 14th Int. Conf. on Defects in Semicond. ICDS-14, ed. by H. G. von Bardeleben, Materials Sciences Forum Vol. 10-12, 1195 (1986).

P. Goerlich, H. Karras, G. Koetitz, and R. Lehmann, *Phys. Status Solidi* 8, 385 (1965).

G. Guillot, C. Benjeddou, P. Leyral, and A. Nouailhat, *J. Lumin.* 31 & 32, 439 (1984).

W. H. Haydl, H. D. Mueller, H. Ennen, W. Koerber, and K. W. Benz, *Appl. Phys. Lett.* 46, 870 (1985).

L. A. Hemstreet in Defects in Semiconductors, ed. by H. J. von Bardeleben, Material Science Forum Vol. 10-12, 85 (Trans. Tech. Ltd., Switzerland, 1986).

T. Ikoma and Y. Mochizuki, *Jpn. J. Appl. Phys.* 24, L935 (1985).

G. F. Imbush in Luminescence of Inorganic Solids ed. by B. DiBartolo (Plenum Press, New York, 1978).

L. F. Johnson, *J. Appl. Phys.* 34, 897 (1963).

L. F. Johnson, J. E. Geusic, and L. G. Van Uitert, *Appl. Phys. Lett.* 7, 127 (1965).

R. Kallenbach, H. J. Reyher, J. Unruh, A. Winnacker, and

H. Ennen, Proc. of the 14th Int. Conf. on Defects in Semicond. ICDS-14, ed. by H. G. von Bardeleben Materials Sciences Forum 10-12, 681 (1986).

A. A. Kaminskii, Laser Crystals (Springer Verlag, Berlin, 1981).

V. A. Kasatkin, F. P. Kesamanly, and B. E. Samorukov, Sov. Phys. Semicond. 12, 974 (1978).

V. A. Kasatkin, F. P. Kesamanly, V. G. Makarenko, and B. E. Samorukov, Sov. Phys. Semicond. 13, 1207 (1979).

V. A. Kasatkin, F. P. Kesamanly, V. G. Makarenkov, Sov. Phys. Semicond. 14, 1092 (1980).

V. A. Kasatkin, F. P. Kesamanly, and B. E. Samorukov, Sov. Phys. Semicond. 15, 352 (1981).

V. A. Kasatkin, V. F. Masterov, V. V. Romanov, B. E. Samorukov, and K. F. Shtel'makh, Sov. Phys. Semicond. 16, 106 (1982).

V. A. Kasatkin and V. P. Savel'ev, Sov. Phys. Semicond. 18, 1022 (1984).

V. A. Kasatkin, Sov. Phys. Semicond. 19, 1174 (1985).

V. A. Kasatkin, A. A. Laurent'ev, and P. A. Rodnyl, Sov. Phys. Semicond. 19, 221 (1985).

W. Katz and J. G. Newman, MRS Bulletin, Vol. 12, No. 6, 40 (1987).

Z. J. Kiss and R. C. Duncan, Proc. IRE 50, 1532 (1962).

P. B. Klein and K. Weiser, Solid State Commun. 41, 365 (1982).

P. B. Klein, J. E. Furneaux, and R. L. Henry, Appl. Phys. Lett. 42, 638 (1983).

P. B. Klein in Extended Abstracts of the 16th (1984 International) Conference on Solid State Devices and Materials, Kobe, Japan, pp. 125-128 (1984).

P. B. Klein, J. E. Furneaux, and R. L. Henry, Phys. Rev. B 29, 1947 (1984).

P. B. Klein in Proceedings of the 1987 Fall Meeting of the MRS, Boston, Dec 1987.

P. B. Klein, Solid State Commun. 65, 1097 (1988).

P. B. Klein and G. S. Pomrenke, Electron. Lett. 24, 1503 (1988).

P. B. Klein, private commun., 1989.

W. Koerber, J. Weber, A. Hangleiter, K. W. Benz, H. Ennen, and H. D. Mueller, J. Cryst. Growth 79, 741 (1986).

W. Koerber and A. Hangleiter, Appl. Phys. Lett. 52, 114 (1988).

W. Koerber, A. Hangleiter, K. Thonke, J. Weber, F. Scholz, K. W. Benz, and H. Ennen, in GaAs and Related Compounds, Heraklion, Greece, 1987 (Inst. Phys. Conf. Ser. No. 91, 1988) p. 303.

W. F. Krupke, Phys. Rev. 145, 325 (1966).

B. Lambert, Y. Toudic, G. Grandpierre, A. Rupert, A. Le Corre, Electron. Lett., 24, 1446 (1988).

G. J. Lasher, F. Stern, and W. Weiser, Injection Laser Study: Second Quarterly Progress Report, 1 Sep - 30 Nov 1963, Contract DA 36-039 AMC-02349 (E) (AD-430696).

K. R. Lea, M. J. M. Leask, and W. P. Wolf, J. Phys. Chem. Solids (Great Britain) 23, 1381 (1962).

G. P. Li and K. L. Wang, J. Appl. Phys. 53, 8653 (1982).

H. J. Lozykowski, Solid State Commun. 66, 755 (1988).

R. M. Macfarlane and R. M. Shelby in Spectroscopy of Solids Containing Rare Earth Ions, ed. by A. A. Kaplyanskii and R. M. Macfarlane (North Holland, New York, 1987).

V. F. Masterov, V. V. Romanov, and B. E. Samorukov, Sov. Phys. Semicond. 12, 955 (1978).

V. F. Masterov, V. V. Romanov, and K. F. Shtel'makh, Sov. Phys. Solid State 25, 824 (1983).

V. F. Masterov, Sov. Phys. Semicond. 18, 1 (1984).

V. F. Masterov and O. D. Khokhryakova, Sov. Phys. Semicond. 21, 1045 (1987) and references therein.

J. A. McHugh in Secondary Ion Mass Spectrometry, ed. by K. F. J. Heinrich and D. E. Newbury, Natl. Bur. Stand. (U.S.) Spec. Publ. 427 (U. S. GPO, Washington DC, 1975) p. 179.

T. Miyashita and T. Manabe, IEEE Trans. Microwave Theory

Tech., MTT-30, 1420 (1982).

G. P. Morgan, D. L. Huber, and W. M. Yen, J. Lumin. 35, 277 (1986).

H. D. Mueller, Photo- und Elektrolumineszenz Seltener Erden in III-V Halbleitern (in German), Diplomarbeit/thesis, Inst. fuer Angewandte Festkoerperphysik der Fraunhofer-Gesellschaft, Freiburg, Fed. Rep. Germany, 1986, pp. 109 - 119.

H. D. Mueller, H. Ennen, J. Schneider, and A. Axmann, J. Appl. Phys. 59, 2210 (1986).

H. Nakagome, K. Takahei, and Y. Homma, J. Cryst. Growth 85, 345 (1987).

J. I. Pankove, Optical Processes in Semiconductors (Dover publications Inc., New York, 1971).

R. G. Pappalardo in Luminescence of Inorganic Solids ed. by B. Di Bartolo (Plenum Press, New York, 1978).

V. V. Petrov, V. S. Prosolovich, Yu. A. Karpov, and V. A. Kharchenko, Sov. Phys. Semicond. 20, 844 (1986).

G. S. Pomrenke, Y. S. Park, and R. L. Hengehold, J. Appl. Phys. 52, 969 (1981).

G. S. Pomrenke, H. Ennen, and W. Haydl, J. Appl. Phys. 59, 601 (1986).

G. Pomrenke, R. Hengehold, Y. Yeo, Bull. Am. Phys. 34, 918 (1989).

S. P. S. Porto and A. Yariv, Proc. IRE 50, 1542 (1962).

S. P. S. Porto and A. Yariv, J. Appl. Phys. 33, 1620 (1962).

S. L. Pyshkin, S. I. Radautsan, and S. V. Slobodchikov, Sov. Phys. Semicond. 1, 847 (1968).

S. L. Pyshkin, Sov. Phys. Semicond., 8, 912 (1975).

H. J. Queisser, Appl. Phys. 10, 275 (1976).

H. J. Queisser, Solid State Electron. 21, 1495 (1978).

H. J. Queisser, Czech. J. Phys. B 30, 373 (1980).

E. Rabinowitch and R. L. Belford, Spectroscopy and Photochemistry of Uranyl Compounds (Macmillan Co., New York,

1964).

J. Raczynska, K. Fronc, J. M. Langer, A. Lemanska, and A. Stapor, Appl. Phys. Lett. 53, 761 (1988).

E. V. K. Rao, A. Sibille, and N. Duhamel, Physica 116B, 449 (1983).

D. Richman, "Rare-Earth Doping of GaAs" in Technical Report No. 2: Synthesis and Characterization of Electronically Active Materials, E. F. Hocking (PI), Contract No. SD-182 ARPA Order 446 (AD452788), 1964.

C. Rochaix, A. Rolland, P. N. Favennec, B. Lambert, A. Le Corre, H. L'Haridon, and M. Salvi, Jpn. J. Appl. Phys. 27, L2348 (1988).

A. Rolland, A. LeCorre, P. N. Favennec, M. Gauneau, B. Lambert, D. LeCrosnier, H. L'Haridon, D. Moutonnet, and C. Rochaix, Electron. Lett. 24, 957 (1988).

W. A. Runciman, B. Thangavadivel, and N. B. Manson, J. Lumin. 24/25, 209 (1981).

G. I. Safaraliev, L. K. Vagabova, and I. Sh. Dadashev, Sov. Phys. Semicond. 21, 235 (1987).

Sargent-Welch Scientific Co., Periodic Table of Elements, 1980.

M. Schulz and H. Weiss, editors, Landholt-Boernstein Numerical Data and Functional Relationships in Science and Technology, Semiconductor Volume (Springer-Verlag, Berlin, 1981) p. 287.

B. O. Seraphin and H. E. Bennet, in Semiconductors and Semimetals (R. K. Willardson and A. C. Beer, eds.) Vol. 3, Academic Press, New York, 1967.

M. J. Sienko and R. A. Plane, Chemistry: Principles and Properties (McGraw-Hill Book Co., New York, 1966).

R. S. Smith, H. D. Mueller, H. Ennen, P. Wennekers, and M. Maier, Appl. Phys. Lett. 50, 49 (1986).

W. V. Smith and P. P. Sorokin, The Laser (McGraw-Hill Book Co., New York, 1966).

J. S. Solomon, Surf. Interf. Anal. 10, 216 (1987).

A. Stapor, J. Raczynska, H. Przybylinska, A. Sienkiewicz, K. Fronc, and J. M. Langer, Proc. of the 14th Int. Conf. on Defects in Semicond. ICDS-14, ed. by H. G. von

Bardleben, Materials Sciences Forum Vol. 10 - 12, 633 (1986).

S. M. Sze, Physics of Semiconductor Devices (John Wiley & Sons, 1981).

B. G. Tagiev, G. M. Niftiev, F. Sh. Aidaev, V. F. Zolin, Ch. M. Briskina, and V. M. Markushev, Opt. Spectrosc. (USSR) 62, 274 (1987).

K. Takahei, K. Uwai, and H. Nakagome, J. Lumin. 40 & 41, 901 (1988).

H. Temkin and W. A. Bonner, J. Appl. Phys. 52, 397 (1981).

H. Temkin, B. V. Dutt, W. A. Bonner, and V. G. Keramidas, J. Appl. Phys. 53, 7526 (1982).

D. G. Thomas, J. J. Hopfield, and W. M. Augustyniak, Phys. Rev. 140, 202 (1965).

Thonke, University of Stuttgart, FRG, unpublished results, 1987; see Ennen, 1987.

R. S. Title, P. P. Sorokin, M. J. Stevenson, G. D. Pettit, J. E. Scardefield, and J. R. Lankard, Phys. Rev. 128, 62 (1962).

P. D. Townsend, Ion Implantation, Sputtering, and Their Application (Academic Press, London, 1976).

W. T. Tsang and R. A. Logan, Appl. Phys. Lett. 49, 1686 (1986).

V. V. Ushakov, A. A. Gippius, V. A. Dravin, and A. V. Spitsyn, Sov. Phys. Semicond. 16, 723 (1982).

K. Uwai, H. Nakagome, and K. Takahei, GaAs and Related Compounds, Las Vegas, USA, 1986 (Inst. Phys. Conf. Ser. No. 83, ed. by W. T. Lindley) p. 87, 1987a.

K. Uwai, H. Nakagome, and K. Takahei, Appl. Phys. Lett. 50, 977 (1987b).

K. Uwai, H. Nakagome, and K. Takahei, Appl. Phys. Lett. 51, 1010 (1987c).

G. E. Valley and H. Wallman, Vacuum Tube Amplifiers (McGraw-Hill Book Co., New York, 1948).

J. P. van der Ziel, M. G. Oberg, and R. A. Logan, Appl. Phys. Lett. 50, 1313 (1987).

J. Wagner, J. Windscheif, and H. Ennen, Phys. Rev. B30, 6230 (1984).

J. Wagner, H. Ennen, and H. D. Mueller, J. Appl. Phys. 59, 1202 (1986).

P. S. Whitney, K. Uwai, H. Nakagome, K. Takahei, Electron. Lett. 24, 741 (1988).

K. Wittmaack, Vacuum (Great Britain) 32, 65 (1982).

W. L. Wolfe and G. J. Zissis, editors, The Infrared Handbook (IRIA, Environmental Research Inst. of Michigan, 1978), p. 5 - 88.

L. C. Beh, W. A. Sibley, and M. J. Suscavage, J. Appl. Phys. 63, 4644 (1988).

L. F. Zakharenkov, V. A. Kasatkin, F. P. Kesamanly, B. E. Samurkov, and M. A. Sokolova, Sov. Phys. Semicon. 15, 946 (1981).

L. F. Zakharenkov, S. I. Markov, V. F. Masterov, E. F. Mitellmakh, Sov. Phys. Semicond. 19, 1132 (1985).

L. F. Zakharenkov, V. F. Masterov, and O. D. Kucharyakova, Sov. Phys. Semicond. 21, 211 (1987).

J. E. Ziegler, J. P. Biersack, and U. Littmark, The Stopping and Range of Ions in Solids (Pergamon, New York, 1985).

VITA


Gernot Siegfried Pomrenke (Hauck) [REDACTED]
[REDACTED]
[REDACTED]

[REDACTED] In 1963 he moved with his mother and stepfather to the United States and became a U.S. citizen in 1967. Upon graduating from Southside High School, Fort Smith, Arkansas, in 1971 he entered the USAF Academy under a congressional nomination from former Senator Fulbright of Arkansas. In June 1975 he was commissioned in the US Air Force and graduated with a Bachelor of Science degree in physics and geography.

Initial assignments were as test engineer with the 475th Test Squadron and software manager (Air Combat Maneuvering Instrumentation system) with the Test and Evaluation Center at Tyndall AFB, Florida. In May 1978 he entered the Air Force Institute of Technology, Wright-Patterson AFB, OH, earning a Master of Science in engineering physics in Dec 1979. A follow-on assignment to the Avionics Lab at WPAFB started his research into III-V Group semiconductors, primarily investigating ion-implanted impurity and defect interactions. From Aug 1982 to Jun 1984, under an AF program (AFSC Exchange Scientist and Engineer Program to the FRG through HQ AFSC/DLXI), he was an exchange scientist with the Fraunhofer Institute for Applied Solid State Physics in Freiburg, Germany, working under Prof. Dr. Juergen Schneider. During this period he became involved with the initial

efforts to investigate rare earth elements in III-V and Group IV semiconductors. He also became familiar with the international R&D community especially in Germany and England.

After teaching various undergraduate physics courses at the USAF Academy in Colorado Springs CO, from 1984 to 1986, and a 1985 summer sabbatical to the Naval Research Lab, he entered the doctoral program at the Air Force Institute of Technology in July 1986. During the fall of 1989 he was reassigned to the Air Force Office of Scientific Research (AFOSR/NE) at Bolling AFB in Washington DC. He has over 15 publications in various scientific journals and has made over 23 presentations at various national and international conferences. He is a member of the American Physical Society, the Ohio Section of the APS, and the Deutsche Physikalische Gesellschaft (German Physical Society).



REPORT DOCUMENTATION PAGE

Form Approved
OMB No. 0704-0188

1a. REPORT SECURITY CLASSIFICATION UNCLASSIFIED			1b. RESTRICTIVE MARKINGS		
2a. SECURITY CLASSIFICATION AUTHORITY			3. DISTRIBUTION/AVAILABILITY OF REPORT Approved for public release; distribution unlimited.		
2b. DECLASSIFICATION/DOWNGRADING SCHEDULE					
4. PERFORMING ORGANIZATION REPORT NUMBER(S) AFIT/DS/ENP/89-4			5. MONITORING ORGANIZATION REPORT NUMBER(S)		
6a. NAME OF PERFORMING ORGANIZATION School of Engineering		6b. OFFICE SYMBOL (If applicable) AFIT/ENP		7a. NAME OF MONITORING ORGANIZATION	
6c. ADDRESS (City, State, and ZIP Code) Air Force Institute of Technology (AU) Wright-Patterson AFB, OHIO 45433			7b. ADDRESS (City, State, and ZIP Code)		
8a. NAME OF FUNDING/SPONSORING ORGANIZATION		8b. OFFICE SYMBOL (If applicable)		9. PROCUREMENT INSTRUMENT IDENTIFICATION NUMBER	
8c. ADDRESS (City, State, and ZIP Code)			10. SOURCE OF FUNDING NUMBERS		
			PROGRAM ELEMENT NO.	PROJECT NO.	TASK NO.
			WORK UNIT ACCESSION NO.		
11. TITLE (Include Security Classification) see Box 19					
12. PERSONAL AUTHOR(S) Gernot S. Pomrenke, B.S., M.S., Maj., USAF					
13a. TYPE OF REPORT PhD Dissertation		13b. TIME COVERED FROM _____ TO _____		14. DATE OF REPORT (Year, Month, Day) 1989 December	
15. PAGE COUNT 315					
16. SUPPLEMENTARY NOTATION					
17. COSATI CODES			18. SUBJECT TERMS (Continue on reverse if necessary and identify by block number)		
FIELD	GROUP	SUB-GROUP			
07	02		photoluminescence, anthanide, actinide, rare-earth,		
20	06		III-V semiconductor, ion implantation, lifetime,		
			gallium arsenide, indium phosphide, AlGaAs		
19. ABSTRACT (Continue on reverse if necessary and identify by block number)					
Title: LUMINESCENCE OF LANTHANIDES AND ACTINIDES IMPLANTED INTO BINARY III-V SEMICONDUCTORS AND AlGaAs					
Author: Major Gernot S. Pomrenke					
Dissertation Chairman: Robert L. Hengehold, PhD Professor of Engineering Physics Chairman Dept. of Engineering Physics					
Abstract on reverse side					
20. DISTRIBUTION/AVAILABILITY OF ABSTRACT <input checked="" type="checkbox"/> UNCLASSIFIED/UNLIMITED <input type="checkbox"/> SAME AS RPT. <input type="checkbox"/> DTIC USERS			21. ABSTRACT SECURITY CLASSIFICATION UNCLASSIFIED		
22a. NAME OF RESPONSIBLE INDIVIDUAL Robert L. Hengehold, PhD			22b. TELEPHONE (Include Area Code) (513) 255-2012		22c. OFFICE SYMBOL AFIT/ENP

Through luminescence experiments it was observed that lanthanides, or rare earths, and also actinides, may be successfully introduced into binary and ternary III-V Group semiconductors. The study supports the feasibility of producing infrared light emitting diodes (LEDs) for the 0.9 to 1.7 μm spectral range. Besides systematic spectral characterization through photoluminescence, excitation mechanisms and decay kinetics were also investigated.

Ytterbium (Yb), erbium (Er), thulium (Tm), praseodymium (Pr), and uranium (U) were successfully implanted into GaAs, InP, GaP, AlAs, or AlGaAs as observed through photoluminescence and also verified by secondary ion mass spectrometry (SIMS). The impurities were implanted through high (1 MeV), intermediate (380, 390 keV), and low (140 keV) energy standard and nonstandard implantation methods, followed by post-implantation annealing using both rapid thermal and conventional furnace annealing. Details on the implantation techniques are given and implantation statistics were determined.

The resulting characteristic sharp 4f- or 5f- emissions were seen around 1.0 μm for Yb^{3+} in InP, GaP, and AlGaAs; 1.5 μm for Er^{3+} in GaAs, InP, GaP, AlAs, and AlGaAs of four different Al mole fractions; 1.2 μm for Tm^{3+} in GaAs and InP; 1.1, 1.3, and 1.6 μm for Pr^{3+} in GaAs and InP; and from 1.6 to 1.7 μm for uranium in GaAs and InP. Preliminary evidence shows Ho-specific emissions in GaAs at 0.94 and 1.18 μm . Tm^{3+} emissions are assigned to transitions between the crystal-field-split spin-orbit levels $^3\text{H}_5 - ^3\text{H}_6$ while for Pr^{3+} , between the levels $^1\text{G}_4 - ^3\text{H}_4$, $^1\text{G}_4 - ^3\text{H}_5$, and $^3\text{F}_3 - ^3\text{H}_4$, respectively. The luminescence studies were performed by using semiconductor substrates of different conductivity, by varying laser excitation, sample temperature, and by varying anneal temperature, time, and technique.

Selected excitation experiments with a tunable dye laser were performed on the different systems in order to understand the excitation mechanism between the semiconductor host and the rare earth ion. It was established that free carriers were needed to excite the rare earth centers but below bandgap states such as donor-acceptor pairs and deep levels are also involved as seen for Er^{3+} and possibly Pr^{3+} . Lifetime measurements show the radiative (~ 1 millisecon for Er^{3+}) and more non-radiative (for Yb^{3+} 12.5 microseconds in InP and 15.5 microseconds in Al_{0.3}Ga_{0.7}As) nature of the different rare earth ions incorporated into the semiconductor.